

The Influence of High Temperature Pyrolysis Melt and Lignin on Cellulose Pyrolysis
Chemistry: A First-principles based Investigation

by

Arul Mozhi Devan Padmanathan

A thesis submitted in partial fulfillment of the requirements for the degree of

Doctor of Philosophy

in

Chemical Engineering

Department of Chemical and Materials Engineering
University of Alberta

© Arul Mozhi Devan Padmanathan, 2023

Abstract

Lignocellulosic biomass pyrolysis for biofuel production shows potential but is challenged with issues of bio-oil instability and low yield. To address these challenges, a bottom-up approach integrating reaction chemistry and transport within biomass particle during pyrolysis is crucial for predicting global performance and engineering parameters. At high pyrolytic temperatures, cellulose undergoes an amorphous transformation into an active-cellulose/melt-phase, making it essential to investigate the influence of this condensed phase environment on cellulose reaction kinetics. Moreover, the pyrolysis product yields from native biomass show stark differences from the pyrolysis of physically mixed synthetic biomass highlighting the role played by lignin-carbohydrate complex (LCC) linkages. Hence, this thesis focuses on investigating the chemistry of the pyrolytic decomposition of cellulose and the influence of condensed phase environment, lignin and LCC linkages on its decomposition.

A novel computational strategy is developed to limit computational cost, employing a hybrid approach that combines density functional theory (DFT) and molecular dynamics (MD) methods. Calculations using this novel strategy reveal two distinct cellulose decomposition regimes transitioning at 900 K, in line with millisecond-scale kinetic experiments. At high temperatures, the reduction in hydrogen bonding and the shift in hydroxymethyl orientations result in a lowered enthalpic barrier within the melt/active phase. As temperature increases, the melt-phase incurs an entropic penalty due to increased degree of freedom exhibited by cellulose chains, reducing the free-energy barrier and leading to an entropy-driven decomposition. Such entropic reductions are significantly less pronounced in the gas phase, indicating that the condensed phase

environment further enhances entropic losses. Furthermore, in native biomass, despite clear evidence for the impact of lignin on cellulose decomposition, its mechanism remains poorly understood. To investigate such condensed phase influence of lignin and LCC, two different environments are modeled: one with covalent linkages between lignin and cellulose, and one without such linkages, under pyrolysis conditions.

The presence of lignin and covalent interactions with cellobiose within the lignin-carbohydrate complex (LCC) and lignin-rich melt-phase have been found to influence the reaction energetics differently. In the LCC melt-phase, there is a promotion of cellulose activation, leading to a significant 107 kJ/mol reduction in the free energy barrier between 100K and 1200K for transglycosylation. This creates two distinct reaction regimes, resembling the behavior observed in pure cellulose. On the other hand, in the lignin-rich melt-phase, the condensed phase environment has no notable impact. Despite the different thermal responses, all three local reaction environments show that the disruption of the hydrogen bonding network and subsequent conformational flexibility in the hydroxymethyl group orientation directly affects the thermal shift in the free-energy barriers for cellobiose activation. Furthermore, the trend in the calculated free energy barriers for cellobiose activation in pure cellobiose and the lignin-rich melt-phase aligns with experimental millisecond-scale kinetics for the pyrolysis of pure cellulose and Loblolly pine.

To also account for the influence of covalent bonding between lignin and cellulose, we have conducted first-principles DFT calculations to investigate the breakdown of cellulose cross-linked with lignin in lignin-carbohydrate complexes (LCCs). The LCC models used

in the study incorporate β -O-4 benzyl ether linkages and are employed to analyze the energetics associated with three mechanisms (transglycosylation, ring contraction, and ring opening) that produce crucial biomass pyrolysis products, namely levoglucosan (LGA), furans, and glycolaldehyde. The examination of activation barriers and reaction energies reveals significant differences induced by LCC linkages on cellulose decomposition kinetics and thermochemistry. Specifically, cross-linked cellobiose in LCC exhibits higher activation barriers (2X) and reaction energies (3-4X) compared to pure cellobiose. The higher reaction energy observed for glycolaldehyde, in contrast to LGA, highlights its preferential formation at higher temperatures due to its more endergonic nature. This reduction in LGA at higher temperatures finds support in the product distribution observed in thin-film bagasse pyrolysis. Moreover, comparing relative experimental yields with the calculated reaction barriers provides evidence suggesting change in the reaction mechanism between cross-linked cellulose in LCC and pure cellulose. This inference is further supported by HOMO-LUMO analysis, which reveals a shift in HOMO orbitals from cellulose to the lignin moiety, suggesting the possibility of inter-moiety mechanisms. In summary, the study sheds light on the intricate effects of LCC linkages on cellulose degradation, highlighting both kinetic and thermochemical alterations in the pyrolysis products formation.

Preface

This thesis is an original work by Arul Mozhi Devan Padmanathan under the supervision of Dr. Samir H. Mushrif.

Chapter 2 of this thesis has been published as Padmanathan, A. M. D.; Mushrif, S. H. Pyrolytic Activation of Cellulose: Energetics and Condensed Phase Effects. *React. Chem. Eng.* **2022**, *7* (5), 1136–1149. I was responsible for the conceptualization, methodology, validation, performing simulations, investigation, data analysis, writing, review, and editing. Dr. S. H. Mushrif was the supervisory author in the conceptualization, investigation, review, and editing.

Chapter 3 of this thesis has been published as Padmanathan, A. M. D.; Vaidya, R.; Mushrif, S. H. Does the Presence of Lignin Affect the Pyrolytic Decomposition of Cellulose? A Condensed Phase Computational Investigation. *Sustainable Energy & Fuels*, 2023, *7*, 3660 – 3674. I was responsible for the conceptualization, methodology, validation, performing simulations, investigation, data analysis, writing, review, and editing. Rahul Vaidya assisted in performing simulations. Dr. S. H. Mushrif was the supervisory author in the conceptualization, investigation, review, and editing.

Chapter 4 of this thesis has been submitted to a peer review journal as Padmanathan, A. M. D.; Beck, S.; Ansari K. B.; Mushrif, S. H. Impact of Lignin-carbohydrate complex (LCC) linkages on cellulose pyrolysis chemistry. I was responsible for the conceptualization, methodology, validation, performing simulations, investigation, data analysis, writing, review, and editing. Seth Beck was responsible for performing CPMD-metadynamics simulations for conformation search. Dr. Khursheed B. Ansari was responsible for conceptualization, methodology and performing thin-film pyrolysis experiments. Dr. S. H. Mushrif was the supervisory author in the conceptualization, investigation, review, and editing.

Acknowledgements

I express my gratitude to the people of the University of Alberta, the City of Edmonton, and the Province of Alberta for their warm and welcoming environment throughout my graduate studies. Their hospitality has made this academic journey truly memorable. I also thank the Canada First Research Excellence Fund as part of the University of Alberta's Future Energy Systems Research Initiative, the Natural Sciences and Engineering Research Council of Canada (NSERC) via their Discovery Grants program and the Digital Research Alliance of Canada for providing computational resources.

I extend my gratitude to Dr. Samir H. Mushrif, my esteemed supervisor, for his exceptional mentorship and constant motivation throughout my Ph.D. journey. The work we have undertaken over the years has been invaluable to my academic and professional growth, and I am truly grateful for the time and effort he dedicated to my development. I deeply cherish the countless discussions, feedback, encouragement, and support I received from him, all of which have been instrumental in shaping my skills, knowledge and honing my capabilities.

In this moment of profound gratitude, I thank my parents, Padmanathan V. RM. and Thangam P for their unwavering love and support. Their care and encouragement have been the driving force behind my achievements. There is no 'I' without my parents, and I owe everything I am today to them. I dedicate every success in my life to my beloved parents, whose sacrifices have paved the way for my academic pursuits.

I would also like to express my heartfelt appreciation to my friends and colleagues, Nilesh Varadan, Shweta Sridharan, Ananthan Santhanakrishnan, Oğuzhan Doğru, Desirée Leistenschneider, José Velasco Calderón and Meghana Jois, who is my family away from home. Their support, motivation, and companionship have been a source of strength throughout my journey. Together, we have shared moments of despair, joy, fun, and adventure, and their presence has taught me invaluable life lessons. I also offer my sincerest thanks to all those that I haven't mentioned and have played a part, big or small, in my growth. Your support has made a profound impact on my life, and I am grateful for each one of you.

Table of Contents

Chapter 1 Introduction	1
1.1 Background	1
1.1.1 Biomass – a renewable source of carbon fuel	1
1.1.2 Lignocellulosic biomass and composition	2
1.1.3 Conversion technologies for lignocellulose utilization	3
1.1.4 Challenges in pyrolysis of lignocellulosic biomass	7
1.2 Thermal decomposition of cellulose	8
1.2.1 Global experimental bio-oil product yields and Kinetic modeling	9
1.2.2 Millisecond scale kinetics and Thin-film experiments	10
1.3 Intricate chemistry and kinetics in pure cellulose	12
1.3.1 Thermal changes in condensed phase using Molecular dynamics (MD)	12
1.3.2 Reaction mechanisms and First principles modelling	14
1.3.3 Condensed phase effects on cellulose reaction chemistry	15
1.3.4 Bottom-up approach for investigating cellulose chemistry	16
1.4 Thermal decomposition of cellulose in lignocellulosic biomass	18
1.4.1 Failure of additive models and interaction between biopolymers	18
1.4.2 Dependence on feed	19
1.4.3 Intricate chemistry and kinetics in native lignocellulosic biomass	20
1.5 Major factors influencing cellulose kinetics and chemistry in biomass	21
1.5.1 Thermal changes in the reaction environment	21
1.5.2 Physical interaction with other biopolymers	22
1.5.3 Covalent bonding in LCC linkages	23
1.6 Motivation of the thesis	24
1.7 Objectives of the thesis	25
1.7.1 Key objectives of chapter 2	26
1.7.2 Key objectives of chapter 3	27
1.7.3 Key objectives of chapter 4	27
1.8 Organization of the thesis	28
1.8.1 Chapter 2: Pyrolytic activation of cellulose: energetics and condensed phase effects	29
1.8.2 Chapter 3: Does the presence of lignin affect the pyrolytic decomposition of cellulose? A condensed phase computational investigation	30

1.8.3 Chapter 4: Impact of Lignin-carbohydrate complex (LCC) linkages on cellulose pyrolysis chemistry.....	30
1.9 Overview of the thesis	31
1.9.1 Computational methodology	33
Chapter 2 Pyrolytic activation of cellulose: Energetics and condensed phase effects.....	37
2.1 Introduction	37
2.2 Computational Methodology.....	42
2.2.1 Condensed phase transition state search (ConTS)	43
2.2.2 Free energy barrier corrections based on Relative Solvation in the condensed phase (ReSolv Method)	45
2.3 Results and discussion	47
2.3.1 Enthalpic barrier for glycosidic bond cleavage using condensed phase TS search.....	47
2.3.2 Condensed phase free-energy barriers using ReSolv method.....	49
2.3.3 Phase change and reaction chemistry	54
2.4 Conclusions	61
Chapter 3 Does the presence of lignin affect the pyrolytic decomposition of cellulose? A condensed phase computational investigation	63
3.1 Introduction	63
3.2 Computational Methodology.....	69
3.2.1 Free energy barrier corrections based on equilibrium solvation in the condensed phase.	71
3.3 Results and Discussions	73
3.3.1 Free energy barriers for competing cellulose decomposition reactions in the <i>melt-phase</i> using the ReSolv method.....	75
3.3.2 Molecular level explanation of <i>melt-phase</i> effects on reaction kinetics.....	79
3.3.3 Comparison with experimental kinetics	86
3.4 Conclusions	89
Chapter 4 Impact of Lignin-carbohydrate complex (LCC) linkages on cellulose pyrolysis chemistry... ..	91
4.1 Introduction	91
4.2 Methodology.....	97
4.2.1 Ab-initio Conformational search.....	97
4.2.2 DFT optimization and Transition State calculations	97
4.2.3 Experimental methods.....	98
4.3 Results and Discussion	99
4.3.1 Activation barriers for competing cellulose decomposition reactions.....	101

4.3.2 Lignin-carbohydrate complex (LCC)	101
4.3.3 Activation barriers for competing cellulose decomposition reactions in the presence of LCC	103
4.3.4 Thin-film pyrolysis experiment product yields for pure cellulose and cross-linked cellulose in native biomass (Bagasse)	110
4.3.5 Reaction kinetics and thermochemistry for cross-linked cellulose (in LCC) decomposition	112
4.4 Conclusions	114
Chapter 5 Conclusions and Future Perspectives	116
5.1 Conclusions	116
5.2 Future Perspectives	118
Bibliography	120
Appendix	155
A.1 Computational methods	155
A.1.1 Force-field method	155
A.1.2 First Principles Methods	157
A.2 Appendix to Chapter 2	158
A.2.1 Condensed phase TS-Search method	158
A.2.2 Dispersion Correction	159
A.2.3 Condensed phase free-energy barrier corrections	160
A.2.4 Simulation parameters	161
A.3 Appendix to Chapter 4	163
A.3.1 Literature review	163
A.3.2 Non-bonded parameters	165
A.3.3 Molecule and system visualizations	166
A.3.4 Molecule Coordinates	167
A.4 Appendix to Chapter 5	173
A.4.1 CPMD-Metadynamics calculations	173
A.4.2 Thin-film Preparation	175
A.4.3 Minimal change in kinetics between LCCs with different linkage sites (C2, C3, C6)	177
A.4.4 Molecule and system visualizations	178

List of Tables

Table 2.1 Dielectric constant in cellobiose melt-phase systems	55
Table 3.1 Enthalpic and entropic contribution to the free energy for cellobiose activation at the low and high temperature regimes in the interfacial LCC melt-phase.	74
Table 4.1 Reaction free energies (kcal/mol) for thermal cleavage of cellobiose via 3 key mechanisms when isolated and when cross-linked to lignin in LCC at C2, C3 and C6 positions.	105
Table 4.2 Thin-film pyrolysis product distribution at 573K-773K for native biomass bagasse and cellulose ¹³⁷	109
Table A.2.1 Computational methods and System configurations.....	158
Table A.2.2 Comparison of finite temperature barriers calculated with and without dispersion corrections	160
Table A.2.3 Non-bonding force-field parameters for cellobiose and its transitions states ..	161
Table A.4.1 Inter- and Intra-moiety hydrogen bond lengths (A) made by the cellobiose moiety when binding at C2, C3 and C6 positions with the lignin dimer.	177

List of Figures

Figure 1.1 Major advantages in fast pyrolysis of biomass.....	7
Figure 1.2 Lignin dimer - Quinone methide intermediate.....	19
Figure 1.3 Knowledge gaps in cellulose chemistry and overview of the thesis	32
Figure 2.1 (a) Atomic nomenclature used in the paper (b) Ring contraction mechanism to form furanic compounds (c) Transglycosylation mechanism to form LGA.....	39
Figure 2.2 Schematic for novel computational strategies that combine QM and MM methods to capture finite temperature condensed phase effects (Condensed phase transition search (ConTS) methodology) and entropic effects (ReSolv method). These strategies enable the <i>calculation of first principles based free energy and enthalpic barriers of glycosidic bond cleavage in the cellobiose condensed phase</i>	44
Figure 2.3 ConTS calculated enthalpic barriers for (a) transglycosylation and (b) ring contraction in the melt-phase environment.....	48
Figure 2.4 Gas phase free energy barrier for glycosidic bond cleavage in cellobiose at different temperatures calculated using hybrid functional M06-2X with 6-31+G (2d,p) basis set.....	50
Figure 2.5 Free energy barrier vs temperature profile for cellulose decomposition via transglycosylation and ring contraction showing two reaction regimes transitioning at 900K. The slope and y-intercept gives the entropic and enthalpic contributions to the <i>free energy barrier, respectively. The tangents are fitted between 500K-900K for the low temperature (blue dash lines) and 900K-1200K for high temperature regime (red dash lines)</i>	51
Figure 2.6 Distribution of hydroxymethyl group dihedral – (a) 100K and 500K, (b) 900K and 1200K. Distribution of O-O distance in hydrogen bonds – (c) 100K and 500K, (d) 900K and 1200K.	53
Figure 2.7 Entropy change in cellobiose molecule without undergoing reaction in a finite temperature melt-phase environment calculated using quasi-harmonic approximations in force-field simulations. The entropy monotonically increases to asymptote above 900K.	56
Figure 2.8 Average number of H bonds around the reacting molecule in a finite temperature melt-phase environment at different temperatures.....	58

Figure 3.1 Molecular visualization and zoomed-in chemical structure schematic of the A) LCC melt-phase with lignin dimers (red) and the cellobiose dimers (black) connected covalently, and B) lignin-rich melt-phase. In either system, one reacting cellobiose molecule *for which the reaction energetics are calculated is shown in a green bubble (ball and stick representation in the bottom molecular visualization), surrounded by lignin, which is not covalently bonded to cellobiose.*..... 69

Figure 3.2 Computational workflow for correcting gas phase free energies using equilibrium solvation free energy to account for finite temperature condensed phase effects. This is followed for both the melt-phase with LCCs (left) and the melt-phase with high lignin *concentration (right) systems.* 70

Figure 3.3 Gas phase free energy barrier for glycosidic bond activation in cellobiose at different temperatures calculated using hybrid functional M06-2X with 6-31+G(2d,p) basis set (reported in earlier publication²⁴⁰)..... 72

Figure 3.4 Free energy barriers for cellulose decomposition via transglycosylation and ring contraction mechanisms at different temperatures in A) LCC melt-phase and B) lignin-rich melt-phase C) pure cellobiose melt-phase..... 73

Figure 3.5 Relative free-energy barrier for cellobiose activation in the melt-phase via (A) transglycosylation mechanism (with respect to the barrier at 1200K) and (B) ring contraction mechanism (with respect to the barrier at 1200K). Average number of intermolecular *hydrogen bonds made by the (C) reactant with the three melt-phases (D) TS of ring contraction (solid line) and transglycosylation (dash line) with the melt-phases.* 80

Figure 3.6 (A) Distribution of O–O distance in intermolecular hydrogen bonds between reacting cellobiose molecule and the LCC melt-phase at 100 K, 500 K, 900 K and 1200 K; (B) Distribution of hydroxymethyl group dihedral angles in free cellobiose molecules (not *directly covalently bonded to lignin dimer*) at 100 K, 500K, 900 K and 1200 K; (C) *Distribution of O–O distance in intermolecular hydrogen bonds between reacting cellobiose molecule and the pure cellobiose melt-phase at 100 K, 500 K, 900 K and 1200 K;* (B) *Distribution of hydroxymethyl group dihedral angles in all cellobiose molecules in the pure cellobiose melt-phase at 100 K, 500K, 900 K and 1200 K.* 81

Figure 3.7 The range of free-energy barrier for cellobiose activation via transglycosylation (black) and ring contraction (red) mechanisms in the gas-phase and 3 melt-phase environments (lignin-rich melt, LCC melt, pure cellobiose) between the 100K-1200K temperatures. 85

Figure 4.1 Gas phase activation free energy barriers for cellobiose decomposition calculated using hybrid functional M06-2X with 6-311+G(d) basis set for transglycosylation, ring contraction and ring opening mechanisms.....	100
Figure 4.2 Free energy barriers for LCC decomposition via A) Transglycosylation B) Ring opening and C) Ring contraction mechanisms.....	103
Figure 4.3 HOMO-LUMO orbitals are visualized using Frontier Orbital analysis performed on isolated cellobiose and cross-linked cellobiose in LCC.	106
Figure 4.4 Yields (wt%) of bio-oil components A. Anhydrosugars, B. Lower oxygenates, C. Furans) in the thin-film pyrolysis of native biomass, bagasse (solid line) and that of pure cellulose (dash line).	108
Figure A.2.1 DFT calculated transition states in condensed phase for (A) Transglycosylation (B) Ring contraction.....	159
Figure A.2.2 DFT calculated activation barriers in crystal structure for Transglycosylation and Ring contraction	159
Figure A.3.2 DFT calculated structures of (A) Quinone methide intermediate (lignin dimer) (B) Lignin-Carbohydrate complex (LCC) molecule.....	166

List of Schemes

- Scheme 1.1 Schematic showing the calculation of condensed phase corrections to gas phase free energy barriers. 34
- Scheme 2.1 Cellulose decomposition model differentiated between the low (blue) and high (red) temperature regimes. At high temperatures, as primary decomposition is accelerated, the rate of secondary reactions in the intermediate liquid are significant.59
- Scheme 2.2 (A) Atomic nomenclature of the monomeric glucose unit (B) Transglycosylation reaction mechanism of cellobiose decomposition to form LGA (C) Ring contraction mechanism of cellobiose decomposition to form furanic compounds (D) LCC linkage between a lignin *moiety (quinone methide intermediate) and the cellobiose dimer*.Scheme 2.3 Cellulose decomposition model differentiated between the low (blue) and high (red) temperature regimes. At high temperatures, as primary decomposition is accelerated, the rate of secondary reactions in the intermediate liquid are significant.59
- Scheme 3.1 (A) Atomic nomenclature of the monomeric glucose unit (B) Transglycosylation reaction mechanism of cellobiose decomposition to form LGA (C) Ring contraction mechanism of cellobiose decomposition to form furanic compounds (D) LCC linkage between a lignin *moiety (quinone methide intermediate) and the cellobiose dimer*. 68
- Scheme 3.2 Schematic showing which melt-phase environments significantly alter cellobiose decomposition reaction kinetics with respect to temperature. 79
- Scheme 3.3 Cellulose decomposition model in the three melt-phases – A) Pure cellobiose, B) Melt-phase with LCC linkages and, C) Lignin-rich melt-phase showing the reaction regimes shift from low (blue) to high (red) temperature regimes. In the higher *temperature regime, as primary decomposition (black arrows) is accelerated, the rate of secondary reactions (green arrows) in the intermediate liquid becomes significant. The two melt-phase environments with lignin seem to alter the reaction kinetics in different ways*. 87
- Scheme 4.1 (A) Atomic nomenclature of the monomeric glucose unit (B) Transglycosylation reaction mechanism of cellobiose decomposition to form LGA (C) Ring contraction mechanism of cellobiose decomposition to form furanic compounds (D) Ring opening mechanism of *cellobiose decomposition to form Glycolaldehyde*. 96
- Scheme 4.2 LCC linkage between a lignin moiety (quinone methide intermediate) and the cellobiose dimer bonded at A) C2 position B) C3 position C) C6 position. 101

Chapter 1 Introduction

1.1 Background

The reliance on biomass as the primary energy source preceded the discovery of fossil fuels. The subsequent identification of coal and, more significantly, crude oil revolutionized the production of high-energy liquid fuels on a large scale. However, the drawbacks associated with fossil fuels, such as environmental impact, supply instability, volatile pricing and political considerations, have necessitated the exploration of alternative sustainable energy sources. While wind, solar, geothermal, tidal, and nuclear energy have been extensively investigated as viable alternatives, biomass stands out as the only option capable of generating a renewable carbon source compatible with existing fossil fuel infrastructure. This renewable carbon source can be gaseous products like renewable natural gas (from waste biomass), which can be blended into the existing pipeline infrastructure, or liquid fuels that can be utilized in conventional combustion engines. Moreover, the carbon cycle is significantly shorter for bio-energy (a few years) as compared to fossil energy (millions of years). The abundance and diverse sources of biomass worldwide make it a crucial resource for ensuring energy independence among nations ¹.

1.1.1 Biomass – a renewable source of carbon fuel

This widely available resource is estimated to possess a global energy potential ranging from 150 to 450 EJ/year by 2050 ². Canadian biomass availability ranges from 64 million green tonnes to 561 million dry tonnes, encompassing energy crops, forest resources, urban waste, agricultural residue, logging, and mill residue ³. In 2006 ⁴, woody biomass accounted for 6% of Canada's energy consumption, with forest resources capable of meeting 60% of the domestic energy requirement ⁵. In terms of fuel production, biomass is classified based on its source. First generation biofuels utilize food-based biomass such as corn sugar or vegetable oil as feedstock, while second generation biofuels utilize the non-edible parts of plants, specifically lignocellulosic biomass ⁶. The commercial production of first generation biofuels, including bioethanol, biodiesel, biogas and sustainable aviation fuel, amounts to approximately 50 billion liters worldwide, annually ⁶. In Canada, ethanol-based sustainable liquid fuel produced from agricultural residue reached approximately 1

billion liters in 2007 ⁷. However, ethanol production has been deemed "environmentally-questionable" due to its negative impact on biodiversity, land use, water consumption⁸ and exacerbating the competition between first generation biofuels and food production. The production of fuel from food crops has been identified as a significant factor contributing to rising food prices ⁹. Consequently, lignocellulosic biomass, encompassing all non-food plant materials, holds tremendous potential in meeting the increasing energy demand.

1.1.2 Lignocellulosic biomass and composition

The recent surge of interest in lignocellulosic biomass can be attributed to advancements in agriculture and biotechnology, which have significantly reduced the production costs compared to crude oil ¹⁰. Lignocellulosic biomass emerges as the most abundant feedstock on Earth ¹¹ among the various biogenic sources. Biomass primarily comprises three major biopolymers: lignin, cellulose, and hemicellulose. Cellulose, a polysaccharide, consists of repeating units of glucose linked by glycosidic bonds ¹², forming a linear chain. Hemicellulose, on the other hand, comprises a diverse range of sugar monomers, such as glucose, xylose, and mannose, forming branched chains. Lignin, a complex polymer, consists of aromatic units such as p-coumaryl alcohol, coniferyl alcohol, and sinapyl alcohol. Additionally, biomass contains trace amounts of alkali and alkali-earth metals (AAEM), pectins, and proteins ¹³. In native biomass, these biopolymers exist as intricate macrostructures, with cellulose arranged in bundles enveloped by hemicellulose and lignin. The composition of these biopolymers and their corresponding repeating oligomer units varies depending on the type of biomass, whether it is derived from herbaceous plants, softwood, or hardwood ¹⁴. Herbaceous plants exhibit varying levels of lignin, hemicelluloses, cellulose, and extractives, ranging from 0–40%, 20–50%, 25–95%, and 4–9%, respectively ^{15,16}. Softwood species typically consist of 33–42% cellulose, 22–40% hemicellulose, 27–32% lignin, and 2–3.5% extractives ¹⁷. In contrast, hardwood species contain 38–51% cellulose, 17–38% hemicellulose, 21–31% lignin, and 3% extractives. The lignin content shows a decreasing trend from hardwoods like oak to softwoods like spruce and pine, and further to herbaceous plants like switchgrass and cornstover ^{18,19}. This variation is also evident in different parts of the plant—for instance, hazelnut shells have high lignin content (51.3 wt%)²⁰, while tree leaves contain negligible²¹ amounts.

1.1.3 Conversion technologies for lignocellulose utilization

A range of technology and process options are available for the conversion of biomass into fuel. The conversion of biomass into useful fuels and chemicals involves multiple process steps and can be achieved through one of three primary techniques: biochemical, liquid phase catalytic, and thermochemical²². Biochemical conversion entails the utilization of microorganisms or enzymes to convert biomass or waste into valuable energy sources. On the other hand, liquid phase catalytic conversion involves the transformation of biomass through chemical reactions. Thermochemical conversion, on the other hand, involves the decomposition of organic components in biomass through the application of heat. The selection of a specific conversion technology depends on various factors, including the feedstock used, the desired end products, environmental principles and financial considerations²³.

1.1.3.1 Biological conversion

Biological conversion involves harnessing specialized microorganisms to convert waste or biomass into valuable products. Processes utilized for the production of gaseous and liquid biofuels include anaerobic digestion and acid fermentation²⁴. During anaerobic digestion, microorganisms transform biomass into biogas, predominantly composed of CH₄ (60-70%) and CO₂ (30-40%), with trace amounts of H₂S²⁵. This process occurs within temperature ranges of 30-35°C or 50-55°C²⁶. Anaerobic digestion consists of three distinct phases: hydrolysis, fermentation, and methanogenesis. Initially, acid-forming bacteria break down complex organic compounds in biomass into simpler substances like acetic and propionic acids, volatile fatty acids, and H₂. Subsequently, methane-producing bacteria convert these acids into CO₂ and CH₄, resulting in the formation of biogas²⁷. The low biomass concentration in the feed stream poses a primary challenge for anaerobic digestion. Alternatively, bioethanol can be produced through the alcoholic fermentation of biomass residues containing fermentable sugars derived from cellulose and hemicellulose. Alcoholic fermentation involves biochemical pathways encompassing hydrolysis and fermentation reactions, leading to the conversion of biomass into alcohols²⁸. The resulting crude alcohol, containing approximately 10-15% ethanol, requires subsequent distillation²⁹. The solid residue remaining after fermentation can be further processed using thermochemical methods. While biological conversion is

often favored for its ability to produce specialty chemicals with high selectivity ³⁰, it does have certain limitations. These include the stability of biological agents, the requirement for pure feedstock, the need for sterile conditions ³¹, narrow operating conditions, and relatively low conversion rates ³².

1.1.3.2 Liquid phase catalytic (inorganic) conversion

Liquid phase catalytic processing of biomass converts biomass into smaller, low oxygen containing molecules ³³. Consequently, chemical conversion of biomass encompasses a diverse range of reactions, including polysaccharide depolymerization, cellulose hydrogenation, sugar and alcohol hydrogenolysis, dehydration and catalytic synthesis of specialty furanic compounds ³⁴. Biomass offers advantages over petrochemicals in the production of functionalized chemicals. While petroleum primarily consists of long-chain hydrocarbons, biomass is highly functionalized. For example, glucose contains one oxygen atom for every carbon atom. However, high functionality and oxygen content can also be a challenge in controlling selectivity of products. Therefore, chemical processes in biomass conversion mainly involve optimizing the functional group type and degree of functionalization. Pentose (xylose) and hexose (fructose or glucose) in biomass can be dehydrated to produce furfural and 5-hydroxymethylfurfural (HMF), which are promising intermediates for synthesizing high-value products. Thus, biomass building blocks are converted into these platform chemicals, which can then be further upgraded to secondary chemicals ³⁵. A notable example is the selective hydrogenation of HMF using Ru/CeO_x catalysts to produce functionalized furans, which serve as precursors for solvents and monomers ³⁶. Additionally, catalytic condensed phase conversion enables the production of 2,5-dimethylfuran (DMF), a fuel additive, from HMF. DMF can also be utilized in Diels-Alder reactions to produce p-xylene ³⁷. It is important to note that although HMF can be converted into various high-value compounds, the availability of HMF on a large scale remains a bottleneck for industrial application. While liquid-phase catalytic conversion is valuable for producing a wide range of targeted products, it is limited by catalyst stability in the aqueous phase and the requirement for pure feedstocks ³⁸.

1.1.3.3 Thermochemical conversion

Thermochemical conversion encompasses a high-temperature reformation process that involves breaking and reforming chemical bonds within organic matter, resulting in the formation of solid biochar, non-condensable/synthesis gas, and highly oxygenated bio-oil. Within the realm of thermochemical conversion, several primary process alternatives exist, including combustion, gasification, liquefaction, and pyrolysis. Combustion involves the burning of biomass in the presence of air, leading to the release of heat and significant emissions of CO₂ into the environment (Fan et al., 2021). Gasification, on the other hand, entails the thermal decomposition of biomass, generating a mixture of gases known as syngas (comprising H₂, CO, CO₂, CH₄, and N₂). This process is carried out at high temperatures with the controlled introduction of oxidizing agents such as steam, air, or O₂ (AlNouss et al., 2020; Shahbaz et al., 2017). Liquefaction involves subjecting biomass to higher temperatures and pressures, allowing for reactions to occur in the liquid phase without the need for moisture removal (Behrendt et al., 2008; Chan et al., 2019; Huang and Yuan, 2015). Pyrolysis, on the other hand, involves thermal treatment of organic compounds in an inert environment, leading to the production of solid biochar, liquid bio-oil, and gaseous fuels (Chan et al., 2019). The condensable gases from pyrolysis undergo room temperature condensation, forming an intermediate liquid known as bio-oil, which predominantly comprises anhydro-sugars (such as levoglucosan), furans, pyrans, and small oxygenates³⁹. Bio-oil derived from pyrolysis can potentially be upgraded into a fuel suitable for direct use in conventional automobiles. Depending on the heating rate, pyrolysis can be categorized as either fast or slow. Slow pyrolysis primarily aims to produce solid char rather than bio-oil. In contrast, fast pyrolysis involves rapidly heating biomass at high temperatures (400°C - 800°C) in the absence of oxygen to yield bio-oil^{40,41}. Currently, there is greater emphasis on liquid production from fast pyrolysis due to several advantages. This approach allows for rapid conversion within seconds⁴², offers flexibility by accommodating various feedstocks without the need for extensive preprocessing, can be implemented on a scalable basis⁴³, supports decentralization to reduced capital and transportation costs¹⁰, and facilitates transportation of the liquid intermediate (bio-oil)^{44,45}. Techno-economic studies indicate that fast pyrolysis exhibits competitiveness, despite lower product

value, owing to significantly lower capital costs, higher process efficiency, and greater yield compared to gasification or biochemical techniques ⁴⁶.

Pyrolysis systems can also be potentially integrated with existing petroleum infrastructure ⁴⁷. For Canada, the production of bio-oil (intermediate in biomass pyrolysis) offers an additional advantage, as it can be used as a diluent in bitumen transportation. The province of Alberta, known for its vast bitumen reserves in the boreal forests of the north, estimates that current technology allows for the extraction of approximately 10% of the bitumen deposits, amounting to 27 billion m³, making Canada the world's third-largest oil reserve ⁴⁸. In 2014, 74% of Alberta's oil production was transported to the United States via pipelines (Alberta Energy; Alberta Energy Regulator; Statistics Canada). Due to its high viscosity, viscosity or friction reduction techniques are employed using diluents like naphtha to reduce the cost of bitumen transport ⁴⁹. Bio-oil, a pyrolysis intermediate derived from lignocellulosic biomass with a viscosity range of 10-350 mPa s ⁵⁰, is a potential diluent that eliminates the need for further separation. Nevertheless, being competitive with petroleum technology or at least parity with conventional fossil fuels is crucial for commercial viability. Comparative studies ⁵¹ show that biomass pyrolysis technology is not competitive with fossil fuels, yet. However, many studies have concluded pyrolysis to be the most promising technology for the production of liquid transportation fuels ^{40,52-54}. The challenge is in the ability to efficiently convert biomass to liquid transport fuel/chemicals. However, pyrolysis offers a cost effective ⁴⁶ pathway for a high yield ⁵⁵ production of liquid product (bio-oil) with sufficient feedstock flexibility. Though the increased research interest to tap into this vast lignocellulosic resource is recent, studies had been conducted as early as 1918 to isolate levoglucosan as a pyrolysis product ⁵⁶. From the above mentioned advantages of pyrolysis (c.f. Figure 1.1) over other conversions techniques, it is clear that pyrolysis is the preferred method for the conversion of biomass to liquid transportation fuels. Therefore, this thesis will focus on pyrolysis technologies for biomass conversion.

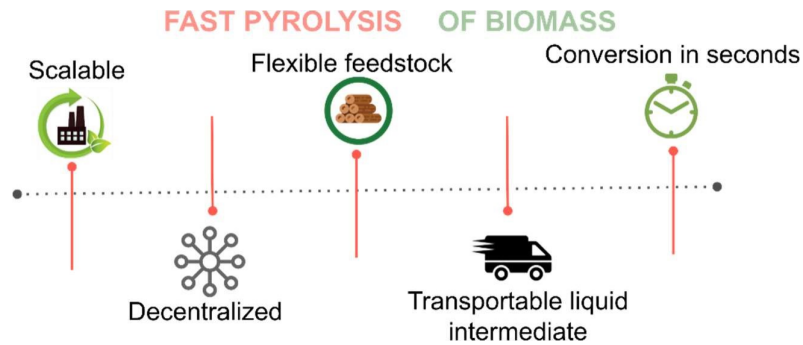


Figure 1.1 Major advantages in fast pyrolysis of biomass

1.1.4 Challenges in pyrolysis of lignocellulosic biomass

There are however many challenges inhibiting the commercialization of pyrolysis ⁵⁷–

1. The corrosive and unstable nature of bio-oil, coupled with its high oxygen content ⁴⁴, poses difficulties in terms of storage and transportation, making it inferior to fossil-based hydrocarbons.
2. Pyrolysis exhibits low yields of bio-oil, and the upgradation of bio-oil also faces challenges in achieving desirable yields.
3. The continuous and economic supply of feedstock introduces uncertainty ⁵⁸, which can impact the overall viability of pyrolysis processes.
4. Efficient upgradation of bio-oil requires advanced catalytic technologies, and the high consumption of hydrogen during upgradation leads to increased operating costs.
5. The characterization of bio-oil is challenging, hindering consistent production and quality control.
6. The removal of char, which is produced during pyrolysis, presents difficulties in inhibiting the circulation of alkali metals within the process cycle. Char formation also limits heat transport rates in the reactor, making scale-up challenging. An ideal pyrolysis reactor should be char-free ⁵⁹.

The application of petrochemical processes for upgradation of bio-oil is hindered by the presence of highly functionalized biomass molecules, characterized by elevated oxygen content and reactivity. Nevertheless, promising alternatives, such as fixed-bed

pyrolysis reactors, have shown potential, achieving approximately 80 wt% bio-oil production without char formation by utilizing H₂ as a sacrificial fuel. However, a fundamental challenge in this context lies in the poorly understood interdisciplinary field of solid phase decompositions⁶⁰. To address these challenges, a key strategy involves gaining a comprehensive understanding of the structural composition of native biomass and its fundamental pyrolysis reactions. In native biomass, cellulose exists in a complex microscopic architecture intertwined with lignin and hemicellulose. A critical review by Collard and Blin⁶¹ delved into the pyrolysis of individual lignocellulosic components, namely cellulose, hemicelluloses, and lignin. They highlighted that the mass superposition of product yields from individual components significantly influences the total product yields for both primary and secondary reactions. As a means to enhance product predictability, researchers have proposed the analysis of individual biomass components (cellulose, hemicellulose and lignin)^{62,63}. Given that dry biomass fuels typically contain approximately 50% cellulose by weight, the kinetics of cellulose pyrolysis assume primary interest in this context, prompting considerable focus on investigating cellulose reaction chemistry compared to other bio-polymers.

1.2 Thermal decomposition of cellulose

Cellulose constitutes a significant proportion (40-50%)⁶⁴ of biomass composition and its thermal decomposition can be initiated at a relatively low temperature of 150 °C⁶⁵, due to its linear homopolysaccharide structure composed of β-D-glucopyranose units. Given its prominence in biomass and the well-known structure, cellulose pyrolysis mechanisms have garnered considerable attention^{64,66}. Despite the presence of hemicellulose and lignin, the cohesive and interlaced cellulosic microfibrils form the fundamental framework of biomass cell walls⁶⁷. The annual production of cellulose surpasses that of all other organic polymers, making an understanding of its thermal decomposition a crucial scientific objective⁴¹. During the pyrolysis process, cellulose undergoes dehydrating, fragmentizing, and condensing reactions, ultimately yielding liquid tar, gaseous products, and residual chars. The comprehension of these fundamental pyrolysis reaction mechanisms represents a critical bottleneck in the development of first-principles based models for particle decomposition, essential for

reactor-level modeling and optimizing reaction conditions. As a result, kinetic studies have been undertaken by early experimentalists in achieving this understanding.

1.2.1 Global experimental bio-oil product yields and Kinetic modeling

Characterizing the evolution of hundreds of compounds from cellulose posed a challenge for researchers, leading them to rely on stoichiometry or yield-based lumped kinetic models. These models, based on TGA experiments, incorporated various factors such as intrinsic kinetics, transport, and phase transitions, resulting in a wide range of reported activation energies, ranging from 50 to 285 kJ mol⁻¹. However, due to the lack of control over secondary reactions, coupled with experimental constraints in measuring fast reaction time that cause mismatch between reaction and measurement timescales, these models are insufficient for understanding the underlying chemistry. To develop a mechanistic understanding of cellulose pyrolysis reactions, it is crucial to maintain the sample in a reaction-controlled regime and continuously analyze product evolution. Experimental studies have utilized micropyrolyzer systems⁶⁸⁻⁷⁰, which feature precise temperature-controlled furnaces and inert carrier gas that sweep the vapors to a gas chromatograph (GC) within the device. For example, Shanks and colleagues employed a micropyrolyzer with a sample size of 6-50 μm to analyze glucose-based carbohydrates⁶⁸. They identified levoglucosan as a major pyrolysis product, with its yield increasing with polymerization. Though cellulose decomposition was previously found to proceed through the formation of levoglucosan⁷¹, it was hypothesized as a precursor for lower molecular weight products (LMWPs)⁷². This sequential reaction model⁷³ was disproven by Shanks and co-workers^{68,69,74} using sample sizes ≤ 50 μm in micropyrolyzer systems. It was observed that levoglucosan (LGA) sublimates before decomposition at 773K, and the pyrolysis products are obtained through competitive reactions. The sequential reactions were found to be a result of secondary reactions (with LGA as a precursor for LMWPs) occurring in the cellulosic melt-phase, which were not adequately limited by experimental constraints.

Although numerous lumped global kinetic models⁷⁵⁻⁸¹ have been proposed, enabling macroscopic predictions of volatilization rate and overall yields, they do not provide a fundamental understanding at a molecular level^{39,47}. These models are limited to specific operating conditions and feedstock compositions, lacking the ability to predict

reaction rates beyond that range, and they are not based on reaction mechanisms [56]. Therefore, advanced experimental and computational techniques are employed to investigate intricate reaction chemistry and calculate kinetics.

1.2.2 Millisecond scale kinetics and Thin-film experiments

Experimental activation energies for cellulose decomposition reported in the literature have shown significant variations, ranging from 13 to 68 kcal/mol⁷³. This creates uncertainty in their ability to differentiate between the two proposed mechanisms – midchain and endchain scission. However, recent advancements in thin-film sample techniques and microreactor technology have allowed for more detailed analysis of cellulose pyrolysis. Mettler et al.⁸² introduced a new thin-film technique (with a size of approximately 1 μm) for sample preparation in mechanistic pyrolysis studies. They argued that transport limitations alter the condensed-phase chemistry, leading to secondary pyrolysis reactions. Their research demonstrated that to study fast pyrolysis at 500°C, the sample dimension should be less than 20 μm to ensure an isothermal kinetically limited regime. Therefore, experimental studies need to design appropriate experiments to capture the primary pyrolysis reactions. Thin films offer the advantage of enabling isothermal, kinetically limited experiments, although they only allow for the analysis of cumulative product yields. However, addressing the temporal mismatch between cellulose chemistry (milliseconds) and chromatography analysis (kiloseconds) is crucial when investigating only the primary reactions⁸³. Reactors must have the ability to control the progression of reactions to quantify products and intermediates over time. Traditional micropyrolyzers undergo complete conversion, making it impossible to analyze intermediate reaction products as a function of reaction time. As early as 2000, Dr. L.D. Schmidt suggested the design of millisecond reactors capable of rapidly adding and removing heat to regulate sample temperatures⁸⁴. Building on this concept, Dauenhauer and colleagues developed a microreactor called the Pulse-Heated Analysis of Solid Reactions (PHASR) reactor⁸³. The PHASR reactor can heat and cool samples in milliseconds using a silicon-based coolant system, allowing control over reaction times as short as 10 ms. This technology enables the analysis of composition within milliseconds, facilitating the measurement of reaction rates.

The use of the PHASR reactor has provided valuable insights into the kinetics of cellulose decomposition at the millisecond scale and the composition of intermediate products. It has revealed changes in reaction mechanisms and kinetics at different temperature regimes. One important discovery is the influence of thermal phase changes, including the formation of an intermediate liquid cellulose known as the "melt-phase". These thermal phase changes impact the structure and hydrogen bonding of cellulose, affecting product formation during decomposition and emphasizing the role of temperature and the melt-phase environment. In studying cellulose decomposition, model molecules such as cellodextrin of different chain lengths and cyclodextrin have been utilized. Cyclodextrin, verified as an appropriate surrogate for cellulose using first-principles methods, shares the same end-group-to-chain-length ratio⁸². Experimental investigations demonstrated that at 550°C, the rate of furan formation was similar for all cellodextrin and cyclodextrin. However, at 400°C, the rate of furan formation was only the same for all cellodextrin when normalized to the polymer chain concentration, indicating that the reaction occurs at polymer chain ends⁸³. This suggests that at 400°C, furan formation is solely from the chain ends, while at 550°C, it can also occur from the mid-chain. This kinetic regime shift from an end-chain to a mid-chain mechanism for furan formation from different cellodextrin molecules was observed at a "reactive melting point" of 467°C. A subsequent study⁸⁵ demonstrated that cyclodextrin pyrolysis follows first-order kinetics at all conditions (550°C < T < 385°C). Below the reactive melting point, the rate of conversion at different temperatures exhibited similar first-order kinetics. Above 467°C, a significant relative difference in the rate of conversion of cyclodextrin was observed, indicating a drastic increase in conversion. By using rate coefficients in the Arrhenius form, a transition at 467°C was identified, above which the activation barrier was 53.7±1.1 kcal/mol, while below 467°C, it was consistently 23.2±1.9 kcal/mol, suggesting a slow end-chain mechanism.

While these studies offer an overall understanding of the kinetics of cellulose decomposition, a comprehensive molecular-level mechanistic understanding of pyrolysis reactions is still lacking. Empirical kinetic models have limitations as they are applicable only to specific operating conditions and feedstock compositions. Hence, it is crucial to establish a fundamental knowledge base of pyrolysis reaction mechanisms to construct mechanistic kinetic models. These newer models incorporate rate

coefficients for elementary reactions obtained from experiments or first-principles calculations^{39,42}. For instance, a kinetic model developed for cellulose pyrolysis accounts for 103 species and 342 reactions, allowing for the estimation of competing reaction pathways within a complex reaction network^{39,86}. Such models provide a quantitative understanding of the system and enable the integration of rate coefficients determined through experiments or first-principles calculations⁸⁷. Moreover, these models can be adapted to various reactor types, reaction conditions, and feedstocks, making them valuable for process scale-up. Their flexibility permits the inclusion of new mechanisms as they are discovered, underscoring the importance of molecular understanding. To address the need for molecular-level insights, experiment-guided simulations employing first-principles molecular modeling are utilized to analyze the energetic aspects of reaction mechanisms. Employing a computational approach to develop biomass conversion technology proves to be more effective and efficient than an empirical approach³³.

1.3 Intricate chemistry and kinetics in pure cellulose

Molecular modeling plays a vital role in gaining insights into phenomena that are otherwise inaccessible through experiments alone⁸⁸. Early experimental ¹³C NMR studies⁸⁹ and kinetic studies^{75–78} have contributed to generating the necessary knowledge on molecular structure and reaction pathways, facilitating computational studies. Cellulose can exist as four different polymorphs (I, II, III and IV)⁹⁰. In plants, cellulose is created as crystalline cellulose I microfibrils⁹¹. Algal cell wall majorly consists of cellulose I α ⁹² while plant cell wall is composed of cellulose I β ⁹³. A study has shown that metastable cellulose I α can easily be converted to I β using a hydrothermal treatment. Therefore, almost all studies in literature deal with cellulose I β structure.

1.3.1 Thermal changes in condensed phase using Molecular dynamics (MD)

Building on experimental findings, several computational studies have focused on analyzing individual biomass components, with cellulose receiving significant attention. In 2000, the native cellulose crystal structure was predicted using two β -1,4 glucopyranose chains⁹⁴. Vietor et al. achieved this by rotating and translating the two chains along the helical axis and estimating the minimum energy for inter-chain

distance using force-field calculations. In 2002, Nishiyama et al.⁹⁵ determined three-dimensional coordinates with a hydrogen bonding system using synchrotron X-ray and neutron fiber diffraction data. This model has since been utilized in numerous computational studies^{96,97}. Molecular dynamics (MD) considers atoms as the basic unit and calculates energy using force-fields, employing a ball and spring model that can simulate physical transformations. Many computational studies have employed force-field-based MD^{98,99} to investigate the thermal response of cellulose at pyrolysis temperatures. These simulations were benchmarked against experimental density, thermal expansion coefficient, dipole moment, and dielectric constant⁹⁹. Cellulose seems to undergo a structural transformation and density reduction between 450K-500K without depolymerization^{97,100}. This reduction in density aligns with other kinetic⁷³, infrared spectroscopy¹⁰¹, and X-ray diffraction^{102,103} studies, which indicated a change in d-spacing with temperature, signifying a crystalline phase transition at 500 K. Hydrogen bonding plays a vital role in understanding these high-temperature cellulose structures, referred to as "active-cellulose" or as "melt-phase" in this thesis. The intra-chain hydrogen bond HO9...O3 breaks completely at 450 K, forming HO9...O3 and HO9...O7 inter-chain bonding. This breaking of the HO9...O3 bond is supported by observations from infrared spectroscopy¹⁰¹. In the cellulose three-dimensional hydrogen bonding network, intra-chain hydrogen bonds decrease, while inter-chain bonds increase^{98,99,104}. Consequently, more stable cellulose sheets are formed as intra-chain bonds stabilize the chain conformation, whereas inter-chain bonds stabilize the sheets¹⁰⁵. The additional intra-sheet hydrogen bonds explain the stability of cellulose at temperatures above 450 K, with only a 20% reduction in total hydrogen bonding but a significant 55% decrease in intra-chain hydrogen bonding⁹⁹. Therefore, thermal phase changes characterized with increased inter-chain hydrogen bonds and a reduction in total and intra-chain hydrogen bonds destabilize the chain conformation, allowing for torsional freedom in cellulose chain.

Further, first principles methods offer the possibility of estimating thermodynamic properties and rate constants for specific chemical reactions without assuming the overall chemical process in advance¹⁰⁶. However, the identification of these specific reactions is guided by experimental data. Once the reactions are identified, first-principles methods can be employed to evaluate the extent of reaction (using rate constants) and the primary products as well as side-products.

1.3.2 Reaction mechanisms and First principles modelling

As previously mentioned, understanding the reaction mechanisms involved in pyrolysis is crucial for the optimal design and operation of reactors³³. The use of first-principles calculations to elucidate chemical reactions and their application in kinetics has been extensively discussed in previous works^{87,107}. However, simulating cellulose microfibrils using first-principles molecular dynamics would require an impractical amount of CPU time⁴⁴. Therefore, first-principles studies have employed tractable surrogate molecules to simplify complex biopolymers. In the literature, surrogate molecules such as glucose^{108,109}, cellobiose^{110,111}, cellotriose¹¹², and cyclodextrin⁸² have been utilized as substitutes for cellulose. These studies have significantly contributed to our knowledge and understanding of the pyrolysis of these individual surrogates and their relevance to the corresponding polymer.

It is known that levoglucosan is the major pyrolysis product⁶⁸, indicating that glycosidic bond cleavage is the dominant mechanism for cellulose decomposition, as revealed by recent computational studies¹¹³. In 1921, an acid-catalyzed/dehydration pathway to levoglucosan with glucose as an intermediate was proposed¹¹⁴. To test this pathway, cellulose was pyrolyzed with glucose, and it was observed that the yield of levoglucosan was only half compared to pyrolyzing cellulose alone¹¹⁵. The authors concluded that glucose was not an intermediate since the levoglucosan yield should have increased or remained constant if it were. Subsequently, free radical mechanisms were proposed, consistent with the knowledge available at that time regarding the thermal decomposition of other stable organic compounds¹¹⁶. Building on this, a multistep mechanism was proposed¹¹⁷, but considering the reactivity of radicals, it is unlikely that all steps occur consistently without side reactions. Nevertheless, this mechanism remained the widely accepted pathway until recently when the activation barrier for this mechanism in the gas phase was calculated to be very high (97.8 kcal/mol at 500°C)¹¹⁸. Ionic mechanisms were also proposed, inspired by the influence of organic salts on cellulose pyrolysis observed through 1H-NMR studies¹¹⁹. With advancements in computational techniques, Assary and Curtis¹⁰⁹ conducted gas phase DFT calculations and proposed a two-step mechanism known as glycosylation, finding an activation energy of 48-53 kcal/mol. This value was close to the experimentally determined activation barrier at that time using DSC-TGA¹²⁰.

Hosoya et al. proposed the first ionic concerted mechanism for the decomposition of methyl β -D glucoside to levoglucosan¹²¹. However, glucose does not accurately capture the electrostatic nature of the glycosidic bond in cellulose. Therefore, this mechanism was adapted to propose a transglycosylation mechanism for cellobiose decomposition, involving simultaneous proton transfer from the methoxy group to the glycosidic oxygen and the formation of a C6-O-C1 bridge³⁴(Figure 1B). Transglycosylation has been reported to have gas phase activation energies in the range of 190-230 kJ/mol^{34,121}. Similar activation energies (201-222 kJ/mol) have been calculated for the glycosylation mechanism¹¹¹. In addition to the formation of levoglucosan through glycosidic bond cleavage, the formation of lower molecular weight products such as glycolaldehyde has also been investigated. The C-C cleavage of cellulose monomers during pyrolysis transforms two carbon fragments into glycolaldehyde⁷¹. However, glycolaldehyde primarily originates from the ring opening of cellulose. The generation mechanisms of lower molecular weight products have also been studied using DFT¹²²⁻¹²⁵, and it has been found that the pyran ring, undergoing dehydration, is more inclined to undergo the ring opening reaction¹²⁶. These two-step ring opening mechanisms involve a series of steps including dehydration and C-C cleavage to form lower oxygenates. A compilation of potential reaction pathways for cellobiose decomposition was performed, and the activation energies calculated using gas phase DFT were compared¹¹³. The lowest activation energy was calculated for transglycosylation (228 kJ/mol), followed by glycosylation (270 kJ/mol) and ring contraction (283.26 kJ/mol) in gas phase environment.

However, high speed photography has shown that cellulose pyrolysis proceeds through a "liquid intermediate" before forming volatiles at 973K¹²⁷. Seconding that, force-field based studies mentioned in section 1.3.1 that analyzed the structural orientation and the thermal response of cellulose, show that at high temperatures, cellulose exists in a "melt-phase". This melt-phase can possibly lead to different pyrolysis reaction chemistry/kinetics compared to cellulose in the gas phase or crystal structure.

1.3.3 Condensed phase effects on cellulose reaction chemistry

The observation of a liquid intermediate known as the "melt-phase," which was supported by high-speed photography and MD calculations⁹⁹, served as the

motivation for researchers to conduct an accelerated ab-initio MD (CPMD-metadynamics) study. In their investigation of cellobiose decomposition, Agarwal et al.⁵² employed multiple collective variables to conduct an unbiased analysis. They found that at 327°C, ring contraction from glucopyranose to glucofuranose is favored, while at 600°C, glycosylation becomes favored with an activation energy of 36 kcal/mol, significantly lower than the value proposed by the study¹¹¹ suggesting the mechanism. Moreover, the study⁵² did not find a low-barrier pathway for pre-LGA formation in the absence of a temperature-appropriate density.

To account for a temperature-dependent variation in reaction mechanisms and mimic the melt-phase environment, a four-molecule periodic system with plausible densities was employed. The results revealed that ring contraction from glucopyranose ring to glucofuranose ring without glycosidic bond cleavage is favored (83.7 kJ/mol) at 600K, while glycosylation (151 kJ/mol) is favored at 873K. The relatively low free energy barrier for ring contraction at low temperatures suggests that depolymerization in the melt-phase to form 'active cellulose' could involve the formation of furanic rings. This temperature-dependent shift in reaction mechanism for cellulose decomposition aligns with the observation of "active cellulose" and is supported by PHASR reactor studies¹²⁸. It should be noted that the local pyrolysis environment in the melt-phase may alter reactivity, rendering the direct relevance of these gas-phase calculations insufficient. Alternatively, investigating hydroxyl catalyzed decomposition in the melt-phase, vicinal OH groups from stacked parallel cellulose sheets were utilized to form hydrogen bonds¹²⁹. This arrangement of cellulose sheets enabled inter-sheet hydroxyl interactions that stabilized the charged transition state. Consequently, catalyzed bond activation by static hydroxyl clusters led to a reduced apparent activation barrier, and the reduction in the activation barrier was proportional to the number of hydroxyl groups participating in the reaction. This finding further supports experimental studies suggesting that a shift in phase with temperature could alter reaction energetics [124] and requires further investigation.

1.3.4 Bottom-up approach for investigating cellulose chemistry

As illustrated in the above sections, it is widely acknowledged that fundamental research plays a crucial role in gradually integrating chemical mechanisms into particle models, enabling the prediction of overall performance and facilitating the engineering

of bio-oil composition ⁴⁴. Therefore, it is essential to gain a comprehensive understanding of the intricate reaction mechanisms occurring during pyrolysis, as it serves as a foundation for advancing macro-scale comprehension, including transport phenomena, process optimization, and selective product distribution. However, the high temperatures at which pyrolysis reactions occur, rapid reaction kinetics, and the complex composition of biomass feedstocks make it extremely challenging for experimental researchers to explore pyrolysis chemistry comprehensively. Moreover, the condensed phase effects induced by thermal phase changes seems to further alter the reaction chemistry. Consequently, researchers have turned their attention to studying the chemistry of individual biomass components, while also recognizing the potential of molecular modeling as an effective tool for investigating condensed phase pyrolysis chemistry. Therefore, a bottom-up approach is adapted to develop such multiscale models encompassing molecular-level investigations of reaction mechanisms which can further be used in particle-level analysis of transport phenomena, and consideration of operating conditions at the reactor level.

In addition to high temperature condensed phase effects in pure cellulose, the intricate macro-structures formed by cellulose, lignin, and hemicellulose in lignocellulosic biomass further complicate studies aimed at understanding fundamental pyrolysis chemistry. Although there is a preliminary understanding of the pyrolysis mechanisms of individual biopolymers like cellulose, such information is not readily available for native biomass. Lignocellulosic biomass fast pyrolysis likely involves a combination of free radical, ionic, and concerted pathways for product formation ^{87,130}. The presence of hemicellulose and lignin in native biomass contributes to the formation of additional compounds such as phenols (primarily derived from lignin) in addition to levoglucosan (LGA), furans, and lower oxygenates. The pyrolysis of native biomass, such as spruce and beech wood, exhibits significant changes in product distribution compared to pure cellulose. This phenomenon is also observed in the pyrolysis of synthetic biomass (model biomass prepared by mixing different extracted biopolymers) containing mixtures of cellulose, hemicellulose, and lignin, where reaction rates slow down, and lignin hinders cellulose breakdown and volatile formation ^{131–133}. Furthermore, repolymerization reactions among lower molecular weight (LMW) compounds to form heavier compounds are promoted by the homogeneity in functional groups, mainly derived from lignin products ^{134–136}. Reducing the lignin content in the feed could

potentially decrease the formation of heavier pyrolysis products and mitigate aging effects. However, biomass pre-treatment to remove lignin and increase polysaccharide content in the feed is expensive and poses environmental challenges¹³⁷. Therefore, it is necessary to investigate the pyrolysis of native biomass in addition to the pyrolysis of individual biopolymers.

1.4 Thermal decomposition of cellulose in lignocellulosic biomass

1.4.1 Failure of additive models and interaction between biopolymers

A simple mathematical model that combines the thermal curves of individual components (lignin, cellulose, hemicellulose) to explain the thermal behavior of native lignocellulosic biomass was proposed¹³⁸. This model suggests that pyrolysis product distribution trends, activation barriers, and kinetic parameters can be predicted using additive models that disregard interactions between biopolymers. However, experimental studies^{139–141} have confirmed that cellulose, hemicellulose, and lignin exhibit catalytic and anti-catalytic effects on each other's decomposition. Recent studies have highlighted the deviation from the additive model and the inability to accurately predict yields of pyrolysis gases (CO, CO₂, CH₄, H₂, C₂H₂, C₂H₄)¹⁴². Nonetheless, there is minimal variation in reaction order between the additive model and experimental pyrolysis, indicating that the pyrolysis mechanism remains largely unchanged¹⁴³. In native biomass, the pyrolysis of cellulose occurs at higher temperatures and the rate of mass loss decreases [26]. These interactions between the biopolymers demonstrate that biomass pyrolysis behavior cannot be explained solely by the individual pyrolysis chemistry of its components^{131,144}. For instance, when spruce and beech wood (both containing approximately 50% cellulose) are pyrolyzed, they yield less than 3% levoglucosan (LGA)¹⁴⁵, whereas pure cellulose can produce a 48% yield when pyrolyzed separately¹⁸. This deviation in kinetics is also observed in the pyrolysis of synthetic biomass containing cellulose and lignin mixtures produced through different mixing methods and over a wide temperature range^{131,132}. However, this deviation between pure cellulose and native/synthetic biomass pyrolysis kinetics is only observed within a specific temperature range. Below and above the cellulose decomposition temperature, the product distribution of both synthetic and native mixtures aligns with additive model predictions, suggesting no interactions¹⁸. Furthermore, lignin exhibits a "liquid phase" above the glass transition temperature

(50-150°C), where its units are redistributed and reallocated. This overlap in the decomposition regime may facilitate CH- π interactions between cellulose and lignin, leading to the enhancement of lignin-derived products such as phenolics^{140,146}. These observations emphasize the existence of interactions between biopolymers during the pyrolytic "melt-phase," but within a narrow temperature range where cellulose and lignin decomposition overlap. Based on the yields obtained from the pyrolysis of native and synthetic samples, no significant interactions were found between xylan (hemicellulose monomer) and lignin, but substantial interactions were observed between cellulose and other components¹³¹. Pyrolysis of native samples after selectively removing one component from cornstover revealed a higher interaction between cellulose and lignin compared to cellulose and hemicellulose¹⁴⁷. Therefore, hemicellulose has been intentionally omitted from the analysis as it does not seem to exert a significant influence on cellulose decomposition.

1.4.2 Dependence on feed

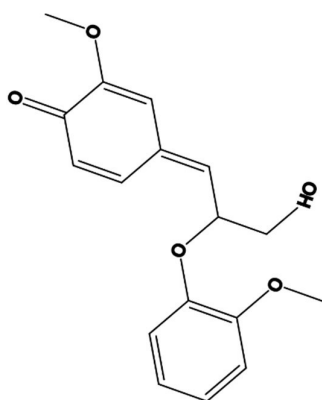


Figure 1.2 Lignin dimer - Quinone methide intermediate

The pyrolysis of herbaceous biomass, such as grass, leads to different product yields compared to woody biomass¹⁹. When herbaceous cellulose-lignin samples are pyrolyzed, there is a decrease of 10.28 wt% in LGA yield, which is compensated by increases of 11.38 wt% in C₁ to C₃ products and 1.45 wt% in furans. In contrast, the pyrolysis of woody biomass shows minimal deviation in product distribution compared to pure cellulose, despite its higher lignin content. While interactions between cellulose and lignin have little effect on char yields in synthetic samples, they promote char formation in native biomass samples^{148,149}. This decrease in LGA yield is also observed in synthetic mixtures of cellulose with hemicellulose, where the presence of

lignin inhibits LGA production by favoring C-C bond cleavage over C-O cleavage. However, the change in product yields, particularly the inhibition of LGA and promotion of furans and C1-C3 compounds, is more pronounced in native samples, especially herbaceous cellulose-lignin samples ^{150,151}.

In lignocellulosic biomass, lignin and hemicellulose form "lignin carbohydrate complexes (LCCs)" ¹⁵². These complexes can involve two types of linkages between lignin and polysaccharides: 1) esterification of phenolic acids, which may participate in lignin polymerization ¹²¹, and 2) α -benzyl ester/ether linkages, where the carboxyl or hydroxyl group in polysaccharides reacts with an intermediate quinone methide (c.f. Figure 1.2) to form these linkages ¹⁵³. These linkages can also occur between lignin and the peripheral cellulose chains of the cellulose microfibrils. In softwood, approximately 50% of lignin is bound to cellulose, while in hardwood, this proportion is around 17% ¹⁵⁴. The variation in pyrolysis products between herbaceous and woody biomass can be attributed to the higher presence of lignin carbohydrate complex (LCC) linkages in herbaceous biomass, which influences product yields, including the reduction in LGA observed experimentally. Understanding the influence of high-temperature biomass melt-phase environments on reaction chemistry requires explicit modeling of molecules in the condensed phase to account for entropic contributions. Accelerated/biased ab-initio molecular dynamics (AIMD) methods can be employed to calculate the free energy barrier by explicitly considering interactions with the local reaction environment ^{113,155}. However, performing accelerated AIMD simulations for multi-molecular LCC systems is computationally intensive ¹³⁷.

1.4.3 Intricate chemistry and kinetics in native lignocellulosic biomass

Verification of the speculated promotion of C-C over C-O cleavage and understanding pyrolytic interactions between biopolymers are best accomplished through computational tools. However, to the best of our knowledge, there have been no first principles studies investigating the competing reaction pathways of cellulose decomposition in the finite temperature biomass melt-phase. This is primarily due to the high computational cost associated with performing ab-initio calculations for condensed phase systems with explicit intramolecular interactions. Computational studies on lignocellulosic biomass in the literature are available only after the 1990s ¹⁵⁶. Some studies ¹⁵⁷ have explored the interaction between lignin and cellulose using

force-field calculations to understand the assembly in wood. These studies found that lignin model molecules can adsorb onto cellulose microfibrils, limiting their mobility. In a complementary study, the importance of hydrogen bonding in lignin-cellulose association was highlighted, with the phenol rings in lignin preferentially oriented parallel to cellulose fibers. More recently, Zhang et al.¹⁵⁸ developed a first principles model of woody biomass, providing a comprehensive list of hydrogen bonds between H-C and covalent bonds between H-L, along with gas phase DFT optimized bond lengths and angles. Although these studies do not directly investigate pyrolysis, they have laid the foundation for molecular modeling of lignocellulosic biomass. However, the applicability of these structures under pyrolysis conditions needs to be verified.

1.5 Major factors influencing cellulose kinetics and chemistry in biomass

1.5.1 Thermal changes in the reaction environment

Considering the importance of understanding the kinetic and chemical shifts in cellulose decomposition, as observed in experimental and computational studies, gaining a molecular-level comprehension of this phenomenon becomes crucial for the development of accurate kinetic models. Previous investigations have indicated that cellulose activation and decomposition predominantly occur through glycosidic bond breakage, resulting in the formation of short-chain anhydro-oligomers with levoglucosan-end¹²⁷. In this context, the primary decomposition of cellulose via glycosidic bond cleavage analyzed herein results in the intermediate liquid, melt-phase formation. While several studies in literature indirectly address the observed thermal shift in cellulose reaction chemistry and kinetics, an in-depth explanation of this phenomenon remains elusive. Seshadri et al.¹⁵⁹ demonstrated that the placement of water molecules to establish hydrogen bonds with glucose's hydroxyl (OH) groups can reduce the enthalpy of activation. Co-pyrolysis of microcrystalline cellulose with fructose indicates a correlation between LGA yield and fructose composition¹⁶⁰. Since fructose does not pyrolyze to form LGA, this suggests that the hydroxyl environment in the reaction mixture promotes LGA formation. Therefore, a review through the lens of molecular modelling is essential to gain mechanistic insights into cellulose decomposition. Mimicking the melt-phase environment by introducing hydroxyl groups from water or small alcoholic products has been shown to catalyze the formation of specific compounds, thereby lowering the enthalpic barrier. These phase-related

modifications exert a noticeable influence on reaction kinetics, as evidenced by millisecond-scale experiments^{83,129}. Based on these observations, it has been hypothesized that cellulose undergoes hydroxyl-catalyzed glycosidic bond cleavage within the melt-phase at lower temperatures (<700K), while direct thermal cleavage becomes prominent at higher temperatures¹²⁹.

This hypothesis finds support in the calculated low activation barrier (23.2±1.9 kcal/mol) below the "reactive melting point" of 740K, when fitting millisecond-scale α -cellodextrin conversion data from PHASR experiments using a first-order kinetics model⁸⁵. Krumm et al. conducted pyrolysis experiments on different chain length cellodextrins using a PHASR reactor and observed that at 823K, the product formation rate per unit mass remained independent of the chain length, indicating an intrachain scission mechanism⁸³. Furthermore, high-temperature conversion of cellulose exhibited a high activation barrier (53.7±1.1 kcal/mol) with a substantial pre-exponential factor (2.4×10^{-16} 1/s) determined from PHASR experiments⁸⁵. The high pre-exponential factor is attributed to the random thermal cleavage of cellulose, where hydroxyl-catalyzed activation is limited by the dynamic nature of the high-temperature cellulose melt-phase, as most glycosidic oxygens are unbound to cellulose hydroxyl groups (active sites)¹²⁹. Notably, DFT studies^{34,129} have solely reported enthalpic barriers ranging from 189.54 to 247 kJ/mol for glycosidic cleavage through non-catalyzed transglycosylation in cellulose derivatives. However clearly, temperature induced shifts in the melt-phase (as detailed in section 1.3.1) seem to significantly influence intrinsic cellulose decomposition energetics leading to a kinetic regime change.

1.5.2 Physical interaction with other biopolymers

In the natural composition of biomass, cellulose is intricately intertwined with lignin and hemicellulose, forming a complex microscopic architecture. While studying isolated biopolymer molecules has provided insights into their individual pyrolysis chemistry, it falls short in predicting or explaining the pyrolysis chemistry of native biomass. Therefore, it is crucial to consider the intricate interactions between biomass components and their impact on cellulose decomposition. The presence of lignin has been associated with micro-explosions and thermal ejection of cellulose intermediates, which enhances the deoxygenation of heavy compounds and impedes

char formation¹⁶¹. A reduced char yield in cellulose with a high lignin composition suggests a hindrance in dehydration reactions. Furthermore, the pyrolysis of maple wood demonstrates an enhanced development of porous structures in the resulting char, indicating the stabilization of lignin intermediates in the melt-phase³⁴. Under pyrolysis conditions, hydrogen-rich cellulose products must escape through the interface between cellulose bundles and lignin, interacting with and stabilizing lignin reactive intermediates. Studies have reported the stabilization of lignin intermediates and the inhibition of oligomerization through in-situ hydrogen sources, such as the formic acid functional group^{162,163}. Consequently, the thermal interaction between high lignin composition and cellulose promotes the formation of levoglucosan (LGA) and weakens competing pathways like dehydration, which contribute to the formation of char precursors^{34,164}. The inhibition of dehydration reactions and the promotion of deoxygenation in heavier compounds, facilitated by the ejection of cellulose intermediates, highlight the significance of non-bonded interactions with other biopolymers.

1.5.3 Covalent bonding in LCC linkages

Despite the importance of cross-linked lignin-carbohydrate complexes (LCCs) in cellulose decomposition, limited research has focused on their role in pyrolysis chemistry. A recent study¹⁶⁵ investigated the pyrolysis products of chemically modified native lignocellulose, where hemicellulose was selectively removed, and compared them to a synthetic cellulose-lignin mixture. The presence of cross-linked lignin was found to have a significant impact on the production of small molecules and furan derivatives, increasing their yield by 97%, while reducing the formation of anhydrosugars by up to 47%. Moreover, cross-linked lignin exhibited a more pronounced effect on lignocellulose pyrolysis by promoting glycosyl ring scission and lignin fragmentation compared to free lignin. However, the specific chemistry and energetics underlying these ring scissions in the LCC molecules remain unclear. Studying the pyrolysis chemistry of cross-linked LCCs is challenging due to the complexity involved in conducting first principles calculations for multimolecular systems and the experimental requirements for isolating LCCs from native biomass through complex pre-treatments. Currently, the only available millisecond-scale data

pertains to woody biomass, which is suggested to have a significantly lower number of LCC linkages compared to herbaceous biomass.

The initial rate of product formation and the Arrhenius plots for the formation of three different cellulose-derived products from the pyrolysis of loblolly wood have been reported ¹⁶⁶. When comparing the millisecond-scale kinetics measured for pure cellulose pyrolysis under similar conditions, a similar increase in rates with temperature is observed. The calculated apparent barriers, assuming first-order kinetics, for pure cellulose decomposition (23.2 ± 1.9 kcal/mol), fall within the same range as the barriers (16.8 – 38.1 kcal/mol) calculated for the formation of the three cellulose-derived products from loblolly wood ¹⁶⁶. It should be noted that these barriers represent the combined effect of a series of reactions during biomass pyrolysis and cannot be directly used for mechanistic interpretations. However, the lack of significant changes in overall kinetics between pure cellulose and woody biomass is expected, as it is the presence of LCC linkages rather than lignin alone that alters product yields ¹⁶⁷. Previous research employing carboxymethylation and subsequent ¹H NMR spectroscopic analysis to identify ether linkages between lignin and cellulose has shown that LCCs are more prevalent in softwood compared to hardwood ¹⁶⁸. However, both pine (softwood) and red oak (hardwood) exhibit minimal deviation in levoglucosan (LGA) yield compared to clean cellulose. In contrast, herbaceous biomass displays significant deviations in LGA yields. This highlights the competition between glycosidic C-O bond cleavage (forming LGA) and C-C bond cleavage (forming furans and C1–C3 products) during cellulose pyrolysis ^{42,68,74}. Furthermore, an LCC bond at the C6 position would hinder the chair-to-boat conformational change, bridge formation, and subsequently affect LGA production. Recent first principles calculations ¹⁶² have demonstrated that these benzyl ether LCC linkages in cellulose residues are thermodynamically favored at the C2 and C3 positions. Therefore, the covalent bonding between cellulose and lignin significantly alters the distribution of pyrolysis products.

1.6 Motivation of the thesis

Pure cellulose samples melt to form a liquid intermediate called ‘active-cellulose’ or ‘melt-phase’ that results from the primary decomposition. Further reactions such as volatile formation and repolymerization undergoes in this *melt-phase* environment

resulting in complex reaction pathways. Due to experimental limitations with the ability to only measure kinetics from weight loss or gas evolution, there are difficulties in identifying the reaction pathways and the intrinsic kinetics. This drawback even with measuring millisecond scale kinetics has been highlighted and elaborated in Section 1.2.2. Computational methods such as molecular modelling and first principles calculations have been carried out to complement the experiments and provide fundamental knowledge on reaction mechanisms and energetics. Still, modelling the finite temperature melt-phase and accounting for explicit interactions with other molecules in the reaction environment has been lacking. Adding further to the complexity, the presence of lignin and hemicellulose seem to alter both the kinetics and the chemistry of cellulose decomposition. Even non-bonded interaction in physically mixed synthetic samples have been shown to alter product yields at certain temperature ranges. Moreover, this influence of other biopolymers on cellulose breakdown is further exacerbated in native biomass as elaborated in Section 1.4. Covalent bonding between the lignin and carbohydrates, known as Lignin carbohydrate complexes, seem to be a major contributing factor. In native biomass, this leads to suppressed yields of anhydro sugars like LGA which is compensated by an increase in C₁ – C₃ products. Despite the clear influence of other biopolymers on cellulose evident from the altered product yields, no reports have focused on developing a mechanistic understanding of cellulose breakdown in biomass. This is mainly because of computational limitations to conduct first principles calculations for large complexes in biomass. Ultimately, the main motivations for this project are the lack of mechanistic understanding on intrinsic cellulose chemistry and kinetics after carefully accounting for 1. The finite temperature melt-phase before volatilization and 2. non-bonded and bonded interactions with other biopolymers in native biomass. Such knowledge of reaction pathways and corresponding energetics will enable better multi-scale modelling and optimization to improve yields and selectivity of desired pyrolysis products.

1.7 Objectives of the thesis

The overall objectives of the thesis are to reveal how changes in the pyrolytic condensed phase induced by temperature or non-bonded interactions with lignin affect cellulose reaction kinetics. In addition to this, covalent bonding in LCCs and their

impact of cellulose chemistry and kinetics are to be identified. The first objective investigating the impact of thermal changes in the condensed phase on cellulose breakdown has been addressed in chapters 2 and 3. Chapter 3 also addresses the impact of the non-bonded interactions between lignin and cellulose inducing changes in the melt-phase configuration on cellulose reaction energetics. Here, it is revealed that the temperature and the interactions with other biopolymers can also create an indirect effect on cellulose reaction chemistry by inducing changes in the finite temperature melt-phase configuration. Chapter 5 deals with the direct influence of covalent bonding in LCCs on cellulose kinetics. Furthermore, thin-film pyrolysis experiments are conducted and compared with first principles calculations to draw qualitative information on the reaction chemistry. The specific objectives addressed in each chapter are detailed below.

1.7.1 Key objectives of chapter 2

- Compute the finite temperature condensed phase energetics for potential cellulose decomposition mechanisms in finite temperature environment with explicit molecules. This allows the investigation of the role of the melt-phase in cellulose exhibiting temperature variant reaction regimes during pyrolysis.
- Key indicators of shift in melt-phase configuration such as hydroxymethyl groups orientations in cellulose residues and hydrogen bond distributions are calculated and analyzed. This offers insights on the significance of the 'reactive melting temperature' (740 K) or the transition temperature at which there is a shift in the kinetics.
- The entropic contributions to the barrier in all reaction regimes. Addressing these queries requires developing a molecular picture of cellulose pyrolysis. Such fundamental knowledge of cellulose activation in the melt-phase will enable accurate calculation of the energetics of competing reactions.

1.7.2 Key objectives of chapter 3

- Compute the finite temperature condensed phase energetics for cellulose decomposition mechanisms under potential lignin reaction environments. These calculations reveal if non-bonded interactions with lignin in the condensed phase influence cellulose decomposition energetics in native biomass *melt-phases*.
- Is furan (C-C cleavage) or LGA (C-O cleavage) formation in cellulose pyrolysis promoted due to the non-bonded, condensed phase interactions with lignin?
- Can the non-bonded interactions with LCC or high lignin content explain the variation in product distribution between native and synthetic samples?

1.7.3 Key objectives of chapter 4

- Utilize ab-initio techniques to model different LCC conformations with varying binding sites – C2, C3, and C6 and calculate their respective electronic energy barriers for cellulose cleavage using Density Functional Theory (DFT). Investigate the influence of potential covalent bond formation sites in the LCC on cellulose decomposition.
- Calculate and compare the energetics of cellulose decompositions mechanisms in cross-linked cellulose found in LCCs and pure cellulose to identify changes in the kinetics and reveal the role of covalent bonding between lignin and carbohydrates in cellulose decomposition.
- Compare reaction energetics and thin-film pyrolysis product yields between cross-linked and pure cellulose samples, to reveal the similarity or dissimilarity in the decomposition chemistry.

1.8 Organization of the thesis

This thesis comprises seven chapters, each contributing to a comprehensive understanding of biomass conversion to energy and the kinetics and chemistry of cellulose pyrolysis. The computational methodology employed in this study is described, providing insights into the novel techniques and tools utilized. Following this, the results section provides a comprehensive analysis of the data, highlighting the key findings and their implications within the context of the research objectives. Finally, each chapter concludes with the main outcomes and contributions of the respective chapters, thereby facilitating an easy grasp of the research progress and overall significance of the study. The organization of the chapters is as follows - Chapter 1 serves as an introduction, providing a broad perspective on biomass conversion, cellulose pyrolysis kinetics and chemistry, and the various molecular-level factors influencing cellulose decomposition. It includes an extensive review of relevant literature to establish the state of the art, as well as specific details regarding each research performed. Chapter 2 delves into the influence of thermal shifts in the finite temperature condensed phase on the primary decomposition of cellulose. The chapter demonstrates how shifts in kinetic regimes align with changes in key indicators, such as alterations in the hydrogen bonding network and the orientation of hydroxymethyl groups in cellulose residues. Chapter 3 focuses on similar shifts in the pyrolytic melt-phase, but with a particular emphasis on the presence of lignin and lignin-carbohydrate complexes (LCCs) alongside cellulose, as found in native biomass. The chapter develops a cellulose decomposition model that facilitates qualitative comparisons between millisecond-scale kinetic experiments and first principles calculations. Chapter 4 investigates the direct impact of covalent bonding with lignin in LCCs on cellulose decomposition. Remarkably, conventional cellulose cleavage mechanisms display approximately double the energy barriers required to cleave cross-linked cellulose within LCCs. In Chapter 5, the cumulative findings and insights derived from the preceding chapters are compiled in a comprehensive conclusion. Additionally, this chapter offers perspectives and potential future research directions based on the obtained results. Chapter 6 serves as a valuable resource for readers, containing supplementary data that support the findings presented throughout the thesis. These appendices correspond to specific chapters. By systematically addressing key aspects

of biomass conversion and cellulose pyrolysis, this thesis presents a thorough investigation into the subject matter.

1.8.1 Chapter 2: Pyrolytic activation of cellulose: energetics and condensed phase effects

The advancement of the pyrolysis process, aimed at enhancing both the quality and yield of bio-oil, encounters significant obstacles due to the limited understanding of the underlying chemistry and transport phenomena. Consequently, this study focuses on investigating the decomposition of cellobiose, a model compound representative of cellulose, during the pyrolysis process. To gain insights into the energetics of glycosidic bond cleavage in cellulose, we employ two innovative computational strategies, considering the influence of the condensed phase and finite temperature effects. Our findings reveal the existence of two distinct reaction regimes, which align well with the observed kinetics in millisecond-scale experiments. Remarkably, these regimes exhibit temperature-dependent variations in decomposition energetics, as demonstrated through both gas and condensed phase simulations, underscoring the substantial impact of entropic contributions on the primary reactions of cellulose. Furthermore, we observe that the disparity in finite temperature enthalpic barriers between the two regimes is magnified in the presence of a condensed phase environment. Notably, the outcomes of this research suggest that the relative destabilization of reactant cellulose, rather than the stabilization of the transition state, plays a crucial role in lowering the reaction barrier with increasing temperature. This insight of reactant destabilization, coupled with the primary influence of entropic contributions in regime changes during decomposition, offers a fresh perspective on the intricate chemistry of cellulose in the condensed phase. By shedding light on the intricate mechanisms underlying cellulose pyrolysis and highlighting the pivotal role of entropic effects, this study paves the way for novel advancements in cellulose chemistry, enabling further exploration of the potential of native biomass as renewable energy resources.

1.8.2 Chapter 3: Does the presence of lignin affect the pyrolytic decomposition of cellulose? A condensed phase computational investigation

This study focuses on simulating key mechanisms involved in cellulose activation and calculating the associated reaction energetics within the condensed phase in native biomass pyrolysis. To model the presence of lignin in the pyrolytic melt, we have employed two condensed phase models: 1. A melt-phase model with lignin-carbohydrate complex (LCC) linkages, and 2. A lignin-rich melt-phase model without LCC bonding. Comparing the results with gas phase calculations, we have observed a substantial reduction of over 100 kJ/mol in the free energy barriers for cellobiose activation through transglycosylation in the LCC melt-phase. Notably, the activation of cellobiose in the LCC melt phase at temperatures below 800 K exhibited greater kinetic feasibility compared to the pure cellobiose condensed phase. Conversely, the presence of lignin in the melt-phase without LCC bonding had minimal impact on cellulose activation, as the free energy barriers were comparable to those observed in the gas phase. Our findings indicate that the breakdown of hydrogen bonds and changes in the orientation of the hydroxymethyl group in cellobiose, induced by temperature variations and the composition of the condensed phase, directly correlate with the reaction energetics, except for the ring contraction mechanism observed in the melt-phase with LCC linkages. Thus, the presence of lignin exhibits contrasting effects on cellulose activation. In the covalently bonded LCC melt-phase, it reduces the activation free energy barrier compared to the pure cellobiose condensed phase. However, in the lignin-rich melt-phase without LCC linkages, the free energy barriers are relatively higher. By unraveling the intricate relationship between lignin and cellulose activation, this work provides valuable insights into the fundamental mechanisms governing biomass pyrolysis chemistry.

1.8.3 Chapter 4: Impact of Lignin-carbohydrate complex (LCC) linkages on cellulose pyrolysis chemistry

The intricate understanding of the role played by cross-linked cellulose and lignin within lignin-carbohydrate complexes (LCC) and its impact on the kinetics and chemistry of cellulose decomposition poses significant challenges due to the complex nature of biomass. To address this, this work combines first-principles molecular simulations and thin-film experiments to investigate key mechanisms involved in the

formation of major bio-oil components, namely Levoglucosan, 5-hydroxymethylfurfural, and glycolaldehyde. These mechanisms include transglycosylation, ring contraction, and ring opening. Through the utilization of ab initio molecular dynamics and metadynamics, LCC molecules containing β -O-4 benzyl ether linkages at the C2, C3, and C6 positions of cellobiose are accurately modeled. Density functional theory (DFT) calculations, based on first principles, are employed to evaluate the reaction energetics associated with cellulose activation through these mechanisms. By comparing activation barriers, reaction energies, and frontier molecular orbital interactions between LCC and pure cellobiose, valuable insights into the influence of LCC linkages are obtained. In addition to computational investigations, experimental product yields from pyrolysis of native herbaceous biomass are measured and compared to those from pure cellulose pyrolysis. The results demonstrate that cross-linked cellobiose within LCC exhibits higher activation barriers (twice as high) and reaction energies (three to four times higher) compared to pure cellobiose, indicating altered kinetics and thermodynamics during cellulose decomposition. Furthermore, the differences between LCC conformers are found to be minimal, suggesting that factors other than C6 position blocking contribute to the product distribution. The analysis of HOMO-LUMO interactions reveals a spatial separation of reaction centers within LCC, indicating the favorability of inter-moiety mechanisms over intra-moiety mechanisms. This observation is supported by qualitative comparisons between computational and experimental yields, which suggest potential differences in kinetics and chemistry induced by LCC. Overall, this study highlights the novel role of covalent bonding between lignin and carbohydrates within LCC in influencing the kinetics and chemistry of cellulose decomposition and the formation of major products. By unraveling these intricate mechanisms, our findings contribute to a deeper understanding of biomass conversion processes and offer potential avenues for improving bio-oil production through tailored lignin-carbohydrate interactions.

1.9 Overview of the thesis

This research comprehensively examines the intricate interplay of condensed phase effects, physical interactions, and covalent bonding with lignin concerning cellulose

reaction chemistry. Figure 1.3 illustrates the key knowledge gaps identified in the existing literature, which our study aims to address.

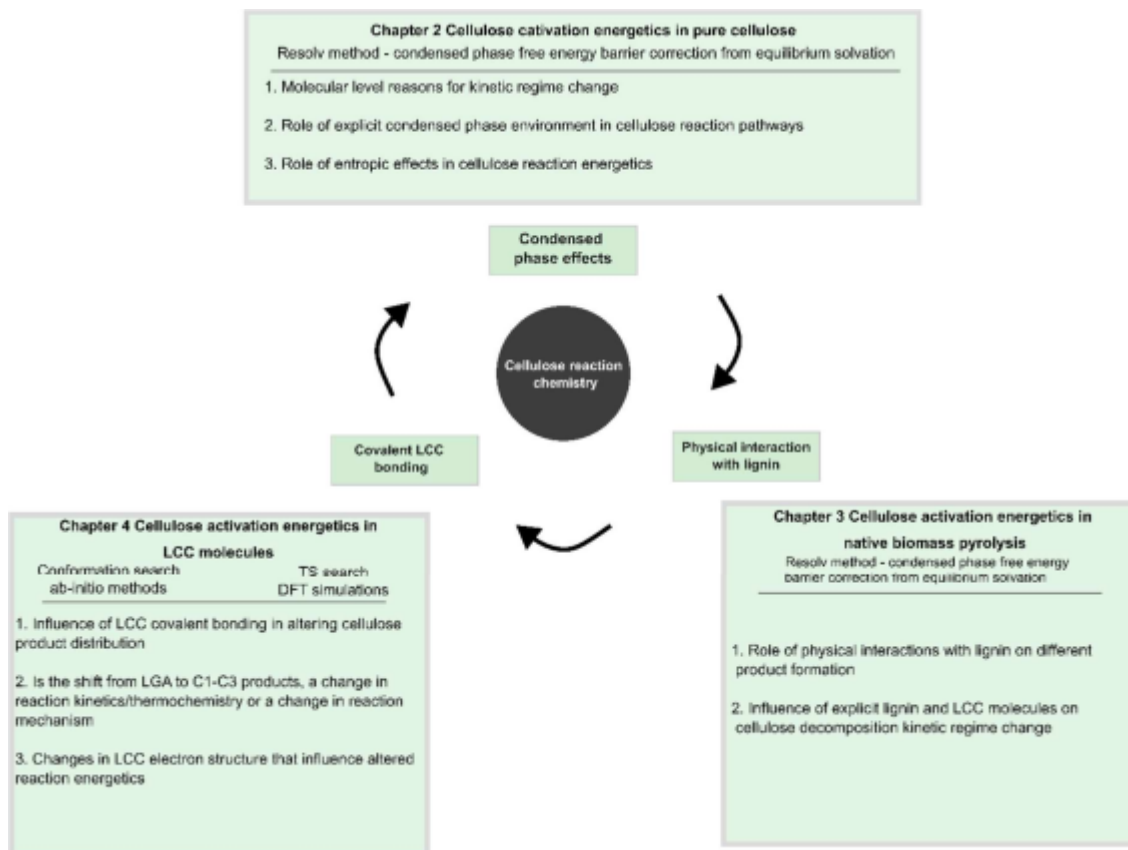


Figure 1.3 Knowledge gaps in cellulose chemistry and overview of the thesis

Our primary approach involves employing first principles calculations to gain insights into how temperature influences the interactions between cellulose and its environment, particularly with lignin. We utilize computational strategies to capture finite-temperature condensed phase effects and elucidate the physical and chemical interactions that impact cellulose chemistry. These first principles techniques are instrumental in providing explanations for previously unexplained experimental observations, notably:

1. Thermal Regime-Change in Cellulose Kinetics: We investigate how finite temperature condensed phase effects alters cellulose kinetics.
2. Change in Product Distribution in Native Biomass Compared to Pure Cellulose: We explore variations in product distribution, specifically the reduction in LGA

compensated by an increase in C1-C3 products when compared to pure cellulose.

1.9.1 Computational methodology

1.9.1.1 Molecular Dynamics Simulations

Molecular dynamics (MD) simulations were performed using GROMACS. Simulations were performed using the OPLS/AA force-field parameters that were chosen that has been benchmarked in published literature for carbohydrate molecules. Each system was simulated for 8 ns in an NVT ensemble with an integration time step of 0.001 ps. This was preceded by a 1 ns of NPT simulation to get the correct density. In all the simulation temperature control was maintained by using the Nosé–Hoover thermostat. No constraints on bonds and angles were applied. Periodic boundary conditions were applied in all directions.

1.9.1.2 Gas phase Transition State (TS) calculations

Gas phase barriers are calculated using an isolated cellobiose molecule. All-electron Density Functional Theory (DFT) calculations were conducted using the Gaussian 09 code. The calculations were carried out employing the hybrid functional M06-2X76 in conjunction with the 6-31+G(2d,p) basis set, a recommended choice for carbohydrate chemistry. Both geometry optimization and Transition State (TS) search calculations were performed without any constraints. The Berny algorithm was employed to determine the TS. Subsequently, frequency calculations were executed to differentiate between saddle points and local minima. To verify the correct positioning of reactants and products on the potential energy surface, Intrinsic Reaction Coordinates (IRCs) were followed in both directions.

1.9.1.3 Condensed phase Transition State calculations

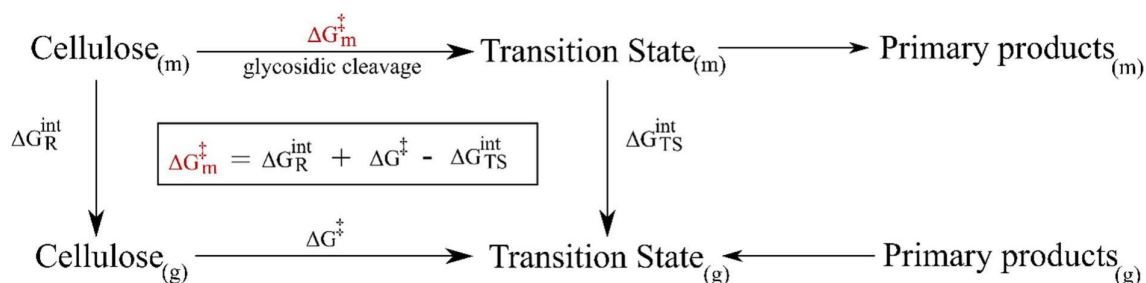
Condensed phase systems are equilibrated to melt-phase configurations using MD simulations. A low cutoff for Lennard-Jones and Coulombic potentials (0.5 nm) is employed to match experimental properties like density and dielectric constant. These configurations serve as reactants for transition state searches, specifically for cellulose decomposition via glycosidic bond cleavage in cellobiose. Transition states are found using Density Functional Theory (DFT) with the Perdew–Burke–Ernzerhof (PBE)

functional, the projector-augmented wave (PAW) pseudopotential, and a 450-eV cutoff energy. Reaction intermediates are optimized, and vibrational frequencies analyzed to confirm transition states. The resulting highest energy images provide enthalpic barriers. However, the method does not include finite temperature entropic contributions or melt-phase dynamics along the reaction coordinate.

1.9.1.4 Thermodynamic Integration Method

The thermodynamic integration (TI) method implementation in GROMACS 2018.7 software is used to calculate interaction free energies. Gas phase reactant and transition state (TS) coordinates serve as the initial configurations. Langevin dynamics and OPLS/AA force-field parameters are utilized. The system configurations are optimized and equilibrated. Pressure equilibration is performed under NPT conditions at 1 atm for 2 ns, establishing the appropriate system volume/phase. Subsequently, TI calculations are conducted under NVT conditions for 8 ns at the relevant temperatures, with 30 λ -windows optimized for intermediate states. Potential derivatives obtained from MD simulations for each λ -window are integrated to determine ΔG^{int} . Combining gas phase calculations and thermodynamic integration results, the free energy barrier for cellulose decomposition in the melt-phase (ΔG_m^\ddagger) is estimated as illustrated in Scheme 1.1.

Scheme 1.1 Schematic showing the calculation of condensed phase corrections to gas phase free energy barriers.



1.9.1.5 Ab-initio Conformation Search

In this approach, both electron density and nuclei are propagated classically. However, simulations are limited to a few hundred picoseconds due to time-step constraints. Since molecular reactions operate on longer timescales, more effective techniques are required. Bias potential methods are employed to guide the system away from

local minima by introducing potentials to fill the Potential Energy Surface (PES), thereby accelerating simulations. Metadynamics combines dynamic and bias potential methods, enabling CPMD-metadynamics simulations to study reaction mechanisms and explore free energy landscapes. All CPMD and metadynamics calculations in this study utilized CPMD code version 4.3.0 with a plane-wave-pseudopotential implementation of Kohn-Sham Density Functional Theory (DFT). We employed the Martins-Trouiller (MT) pseudopotential, coupled with the revised Perdew-Burke-Ernzerhof (revPBE) functional within the generalized gradient approximation (GGA) for CPMD calculations. The plane-wave energy cutoff was set at 70 Rydberg, and a single k-point (Γ -point) was used for Brillouin zone integration in reciprocal space. To ensure that the systems remained on the Born-Oppenheimer surface during molecular dynamics simulations, we monitored energies, including the fictitious electronic kinetic energy. Two torsion angles served as collective variables to enhance CPMD sampling, exploring conformations with significant energy barriers via the metadynamics technique. Low-energy conformers were extracted from the constructed free energy surfaces. Subsequently, all structures corresponding to minima were optimized using all-electron DFT calculations.

1.9.1.6 Post processing

Hydrogen bonding

Changes in the hydrogen bonding and hydroxymethyl group conformations are calculated from the MD trajectories. Number of hydrogen bond (donor-acceptor distances $<4.5 \text{ \AA}$ and \hat{H} angle $>150^\circ$) and bond distance distributions were calculated using in-built GROMACS commands. Dihedral angles are calculated for O₅-C₅-C₆-O₆ (hydroxymethyl group) and -60° , 60° and 180° corresponds to the tg, gt and gg conformations, respectively.

Frontier Molecular Orbitals (HOMO-LUMO)

Frontier Molecular Orbital Theory defines the Highest Occupied Molecular Orbital (HOMO) and the Lowest Unoccupied Molecular Orbital (LUMO). HOMO reflects electron acceptance ability, while LUMO indicates electron provision capacity. The HOMO and the LUMO orbitals are visualized for molecule conformers from DFT calculations using the Avogadro software. These frontier orbitals play a critical role in

chemical reactions, with electron transfer primarily occurring here. The HOMO-LUMO gap, representing the energy difference between reactants' HOMO and LUMO, gauges interaction strength. Smaller gaps imply stronger bonding and greater reactivity. The Frontier Molecular Orbital approach, encompassing HOMO and LUMO, is widely used in quantum calculations to study interaction tendencies and potential sites of electron transfer.

Chapter 2 Pyrolytic activation of cellulose: Energetics and condensed phase effects

Reprinted with permission from RSC React. Chem. Eng., 2022,7, 1136-1149 © 2023 Royal Society of Chemistry.

2.1 Introduction

Second generation lignocellulosic biomass is the largest renewable natural resource to produce carbon-based liquid fuels¹⁶⁰, circumventing the food-to-fuel pipeline^{8,169}. It offers a route for renewable generation of fuels and commodity chemicals¹⁷⁰⁻¹⁷⁵ by pyrolyzing non-food parts to renewable crude oil (bio-oil)¹²⁷. To produce bio-based transportation fuel, fast pyrolysis is a promising⁵³ technology in which biopolymers are cracked thermally, in the absence of oxygen⁴⁷. Pyrolysis is also one of the very few processes that are amenable for decentralized processing of biomass². Though, the liquid product of pyrolysis, bio-oil, can be transported economically, its highly oxygenated nature requires further treatment^{176,177}. Production of high quality and quantity of bio-oil by reducing its oxygen content would enable downstream integration within existing petroleum infrastructure which is key to the commercialization of pyrolysis technology⁴⁷. The yield and quality of bio-oil rely on the interplay between reactions and transport in the pyrolysis reactor and hence its optimization would require a detailed mechanistic understanding of pyrolysis chemistry¹⁷⁸⁻¹⁸⁰. Consequently, developing a fundamental understanding of lignocellulosic biomass decomposition chemistry during pyrolysis in the condensed phase was identified as the primary challenge for biomass pyrolysis¹⁷⁸.

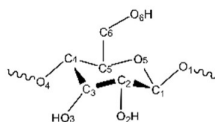
Since, lignocellulose majorly consists of cellulose (40-50%)⁶⁴ which is the most abundant biopolymer on earth⁹⁰, understanding cellulose chemistry is crucial in developing fundamental insights into biomass pyrolysis chemistry. Early experimental studies⁷⁶⁻⁷⁸ could only measure global product distributions of cellulose pyrolysis using thermogravimetric analysis (TGA). These global conversion data have been used to develop numerous lumped kinetic models⁸¹ with activation energies ranging from 50 to 285 kJ/mol, suggesting that they represent the combined effect of intrinsic kinetics, transport and phase transition. At low temperatures (<568K), well accepted models such as Broido-Shafizadeh⁷⁸ and Diebold⁷⁶ report an initiation period for the activation of cellulose before its decomposition through first order competing reactions

for the formation of char and volatiles. “Active cellulose” was observed using ^{13}C -CPMAS NMR as an amorphous cellulosic intermediate with a low degree of polymerization (DP) of 200-400⁴² during the pyrolysis of microcrystalline cellulose at 573K¹⁸¹. Diffraction studies^{102,103,182–184}, 2D moving window infrared spectroscopy studies^{185,186} and other experimental studies^{187–189} have shown an anisotropic expansion, abrupt change in hydrogen (H) bonding and other similar unassigned structural changes between 450K–550K. This amorphous, low density and low DP cellulosic environment will be referred to as “*melt-phase*” in this paper. Such transitions in the phase that change hydrogen bonding could possibly alter reaction chemistry of cellulose during pyrolytic decomposition¹⁹⁰. In contrast, at high temperatures, other kinetic models^{60,75,77,191,192} have proposed direct first order decomposition to volatiles without the initial activation step. However, either type show large variations in their kinetic parameters¹⁹³ because of the inability to limit transport effects and secondary reactions. The experimental limitations render these models irrelevant for developing mechanistic understanding of cellulose pyrolysis chemistry.

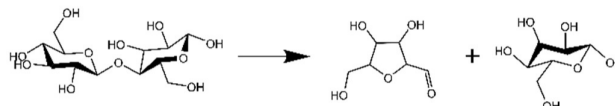
More recently, Mettler et al.⁸² developed thin-film sample techniques (size $\approx 1\mu\text{m}$) to study pyrolysis. Thin films enable preparation of appropriate sample dimension ($\leq 20\mu\text{m}$ at 773K) to conduct mechanistic pyrolysis experiments in an isothermal, kinetically limited regime. However, even with thin-films, only cumulative product yields can be analyzed because of the temporal mismatch between reaction chemistry and chromatography analysis equipment¹⁹⁴. Intrinsic kinetics can only be studied if the time evolution of pyrolysis products can be measured. Recently, a novel microreactor developed for Pulse-Heated Analysis of Solid Reactions (PHASR) with the ability to control reaction progression has enabled intermediate product composition analysis to measure milliseconds scale⁸⁴ reaction kinetics. Fragmentation kinetics of α -cyclodextrin and volatile furan product formation were measured using PHASR reactor¹⁹⁴. The measured transition between the two kinetic regimes at 740K was suggested to be a change from end-chain scission to mid-chain scission mechanism. First order kinetics were assumed to calculate the barriers and rate coefficients from the kinetic data¹²⁸. The resulting enthalpic barriers were $23.2\pm 1.9\text{ kcal/mol}$ ($97.07\pm 7.95\text{ kJ/mol}$) and $53.7\pm 1.1\text{ kcal/mol}$ ($224.68\pm 4.6\text{ kJ/mol}$) at the low and high temperature regimes, respectively. For the first time millisecond scale intrinsic kinetics were measured and was demonstrated that cellulose reactivity is altered by the thermal phase changes.

Moreover, primary decomposition of cellulose initiates via glycosidic bond cleavage making up the phase for secondary reactions.

a. Atomic nomenclature



b. Concerted Ring contraction



c. Concerted Transglycosylation

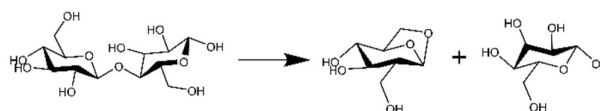


Figure 2.1 (a) Atomic nomenclature used in the paper (b) Ring contraction mechanism to form furanic compounds (c) Transglycosylation mechanism to form LGA.

This thermal phase change leads to a short-lived intermediate liquid cellulose⁵⁹, the formation of which is understood by studying the structure and hydrogen bonding of native cellulose. In biomass, cellulosic chains are connected by inter-chain hydrogen bonds, making polymeric sheets which are stacked on the top of each other¹⁹⁵. Synchrotron X-ray and Neutron fiber diffraction^{95,196} revealed three-dimensional atomic configuration and hydrogen bonding in cellulose I β . Polymer chains are strained to facilitate energetically favorable H bonding¹⁹⁶ which results in lowering the electronic energy¹⁹⁷. The balance between the increased strain energy and the decreased electronic energy associated with forming the H bonds determine the stability of the H bonds. Though the H bonds hold the chains rigid, each glucose residue has a degree of torsional freedom that determines the orientation of the hydroxymethyl group and the shape of the whole saccharide molecule – boat/chair¹⁹⁸. Such change in conformation is known to influence the product formation during primary cellulose decomposition¹⁹⁰. In aqueous solutions, glucose is present as *gg* or *gt* conformer, where the position of O₆ atom is gauche (*g*) to O₅ and gauche (*g*)/trans (*t*) to C₄ (refer Figure 2.1a for atom labelling). X-Ray fiber diffraction¹⁹⁹ and ¹³C-NMR²⁰⁰ studies show that glucose residues have *tg* conformation in native cellulose. Many

studies ^{102,182–184} have simulated the thermal response of crystalline cellulose under pyrolysis conditions and found a discontinuous change in lattice parameters, thermal and spectral properties at the 450K-550K range, echoing the experimental observations. These changes indicate a ‘phase transition’ ⁹⁸ as the density decreases non-linearly ²⁰¹ to form the *melt-phase*.

Molecular mechanics based calculations ⁹⁹ show *melt-phase* cellulose arrangement forms stable sheets with increased inter-chain H bonds. However, a 20% and 55% reduction in total and intra-chain H bonds destabilizes the chain conformation ¹⁰⁵ gaining torsional freedom. The hydroxymethyl group orientation is determined by the degree of torsional freedom and with temperature increase, force-field simulations indicate a shift from *tg* to *gg* or *gt* conformation ^{201,202}. An analysis of systematic variation of torsional parameters suggested an entropy gain by adopting *gg/gt* conformer over *tg* ¹⁹⁸. Therefore, “*phase transition*” can be associated with entropy gain that stabilizes high temperature structures and could significantly alter the energetics of decomposition. Moreover, mimicking *melt-phase* reaction environment by positioning hydroxyl groups of water or small alcoholic products to catalyze the formation of LGA from glucose resulted in a reduced enthalpic barrier ¹⁹⁰. These changes in phase could potentially alter reaction kinetics resulting in two regimes as observed in millisecond scale kinetic experiments ¹⁹⁴. For this reason, knowledge of the local pyrolysis environment under reaction conditions is crucial in understanding cellulose decomposition chemistry and kinetics.

Developing molecular insights of the interactions in the *melt-phase* and estimating the resulting low barrier for pyrolytic C-O bond activation is currently inaccessible to experiments alone ¹²⁸. Therefore, molecular modelling methods are employed. Due to computational limitations in simulating large cellulose microfibrils ¹⁷⁸, first principles studies have used tractable surrogate molecules to simplify complex biopolymers. In literature, glucose ^{108,109}, cellobiose ^{110,111}, cellotriose ¹¹² and cyclodextrin ⁸² have been used as surrogate molecules for cellulose. Some studies ^{82,118} have shown the formation of volatiles (furans), HMF, formic acid and CO directly from cellulose. However, the intermediates of cellulose pyrolysis have short-chain anhydro-oligomers with levoglucosan-end ¹²⁷ indicating that cellulose decomposition proceeds dominantly by glycosidic bond cleavage. This agrees with other studies ⁵² that suggest

levoglucosan (LGA) is the kinetically favored product. Multi-step high temperature homolytic^{116,203} and heterolytic^{119,128} mechanisms with free radical and ionic intermediates, respectively have been proposed for glycosidic cleavage. However, Density Functional Theory (DFT) calculations for these mechanisms in methyl-cellulbiose with implicit solvation resulted in high activation barriers (>400 kJ/mol at 773K)¹¹⁸. Many studies^{52,111,118,122} have shown that concerted mechanisms are more favorable than homo/hetero-lytic cleavage of the glycosidic bond. The activation barrier for these concerted mechanisms in gas phase vary anywhere between 200-300 kJ/mol^{111,118,122,190,204}. However, as mentioned earlier, the local pyrolysis environment in *melt-phase* can significantly alter the reactivity rendering the direct relevance of these gas phase calculations insufficient. Moreover, ab-initio calculations using biasing methods found no low-barrier pathway for pre-LGA formation in the absence of temperature-appropriate density⁵². A temperature dependent variation in reaction mechanisms was calculated in a four-molecule periodic system with plausible densities to mimic *melt-phase* environment. Ring contraction from glucopyranose ring to glucofuranose ring without glycosidic bond cleavage was reported to be favored (83.7 kJ/mol) at 600K and glycosylation (151 kJ/mol) at 873K. The low free energy barrier for ring contraction at low temperatures suggests that depolymerization in the *melt-phase* to form 'active cellulose' could also include the formation of furanic rings. Alternatively, vicinal OH groups from stacked parallel cellulose sheets were used to form H bonds to investigate hydroxyl catalyzed decomposition in *melt-phase*¹²⁹. Cellulose sheets were arranged to form inter-sheet hydroxyl interactions that stabilize the charged transition state. Such catalyzed bond activation by static hydroxyl clusters results in a reduced apparent activation barrier. Also, the reduction in activation barrier was proportional to the number of hydroxyl groups participating in the reaction. This only reinforces the experimental studies that suggest shift in phase with temperature could alter reaction energetics¹⁹⁴.

Nevertheless, finite temperature dynamic effects, influence of entropy gained to stabilize high temperature structures on cellulose reactivity and the associated free energies remain unknown. The immediate knowledge gaps in understanding pyrolytic decomposition of cellulose in *melt-phase* are – 1. The role of the *melt-phase* in cellulose exhibiting temperature variant reaction regimes during pyrolysis, 2. The significance of 'reactive melting temperature' (740K) or the transition temperature at

which there is a shift in the kinetics and 3. The entropic contributions to the barrier in both reaction regimes. Addressing these queries requires developing a molecular picture of cellulose pyrolysis. Such fundamental knowledge of cellulose activation in the *melt-phase* will enable accurate calculation of the energetics of competing reactions leading to their integration in kinetic/transport/reactor models and eventually in prediction and optimization of bio-oil production.

To address these gaps, a careful analysis of phase transition on the reaction environment and the relative stabilization effects on reactive species is needed. In this work, a combination of classical molecular dynamics (MD) and density functional theory (DFT) approaches is used to evaluate the role of finite temperature *melt-phase* environment on cellulose primary decomposition reactions. First principle DFT calculations are performed for cellobiose systems equilibrated with MD to capture explicit interactions in the reaction environment. A novel computational strategy is employed to estimate free energy barriers for cellulose decomposition in the *melt-phase* using gas phase barriers and relative free energies of interaction. The results suggest that the entropic contributions induced by melt phase formation significantly influence the decomposition mechanism. This work provides broader insights into the role of *melt-phase* hydrogen bonding and molecular conformations on cellulose reaction chemistry at different temperatures.

2.2 Computational Methodology

Since cellulose gains entropy to stabilize high-temperature structures, the influence of melt phase formation on reaction chemistry can only be probed by accounting for explicit molecules in the condensed phase and the entropic contributions. The free energy barrier can be captured using accelerated/biased ab-initio MD (AIMD) methods by explicitly defining interactions with the local reaction environment^{52,82}. However, performing accelerated AIMD for multi-molecular cellobiose systems is computationally very expensive¹⁷⁸. Thus, cellulose decomposition in the condensed phase is examined using two novel and different methods described below to accurately capture enthalpic and finite temperature entropic contributions to the free energy barrier. These strategies employ a combination of quantum mechanics (QM) and molecular mechanics (MM) approaches to circumvent the computationally expensive AIMD calculations. First ConTS method (described in detail in Section

2.2.1) enables the calculation of enthalpic activation barriers in the condensed phase system with all molecules treated using QM (static DFT). However, the condensed phase is pre-equilibrated using MM based MD simulations prior to QM calculations. Finite temperature effects cannot be captured using ConTS since it does not model reaction dynamics. To capture finite temperature effects and entropic contributions, the second ReSolv method (described in detail in Section 2.2.2) is implemented. In this method, activation free energy barriers are calculated in the gas phase using QM and corrected with finite temperature MM based free energy of solvation (of the reactant and the TS), which is computed using molecular dynamics (MD) based Thermodynamic Integration techniques. Additionally, the molecular mechanism of de-/stabilization offered with the *melt-phase* formation on the reactive species is analysed by calculating the changes in the hydrogen bonding and hydroxymethyl group conformations from the MD trajectories. The strategies used here to quantify the influence of cellobiose phase transition on reaction energetics would also enable comparison with the experimental kinetic data ^{128,194} that suggests two temperature dependent decomposition regimes.

2.2.1 Condensed phase transition state search (ConTS)

Forcefield based MD simulations are performed using GROMACS 2018.7 for an 8 residue cellobiose system at two temperatures (500K, 1200K) which are at the extremes of the pyrolysis range. Simulations were performed using OPLS/AA forcefield ²⁰⁵ parameters (Non-bonding parameters provided in Table S3). At each temperature, the simulation is run for 8ns in an NVT ensemble with an integration time step of 0.001 ps where the temperature is maintained by Nosé-Hoover thermostat. Prior to this, the system was equilibrated to the appropriate temperature and pressure (1bar). The neighbor list is updated every 0.01 ps and all averaged observables are recorded every 0.01 ps along the trajectory. Periodic boundary conditions are applied in all directions with no bond/angle constraints on atoms. The cut-off for Lennard-Jones and Coulombic potential was set at 0.5 nm. The equilibrated system coordinates give the temperature appropriate *melt-phase* configurations. The resulting low (500K) and high temperature (1200K) systems are used as reactant conformations for transition state search using DFT.

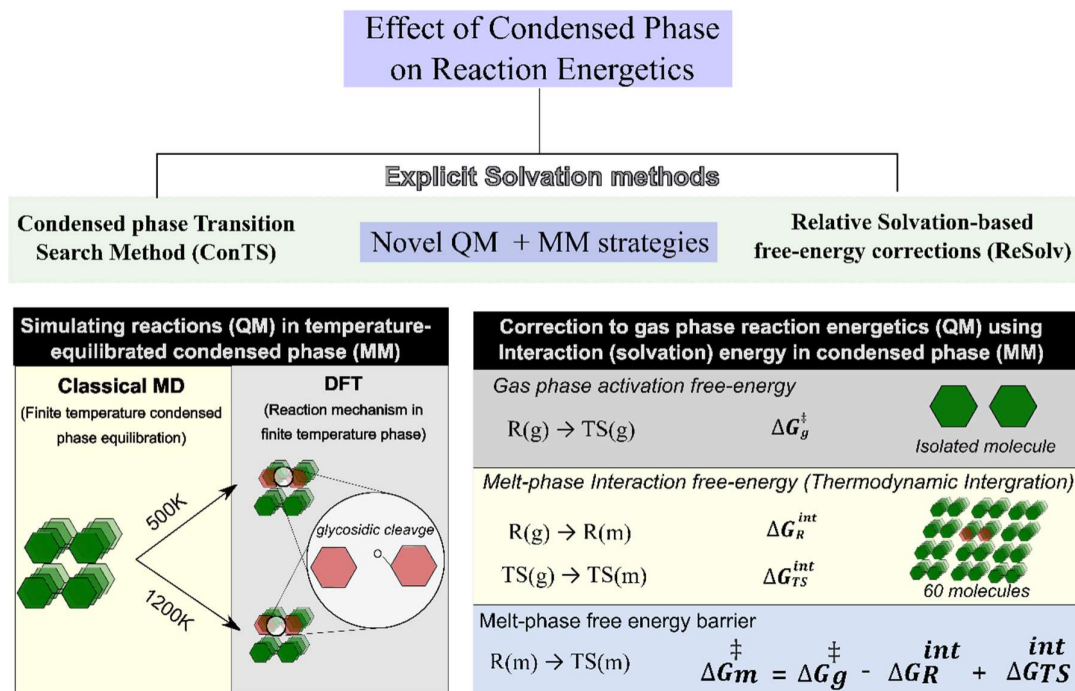


Figure 2.2 Schematic for novel computational strategies that combine QM and MM methods to capture finite temperature condensed phase effects (Condensed phase transition search (ConTS) methodology) and entropic effects (ReSolv method). These strategies enable the calculation of first principles based free energy and enthalpic barriers of glycosidic bond cleavage in the cellobiose condensed phase.

As shown in Figure 2.2, after MD simulations at 500K and 1200K, the transition states for decomposition reactions via glycosidic bond cleavage of cellobiose is calculated with DFT methods. TS was searched using Nudged elastic band (NEB) method implementation on Vienna ab initio simulation program (VASP). The series of images along the reaction coordinate are connected by a force constant of 0.2 eV/Å. These DFT calculations are performed using Perdew–Burke–Ernzerhof (PBE) which is a nonlocal exchange correlation functional of the generalized gradient approximation (GGA). The core electrons are represented by the projector-augmented wave (PAW) pseudopotential and the plane wave basis set is constructed with a cutoff energy of 450 eV. The $1 \times 1 \times 1$ Monkhorst–Pack k-points grid was found to be sufficient to sample the Brillouin zone. Geometry and force convergence criteria are set to be 10^{-6} eV and 0.04 eV/Å, respectively. Calculations performed with dispersion corrected DFT using Grimme method and PBE revealed negligible deviation (Table S2). The reaction intermediates (Figure S1) are optimized, and the frequencies are visualized to confirm

that the TS corresponds to the desired reaction. The highest energy images are used to calculate the TS and the corresponding enthalpic barriers. ConTS enables accurate calculation of first principles enthalpic barriers in the condensed phase environment. However, to include finite temperature entropic contributions, dynamics of the *melt-phase* along the reaction coordinate will have to be simulated. Therefore, the second method (ReSolv) aims at capturing solvent (*melt-phase*) dynamics (MM) around QM calculated reactant and TS in the gas phase.

2.2.2 Free energy barrier corrections based on Relative Solvation in the condensed phase (ReSolv Method)

The formulation of this novel technique to calculate free energy barrier corrections in condensed phase, involves the dissociation of the reaction into multiple associated reactions in a Bordwell thermodynamic cycle, ²⁰⁶ as presented in Figure 2.2. The reaction in *melt-phase* ($R_{(m)} \rightarrow TS_{(m)}$) is represented as a combination of associated reactions. This Bordwell cycle is used to estimate the free energy barrier in *melt-phase* by calculating the barrier in gas-phase and the relative interaction energies of the cellulose reacting species (reactant and TS) in the *melt-phase*. Gas phase barrier calculations are explained in Section 2.2.2.1. While the relative interaction free energies of the reacting specimen in *melt-phase* are calculated with thermodynamic integration considering intermediate states connected by a coupling parameter λ . Theory and computational procedures for the free energy calculations using thermodynamic integration (TI) are found elsewhere ²⁰⁷.

2.2.2.1 Gas phase barrier

All-electron DFT calculation were performed using Gaussian 09 code for an isolated cellobiose molecule. Calculations were performed using the hybrid functional M06-2X ²⁰⁸ with 6-31+G(2d,p) basis set as it has been recommended for carbohydrate chemistry ^{118,209–211}. Geometry optimization and TS search calculations are carried out with no constraints. Beryn algorithm is used for TS search. Subsequently, frequency calculations are performed to distinguish between the saddle point and local minima. Intrinsic reaction coordinates (IRCs) are followed in both directions to ensure that it corresponds to the correct reactant and product on the potential energy surface. These barriers are calculated at 1 atm and four temperatures (100K, 500K, 900K, 1200K).

Free energy barrier computed using temperature dependent entropic corrections is reported in Section 2.3.

2.2.2.2 Interaction energy

Thermodynamic integration (TI) method^{155,207} implementation on GROMACS 2018.7 is used to calculate the free energy of interaction at four temperatures (100K, 500K, 900K, 1200K) for 60 residue cellobiose system. The reactant and TS coordinates from gas phase calculations are used as the starting conformation for the reacting specimen. Langevin dynamics is used along with OPLS/AA force-field parameters. The initial system configurations are first energy optimized and equilibrated. Pressure equilibration is performed in an NPT ensemble at 1 atm for 2 ns and the resulting configurations are used to set the appropriate system volume/phase. TI calculations are then carried out in an NVT ensemble for 8 ns at the respective temperatures. The number of intermediate states (λ -windows) is optimized, and 30 λ -windows are found to be sufficient. The potential derivatives calculated from the MD simulations for each λ -window are integrated to compute ΔG^{int} . The free energies (ΔG^{int} , ΔG^\ddagger) from gas phase calculations and thermodynamic integration are used to estimate the free energy barrier for cellulose decomposition in *melt-phase* (ΔG^\ddagger) as shown in Figure 2.2. The enthalpic (ΔH^\ddagger) and entropic (ΔS^\ddagger) contributions to the free-energy barrier are further calculated from the slope and intercept of ΔG^\ddagger vs. temperature plot.

In summary, ConTS (section 2.2.1) calculates the enthalpic barrier in the condensed phase using DFT, but without dynamic effects. These first-principles enthalpic barriers are calculated for glycosidic bond cleavage in cellobiose *melt-phase* and the influence of temperature in ConTS is indirectly captured by pre-equilibrating the *melt-phase* around the reactant using MD simulations. However, in the *melt-phase* at temperatures above 450K⁹⁹, cellulose is known to gain torsional entropy. The entropy of transition has been roughly estimated by varying torsional parameters to be 26 J/K-mol¹⁹⁸. Accounting for these entropic contributions and developing a mechanistic understanding is crucial for explaining cellulose chemistry in the *melt-phase*. Hence, in the ReSolv method, the gas phase DFT computed free energy barriers are corrected using finite temperature interaction energies with the *melt-phase*, calculated using MM based MD simulations. Additionally, the enthalpic contribution to the free energy barrier calculated using ReSolv method can be compared to the enthalpic barrier calculated

using ConTS. As evident from the discussion, the approaches employed in these strategies are mutually exclusive. Therefore, agreement between the results of these two independent techniques would also validate their application in this study for calculating cellulose decomposition energetics.

2.3 Results and discussion

Cellulose activation has been shown to dominantly initiate either by glycosidic bond cleavage () or by ring contraction (from pyranose to furanose rings, c.f. Figure 2.1b) at low pyrolysis temperatures (600K) ⁵² . Comparison of potential reaction mechanisms for glycosidic bond cleavage using gas phase enthalpic barriers favored transglycosylation ²⁰⁴ . Moreover, transglycosylation (Figure 2.1c) and ring contraction w/ C-O cleavage (Figure 2.1b) mechanisms lead to the formation of dominant cellulose pyrolysis products – LGA and furans. Therefore, these two mechanisms are used in the current study as representative primary reaction mechanisms to investigate cellulose decomposition. The ring contraction is a concerted mechanism that undergoes simultaneous ring reorganization and glycosidic bond cleavage.

2.3.1 Enthalpic barrier for glycosidic bond cleavage using condensed phase TS search

DFT calculations performed for the glycosidic bond cleavage via transglycosylation and ring contraction in a cellobiose crystal structure ¹⁹⁶ environment predicted activation barrier of 241 kJ/mol and 251.83 kJ/mol, respectively (Figure A.2). However, to capture the influence of molecular rearrangements in the melt phase on decomposition mechanisms, ConTS calculations are performed. First, cellobiose crystal structure systems having explicit intermolecular hydrogen bonding are equilibrated at finite temperature using MD (Section 2.2.1). The resulting system configurations after the production run are used to calculate the transition state and finite temperature activation barrier for glycosidic bond cleavage in the *melt-phase* system. Calculations revealed that at 500K the enthalpic barrier for transglycosylation in the *melt-phase* environment is 249.5 kJ/mol (*cf* Figure 2.3). These low temperature condensed phase barriers are in line with the reported range of 189.54 – 247 kJ/mol ^{118,122,129,190,204} for glycosidic cleavage through noncatalyzed transglycosylation in cellulose derivatives. To also capture the influence of the high temperature *melt-phase*

environment at the other extreme of pyrolysis operating temperatures, ConTS calculations were performed at 1200K. The computed enthalpic barrier for glycosidic C-O cleavage via transglycosylation in cellobiose *melt-phase* at 1200K is only 164.66 kJ/mol (*cf* Figure 2.3). It has to be noted that such low enthalpic barriers for glycosidic bond cleavage in a non-catalyzed system has not been reported before. Similar to the millisecond-scale kinetics experiments ¹⁹⁴, ConTS calculations show two reaction regimes – high enthalpic barrier at low temperature (500K), and low enthalpic barrier at high temperature (1200K). The low enthalpic barrier is in the range of the barrier reported for OH-catalyzed LGA formation in earlier studies ^{73,129,190}, though such catalyzation would not be possible at this high temperature. Figure 2.3 also shows a similar reduction in the enthalpic barrier for ring contraction mechanism from 456.53 kJ/mol at 500K to 294.28 kJ/mol at 1200K.

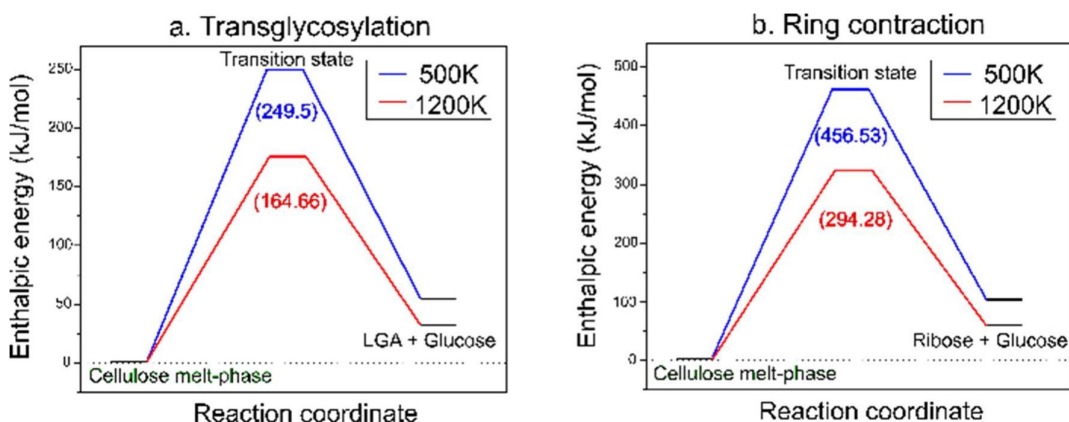


Figure 2.3 ConTS calculated enthalpic barriers for (a) transglycosylation and (b) ring contraction in the melt-phase environment.

In literature, cellulose has been hypothesized to undergo hydroxyl-catalyzed glycosidic bond cleavage (low barrier) in the *melt-phase* at lower temperatures (<740K) and direct thermal cleavage at higher temperatures (high barrier) ¹²⁹. External hydrogen bonding with water or alcohol groups has been shown to promote LGA formation from glucose by stabilizing the charged transition state ¹⁹⁰. Nearby hydroxyl groups could have similar catalytic effect during pyrolysis ¹⁵⁹. Maliekkal et al. ¹²⁹ performed DFT calculations and found that in stacked cellulose sheets, intersheet hydroxyl groups help stabilize charged transition states promoting proton transfer. The intrinsic activation barrier for such hydroxyl catalyzed transglycosylation has been

reported to be 154.39 kJ/mol which decreased further (134.31 kJ/mol) on binding with additional hydroxyl groups. Also, an even lower free energy barrier (139.33 kJ/mol) was calculated using constrained AIMD simulations. Though hydroxyl groups promoting cellulose decomposition is demonstrated, such reactions were not studied in an unconstrained *melt-phase* environment. The DFT studies discussed above have used constrained/static clusters to validate the effects of vicinal hydroxyl groups while the temperature induced changes in the condensed phase molecular environment and their influence on the reaction kinetics was unaccounted. Parity with experiments showing low activation barrier (224.68 ± 4.602 kJ/mol) is obtained only when low temperature experimental conversion is fitted with first order kinetics¹²⁸. The higher ConTS barrier calculated in the lower temperature regime and the lack of catalytic action (not observed while visualizing the structure) essentially provides evidence contrary to the hydroxyl-catalyzed model of cellulose decomposition.

2.3.2 Condensed phase free-energy barriers using ReSolv method

ReSolv method described in Section 2.2.2 is used to calculate the free energy barrier in condensed phase by correcting the gas phase barrier. Therefore here, finite temperature gas phase cellobiose decomposition is shown first before presenting the corresponding energetics in the melt-phase.

2.3.2.1 Gas phase decomposition

Gas phase calculation was performed using Gaussian 09 code for an isolated cellobiose. The free energy barriers for C-O bond cleavage via transglycosylation and ring contraction at 100K, 500K, 900K and 1200K are shown in Figure 2.4. The free energy barriers for both mechanisms show a clear transition with temperature (Figure 2.4). The barrier for transglycosylation reduces from 255.16 kJ/mol at 100K to 227.88 kJ/mol at 1200K whereas for ring contraction mechanism, it reduces from 255.16 kJ/mol at 100K to 227.88 kJ/mol at 1200K. As expected, at 500K our calculations revealed similar enthalpic barriers for glycosidic bond cleavage reported by Arora et al.²⁰⁴. Transglycosylation only involves a bridge formation while ring contraction involves ring cleaving and reorganization. Figure 2.4 shows that transglycosylation is favored over ring contraction in the gas phase at all temperatures, matching both the ConTS calculations and previous DFT studies²⁰⁴.

The gas phase barrier for either mechanism shows two decomposition regimes, resembling the ConTS calculations – 1. Low temperature, high barrier & 2. High temperature, low barrier. Since the calculations are performed for an isolated molecule, this suggests that during pyrolysis, the entropy of the reacting molecule also plays a role in bringing down the barrier slightly. The gas phase DFT calculated reactant and transition state conformations are then used to calculate the interaction free energies of the reacting species (reactant, TS) using the thermodynamic integration method, as described in section 2.2.2.

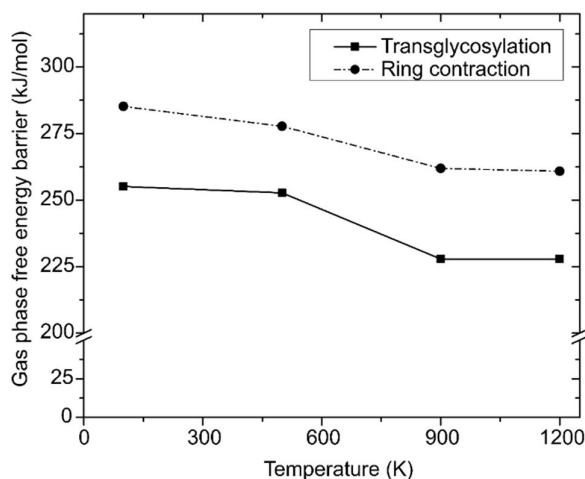


Figure 2.4 Gas phase free energy barrier for glycosidic bond cleavage in cellobiose at different temperatures calculated using hybrid functional M06-2X with 6-31+G (2d,p) basis set.

2.3.2.2 Melt-phase decomposition

The formalism presented in Figure 2.2 is used to calculate the Gibbs free energy barriers for transglycosylation and ring contraction of one reacting cellobiose molecule in the *melt-phase* at different temperatures, as shown in Figure 2.5. The activation free energy barrier in the *melt-phase* environment decreases almost linearly with increasing temperatures and asymptotes above 900K. At these higher temperatures, the free energy barriers are constant at ~105 kJ/mol and ~323 kJ/mol for transglycosylation (LGA formation) and ring contraction (furan formation), respectively. Consequently, the reduction in the (free) energy barriers from 100K to 900K for the two mechanisms are 267.76 kJ/mol and 159.18 kJ/mol suggesting that the presence of finite temperature melt phase environment has a stronger influence on

transglycosylation. This reduction in the *melt-phase* barrier is a magnitude greater than what is calculated in gas phase for transglycosylation (27.29 kJ/mol) and ring-contraction (23.29 kJ/mol), highlighting the influence of melt phase interactions. Similar high temperature low free-energy barriers for pre-LGA (151 kJ/mol) formation compared to pre-HMF (furanic) (205 kJ/mol) formation using accelerated AIMD simulations at 873K ⁵² has been reported previously. This validates the novel approach used in this study to compare the influence of the finite temperature condensed phase environment on cellulose decomposition chemistry.

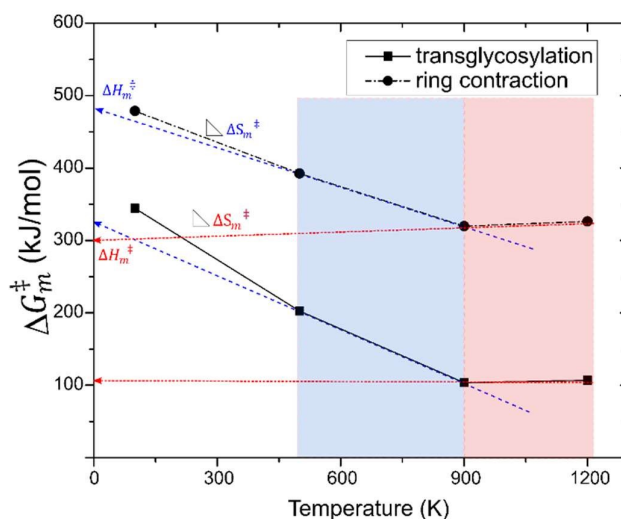


Figure 2.5 Free energy barrier vs temperature profile for cellulose decomposition via transglycosylation and ring contraction showing two reaction regimes transitioning at 900K. The slope and y-intercept gives the entropic and enthalpic contributions to the free energy barrier, respectively. The tangents are fitted between 500K-900K for the low temperature (blue dash lines) and 900K-1200K for high temperature regime (red dash lines).

The slope and y-intercept of the free-energy vs temperatures plot (Figure 2.5) gives the entropic and enthalpic contributions, respectively. At low temperatures, the free energy barrier decreases almost linearly having a common tangent intercept and slope at any given temperature (<900K). The constant slope of the free energy barrier curve is indicative of the constant gain in entropy (ΔS^\ddagger) of 334.69 J/mol-K for LGA formation and 198.98 J/mol-K for furan formation during phase transition in cellulose *melt-phase*. At higher temperatures, the free energy barrier curve flattens indicating that the entropic contribution to the barrier is zero, making it an enthalpy-controlled regime.

The linear slopes of the low and high temperature curves form two decomposition regimes. These regimes transitioning at ~800-900K is similar to the experimentally measured millisecond scale kinetic regimes transitioning at 740K¹⁹⁴. As seen in Figure 2.5, the enthalpic barriers of the two regimes are calculated from the y-intercept of the tangent to the free energy curve at 700K (average of 500K-900K) and 1050K (average of 900K-1200K). For transglycosylation, the enthalpic barrier reduces from 320 kJ/mol to 120 kJ/mol while for ring contraction, it reduces from 480 kJ/mol to 299 kJ/mol with increase in temperature. The high enthalpic barrier at low temperatures and low enthalpic barrier at temperatures above 900K agrees with the ConTS calculations performed in *melt-phase* environment (Figure 2.3) which is reported in Section 2.3.1.

Two cellulose decomposition regimes in the *melt-phase* have been identified with both free energy barrier corrections and ConTS calculations –

1. High enthalpic & free-energy barrier at low temperatures (500K-800K), and
2. Low enthalpic & free-energy barrier at high temperatures (800K-1200K).

The enthalpic barriers (ΔH^\ddagger) estimated from Fig. 5 for transglycosylation and ring contraction between 500K-900K are 300 kJ/mol and 480 kJ/mol, respectively. In the higher temperature regime (900K-1200K), the enthalpic barriers (ΔH^\ddagger) are 120 kJ/mol and 300 kJ/mol. These barriers show excellent match with first principles DFT based ConTS calculations presented in Figure 2.3 – 249.5 kJ/mol & 456.53 kJ/mol at 500K, and 164.66 kJ/mol & 294.28 kJ/mol at 1200K for transglycosylation and ring contraction, respectively. Previous DFT studies had suggested catalytic activation by vicinal hydroxyl groups to be the primary mode of glycosidic activation at low temperatures^{129,212}. However, the evidence presented here strongly suggests that when accounted for condensed phase and finite temperature effects, the reorganization of neighboring molecules from crystal phase to melt phase significantly influences cellulose chemistry. Throughout the temperature range (100K-1200K), transglycosylation has a lower energy barrier compared to ring contraction, similar to the trend reported using both ConTS and gas phase calculations. It has to be noted that AIMD-metadynamics⁵² study reported low free-energy barriers (83.7 kJ/mol) for ring contraction from glucopyranose ring to the glucofuranose ring, but without the glycosidic bond cleavage. The higher free-energy barriers calculated for the concerted

ring contraction mechanism studied herein indicate that direct glycosidic bond cleavage while the cellulose ring undergoes contraction (Figure 2.1c) is less favorable in the *melt-phase* (Figure 2.5). The difference in the absolute free energy barriers and the slope of reduction in barrier between the mechanisms with temperature indicate that the structural changes undergoing during phase transition in the cellulose *melt-phase* environment favors transglycosylation over ring contraction. This difference in the barriers and therefore the kinetic feasibility of transglycosylation over ring contraction only seems to increase with temperature.

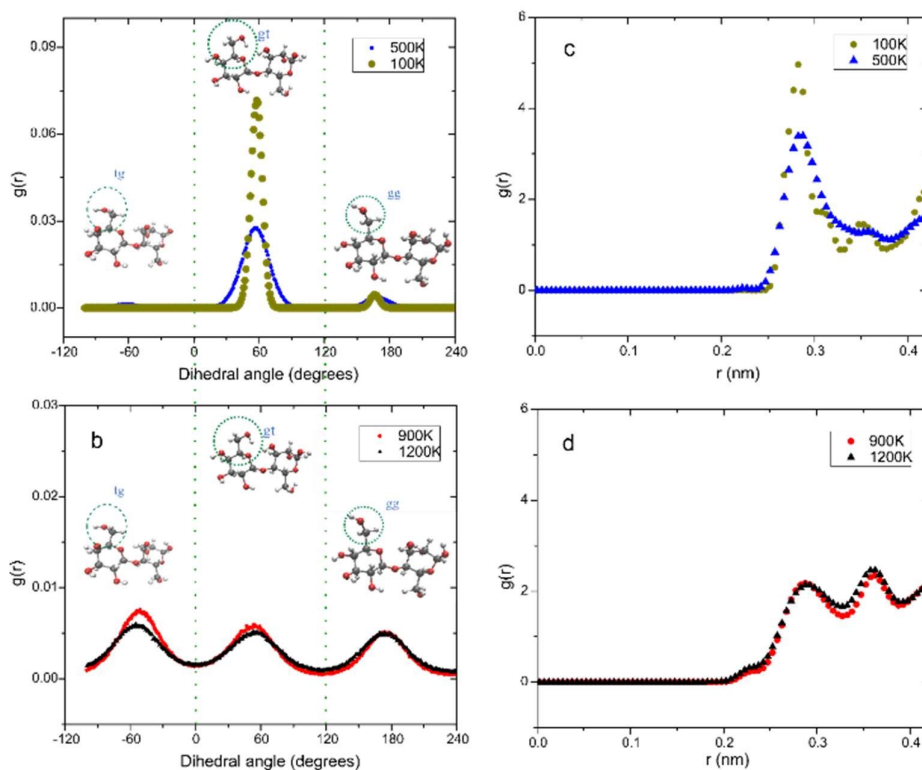


Figure 2.6 Distribution of hydroxymethyl group dihedral – (a) 100K and 500K, (b) 900K and 1200K. Distribution of O-O distance in hydrogen bonds – (c) 100K and 500K, (d) 900K and 1200K.

During phase transition between 500K-900K, ΔH^\ddagger and ΔS^\ddagger have constant positive values. In this regime, the enthalpic contribution to the free energy remains constant while the entropic contribution ($T\Delta S^\ddagger$) increases due to increase in temperature. This is therefore an entropy-controlled regime as the increase the entropic contribution ultimately lowers the free-energy barrier. However, in the high temperature regime (>900K), ΔH^\ddagger has a constant positive value but ΔS^\ddagger is negligible, making it an

enthalpy-controlled regime. This suggests that glycosidic bond cleavage is increasingly promoted as a function of temperature only until 900K, after which the barrier for cleavage remains constant ($\Delta G^\ddagger \approx \Delta H^\ddagger$). To better understand this decomposition energetics and the regime change, molecular details of the interactions in the melt phase are investigated. A detailed molecular interpretation of the energy diagrams is presented below.

2.3.3 Phase change and reaction chemistry

Molecular level changes in cellobiose *melt-phase* systems, at pyrolysis conditions, are studied by calculating the relative distribution of hydroxymethyl dihedrals & hydrogen bonds (Figure 2.6), dielectric constant (Table 2.1) and entropy changes with temperature (Figure 2.7) using MD simulations. These changes are then correlated to the changes in entropic and enthalpic contributions to the free-energy barriers, as a function of temperature.

2.3.3.1 Hydroxymethyl group orientation

There are 60 cellobiose molecules in the system and therefore 240 hydroxymethyl groups are analyzed here. The dihedral angles (O5-C5-C6-O6) -60° , 60° , 180° correspond to the *tg*, *gt* and *gg* conformations, respectively. Figure 2.6a shows that at low temperatures, the hydroxymethyl groups are predominantly oriented in *gt* conformation.

The distribution of *gt* conformer reduces with temperature (500K) at the cost of forming *gg* conformers. This is consistent with the change from *tg* in crystal structure to *gg* conformer calculated for non-rotating center cellulose chain using force-field calculations by Zhang et al.²⁰². Above 900K, the distribution of hydroxymethyl dihedrals (Figure 2.6b) show that all conformations are equally accessible because of the complete disruption of the hydrogen bonding network. Cellulose chains have been reported to gain torsional entropy during “phase change” to stabilize the high temperature *melt-phase* structures. As the chains rotate, the hydroxymethyl group gains extra degrees of freedom to change orientations^{98,198}. Figure 2.6a and 6b suggests that this change in conformation continues until 900K after which all conformers are equally accessible. Since concerted transglycosylation mechanism involves simultaneous protonation of the glycosidic bond by the hydroxymethyl group

and formation of C6–O–C1 (Figure 2.1c) bridge, any shift in hydroxymethyl conformations from the crystal arrangement could decrease the barrier for bridge formation. In general, the shift in conformation is a measure of torsional freedom in cellulose chains. With limited degrees of freedom even ring-contraction mechanism exhibits a higher barrier at low temperatures. Such influence of hydroxymethyl group orientation on the energy barrier is further elaborated in Section 2.3.3.3.

Table 2.1 Dielectric constant in cellobiose melt-phase systems

Temperature (K)	Dielectric Constant
500	3.89
900	4.27
1200	2.37

2.3.3.2 Hydrogen bonding

The distribution of H bonds in cellobiose *melt-phase* are shown in Figure 2.6c and 6b. At low temperatures, the hydrogen bond lengths are short with a peak O–O distance of 2.7 Å. Similar elongation of H bonds at higher temperatures have been reported earlier⁹⁸. Neutron crystallography studies^{195,213} performed at ambient temperature found that the H atom covalently bonded to O2 can either form H-bond with O6 of the inner or outer chain in cellulose microfibrils. Depending on the location of the H atom, cellulose forms unidirectional infinite network of H bonds. X-ray diffraction and force-field studies have shown that in the crystal structure, the hydroxymethyl groups are in the tg conformation^{196,202} which is in alignment with O2 forming intrachain H-bonds with O6 (refer Figure 2.1a for nomenclature). Similarly, other force-field based MD studies^{90,98,195,198,201,202} have found abrupt changes in thermophysical properties of cellulose above 450K. The directionality of this infinite network of H-bonds is analyzed by calculating dielectric constant for cellobiose systems (Table 2.1). Dielectric constant remains higher and relatively invariable at the low temperatures (500K–900K) indicating certain directionality of hydrogen bonds. With increasing temperatures, directional hydrogen bonding is disrupted, increasing torsional freedom in cellulose

chains. This enables the possibility of taking different hydroxymethyl conformations and consequently increases the entropy in the system. Figure 2.7 shows the entropy gained (ΔS) by a cellobiose molecule without undergoing reaction in *melt-phase* at different temperatures, calculated using quasi-harmonic approximations in force-field simulations. Since the entropy is calculated for an intact cellobiose molecule, the entropy gained is due to the disruption of H-bonds in the *melt-phase*. ΔS increases until 900K, and asymptotes with further increase in temperature. There is a monotonic increase of 604.55 J/K-mol from 500K-900K is due to the disruption of the hydrogen bonds. The modest entropy gain beyond 900K (Figure 2.7) indicates that all degrees of freedom available through the complete disruption of the hydrogen bonding has been gained. The drop in dielectric constant from 900K to 1200K (Table 2.1) and the negligible entropy gain above 900K (Figure 2.7) corroborates that the directional H-bonding network in cellulose melt phase is completely disrupted beyond 900K.

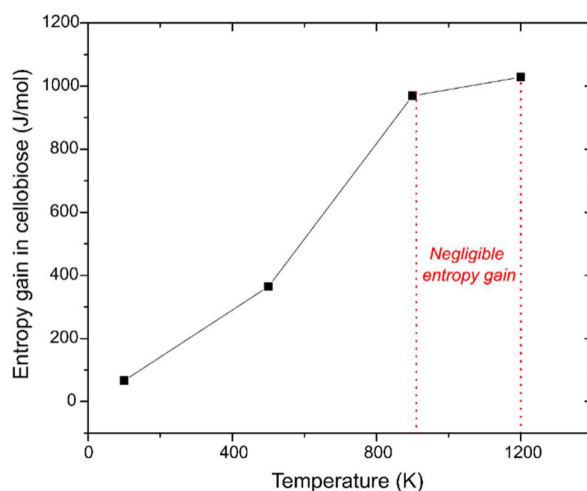


Figure 2.7 Entropy change in cellobiose molecule without undergoing reaction in a finite temperature melt-phase environment calculated using quasi-harmonic approximations in force-field simulations. The entropy monotonically increases to asymptote above 900K.

The average number of intermolecular hydrogen bonds (distance: $<4.5 \text{ \AA}$, angle: 150°) formed by the reacting cellobiose molecule and the TS species with the condensed phase is presented in Figure 2.8. In the low temperature regime, the intact cellobiose molecule forms higher number of hydrogen bonds followed by the TS of ring contraction and transglycosylation which rapidly decreases with temperature. In

contrast, at higher temperatures (>900K), the number of H-bonds formed by all species is reduced to a minimum value. The decrease in the average number of hydrogen bonds between 100K-1200K is 75% for cellobiose, 69% and 67 % for the TS of ring contraction and transglycosylation, respectively. This difference in the % reduction of the H-bonds with temperature suggests that the melt phase is more destabilizing for the reactant cellobiose compared to the TS. These changes in hydrogen bonding and hydroxymethyl conformations indicate a 'phase transition' characterized by amorphous expansion to a lower density state.

2.3.3.3 Influence of condensed phase on cellulose decomposition chemistry

To form cyclic products like LGA and furans, the glucose residues in cellulose must shift from the ground state chair conformer to boat conformer ¹⁹⁰. In the boat conformation, after glycosidic bond cleavage, C1 (carbocation) is more accessible to the hydroxymethyl arm for transglycosylation or C2-C3 bond fragmentation for ring contraction. At low temperatures, the hydroxymethyl arm is locked away from the glycosidic oxygen by strong hydrogen bonds in the condensed phase. Additional energy is required for conformational change enabling C2-C3 bond fragmentation in ring contraction and for the breaking of the hydrogen bonds before the attack of O6 on C1 in transglycosylation. This additional energy is reflected in the higher enthalpic barriers (ΔH^\ddagger) at the low temperature reaction regime (100K-900K) reported in Figures 2.5 and 2.6. The high dielectric cellulosic *melt-phase* (Table 2.1) in this lower temperature regime also provides a polar environment. Similar polar environments (solvent) have shown to increase activation barrier for acid-catalyzed dehydration of xylose to furfural ²¹⁴ by enhancing reactant solvation. High dielectric melt phase, therefore, enhances cellobiose intermolecular self-solvation having only a fractional effect on the charged TS. However, the TS has higher entropy than the reactant cellobiose molecule and with the melt phase formation, this activation entropy (ΔS c.f. Figure 2.7) further amplifies as the hydrogen bonds in the local environment weaken, stretch, and break providing torsional freedom for conformational change in hydroxymethyl groups. Hence in the low temperature *melt-phase* (100K-900K), entropy contributes ($T\Delta S^\ddagger$) to reducing the free energy barrier for glycosidic bond cleavage as a function of temperature. ΔS^\ddagger calculated from the free-energy profile (Figure 2.5) in this regime is 334.69 J/mol-K and 198.98 J/mol-K for

transglycosylation and ring contraction, respectively. As explained in Section 2.3.2.2, this is an entropy-controlled regime as ΔS^\ddagger is non-trivial with the molecular rearrangements providing extra degrees of freedom. Therefore, in the low temperature regime, cellulose has a constant enthalpic contribution to the free-energy barrier for glycosidic bond cleavage, and the reduction in free energy barrier is mainly due to entropic contributions.

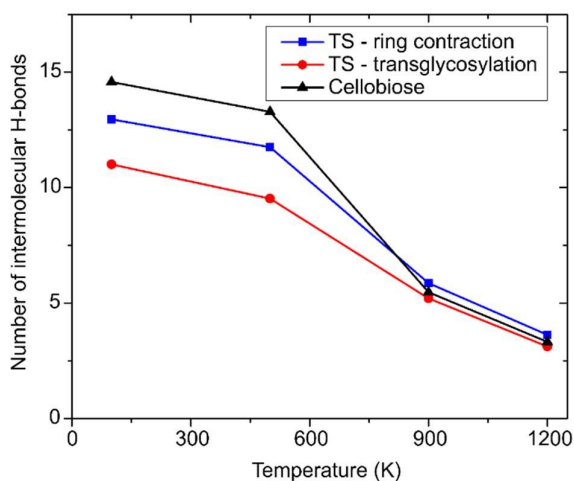


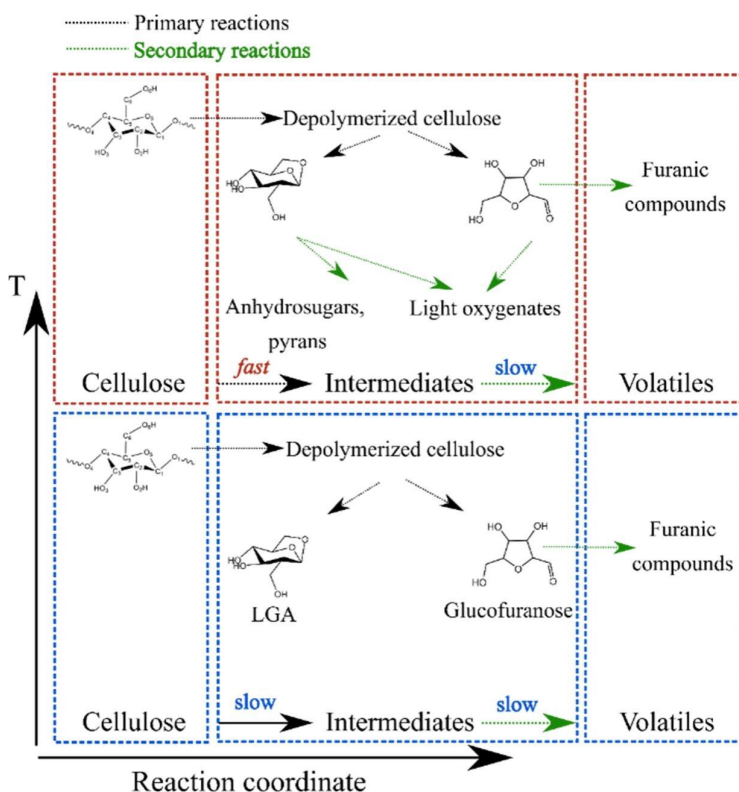
Figure 2.8 Average number of H bonds around the reacting molecule in a finite temperature melt-phase environment at different temperatures

ΔS^\ddagger for glycosidic cleavage in cellobiose *melt-phase* is positive only until the hydrogen bonding network is completely disrupted and the hydroxymethyl groups gain conformational freedom. This complete transition in phase occurs beyond 900K, as shown in Figs. 7d, 8, 9 and Table 2.1. In the high temperature reaction regime (>900K), the lower dielectric melt phase no longer preferentially enhances reactant cellobiose self-solvation. The difference in entropy (ΔS^\ddagger) between the TS and cellobiose molecule is negligible (Figure 2.5), making it an enthalpy-controlled regime. High temperature *melt-phase* environment is relatively destabilizing for the reacting cellobiose molecule because of the disrupted hydrogen bonding network. Here, C1 is more accessible to the hydroxymethyl arm for the formation of LGA via transglycosylation.

Similarly increased conformational freedom enables C2-C3 bond cleavage for ring contraction, therefore having a low enthalpic barrier for either mechanism is reflected in Figs. 5 and 6. This reduced high temperature barrier could either be due to the

stabilization of TS or destabilization of the reactant cellobiose. As the hydrogen bonding network in cellulosic phase is disrupted with temperature, the percentage reduction in the average number of intermolecular hydrogen bonds made with the melt phase is greater for reactant cellobiose than for the TS (Figure 2.8). This along with the reduced dielectric constant (Table 2.1) suggests a relative destabilization of the reactant cellobiose molecule with phase transition. Such destabilization of the cellobiose during melt phase formation has been reported here for the first time, providing a novel outlook on cellulose decomposition in the *melt-phase*.

Scheme 2.1 Cellulose decomposition model differentiated between the low (blue) and high (red) temperature regimes. At high temperatures, as primary decomposition is accelerated, the rate of secondary reactions in the intermediate liquid are significant.



In recent experimental studies ^{128,194}, cellulose weight loss and furan formation rate are measured to study the millisecond scale intrinsic kinetics. When comparing the above explained low-temperatures-high-barrier and high-temperature-low-barrier regimes with the barriers calculated from experimental kinetics ¹²⁸, there is an apparent contradiction. When fitted with first order kinetics to the millisecond scale

data from PHASR reactor, experiments suggested low-temperatures-low-barrier and high-temperature-high-barrier regimes. The trend of enthalpic barrier with respect to temperature seem flipped. But such direct comparisons between computed energetics of elementary steps and measured kinetics of bulk decomposition reactions might not be possible. Unreacted α -Cyclodextrin is quantified to calculate the rate of cellulose consumption while gas chromatography mass spectroscopy is used to measure the rate of furan production. High speed photography has shown that cellulose pyrolysis proceeds through a “liquid intermediate” before forming volatiles at 973K⁵⁹. Scheme 2.1 illustrates the decomposition of cellulose to volatiles through the liquid intermediate along the reaction coordinate at the two temperature dependent regimes. It can be inferred from this model that both the experimental measurements do not exclude the secondary reactions occurring in that intermediate (Scheme 2.1). Therefore, a quantitative relationship cannot be established between the current experimental kinetic data that includes secondary reactions and first principles calculations of cellulose primary decomposition.

Having said that, the experimentally measured millisecond scale rate of cellulose decomposition and furan production show two regimes, transitioning at 740K¹²⁸, agreeing with the results presented here. The rate of cellulose decomposition and furan production as a function of temperature are similar at lower temperatures. Whereas above 740K, the rate of cellulose decomposition increases relatively rapidly compared to that of furan production. This suggests that at low temperatures, the rate of primary decomposition of cellulose to intermediates is comparable with the rate of secondary decomposition to volatiles like furans. However, at higher temperatures, the rate of primary decomposition is much faster compared to the rate of secondary decomposition. This higher rate of primary cellulose decomposition compared to volatile products formation at high temperatures agree with the low enthalpic barrier calculated for glycosidic bond cleavage in this study. Further direct comparison of computational results with the entangled kinetics of phase transition, primary and secondary reactions happening in experiments would require elaborate multiscale kinetic modelling, tracking multiple possible reactions.

2.4 Conclusions

Cellulose primary decomposition reactions (transglycosylation and ring contraction) via glycosidic bond cleavage in the condensed phase pyrolysis environment are investigated between 100K-1200K. Two novel computational strategies are implemented: (i) ConTS method, where first principles enthalpic barriers are calculated with explicit condensed phase molecules in the reaction environment (that are equilibrated by molecular mechanics based MD simulations) and (ii) ReSolv method where gas phase first principles calculated free energy barriers are corrected using molecular mechanics based solvation free energies (with finite temperature effects) of the reacting species in the condensed phase. The free-energy barrier calculated using the ReSolv method as a function temperature is then used to estimate the enthalpic and entropic contributions for glycosidic bond cleavage. Both methods independently estimate high enthalpic barriers (ΔH^\ddagger) at low temperatures and low enthalpic barriers at high temperatures for the glycosidic C-O cleavage. These techniques allow utilizing a first-principles based approach to simulate finite temperature, condensed phase pyrolysis chemistry without having to use computationally expensive *ab initio* molecular dynamics.

Cellulose decomposition exhibits two distinct regimes transitioning at 900K. These two regimes have different enthalpic (ΔH^\ddagger) and entropic ($T\Delta S^\ddagger$) contributions to the free energy barrier. Both C-O cleavage mechanisms studied require conformational change from chair to boat. In the low temperature regime (100K-900K), the additional energy required to break the directional hydrogen bonding and to create the torsional freedom to change conformations is reflected in the higher ΔH^\ddagger . The high dielectric *melt-phase* in this regime, also enables self-solvation of the proton-donating reactant over the TS. However, ΔS^\ddagger takes constant positive values resulting in the lowering of the free-energy barrier with increase in temperature. Since the enthalpic contribution is constant and the total entropic contribution ($T\Delta S^\ddagger$) changes, it is an entropy-controlled regime. This is accompanied by the gradual disruption of the hydrogen bonding network and gaining conformational flexibility in hydroxymethyl group orientation, suggesting a transition in phase at 500K-900K. High temperature (>900K) *melt-phase* formation involved the complete disruption of directional hydrogen bonding allowing increased torsional freedom, in turn resulting in a lower enthalpic barrier. This

is due to the destabilization of the proton-donating cellobiose reactant in the high temperature regime. Unlike the hydroxyl catalyzed mechanism proposed in the literature where the charged TS is stabilized by vicinal hydroxyls, the present work suggests that the relative destabilization of cellulose leads to lower barrier for cellulose activation above 900K. In this high temperature regime, ΔS^\ddagger is negligible in the condensed phase. Gas phase DFT calculations revealed similar results, however, the activation entropy gained at 100K-900K is much higher in the presence of condensed phase. The increased favorability of glycosidic bond cleavage when the entropic contributions in the finite temperature melt-phase are included, establishes that it is an entropy-driven regime change. Furthermore, experimental studies measuring millisecond scale kinetics reported a higher increase in the rate of primary cellulose decomposition compared to volatile products formation above 740K. Qualitative comparisons made here, reveal coherence between calculated energetics for primary decomposition and experimental kinetics. Therefore, the two computational strategies (ConTS, ReSolv) and qualitative comparison with experiments yield strong evidence for entropic activation and resulting reactant destabilization leading to a lower activation barrier for glycosidic cleavage at high temperatures.

Chapter 3 Does the presence of lignin affect the pyrolytic decomposition of cellulose? A condensed phase computational investigation

*Reprinted with permission from RSC Sustainable Energy Fuels, 2023,7, 3660-3674
© 2023 Royal Society of Chemistry*

3.1 Introduction

Despite the promise of decentralized processing of biomass and subsequent lower transportation cost of intermediate bio-oil²¹⁵, pyrolysis technology has not yet grown to commercial viability. A major roadblock stopping the maturity of pyrolysis is the instability of bio-oil, which undergoes physicochemical changes (aging) during storage and transport,^{216,217} such as increase in viscosity due to re-polymerization²¹⁸. Such changes are induced by homogeneity in functional groups promoting repolymerization reactions among lower molecular weight (LMW) compounds to form heavier compounds, which are mainly lignin derived products^{134–136,219}. Lignin cannot be simply separated from the native biomass feed to inhibit repolymerization as isolating the biopolymers is expensive and not environmentally friendly. Therefore, fundamental understanding of reaction mechanisms and molecular level interactions between cellulose and other biopolymers is crucial to engineer biomass processing techniques that can optimize desired products in bio-oil^{34,137}. The lack of understanding of fundamental biomass chemistry presents a serious challenge to reduce repolymerization of lignin products and for greater access to cellulose products. The development of such fundamental knowledge is hindered by the multiscale structure of biomass. Unlike petrochemical feed, biomass spans eleven orders of magnitude in length from C-C, C-H, C-O, O-H bonds which makeup hemicellulose, lignin that binds to cellulose microfibrils in the cell wall, to the multi-cellular plant macrostructure⁴⁴. This gives rise to complex interactions between the biopolymers and the pyrolysis behaviour of the three individual biomass components in isolation will have to be distinguished from that in native biomass^{220,221}.

In one of the first reviews on biomass pyrolysis, Antal M. J.¹³⁸ suggested that a simple mathematical model superimposing thermal curves of individual components (lignin, cellulose, hemicellulose) should explain the thermal behaviour of native lignocellulosic biomass. This suggested that pyrolysis product distribution trends, global lumped

activation barriers and other kinetic parameters can be predicted with additive models that ignore any interactions between individual biopolymers. Following this, numerous studies have focused on using an additive model that combines pyrolysis kinetics of isolated biopolymers to explain the native biomass pyrolysis kinetics. The equipment, feedstock, temperature ramp and conclusions in those studies have been compiled in the supporting information (Tables S1 and S2 in the supporting information). Pyrolysis experiments performed to evaluate the additive models were conducted using a wide range of feeds like – 1. Woody biomass (like cedar, pine, beech, thistle, spruce, oak), 2. Herbaceous biomass (like rice straw, corn stalk, peanut vine, sugarcane bagasse), 3. Waste biomass (like waste wood chips, olive husk, hazelnut shells, palm oil waste), 4. Treated biomass (selective removal of individual biopolymers through chemical treating) and 5. Synthetic biomass (blending of commercial biopolymers using various mixing techniques). Raveendran et al.²²² used 14 different biomass feeds to show that char, liquid and gas yields in thermogravimetric analyzer (TGA) and a packed bed reactor can be predicted with a simple additive model. Following this, a regression model to predict hemicellulose, cellulose and lignin content from weight loss measurements worked well for synthetic samples while failing for palm oil waste²²³. This deviation in their model predictions was attributed to the mineral salt content in the native biomass feed. To avoid any anti-/catalytic effect by inorganic compounds, some studies^{224,225} acid washed the feedstock to remove mineral content. De-mineralized biomass corroborated with their additive model, deviating only for herbaceous (thistle) biomass. Similar studies^{226–230} showed the usefulness of additive kinetic models to predict activation energy, peak decomposition temperature and product composition. As highlighted in Table S1, most early experiments reported no significant interactions under the high temperature pyrolysis melting conditions. However, these studies used TGA or other reactor set-up which are limited by transport and a slow ramp temperature. They are plagued with these limitations and can only predict global kinetic parameters or product yield (char, liquid, gas). Recent experiments conducted in an entrained flow reactor¹⁴² under isothermal conditions showed that the additive law cannot even accurately predict pyrolysis gas (CO, CO₂, CH₄, H₂, C₂H₂, C₂H₄) yields which is in contrast to the previous studies reported in Table S1. This renders the use of TGA without adequate heating rate and weight loss measurements limited in its scope for understanding the molecular level interactions

of biomass components¹⁹. Therefore, a critical analysis of the limitations of equipment used, feed and pyrolysis temperatures are to be carefully considered to draw inferences about intrinsic chemistry from experiments.

Supporting this conclusion, lately many studies (Table S2) have suggested interactions between the biomass components and the failure of superposition/additive models in calculating product distributions. Using an ampoule reactor at gasification temperatures (600 C, 800 C), Hosaya et al.^{143,231} showed that the simple additive law is not sufficient to explain water soluble sugar fraction and secondary char formation. This deviation from the additive model indicating interactions during pyrolysis appear to occur in the solid, liquid and vapor phases increasing the gasification of cellulose-derived products. Spruce and beech wood (~50% cellulose) produced less than 3% levoglucosan (LGA)¹⁴⁵ while the cellulose content in them can produce 48% yield when pyrolyzed separately¹⁸. This change in kinetics with respect to pure cellulose is also noticed in the pyrolysis of synthetic biomass with cellulose and lignin mixtures made with different mixing methods at a wide temperature range^{131,132}. The reaction rates slow down suggesting that lignin inhibits cellulose pyrolysis and has a negative effect on volatiles formation¹³³. However, such a deviation in the kinetics between the pyrolysis of pure cellulose and of native/synthetic biomass is only noticed in a particular temperature window. This can possibly be explained by the overlapping of biopolymer decomposition temperatures in the pyrolytic melt. Biomass pyrolysis process involves – moisture evolution (<220°C), hemicellulose decomposition (220-315°C), cellulose decomposition (315-400°C) and lignin decomposition (>400°C)²²³. Though the three biopolymers decompose at different rates and in different temperature ranges, there is significant overlap. Higher interactions between cellulose and lignin are reported because of the overlap in the temperature range (313-438°C) at which the maximum weight loss rate for lignin and cellulose occur. Below and above the cellulose decomposition temperature, the product distribution of both synthetic and native mixtures matches additive model predictions, indicating no interactions¹⁸. This splits biomass pyrolysis into three kinetic temperature regimes where pyrolytic interactions between biopolymers is only present in regime 2 (313-438°C)¹⁴⁷. Before cellulose decomposition, in regime 1 (220-305°C), hemicellulose decomposes while lignin and cellulose pyrolyze to its oligomers without any thermal interactions. Likewise, in regime 3 (>438°C), cellulose is pyrolyzed leaving lignin to its slow

decomposition with no interactions. However, in regime 2, cellulose is reported to de-crystallize to an amorphous “liquid phase” (*melt-phase*) beyond 230°C²³². Similarly, lignin takes a “liquid-like phase” with the units redistributed and reallocated above the glass transition temperature (50-150°C). This overlap in regime 2 (313-438°C) could lead to CH- π interactions between cellulose and lignin, enhancing lignin-derived products such as phenolics^{140,146}. These observations highlight that in the pyrolytic *melt-phase*, interactions between the biopolymers indeed exist but in a narrow temperature range with the overlapping of cellulose and lignin decomposition. Therefore, this paper is focused on the influences of lignin on cellulose decomposition.

Previous studies have also shown that in addition to temperature, the feedstock also influences the validity of the additive models. Product yields from the pyrolysis of woody biomass differ from that of herbaceous biomass¹⁹. Herbaceous biomass (cornstover, switchgrass) and woody biomass (pine, redwood) were chemically treated to isolate hemicellulose. The treated herbaceous cellulose-lignin when pyrolyzed, produced a lower LGA yield of 10.28 wt%, compared to clean cellulose. The offset in LGA yield is compensated by 11.38 wt% and 1.45 wt% increase in C₁ to C₃ products and furans, respectively. However, for the pyrolysis of woody biomass, despite the higher lignin content compared to herbaceous biomass, the deviation in pyrolysis product distribution from pure cellulose is minimum. This variation between herbaceous and woody biomass was speculated to be because of higher lignin carbohydrate complex (LCC) linkages. In the cell wall, some cellulose and lignin are covalently bonded by ester/ether linkages^{154,233,234} forming LCCs¹⁶⁸. Predominant of the studies^{235,236} have reported LCC linkages in the C₆ position (refer Scheme 3.1). This would be coherent with reduced LGA yield as similar inhibition of LGA has been shown in polysaccharides with 1,6-glycosidic linkages (similar to LCC linkages) compared to 1,4- or 1,3-glycosidic linkages⁶⁸. Moreover, the oxygen containing covalent linkages between cellulose and lignin in cornstover and *A. cunninghamii* wood were measured using an isotope method and indeed herbaceous biomass was found to have higher LCC linkages compared to woody biomass²³⁷. Covalent bonding between lignin and cellulose in LCC could very well explain the difference between the pyrolysis of herbaceous and woody biomass. Therefore, it is important to consider LCCs while studying pyrolysis of native biomass or co-pyrolysis of cellulose and lignin. However, fewer LCC covalent bonds alone cannot explain the little influence of lignin

molecules in pyrolysis of the woody feed. This highlights the competition between glycosidic C-O bond cleavage (forming LGA) and C-C bond cleavage (forming furans & C₁-C₃ products) in cellulose pyrolysis^{68,74,238}. The high lignin content in woody biomass is known to cause micro-explosions and thermal ejection of cellulose intermediates which promotes deoxygenation of heavy compounds and hinder char formation¹⁶¹. This reduction in char yield is suggested to indicate the inhibition of dehydration reactions in cellulose with high lignin composition. Also, the char exhibits an enhanced development of porous structures in the pyrolysis of maple wood indicating the stabilization of lignin intermediates in the *melt-phase*³⁴. For this to happen under pyrolysis conditions, hydrogen rich cellulose products will have to escape through the interface between cellulose bundles and lignin, in the process of interacting and stabilizing lignin reactive intermediates. Such stabilization of lignin intermediates and inhibition of oligomerization by in-situ hydrogen sources (formic acid functional group) have been reported^{162,163}. Therefore, thermal interaction of high composition lignin and cellulose promoted LGA formation and weakened competing pathways such as dehydration, which form char precursors^{34,164}.

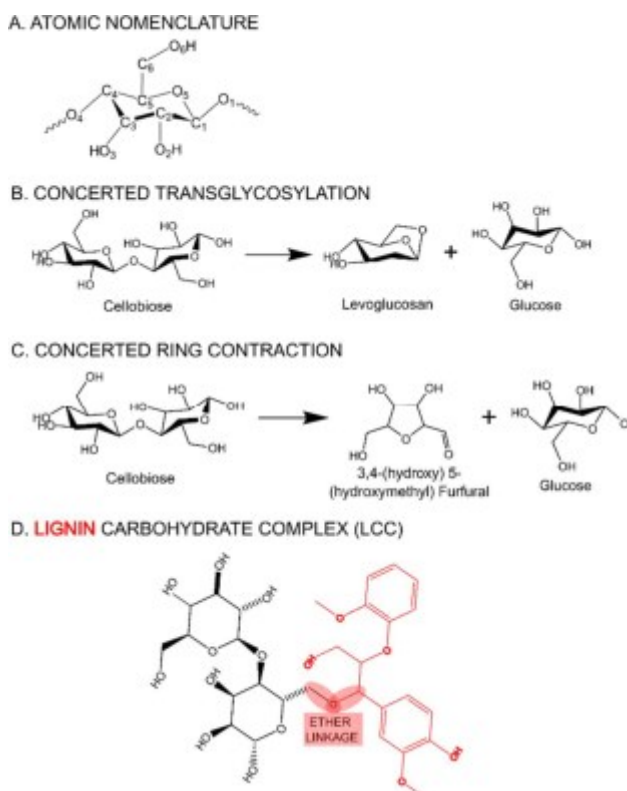
Summarizing the literature, it can be said that in the biomass matrix, cellulose exists in bundles (microfibrils) that are held together by lignin, which are connected by LCC linkages. But when pyrolyzed, the microscopic architecture in the cell wall breaks down to form a “liquid-like” phase with the surface lignin melting first and covering the microfibrils³⁴. This liquid intermediate ‘*melt-phase*’ has been shown for cellulose pyrolysis using high speed photography²³⁹. Moreover, cellulose intermediates have been speculated to escape through interacting with lignin before decomposition. During the pyrolysis of native biomass, cellulose chemistry is influenced by covalent bonding in LCCs or high lignin composition. Therefore, two lignin-cellulose ‘*melt-phase*’ environments are modelled in this work to investigate the effect of lignin on cellulose condensed phase pyrolytic decomposition –

Melt-phase with LCCs – The system has LCC linkages between cellulose surrogate (cellobiose) and lignin surrogate (quinone methide intermediate) and 12 cellobiose molecules (*c.f.* Figure 3.1A).

Melt-phase with high lignin composition (lignin-rich) – Reacting cellobiose molecule surrounded by lignin dimer (quinone methide intermediate) molecules (*c.f.* Figure 3.1B).

Key knowledge gaps that we attempt to bridge in this paper are – 1. Does the presence of lignin in the condensed phase influence cellulose decomposition energetics in native biomass *melt-phases*? 2. Can the presence of LCC linkages or high lignin content explain the variation in product distribution between woody and herbaceous feed? 3. Is furan (C-C cleavage) or LGA (C-O cleavage) formation in cellulose pyrolysis promoted due to the non-bonded, condensed phase interactions with lignin?

Scheme 3.1 (A) Atomic nomenclature of the monomeric glucose unit (B) Transglycosylation reaction mechanism of cellobiose decomposition to form LGA (C) Ring contraction mechanism of cellobiose decomposition to form furanic compounds (D) LCC linkage between a lignin moiety (quinone methide intermediate) and the cellobiose dimer.



3.2 Computational Methodology

A novel computational strategy (ReSolv method) was introduced and exemplified in our previous work²⁴⁰. This strategy employs a combination of quantum mechanics (QM) and molecular mechanics (MM) approaches to circumvent the computationally expensive *ab initio* molecular dynamics (AIMD) calculations. Activation free energy barriers are calculated in the gas phase using QM based density functional theory (DFT) methods. This gas phase free energy is further corrected to account for the finite temperature condensed phase using MM based equilibrium solvation for the reactant and TS. The free energy of interaction in equilibrium solvation is computed using Thermodynamic Integration techniques²⁴¹. The specific methodology is further elaborated in Section 3.2.1.

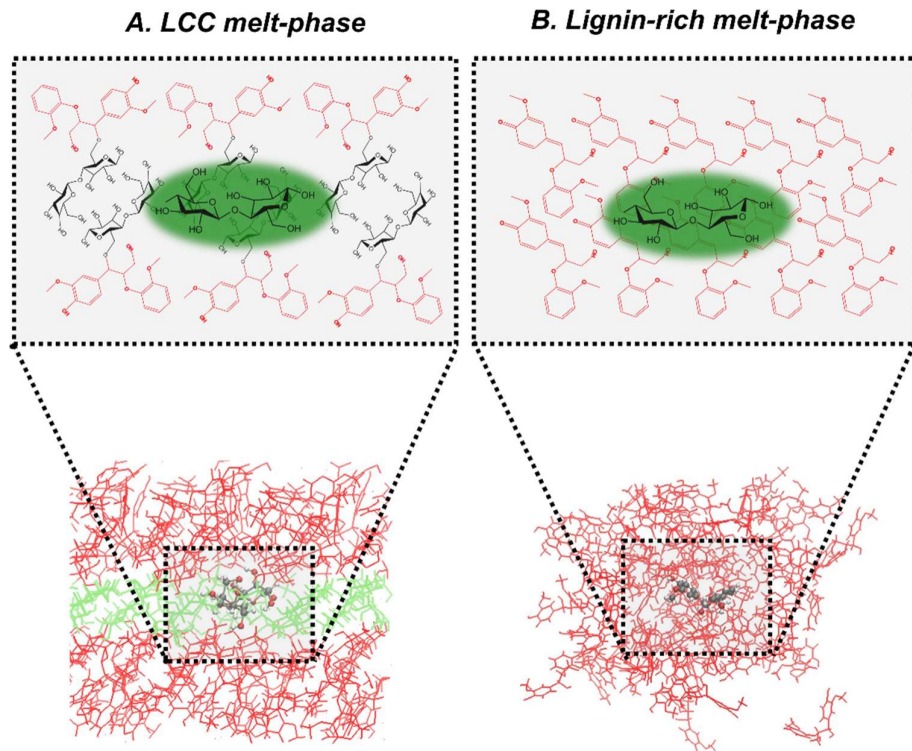


Figure 3.1 Molecular visualization and zoomed-in chemical structure schematic of the A) LCC melt-phase with lignin dimers (red) and the cellobiose dimers (black) connected covalently, and B) lignin-rich melt-phase. In either system, one reacting cellobiose molecule for which the reaction energetics are calculated is shown in a green bubble (ball and stick representation in the bottom molecular visualization), surrounded by lignin, which is not covalently bonded to cellobiose.

Several studies used cellobiose as a model molecule to propose a 2-step mechanism for levoglucosan formation¹¹¹, demonstrated the energetic favourability of concerted mechanisms²⁴², investigated the catalytic effects of inorganic compounds²⁰⁴, and explored the impact of the three-dimensional hydroxyl environment on activation dynamics²¹². Therefore, cellobiose is used as a model and the nomenclature in Scheme 3.1A will be followed throughout the manuscript. The equilibrium solvation method (ReSolv) is used to calculate the free energy barriers for cellulose decomposition via transglycosylation and ring contraction mechanisms (refer Scheme 3.1B, 1C). Two ‘*melt-phase*’ systems with lignin have been modelled to capture their respective condensed phase effects on cellulose chemistry – 1. with LCCs and 2. with high lignin composition. The results are also compared to the ‘*melt-phase*’ system with pure cellulose from our previous work.

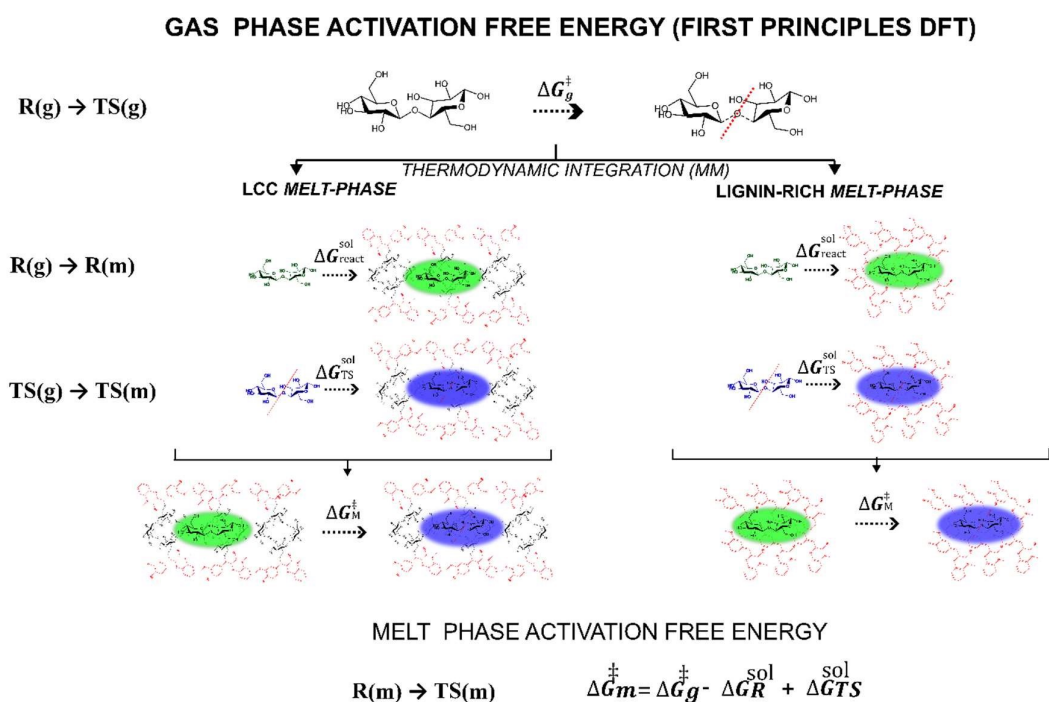


Figure 3.2 Computational workflow for correcting gas phase free energies using equilibrium solvation free energy to account for finite temperature condensed phase effects. This is followed for both the melt-phase with LCCs (left) and the melt-phase with high lignin concentration (right) systems.

3.2.1 Free energy barrier corrections based on equilibrium solvation in the condensed phase.

The formulation of this novel technique to calculate free energy barriers in condensed phase, involves the dissociation of the reaction into multiple associated reactions in a Bordwell thermodynamic cycle²⁴³ (c.f. Figure 3.2). First, the activation free energy (ΔG^\ddagger) for a particular reaction mechanism is calculated using gas phase DFT. Then, the reaction intermediates (reactant and transition state) from the gas phase calculations are constrained and transferred into the *melt-phase* system. These *melt-phase* systems are constructed to capture explicit finite temperature condensed phase effects on the intermediates. So, thermodynamic integration method^{155,207} is used to calculate the equilibrium solvation free energies (ΔG^{sol}) of the reaction intermediates in the *melt-phase* system. The difference between the solvation free energy of the transition state (ΔG_{TS}^{sol}) and of the reactant (ΔG_{react}^{sol}) is the *melt-phase* correction factor. This *melt-phase* correction factor ($\Delta G_{TS}^{sol} - \Delta G_{react}^{sol}$) is further added to the DFT calculated gas phase barrier (ΔG^\ddagger), to estimate the free energy barrier in the *melt-phase* (ΔG_m^\ddagger). This correction factor is unique to the particular reaction mechanism and the *melt-phase* system. The specific methods used for gas phase, equilibrium solvation and post-processing calculations are mentioned below.

3.2.1.1 Gas phase

All-electron DFT calculations were performed using Gaussian 09 code for the cellobiose molecule in gas phase. Hybrid functional M06-2X 76 with 6-31+G(2d,p) basis set is used as it has been recommended for carbohydrate chemistry^{242,244–246}. Geometry optimizations and TS searches performed using Berny algorithm were unconstrained. Subsequently, frequency calculations are performed to distinguish between the saddle point and local minima. Intrinsic reaction coordinates (IRCs) are followed in both directions to ensure that the TS corresponds to the correct reactant and product on the potential energy surface. These barriers are calculated at 1 atm and four temperatures (100K, 500K, 900K, 1200K). Free energy barriers computed in the gas phase for cellobiose activation via transglycosylation and ring contraction have been reported in our previous work²⁴⁰.

3.2.1.2 Equilibrium solvation

Thermodynamic integration (TI) method^{241,247} as implemented in GROMACS 2018.7, is used to calculate the equilibrium solvation free energy at four temperatures (100K, 500K, 900K, 1200K) for the two biomass *melt-phase* systems (*c.f.* Figure 3.2). The selection of temperature range encompasses both, the investigation of crystal structure effects (100K) and the comprehensive range for thermochemical conversion of biomass (473-1273K), as inferred from an extensive analysis of previous studies and the corresponding peak reactor temperatures²⁴⁸. The reactant and TS coordinates from gas are constrained and inserted in the *melt-phase* system. Langevin dynamics is used along with OPLS/AA force-field parameters. The initial system configurations are first energy optimized and equilibrated. Pressure equilibration is performed in an NPT ensemble at 1 atm for 2 ns and the resulting configurations are used to set the appropriate system volume/phase. TI calculations are then carried out in an NVT ensemble for 8 ns at respective temperatures. The number of intermediate states (λ -windows) is optimized, and 30 λ -windows was found to be sufficient. The potential derivatives calculated from the MD simulations for each λ -window are integrated to compute ΔG^{sol} .

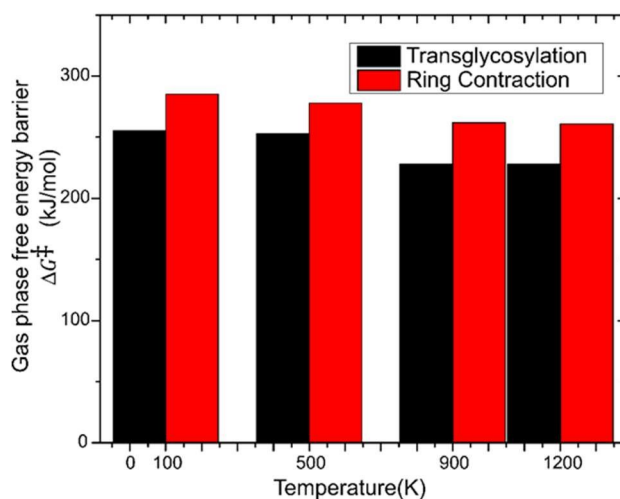


Figure 3.3 Gas phase free energy barrier for glycosidic bond activation in cellobiose at different temperatures calculated using hybrid functional M06-2X with 6-31+G(2d,p) basis set (reported in earlier publication²⁴⁰)

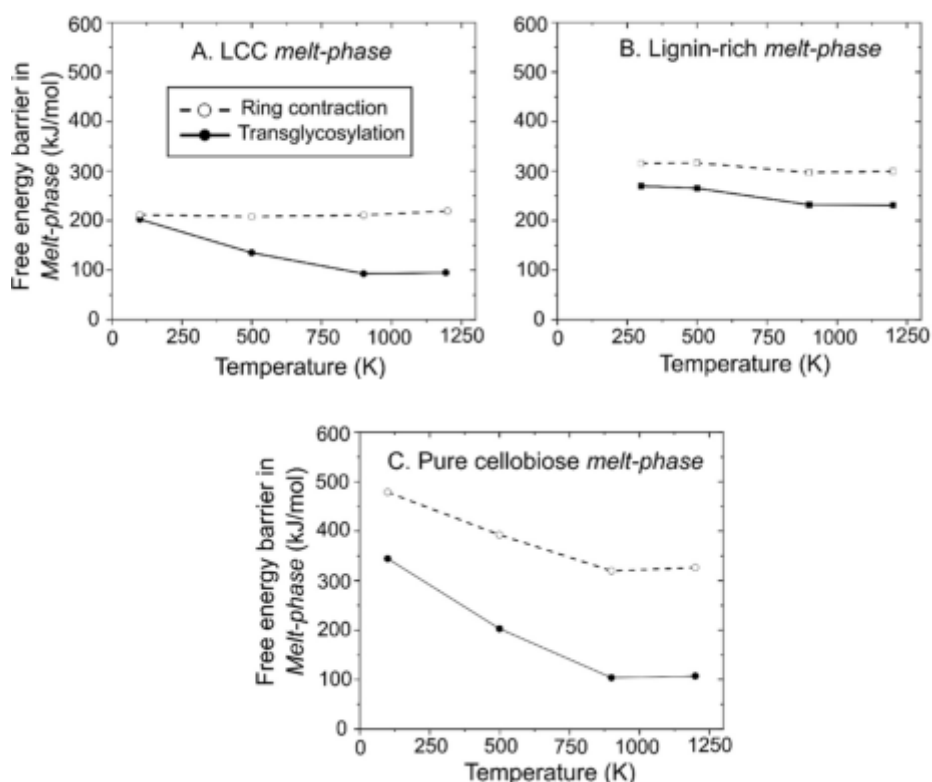


Figure 3.4 Free energy barriers for cellulose decomposition via transglycosylation and ring contraction mechanisms at different temperatures in A) LCC melt-phase and B) lignin-rich melt-phase C) pure cellobiose melt-phase.

3.3 Results and Discussions

Under pyrolysis conditions, cellulose is reported to decompose via competing glycosidic C-O bond cleavage (LGA formation) and C-C bond cleavage (furan, C₁- C₃ products). Hence, the most favorable cellobiose activation mechanisms are simulated – Transglycosylation and ring contraction¹¹³. In transglycosylation mechanism, the C₁-O₁ bond is simultaneously cleaved as the hydrogen from hydroxymethyl tail protonates it, making a C₆-O₆-C₁ bridge (Scheme 3.1B) to form LGA and glucose. Ring contraction is also a concerted mechanism involving C-C bond cleavage and ring reorganization (Scheme 3.1C) to form 3,4-(hydroxyl) 5-(hydroxymethyl) furfural and glucose. Finally, molecular interactions that affect cellobiose chemistry in the condensed phase are

investigated and delineated using hydrogen bonding analysis and hydroxymethyl group orientations.

Table 3.1 Enthalpic and entropic contribution to the free energy for cellobiose activation at the low and high temperature regimes in the interfacial LCC melt-phase.

<i>Melt-phase</i>	Mechanism	Thermal regime	Enthalpic contribution to the free energy (kJ/mol)	Entropic contribution to the free energy (kJ/mol/K)
LCC	Transglycosylation	< 800K	212.13	-0.1372
		800-1200K	86.98	0.0065
	Ring-contraction	< 800K	210.92	-0.0011
		800-1200K	185.60	0.0282
Pure Cellobiose	Transglycosylation	< 800K	389.45	-0.3347
		800-1200K	82.14	0.0106
	Ring-contraction	< 800K	468.73	-0.2331
		800-1200K	237.71	0.0219

3.3.1 Free energy barriers for competing cellulose decomposition reactions in the *melt-phase* using the ReSolv method

As described in Section 3.2, DFT calculations were first performed to determine the free energy barriers in the gas phase (Figure 3.3). The barrier for transglycosylation reduces from 255.16 kJ/mol at 100K to 227.88 kJ/mol at 1200K; whereas for ring contraction mechanism, it reduces from 285.16 kJ/mol at 100K to 260.87 kJ/mol at 1200K. Transglycosylation is slightly favoured over ring contraction in the gas phase at all temperatures, in agreement with previous DFT studies^{113,240}. Figure 3.3 shows a drop in the activation free energy barrier above 500K for the breakdown of an isolated cellobiose molecule. This drop indicates that gain in configurational entropy by breaking intramolecular hydrogen bonds play a role in bringing down the barrier.

3.3.1.1 Cellobiose Decomposition in melt-phase with LCCs

The melt-phase system with LCCs was modelled as shown in Figure 3.1A. The free-energy barrier for transglycosylation (C-O cleavage) and ring contraction (C-C cleavage) mechanisms in the LCC *melt-phase* environment is shown in Fig 4A. The free energy barrier for transglycosylation decreases with temperature from 202.62 kJ/mol at 100K to 94.82 kJ/mol at 1200K. The drop in activation free energy barrier plateaus beyond 800K (~100kJ/mol). Such a trend is not noticed for ring contraction and the free energy barriers remained between 200-220 kJ/mol at all temperatures. The barrier dropped by 107.8 kJ/mol between 100K-1200K for transglycosylation while in the same interval, the barrier increased by 7.56 kJ/mol for ring contraction. This reveals that the activation free energy is significantly influenced by the finite temperature for transglycosylation in the melt phase environment with LCCs. This significant reduction in the activation barriers points to a reaction regime change and such a change has been reported in our previous work²⁴⁰ for both decomposition reactions (transglycosylation and ring contraction) in pure cellulose *melt-phase* (*c.f.* Figure 3.4C). Contrarily, ring contraction mechanism in the LCC *melt-phase* does not exhibit such entropy driven regime change which will be discussed further in Section 3.3.2.

The slope and intercept of the free-energy profiles provide the activation entropy (ΔS^\ddagger) and enthalpy (ΔH^\ddagger), respectively. The entropic and enthalpic barriers calculated from Figure 3.4A for cellobiose decomposition in the LCC *melt-phase* have been compiled in Table 3.1. For transglycosylation mechanism, the entropic contribution (ΔS^\ddagger) to the free-energy barrier is higher (-0.1372 kJ/K/mol) at lower temperatures (<800K) which then shifts to a negligible value (0.0065 kJ/K/mol) at higher temperatures. There are two distinct reaction regimes transitioning around 800K, similar to what was observed in the millisecond scale kinetic experiments conducted for pure cellulose in the absence of lignin^{128,194}. The enthalpic barrier (ΔH^\ddagger) for transglycosylation (*c.f.* Table 3.1) shifts from 212.13 kJ/mol at low temperatures (<800K) to 86.98 kJ/mol at higher temperatures (800K-1200K). Therefore, two reaction regimes have been identified – 1. High activation enthalpy and free-energy barrier at low temperatures (500K-800K), 2. Low activation enthalpy and low free-energy barrier at high temperatures (800K-1200K). For ring contraction mechanism however, as temperature doesn't have a major influence on the reaction energetics in the LCC melt-phase (*c.f.* Figure 3.4A), changes in entropic enthalpic contributions are negligible. The entropic contribution (ΔS^\ddagger) to the free-energy barrier barely changes with temperature (-0.0011 kJ/K/mol to 0.0282 kJ/K/mol). Similarly, the change in enthalpic barrier (ΔH^\ddagger) is also small, from 210.92 to 185.6 kJ/mol (Table 3.1). The free-energy barriers for ring contraction are higher than transglycosylation throughout the temperature range (100K-1200K). Only few computational studies have focused on understanding the role of lignin in cellobiose activation and none have the condensed phase effects because of LCCs. Therefore, comparisons are made with reaction barriers calculated in pure cellulose systems. Similar low free-energy barriers have been reported earlier using accelerated AIMD simulations at 873 K for pre-LGA formation (151 kJ/mol) and pre-HMF (furanic) (205 kJ/mol) formation⁵². These ab-initio barriers are in coherence with the high temperature (900K) free-energy barriers calculated in this study for LGA formation (92.856 kJ/mol) and furan formation (210.976 kJ/mol).

3.3.1.2 Cellobiose Decomposition in lignin-rich *melt-phase*

Figure 3.4B shows the free energy barriers for transglycosylation and ring-contraction reactions of cellobiose in the *melt-phase* environment with high lignin composition, but without covalent LCC linkages. For transglycosylation mechanism, the free energy barrier drops from 269.96 kJ/mol to 231.26 kJ/mol between 300K-1200K. Similarly, for the ring contraction mechanism, the barrier drops from 315.68 kJ/mol to 299.73 kJ/mol in the same temperature range. These small change in barriers (transglycosylation - 38.7 kJ/mol and ring contraction - 15.97 kJ/mol) in the lignin melt-phase is comparable with the change in gas phase barriers (transglycosylation- 27.29 kJ/mol and ring contraction - 24.29 kJ/mol). They follow the same trend as gas phase barriers with no significant change in reaction kinetics. Also conforming to other melt-phase environments (with LCC and pure cellobiose), transglycosylation (C-O bond cleavage) is favored over ring contraction (C-C cleavage) even in the lignin-rich *melt-phase*. However, unlike the large temperature driven promotion of transglycosylation in the LCC *melt-phase* (Figure 3.4A), thermal and condensed phase effects are negligible for either mechanism in the lignin-rich *melt-phase* (Figure 3.4B). This could be because of the absence of a thermal change in the melt phase environment, as was reported for pure cellulose systems^{99,240}. The large entropic contributions to the free-energy barrier gained by the thermal shift in the pure cellobiose *melt-phase* and in LCC melt-phase is not present in the lignin-rich *melt-phase*, making it an enthalpy-controlled regime ($\Delta G_m^\ddagger \approx \Delta H_m^\ddagger$). Cellobiose decomposition energetics in two distinct condensed phase environments containing lignin – 1. LCC *melt-phase*, 2. Lignin-rich *melt-phase* (high lignin content) have been presented here for the first time. The finite temperature condensed phase effects have a significant impact only for transglycosylation reaction mechanism in the LCC *melt-phase*. Such significant influence (unlike that in pure cellobiose environment, Figure 3.4C) is not observed for transglycosylation in the lignin-rich *melt-phase* or ring contraction mechanism in either *melt-phase* environments.

3.3.1.3 Comparison with cellobiose decomposition kinetics in the absence of lignin

In pure cellobiose condensed phase environment, the free energy barrier for both transglycosylation and ring contraction mechanisms decrease significantly with the

increase in temperature. This leads to two thermal reaction regimes with different enthalpic barriers transitioning above 800K²⁴⁰. These enthalpic (ΔH_m^\ddagger) and the entropic contributions (ΔS_m^\ddagger) to the free-energy barrier in the high and low temperature regimes have been published in our previous work and are compiled in Table 3.1. The enthalpic barrier (ΔH_m^\ddagger) (Table 3.1) for transglycosylation shifts from 389.45 kJ/mol at low temperatures (500K-800K) to 82.14 kJ/mol at higher temperatures (800K-1200K). Similarly, for ring contraction it shifts from 468.73 kJ/mol to 237.71 kJ/mol in the low and high temperature regimes. The temperature induced drop in the free energy barrier is due to entropic contributions from the increased degree of freedom within the cellobiose *melt-phase*. The rapid formation of *melt-phase* (from cellobiose crystalline phase) has shown to decrease intra-sheet hydrogen bonding⁹⁹ amongst cellobiose molecules. This leads to increased access to the boat conformation in cellobiose residues. The change from chair to boat conformation is a necessary step for glycosidic bond activation and easier access to this boat conformer would be expected to reduce the activation barrier. Change in conformation was suggested to be the primary mode of cellulose activation as compared to catalytic activation by vicinal hydroxyl groups¹²⁹. Analysis of cellobiose decomposition in its own *melt-phase* in the absence of lignin also suggested that the conformational entropy (higher degrees of freedom) gained with breaking hydrogen bonds between the pyrolytic condensed phase (*melt-phase*) and the reactant was a key factor²⁴⁰. Such rapid change in the reaction environment and the corresponding thermal regime change or *melt-phase* (condensed phase) induced promotion/inhibition of reaction mechanisms is not seen in the lignin-rich *melt-phase, without LCC linkages*. The hydrophobic cellobiose molecule have negligible interactions with the aromatic molecules in the lignin-rich *melt-phase*. The lignin-rich environment does not exhibit the drastic decrease in the density, as seen in pure cellobiose environments to alter cellobiose reaction chemistry. The free energy barrier profile in the lignin-rich *melt-phase, without LCC linkages* (c.f. Figure 3.4B) can be correlated to hydrophobicity and the lack of interactions between the cellobiose and the surrounding lignin condensed phase.

Two primary cellobiose decomposition reaction mechanisms have been investigated in pure cellobiose and in melt-phase environments in the presence of lignin (with and without LCC linkages). Scheme 3.2 summarizes if finite temperature *melt-phase* effects significantly alter cellulose activation via transglycosylation and ring contraction in these systems. To further understand molecular interactions that lead to shifts in reaction energetics, they are correlated to changes in the *melt-phase*. The lignin containing *melt-phase* environments are studied in detail using distributions of hydrogen bond and hydroxymethyl group orientations to develop a molecular interpretation of the energy diagrams and are presented below.

Scheme 3.2 Schematic showing which melt-phase environments significantly alter cellobiose decomposition reaction kinetics with respect to temperature.

	Melt-phase w/ pure Cellobiose	Melt-phase w/ LCC	Melt-phase w/ high lignin composition
Transglycosylation	Significantly altered reaction kinetics with temperature	Significantly altered reaction kinetics with temperature	Minimal change in reaction kinetics with temperature
Ring contraction	Significantly altered reaction kinetics with temperature	Minimal change in reaction kinetics with temperature	Minimal change in reaction kinetics with temperature

3.3.2 Molecular level explanation of *melt-phase* effects on reaction kinetics

Multiple works^{99,198,202} studying the thermal behaviour of bulk cellulose and its oligomers have reported change in density, dipole moment, dielectric constant, torsional entropy, thermal expansion coefficient, hydrogen bonding and IR spectrum above 450-500K. Despite this, to the best of our knowledge, no one has investigated if these thermal responses are also exhibited in the presence of lignin in the biomass matrix. The branched phenolic polymer lignin could distort the organized hydrogen bonding network of polysaccharide cellobiose systems even at lower temperatures and suppress the rapid thermal expansion at high temperatures. This would limit the drastic changes in phase with temperature and in turn may limit its role in cellobiose reaction chemistry. To investigate this, first the molecular level interactions of the condensed phase with the reacting species for the transglycosylation mechanism are analyzed and then it is

extended to the ring contraction mechanism. The activation free energy barriers at different temperatures, relative to the barrier corresponding to 1200K (Figures 3.5A, B), are reported and are correlated to the average number of hydrogen bonds between the reacting species and the *melt-phase* environment (Figures 3.5C, D).

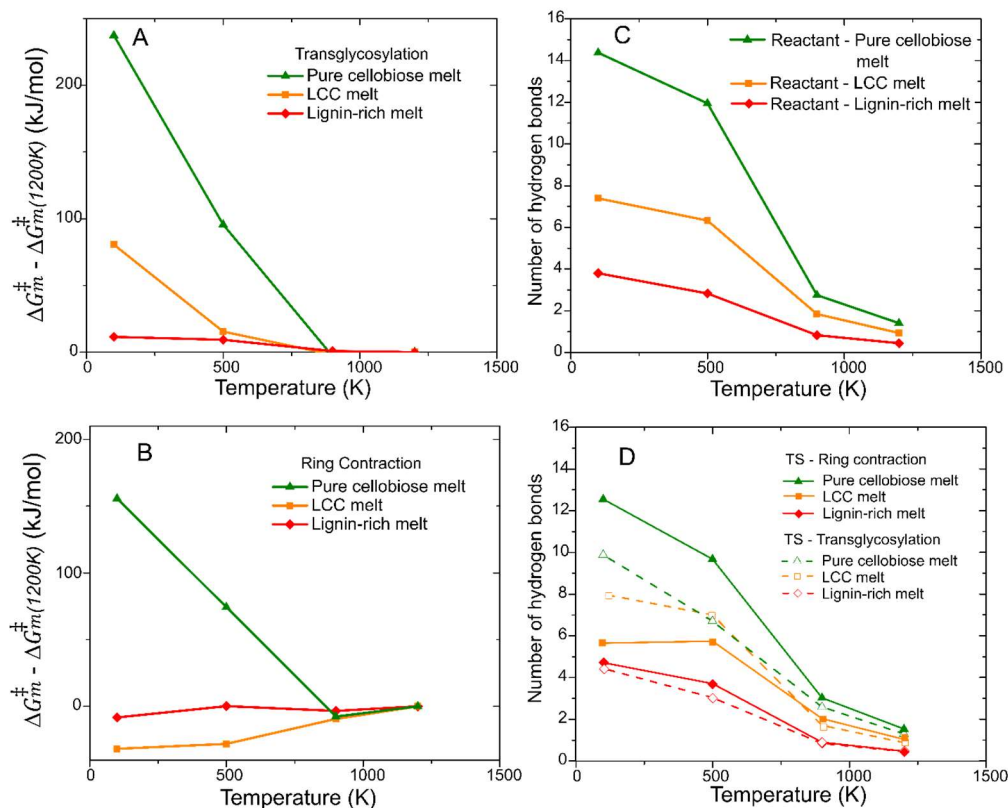


Figure 3.5 Relative free-energy barrier for cellobiose activation in the melt-phase via (A) transglycosylation mechanism (with respect to the barrier at 1200K) and (B) ring contraction mechanism (with respect to the barrier at 1200K). Average number of intermolecular *hydrogen bonds made by the* (C) *reactant with the three melt-phases* (D) *TS of ring contraction (solid line) and transglycosylation (dash line) with the melt-phases.*

Also, the distribution of these hydrogen bond distances (Figure 3.6A) and the distribution of hydroxymethyl group orientation for cellobiose (Figure 3.6B) in the LCC *melt-phase* are calculated to substantiate the destabilizing effect as a function of temperature. Further, this is compared to hydrogen bond distances (Figure 3.6C) and hydroxymethyl group orientation distribution (Figure 3.6D) in pure cellobiose *melt-phase*. These plots reveal the temperature induced changes in the *melt-phase*, and in turn the local reaction environment, that influences reaction energetics. Lastly, molecular level explanation of

the role played by lignin in cellulose decomposition chemistry via altering the high temperature condensed phase environment is discussed and compared to reported experimental findings.

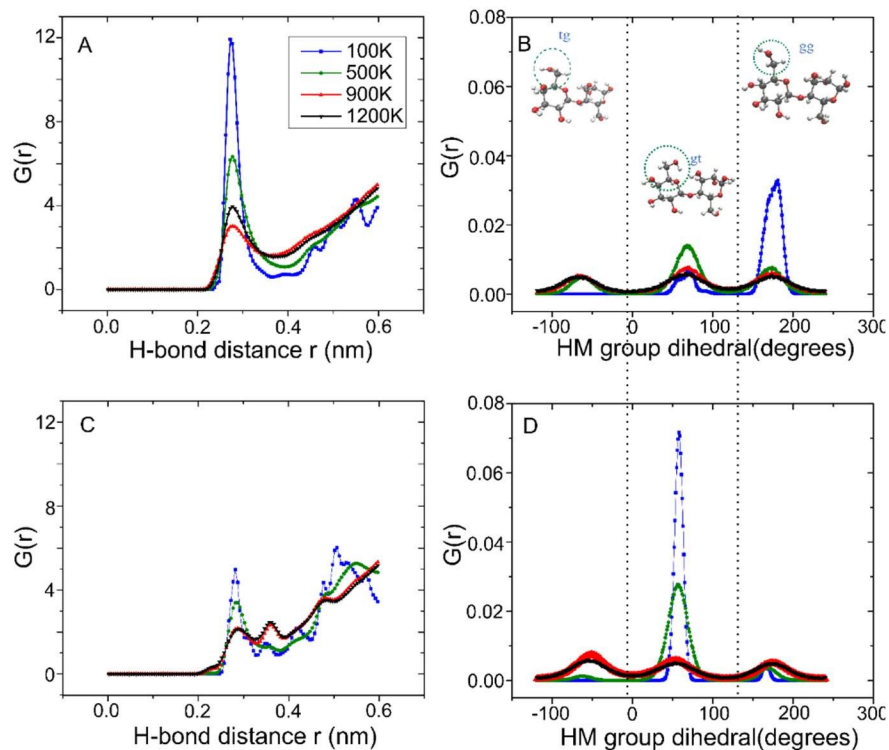


Figure 3.6 (A) Distribution of O–O distance in intermolecular hydrogen bonds between reacting cellobiose molecule and the LCC melt-phase at 100 K, 500 K, 900 K and 1200 K; (B) Distribution of hydroxymethyl group dihedral angles in free cellobiose molecules (not directly covalently bonded to lignin dimer) at 100 K, 500K, 900 K and 1200 K; (C) Distribution of O–O distance in intermolecular hydrogen bonds between reacting cellobiose molecule and the pure cellobiose melt-phase at 100 K, 500 K, 900 K and 1200 K; (D) Distribution of hydroxymethyl group dihedral angles in all cellobiose molecules in the pure cellobiose melt-phase at 100 K, 500K, 900 K and 1200 K.

3.3.2.1 Thermal changes in the condensed phase directly influencing reaction energetics

To analyse *melt-phase* effects, free-energy barriers for transglycosylation mechanism, relative to those at 1200 K in the same *melt-phase* (*c.f.* Figure 3.5A) are reported here. This is done to highlight the thermal influence that alters phase change and affects cellobiose activation. While the free energy for cellobiose activation drops via

transglycosylation by 237.3 kJ/mol in the pure cellobiose melt between 100-1200K, it only reduces by 80.52 kJ/mol and even lower by 11.42 kJ/mol in the *melt-phase* with LCCs and without LCCs (lignin-rich), respectively. This trend is also clearly followed by the drop in the number of intermolecular hydrogen bonds made by the reactant with the surrounding *melt-phase* environment (*c.f.* Figure 3.5C). The number of intermolecular hydrogen bonds made by the reactant cellobiose between 100K-1200K drops by 12.97, 6.45 and 3.36 in the pure cellobiose, LCC and lignin-rich *melt-phases*, respectively. This correlation suggests that the disruption of hydrogen bonds has a direct impact on cellobiose activation via transglycosylation in the pyrolytic *melt-phase*. Similarly, for the ring contraction mechanism, free-energy barriers relative to those at 1200 K in the same *melt-phase* (*c.f.* Figure 3.5B) are reported along with the number of intermolecular hydrogen bonds formed by the TS of both mechanisms with the condensed phase (*c.f.* Figure 3.5D). While in the pure cellobiose melt, the free energy for cellobiose activation via ring contraction drops by 155.6 kJ/mol between 100K-1200K, it marginally increases by 31.85 kJ/mol and by 8.33 kJ/mol in the LCC and lignin-rich *melt-phases*, respectively. The trend in pure cellobiose melt phase and in the lignin-rich melt phase agrees with that observed for transglycosylation (*c.f.* Figure 3.5A). However, in the LCC melt-phase, cellulose activation via ring contraction exhibits little change with temperature. The number of intermolecular hydrogen bonds (*c.f.* Figure 3.5D) made by the TS for ring contraction between 100K-1200K drops by 11.02, 4.25 and 4.61 in the pure cellobiose, LCC and lignin-rich *melt-phases*, respectively. Similarly, the drop in hydrogen bonds with the TS for transglycosylation are 8.58, 7.12 and 3.99 in the pure cellobiose, LCC and lignin-rich *melt-phases*, respectively. While the drop in hydrogen bonds with the TS of ring contraction is smaller in the LCC melt-phase, as compared to that in transglycosylation, the trend doesn't directly correspond to that of relative activation free energy barriers (*c.f.* Figure 3.5B). The drop in hydrogen bonds with the TS suggests that there isn't a preferential stabilization of the TS by vicinal hydroxyl groups forming hydrogen bonds, as reported by some studies¹²⁹.

Cellobiose forms intramolecular hydrogen bonds ($O_5 \dots H \dots O_6$) between the ring oxygen and the hydroxymethyl (HM) group of the neighboring residue. As this hydrogen bond breaks, the molecule gains torsional freedom for conformational change and the HM

group interacts with the glycosidic oxygen initiating transglycosylation mechanism. The reduction in the number of intermolecular hydrogen bonds with respect to temperature in all *melt-phases* indicate the complete disruption of hydrogen bonding network. This hydrogen bonding network has been reported to be ordered and long-range in the pure cellobiose *melt-phase*. While in the lignin-rich *melt-phase* (c.f. Figure 3.5C), hydrogen bonding doesn't seem to be predominant, showing it's not a significant mode of interaction between the reactant cellobiose and the lignin-rich *melt-phase*, *without LCC*. Lignin undergoes phase transition at lower temperatures (323K-423K) compared to cellobiose (450K-500K) but the lignin-rich *melt-phase* does not undergo the vast change in hydrogen bonding, as observed in pure cellobiose *melt-phase*. This could be because of the large unidirectional network of hydrogen bonds formed in cellobiose crystal structure at low temperatures which is not available for the lignin-rich *melt-phase*. This lack of significant hydrogen bonding in lignin-rich *melt-phase* even at 100K seems to explain the corresponding minimal change in cellobiose activation barrier with temperature (Figure 3.4B). To further validate if changes in the LCC *melt-phase* correspond to changes in reaction energetics, the hydroxymethyl (HM) group and hydrogen bond distributions are calculated and compared to those in pure cellobiose *melt-phase* (c.f. Figure 3.6). Hydrogen bonding in cellobiose and LCC molecules is predominantly facilitated by the hydroxyl groups (-OH). The resulting distribution of O-O distances within these different hydrogen bonds have been plotted in Figure 3.6A and 6C. Just like the drop in the number of intermolecular hydrogen bonds (c.f. Figure 3.5A), the hydrogen bond distance distribution also shows a decrease in peak intensity with increase in temperature from 100K to 1200K. Despite this decrease, the hydrogen bond length remains at 0.35 nm (c.f. Figure 3.6A). This is different than what is observed in the pure cellobiose *melt-phase* (c.f. Figure 3.6C)²⁴⁰, where the hydrogen bond distribution peaks are much smaller and shift from shorter (<3.5 Å) to longer (>3.5 Å) hydrogen bonds at higher temperatures. As the cellobiose molecule gains torsional freedom with breaking hydrogen bonds, the HM group shifts orientation making it a good measure of conformational change from chair to boat. As shown in Figure 3.6B, at 100K in the LCC *melt-phase*, the HM group orientations are constrained to the gg conformation. With increasing temperature, they start shifting to gt and tg conformations, as the peak intensities coincide, making all orientations

equally accessible beyond 500K. The corresponding HM group orientation distributions (*c.f.* Figure 3.6D) in pure cellobiose melt are similar at higher temperatures. However, at 100K, with the presence of LCC, the cellobiose molecules prefer the gg conformation rather than the gt conformation. The thermal shift from a particular orientation to all conformations being equally accessible is significant even at 500K in the LCC *melt-phase* (*c.f.* Figure 3.6B) whereas it is only significant beyond 900K in pure bulk cellobiose (*c.f.* Figure 3.6D). This hydrogen bond network breakdown and increased torsional freedom to access all HM orientations at a lower temperature compared pure cellobiose *melt-phase* indicates that the presence of covalently bonded lignin promotes thermal phase change. The larger size of the phenolic LCC molecule potentially restricts and disrupts the cohesive interactions between cellobiose molecules, and in turn limiting the long range ordered hydrogen bond network, as seen in pure cellobiose *melt-phase*. Therefore, the change in phase, i.e., decrease in the number of hydrogen bonds and corresponding increase in torsional freedom directly maps to the decrease in free energy barrier for cellobiose activation via transglycosylation in all *melt-phases*. However, in the LCC melt-phase, the reduction in barrier influenced by the breaking intermolecular hydrogen bonds is not seen for the ring contraction mechanism. While the broken hydrogen bonds providing higher access to the hydroxymethyl group is key for transglycosylation mechanism, it is not in ring contraction mechanism. This indicates that though thermal ‘phase-change’ is a key factor, reaction chemistry is also dependent on the mechanisms and the corresponding reaction intermediates. To summarize the effect of temperature and of condensed phase environment on cellulose activation, free energy barriers in all *melt-phases* are plotted in Figure 3.7 in the entire range of 100K-1200K.

Therefore, in the lignin-rich reaction environment without any LCC bonding, there is little interaction between the reactant cellobiose, and the lignin melt-phase. Whereas in pure cellobiose, there are significant interactions and those change with temperature. The magnitude of this change is measured from the drop in intermolecular hydrogen bonds between the reactant and the condensed phase and it correlates well with the change in the relative free-energy barriers (*c.f.* Figure 3.5A) in both pure cellobiose and lignin-rich melt-phases. Nevertheless, in the LCC melt-phase the drop in hydrogen bonding is significant with respect to temperature, but lower than that in pure cellobiose melt-phase.

Fewer intermolecular hydrogen bonds might enable a greater degree of torsional freedom in the reacting cellobiose residue allowing a lower activation barrier as seen for transglycosylation in Figure 3.4A. However, in the same LCC melt-phase, this reduction in barrier influenced by the breaking intermolecular hydrogen bonds is not seen for the ring contraction mechanism.

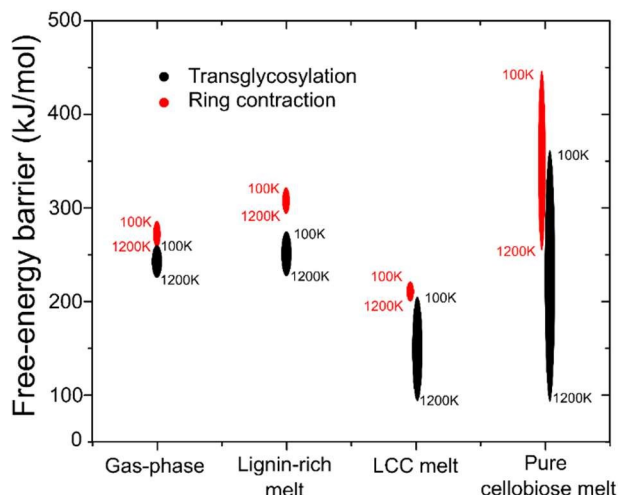


Figure 3.7 The range of free-energy barrier for cellobiose activation via transglycosylation (black) and ring contraction (red) mechanisms in the gas-phase and 3 melt-phase environments (lignin-rich melt, LCC melt, pure cellobiose) between the 100K-1200K temperatures.

3.3.2.2 Thermal influence of *melt-phase* varies with reaction mechanism

In Figure 3.7, higher spread indicates significant influence of temperature on the activation free energy barriers in the respective *melt-phase*. It can be noticed that the spread is large for transglycosylation in pure cellobiose *melt-phase* (267.7555 kJ/mol) and LCC *melt-phase* (109.7655 kJ/mol) in addition to ring contraction in pure cellobiose *melt-phase* (186.27 kJ/mol). Whereas in other *melt-phases* and in the gas phase its minimal (< 25 kJ/mol). Transglycosylation seems to be greatly promoted with breaking hydrogen bonds, shifting hydroxymethyl groups and increased torsional freedom in pure cellobiose and in LCC-melt phase. Thermal shifts in the condensed phase greatly increases the degree of freedom of the hydroxymethyl group that is bound by intermolecular hydrogen bonds in the cellobiose crystal structure. Since, in transglycosylation, the activation initiates via the protonation of the glycosidic oxygen by the hydroxymethyl tail, thermal shifts in the condensed phase also significantly influence

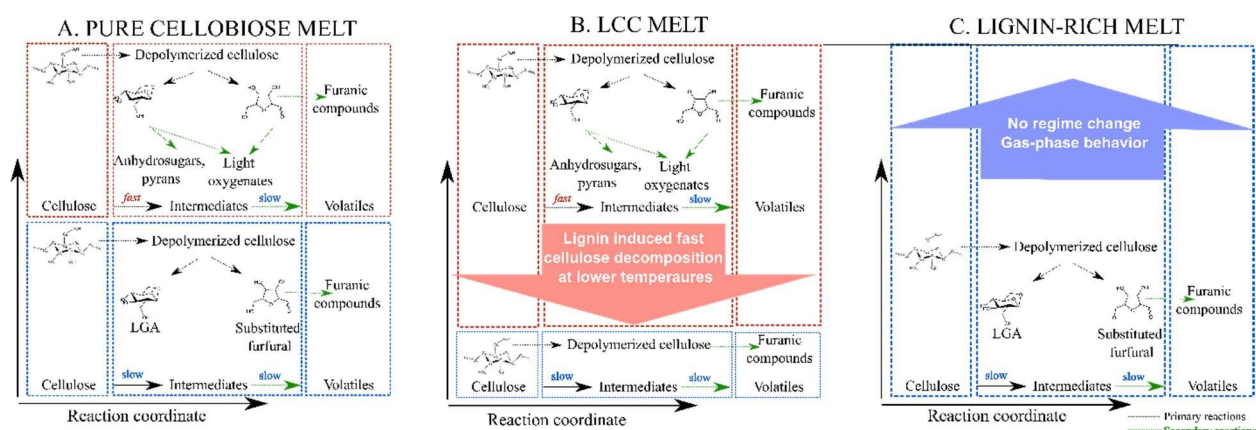
the activation barrier for transglycosylation. Also, it can be seen from Figure 3.7 that the lowest barrier for cellobiose activation calculated at 1200K is comparable in both the pure cellobiose and the LCC *melt-phases*. Unlike this, in the case of ring contraction, even the highest barrier for cellobiose activation calculated at 100K in the LCC *melt-phase* is significantly lower (by 52.15 kJ/mol) than the lowest barrier calculated in the pure cellobiose *melt-phase* at 1200K. This indicates that the presence of lignin in the LCC *melt-phase* system already promotes ring contraction to a much higher extent than the finite temperature effects in pure cellobiose *melt-phase*. Also, in the ring contraction mechanism, the protonation of the glycosidic bond (C₁-O₁) is carried out by the hydroxyl group attached to the adjacent C₂ ring carbon. Because of which, it doesn't benefit from increased degrees of freedom to the extent transglycosylation does. Looking at the entire picture, it can be stated that the presence of lignin in the LCC *melt-phase* promotes ring contraction to the extent that no further temperature induced reduction in the barrier is possible. Therefore, though the thermal 'phase-change' is a key indicator to predict shifts in cellulose decomposition energetics, the mechanism of decomposition seems to play a role too. Vast thermal shifts in the condensed phase will not promote cellulose activation if the reaction mechanism does not benefit from those additional degrees of freedom.

3.3.3 Comparison with experimental kinetics

High speed photography has captured cellulose pyrolyzing via a 'liquid/melt intermediate' to form volatiles²³⁹. Numerous reactions take place in such reactive boiling of cellulose, limiting direct comparison of experimental kinetics and first principles calculations without an elaborate multiscale kinetic model incorporating all reactions. However, recent state-of-the-art reactors (PHASR)¹⁹⁴ capture millisecond scale intrinsic kinetics by controlling reaction progression. Product formation measured using a gas chromatography-mass spectroscopy and the weight loss measurement from the unreacted feed are used to calculate experimental kinetics. Further, when fitted with first order kinetics, the corresponding activation barriers can be calculated¹²⁸. Both the weight loss and product formation measurements include secondary reactions and do not only capture the primary activation of cellulose that has been reported in this paper. Millisecond scale kinetic experiments conducted using a pure cellulose surrogate (α -cyclodextrin)¹⁹⁴, exhibited a

regime change with a shift in the apparent activation barrier. Scheme 3.3 illustrates the decomposition of cellulose to volatiles through the liquid intermediate along the reaction coordinate showing the shift in reaction regimes. As a function of temperature, the rates of cellulose decomposition and furan production are similar at lower temperatures but above 740 K, the rate of cellulose decomposition increases rapidly compared to that of furan production. This suggests that primary reactions (black arrows in Scheme 3.3) and secondary reactions (green arrows in Scheme 3.3) have comparable rate at low temperatures. Whereas at higher temperatures, secondary reactions are the rate determining step for the formation of volatile products. This agreed with the free-energy barrier calculations for cellobiose activation in pure cellobiose melt-phase²⁴⁰ and a cellulose decomposition model was developed to draw fundamental insights from first principles calculations and extending to overall reaction kinetics for comparison with experiments.

Scheme 3.3 Cellulose decomposition model in the three melt-phases – A) Pure cellobiose, B) Melt-phase with LCC linkages and, C) Lignin-rich melt-phase showing the reaction regimes shift from low (blue) to high (red) temperature regimes. In the higher temperature regime, as primary decomposition (black arrows) is accelerated, the rate of secondary reactions (green arrows) in the intermediate liquid becomes significant. The two melt-phase environments with lignin seem to alter the reaction kinetics in different ways.



Scheme 3.3 attempts to extend this decomposition model to also illustrate the influence of lignin on cellulose primary and secondary decomposition by taking experimental insights on regime change in native biomass pyrolysis into account. In the lignin-rich melt-

phase, lignin barely affects gas-phase barriers for cellulose activation with no regime change and in the LCC *melt-phase*, regime change occurs at a lower temperature compared to that in pure cellobiose. Recent millisecond scale kinetic experiments have been reported for the pyrolysis of Loblolly pine¹⁶⁶ between 673K-733K. This temperature range is below the regime change temperature (740K) in the pyrolysis of pure cellulose surrogate¹⁹⁴. The rate of formation of six different biomass pyrolysis products were measured and the apparent activation barriers were calculated. Out of the 6 products that were measured, LGA and 5-HMF are of interest as they are the products of transglycosylation and ring contraction (furan-formation) mechanisms, respectively, as investigated in this paper. Since this is one of the only studies available in literature that offer insights into reaction mechanisms in biomass pyrolysis, qualitative comparison with first principles reaction energetics is drawn. The barrier for the formation of LGA (70.29 kJ/mol) was lower than that for the formation of 5-HMF (93.30 kJ/mol). This strongly supports the calculations presented here – ring contraction mechanism (furan formation) has higher activation barriers compared to transglycosylation mechanism (LGA formation) in all melt-phase environments. Also, these apparent activation barriers measured from experiments for native biomass samples did not exhibit a regime change, similar to the minimal change with temperature in LCC and lignin-rich *melt-phases*. However, in the same temperature range, the apparent barrier for furan formation in native biomass is comparable to the apparent barrier (75.30 kJ/mol) reported in pure cellulose samples. Similarly, even for the pyrolysis of synthetic mixtures of lignin and cellulose¹³³, the measured reaction rates reduced when compared to pure cellulose pyrolysis. Such increased barriers leading to reduced reaction rates in the native and synthetic biomass matches the higher barrier in lignin-rich *melt-phase* compared to that in pure cellobiose *melt-phase* (*c.f.* Figure 3.4) between 673K-733K. Therefore, pyrolysis of lignin-rich woody loblolly pine seems to agree to the thermal activation of cellulose in lignin-rich melt-phase modelled in this work. Similar experiments measuring LGA and furan formation even at temperatures >740K for different biomass samples would be valuable in further validating our results. Moreover, transglycosylation (LGA-formation) is promoted over ring contraction in all melt-phase environments and in the LCC *melt-phase*, the regime change is pushed to a lower temperature promoting cellobiose

decomposition. Whereas, in the lignin-rich *melt-phase* the finite temperature condensed phase corrections ($\Delta G_{TS}^{sol} - \Delta G_{react}^{sol}$) barely alter the relative stabilization of the TS for either mechanism. This highlights the lack of thermal regime change (as shown in Scheme 3.3) or *melt-phase* (condensed phase) induced promotion/inhibition of reaction mechanisms in the lignin-rich *melt-phase* (c.f. Figure 3.5A).

3.4 Conclusions

Cellulose primary decomposition reactions via two key mechanisms (transglycosylation and ring contraction) in the condensed phase biomass pyrolysis environment are investigated between 100K-1200K. In the native biomass, high temperature melting leads to distinct local reaction environments – 1. *Melt-phase* with covalent lignin carbohydrate complex (LCCs) linkages, 2. Lignin-rich *melt-phase*, without LCC linkages and 3. Pure cellulose *melt-phase*. To investigate the influence of lignin on cellulose decomposition in the native biomass, the LCC and lignin-rich *melt-phases* are modelled using the quinone methide intermediate and cellobiose as surrogates for lignin and cellulose, respectively. A novel equilibrium solvation technique (ReSolv method) is employed to compute condensed phase free energy barriers for cellobiose activation.

In the pure cellobiose melt, cellobiose has been reported to exhibit two distinct regimes with different enthalpic (ΔH^\ddagger) and entropic ($T\Delta S^\ddagger$) contributions to the free energy barrier transitioning at 900K. With this regime change the free energy barrier drops significantly (by 264 kJ/mol for transglycosylation and 179 kJ/mol for ring contraction) between 100K-1200K. Calculations performed in this work probing the role of lignin in cellulose activation show that the two *melt-phases* with lignin alter reaction energetics differently. In the LCC *melt-phase*, cellulose activation is promoted with a 107 kJ/mol decrease in the free energy barrier between 100K-1200K for transglycosylation making two reaction regimes transitioning at a lower temperature (~ 800 K). While in the lignin-rich *melt-phase*, there is no influence of the condensed phase environment and activation free energy barriers remain very similar to those in the gas phase. In pure cellobiose melt phase, the high temperature (>900 K) *melt-phase* formation involves the complete disruption of directional hydrogen bonding allowing increased torsional freedom in the *melt-phase*. Similarly, in the LCC melt-phase, a more modest drop in the number of intermolecular hydrogen

bonds is reported. Unlike the other two systems, in lignin-rich *melt-phase*, such drastic shifts are not observed with change in temperature. Despite the different thermal responses, in all three local reaction environments, the thermal shift in the condensed phase with the disruption of the hydrogen bonding network and in turn the conformational flexibility in hydroxymethyl group orientation seem to directly map onto the thermal shift in the free-energy barriers for cellobiose activation. However, ring contraction in the LCC melt-phase is an exception. As the presence of lignin already significantly decreases the barrier for cellulose activation via ring contraction, temperature induced shifts in the melt phase don't contribute to further reducing the barrier. The increased favorability of glycosidic bond cleavage when the entropic contributions in the finite temperature melt-phase are included, establishes the significance of condensed phase effects. Experimental studies measuring millisecond scale kinetics for the pyrolysis of Loblolly pine (lignin-rich woody biomass with low LCC linkages compared to herbaceous biomass) and pure cellulose reported a higher barrier for furan formation in Loblolly pine. This aligns with the calculated barriers for cellobiose activation in the pure cellobiose and lignin-rich *melt-phase*. For the first time, the influence of lignin and finite temperature condensed phase on cellobiose primary decomposition has been investigated. Comparison between the barriers calculated by the ReSolv method and the experiments yield strong evidence for significant influence of lignin on cellobiose activation leading to a higher barrier.

Chapter 4 Impact of Lignin-carbohydrate complex (LCC) linkages on cellulose pyrolysis chemistry

4.1 Introduction

Lignocellulosic biomass, the largest renewable natural resource²⁴⁹ for carbon-based liquid fuels, offers a promising solution for sustainable fuel and chemical production. By utilizing fast pyrolysis, a decentralizable processing technology, biopolymers can be thermally cracked without oxygen, yielding renewable crude oil (bio-oil)⁸. During pyrolysis, biomass is heated in the absence of oxygen to produce a mixture of bio-oil, biochar, and volatile gases. Despite the potential benefits of decentralized biomass processing and lower transportation costs, the commercial viability of pyrolysis technology has been hindered by the instability of bio-oil during storage and transport. Also, the highly oxygenated nature of bio-oil¹⁶⁹ necessitates further treatment for integration into existing petroleum infrastructure. Despite extensive attempts over past couple of decades to improve targeted bio-oil production, minimize lignin repolymerization, and enhance the accessibility of cellulose-derived products, the advancement of biomass deconstruction techniques has faced obstacles due to limited understanding of the underlying chemistry. Therefore, understanding the chemistry of biomass decomposition and molecular interactions between cellulose and other biopolymers is crucial for systematic and bottom-up optimization of the pyrolysis process and for improving the yield and quality of the resulting products.

The intricate microscopic structure of native biomass in the plant cell wall involves the complex intermingling of cellulose, lignin, and hemicellulose²⁴⁹. To facilitate a clearer understanding of biomass decomposition, researchers have focused on studying isolated biopolymers chemistry. Among the primary components of biomass, cellulose garnered significant attention due to its rapid decomposition during pyrolysis, leading to the production of substantial quantities of desirable volatile compounds. Multiscale molecular modelling and first principles-based calculations have enabled the discovery of molecular level mechanisms that are inaccessible to experiments alone. First-principles modeling has played a crucial role in advancing our understanding of the intricate mechanisms and

kinetics involved in cellulose pyrolysis^{33,118}. Previous research has mainly concentrated on investigating the initial steps of cellulose pyrolysis, specifically the depolymerization of cellulose chains and the formation of various small molecules. The thermal decomposition of cellulose during pyrolysis produces levoglucosan (LG)^{250,251} as a dominant product followed by furanic compounds like 5-hydroxymethyl-furfural (5-HMF) and light oxygenates like glycolaldehyde (GA). Moreover, multiple Density Functional Theory (DFT) studies^{111,118,252} have proven that concerted mechanisms, such as transglycosylation and ring contraction, are more favorable, compared to homolytic or heterolytic cleavage of glycosidic C–O bonds during LG formation. Transglycosylation, specifically, has been proposed as a favorable pathway for glycosidic bond cleavage²⁵³. Concerted transglycosylation mechanism involves simultaneous protonation of the glycosidic bond by the C6-hydroxymethyl group and the formation of a C6-O-C1 bridge (*c.f.* Scheme 4.1 for atomic nomenclature). Ab initio molecular dynamics (AIMD)-metadynamics simulations have revealed that major volatiles, including furans, can be directly generated from cellulose through ring contraction, without the involvement of small-molecule intermediates like glucose or levoglucosan (LGA)⁵². Free energy barriers reported for pyranose ring contraction, ring opening, rearrangement, or ring fragmentation during pyrolysis, leading to the formation of pre-LGA and pre-furans revealed ring contraction as the dominant mechanism at 327 °C. Concerted ring contraction mechanism involves the simultaneous protonation of the glycosidic bond and C2-C3 bond fragmentation to form C1-C3 bond, changing to a furanose ring from pyranose. The reorganization of the ring structure leads to the formation of 3,4-(hydroxyl) 5-(hydroxymethyl) furfural and glucose. These mechanisms to form major pyranic and furanic compounds have been previously investigated in both gas-phase²⁵³ and in condensed-phase environments²⁴⁰. Piskorz et al.⁷¹ proposed that the two carbon fragments resulting from the cleavage of cellulose monomers during pyrolysis are transformed into glycolaldehyde (GA), a major pyrolysis derived bio-oil product. The mechanisms for small molecular weight products, such as GA, have also been studied using DFT^{123–125,254} and a minor fraction of GA has been suggested to be produced from the secondary cleavage of LG²⁵⁵. However, GA primarily originates from the ring opening of cellulose, particularly through the cleavage of C1–C2, C5–C6, and C3–C4 bonds in the

cellulose monomer. DFT calculations showed that the pyran ring, undergoing dehydration, is more inclined to undergo the ring opening reaction¹²⁶. 1,2 dehydration mechanism has been found to be the most prevalent, surpassing alcohol dehydration^{256,257}. Detailed insights into such retro-aldol reactions, which are the primary routes for GA production, have been provided by Assary and Curtiss¹⁰⁹ and further supported by Zhang et al.²⁵⁸. Ring opening leads to reactants through a series of steps involving dehydration, cleavage, and isomeric formation of glycolaldehyde (GA). As depicted in Scheme 4.1, the ring opening process initiates with the 1-2 dehydration of cellobiose, followed by the cleavage of C4'–C5' and C1'–O5' bonds, resulting in the opening of the pyran ring. This leads to the formation of two C=C double bonds (C1'–C2' and C5'–C6') and glycolaldehyde. While the aforementioned discussion provides valuable insights into the chemistry of cellulose pyrolysis, with a primary focus on the primary and secondary reactions of cellulose decomposition, there remains a lack of integrated research addressing the mechanism of the initial stage of cellulose pyrolysis in the context of covalent bonding with other plant biopolymers in the plant cell wall.

It is well known that the presence of lignin in native biomass contributes to the formation of additional compounds such as phenols (derived primarily from lignin), in addition to furans and levoglucosan (LGA). However, the pyrolysis of native biomass, such as spruce and beech wood, exhibits a significant change in the distribution of cellulose derived components too, as compared to pure cellulose pyrolysis. While the cellulose content in these biomasses can potentially yield up to 48% levoglucosan when pyrolyzed separately, the actual LGA yield is less than 3%^{18,145}. This phenomenon is also observed in the pyrolysis of synthetic biomass (model biomass prepared by mixing different extracted biopolymers) containing cellulose and lignin mixtures, where the reaction rates slow down, and lignin hinders in cellulose breakdown and volatile formation^{131–133}. Additionally, the product yields from the pyrolysis of herbaceous biomass (e.g., cornstover, switchgrass) also differ from those of woody biomass (e.g., pine, redwood)²⁵⁹. The herbaceous cellulose-lignin sample results in a 10.28 wt% lower LGA yield which is compensated by 11.38 wt% and 1.45 wt% increase in C₁ to C₃ products and furans, respectively. However, in the pyrolysis of woody biomass, despite the higher lignin content, the deviation in product distribution from pure cellulose is minimal. This variation

between herbaceous and woody biomass is attributed to higher lignin carbohydrate complex (LCC) linkages in herbaceous biomass. While modelling isolated biopolymer molecules has been useful in understanding their individual pyrolysis chemistries, they don't allow the prediction or even can explain the pyrolysis chemistry of native biomass. It is therefore important to consider the complex linkages between biomass components and their influence on cellulose decomposition. Lignin-carbohydrate complexes (LCC) play a vital role in wood structure, with a considerable portion of lignin (all in coniferous ²⁶⁰ and 47-60% in deciduous ²⁶¹) forming covalent bonds with carbohydrates. In softwood, approximately 50% of lignin is bound to cellulose, while in hardwood, this proportion is around 17%¹⁵⁴. The presence of LCCs poses challenges in isolating biomass components with high yield and purity^{150,151}, mainly due to the reduced accessibility of carbohydrates^{148,149} and the stability of these covalent bonds²⁶² between lignin and carbohydrates to extraction via alkaline treatment. Traditionally, research on LCCs has focused on cleaving these bonds for extraction purposes, employing indirect wet chemistry methods such as selective acid/alkaline hydrolysis²⁶⁰ followed by FT-IR spectroscopy for analysis. However, for a more comprehensive understanding of the molecular structure, direct techniques like two-dimensional nuclear magnetic resonance (2D NMR), particularly HSQC spectroscopy, are commonly utilized. Among the eight identified types of LCC linkages^{149,233,234,263,264}, benzyl ether, benzyl ester, and phenyl glycosidic linkages are frequently observed²⁶⁴, exhibiting varying strengths under different conditions. Benzyl ether bonds are dominant in softwood LCCs and are notably more stable and prevalent. Herbaceous biomass, particularly in grass cell walls, displays a higher occurrence of LCC linkages, where benzyl ether linkages crosslink lignin and polysaccharides (Kajikawa et al., 2000). A study conducted by Watanabe et al. in 1989 employed a comprehensive technique involving cellulase digestion, adsorption chromatography, acetylation, DDQ (2,3-dichloro-5,6-dicyano-1,4-benzoquinone) oxidation, and methylation to provide direct evidence of binding sites between lignin and carbohydrates. The majority of studies^{235,265} have reported LCC linkages at the C6 position of the sugar, although acetylation at the C2 and C3 positions, indicating LCC linkages, has been observed in mannose and xylan molecules²⁶⁵⁻²⁶⁷. Recent first principles-based calculations ³⁴ studying the reaction energies of LCC formation at

different bonding sites on glucose demonstrated minimal differences of less than 5 kJ/mol, indicating thermodynamic preference for LCC formation at any of the three positions (C6, C3, or C2) (*c.f.* Scheme 4.1A).

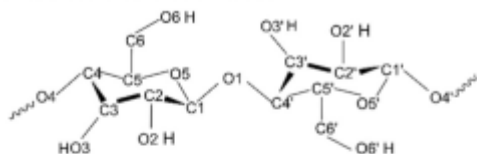
Cross-linked cellulose in these LCC heteromolecules may exhibit distinct chemical properties compared to pure cellulose. LCC linkages formed at the C6 position in particular can inhibit levoglucosan (LGA) formation, similar to the inhibition observed in polysaccharides with 1,6-glycosidic linkages as opposed to 1,4- or 1,3-glycosidic linkages⁶⁸. This inhibition of LGA formation by the benzyl ether LCC linkage at the C6 position aligns with the measured decrease in LGA yield and the subsequent increase in C1-C3 products observed in the pyrolysis of native biomass, particularly herbaceous biomass. This suggests that the LCCs could potentially alter cellulose reaction pathways and energetics because of the covalent cross-linking between lignin and cellulose. However, despite the significance of cross-linked LCC linkages in cellulose decomposition, only one recent study, to the best of our knowledge, has investigated their role in pyrolysis chemistry. The study compared the pyrolysis products of chemically tailored native lignocellulose with selective removal of hemicellulose to a synthetic cellulose-lignin mixture¹⁶⁵. The presence of cross-linked lignin was found to significantly influence the production of small molecules and furan derivatives, increasing their yield by 97%, while hindering the generation of anhydrosugars by up to 47%. Additionally, cross-linked lignin exhibited a more pronounced effect on lignocellulose pyrolysis by promoting glycosyl ring scission and lignin fragmentation compared to free lignin. However, the specific chemistry and energetics underlying these ring scissions in the LCC molecule remain unknown. Studying cellulose pyrolysis chemistry in cross-linked LCCs is limited by the complex nature of conducting first principles calculations for multimolecular systems and the experimental difficulties associated with complex pre-treatments for the isolation of these LCCs from native biomass.

In order to gain understanding of the impact of lignin-carbohydrate linkages on cellulose pyrolysis chemistry, it is crucial to address several significant knowledge gaps - 1) the role of cross-linked LCC linkages in cellulose decomposition energetics, 2) the similarity or dissimilarity in the decomposition chemistry and kinetics between pure cellulose and

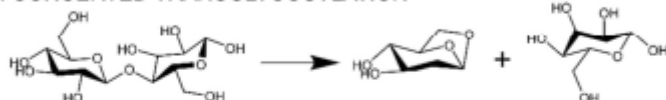
cross-linked cellulose moieties within LCC, and 3) the influence of the lignin binding site on cellulose decomposition. This study aims to address these gaps by employing a combination of first principles calculations and thin-film pyrolysis experiments. Specifically, the study will utilize ab-initio techniques to model different LCC conformations with varying binding sites – C2, C3, and C6 (*c.f.* Scheme 4.1A) and calculate their respective energy barriers and reaction energies using Density Functional Theory (DFT). These calculations will be compared to the energetics calculated for the pyrolysis of pure cellulose. By investigating the decomposition chemistry using model molecules and subsequently validating the findings through experiments, this paper will provide novel insights into the role of LCC linkages and the impact of lignin-cellulose binding sites on cellulose decomposition.

Scheme 4.1 (A) Atomic nomenclature of the monomeric glucose unit (B) Transglycosylation reaction mechanism of cellobiose decomposition to form LGA (C) Ring contraction mechanism of cellobiose decomposition to form furanic compounds (D) Ring opening mechanism of cellobiose decomposition to form Glycolaldehyde.

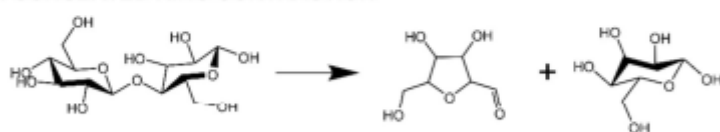
A. ATOMIC NOMENCLATURE



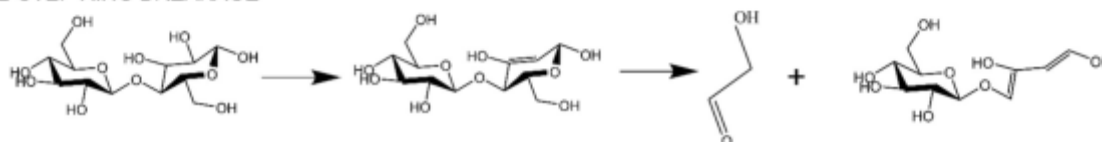
B. CONCERTED TRANSGLYCOSYLATION



C. CONCERTED RING CONTRACTION



D. 2-STEP RING BREAKAGE



4.2 Methodology

4.2.1 Ab-initio Conformational search

To ensure accurate computation of activation and reaction energies, it is crucial to thoroughly explore the conformational space of the LCC molecule (model cellobiose and lignin compounds covalently bonded via an LCC linkage). In this study, Car-Parrinello molecular dynamics (CPMD) combined with metadynamics (CPMD-metadynamics) was utilized to calculate the free energy surface (FES) as a function of torsional angles within the LCC molecule. The selection of torsion angles aimed to enable extensive sampling of the system, which would not be feasible within reasonable computational timeframes using thermal energy alone. The methods and parameters closely followed the procedures outlined by Beck et al.²⁶⁸. Conformers corresponding to the lowest minima on the FES were subsequently subjected to density functional theory (DFT) optimization and further calculation of the transition state for the cleavage of cellulose moiety in the LCCs through transglycosylation, ring contraction, and ring opening. The computational details are further elaborated in SI.

4.2.2 DFT optimization and Transition State calculations

The Gaussian 09 code²⁶⁹ was utilized to perform all-electron DFT calculations, aiming to compare the relative stabilities and to further optimize the lowest energy sample conformers identified through CPMD-metadynamics. Considering the large number of generated starting conformers, a step-wise improvement strategy was adopted for the basis set selection. The output of a less sophisticated basis set served as the input for a more advanced one, providing a systematic approach for conformational screening, with each level of theory screening the lowest energy conformers. Each conformer underwent complete geometry optimization at each level of theory, without imposing constraints on the atoms. Subsequently, frequency calculations were performed to ensure the absence of spurious frequencies in the reactant and product compounds. The hybrid functional RM06-2X was employed in all stages of optimization up to the 6-311+G(d) basis set, as it has been demonstrated to provide sufficient accuracy for modeling cellulose-derived molecules^{118,210,211,244}. Transition state (TS) searches were conducted using the Berny

algorithm for both unconstrained cellobiose and LCC molecules, focusing on transglycosylation, ring contraction, and ring opening mechanisms (Scheme 4.1). Following the TS searches, frequency calculations were carried out to differentiate between saddle points and local minima, determined by the presence or absence of an imaginary frequency (corresponding to the reaction coordinate), respectively. Intrinsic reaction coordinates (IRCs) were traced in both directions to verify that the TS corresponded to the correct reactant and product on the potential energy surface. The reported reaction free energies were determined at 1 atm and 500K. A convergence criterion of 1.00D-06 in energy change was selected for the self-consistent field (SCF) calculations to determine the electronic structure configuration. Similar activation barriers for cellobiose activation via transglycosylation and ring contraction have been previously reported in our earlier work ²⁴⁰.

4.2.3 Experimental methods

4.2.3.1 Materials and thin-film preparation

The bagasse sample was acquired from a local juice shop and washed and oven dried at 110 °C for 2 hrs. After drying, it was grinded to reduce the size. The grinded bagasse was sieved with 60 Mesh and used for thin-film preparation. 1.0% (weight basis) of dry bagasse was taken in deionized (DI) water for Thin-film preparation. Bagasse did not dissolve in DI water and resulted in a suspension. 25 μ L of 1.0 wt % suspension was transferred into the pyrolysis crucible. The water was removed using room temperature evacuation, leaving behind a micrometer scale film of bagasse ^{252,270,271}. The thickness of the thin-film was measured using a digital microscope (Leica, model DVM6) as shown in Figure S1 (in the SI). Image analysis showed that bagasse thin-films were ~50-70 μ m thick indicating a reaction-controlled pyrolysis regime ²⁷⁰.

4.2.3.2 Pyrolysis experiments

Thin-films of bagasse were pyrolyzed in a micropyrolyzer (PY-3030S, Frontier Laboratories Ltd., Japan). The weight of the bagasse sample used for the thin-film pyrolysis experiments was 50 μ g. The heating rate of the bagasse thin-films in a micropyrolyzer was 3 – 5 orders of magnitude faster than traditional heating rates in

pyrolysis techniques. Identification and quantification of pyrolysis volatile products (condensable volatiles and non-condensable gases) were conducted using a gas chromatograph (GC) (Agilent, model 7890B)/mass spectrometer (MS) (model 5977B MSD) connected in-line with the micropyrolyzer. The pyrolysis volatile products were removed instantly from the micropyrolyzer through helium gas flowing continuously. The detection of condensable pyrolysis volatile compounds and non-condensable gases was done using Agilent J&W DB-5 and Agilent J&W HP-PLOT-Q GC columns, respectively, with a maximum operating temperature of 320 °C and having the same dimensions (i.e., 30 m × 320 μm × 1.5 μm, length × internal diameter × film). Initially, the oven temperature was set to 35 °C, and then a ramp of 3.5 °C/min was provided to reach a final oven temperature up to 250 °C during analysis. A sample split time (~2 min) was also set in the GC program to separate non-condensable gases and condensable volatile products (especially forming bio-oil) into two separate columns (i.e., HP-PLOT-Q for non-condensable gases and J&W DB-5 for condensable volatile compounds) in order to achieve their analysis simultaneously. The quantification of char was done post-pyrolysis using combustion technique. The pulse of oxygen was applied to the micropyrolyzer at 700 °C and equivalent amount of combustion gas (or carbon dioxide) was measure for char quantification. The details of the thin-film pyrolysis experimental procedure and product characterization are reported elsewhere ²⁷¹.

The yields of bio-oil and non-condensable gases were obtained by summing the yields of condensable pyrolysis products and the yields of carbon dioxide/carbon monoxide, respectively. Further, the quantification of individual pyrolysis products (forming bio-oil and non-condensable gases) was performed using calibration of the standards with average error. Bagasse thin-film pyrolysis experiments were conducted in triplicate, and the average values (product yields, % weight basis) are reported.

4.3 Results and Discussion

Cellulose undergoes decomposition under pyrolysis conditions through competing reactions involving the cleavage of glycosidic C-O bonds (yielding LGA) and C-C bonds (yielding furan and C₁-C₃ products). DFT calculations show that concerted transglycosylation and ring contraction (*c.f.* Scheme 4.1) are the most favorable pathways

for the glycosidic bond cleavage²⁰⁴, while 2-step retro-aldol ring opening has reported be the predominant pathway for the formation of lower molecular weight compounds. The opening of the pyran ring initiates with a dehydration step followed by a ring opening step to form glycolaldehyde (GA), one of the major products in bio-oil¹²⁶(*c.f.* Scheme 4.1). Transglycosylation, ring contraction and 2-step ring opening mechanisms contribute to the formation of major cellulose pyrolysis products, LGA, furans and GA, and are used as representative primary reaction pathways in this study. Also, dimers cellobiose and quinone methide intermediate²⁶⁸ are used as surrogates for cellulose and lignin polymer, respectively.

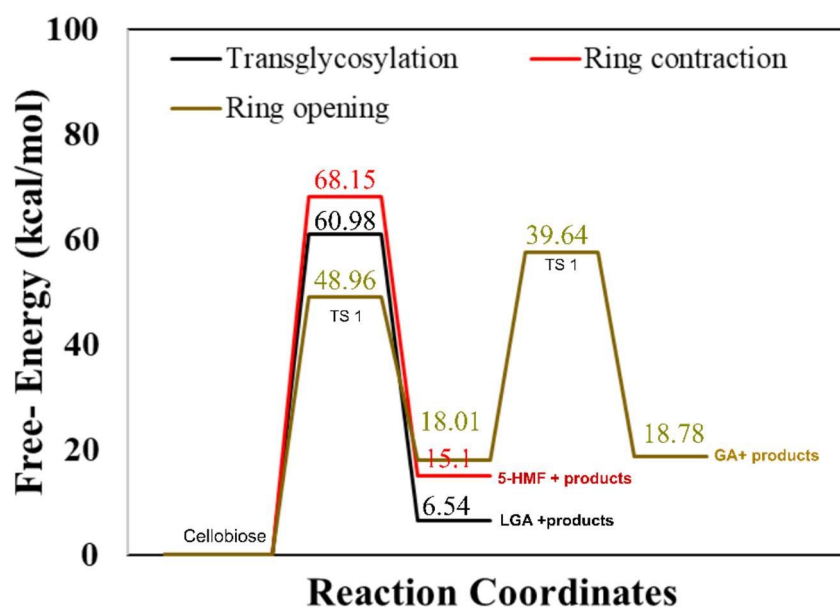
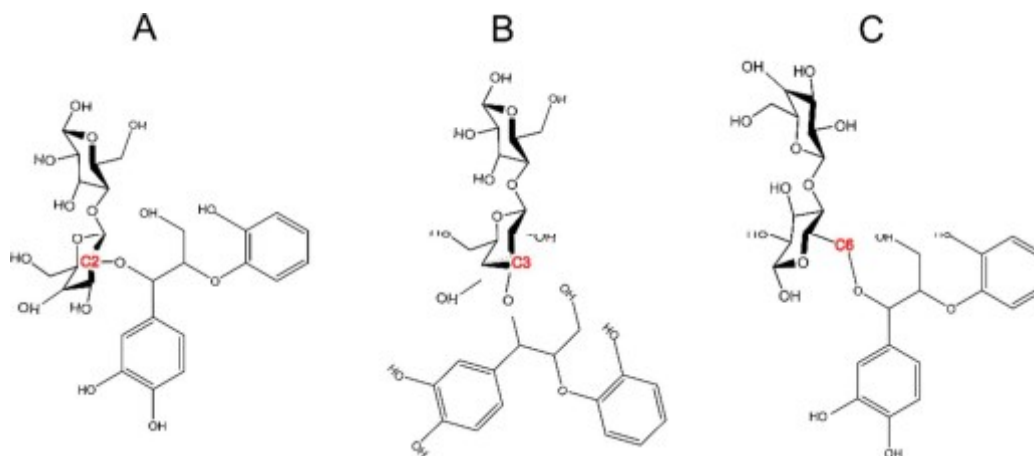


Figure 4.1 Gas phase activation free energy barriers for cellobiose decomposition calculated using hybrid functional M06-2X with 6-311+G(d) basis set for transglycosylation, ring contraction and ring opening mechanisms.

4.3.1 Activation barriers for competing cellulose decomposition reactions

As described in methodology, DFT calculations were performed for an isolated cellobiose molecule. The results, as presented in Figure 4.1, illustrate the energy diagram for transglycosylation, ring contraction, and ring opening mechanisms at a temperature of 500 K. The calculated activation barriers for transglycosylation and ring contraction were determined to be 60.98 kcal/mol and 68.15 kcal/mol, respectively. The barriers for the two-step ring opening mechanism were calculated to be significantly lower, 48.96 kcal/mol and 39.64 kcal/mol. Transglycosylation involves the formation of a bridge, while both ring opening and ring contraction entail the reorganization and cleavage of the ring structure. The results depicted in Figure 4.1 demonstrate that transglycosylation is favored over ring contraction, which aligns with previous findings from DFT studies¹⁰⁹. Additionally, the stepwise barriers for ring opening are the lowest among the investigated mechanisms.

Scheme 4.2 LCC linkage between a lignin moiety (quinone methide intermediate) and the cellobiose dimer bonded at A) C2 position B) C3 position C) C6 position.



4.3.2 Lignin-carbohydrate complex (LCC)

The formation of lignin carbohydrate complex (LCCs) linkages has recently gained attention due to their significant role in the recalcitrant nature of biomass^{142,272}. LCCs are formed as a result of side reactions during the formation of the predominant β -O-4 linkage in lignin. During the formation of the β -O-4 linkage, a quinone methide (QM) intermediate

is generated, which undergoes re-aromatization through nucleophilic addition at the α -carbon. Traditionally, it has been assumed that this intermediate reacts exclusively with water^{273,274}, leading to only physical interactions between lignin and cellulose in the cell wall. However, Beck et al.³⁴ provided direct evidence of the molecular mechanism behind the formation of benzyl ether and benzyl ester LCC linkages through the speculated lignin-cellobiose polymerization pathway. These LCCs, formed through covalent bonding between cellobiose and lignin, were found to be thermodynamically more stable than the nucleophilic addition of water. Since, among various LCC linkages, benzyl ether LCCs are prevalent and stable²⁷⁵, the cross-linking between cellobiose and the quinone methide intermediate were made via a benzyl ether bond. While these covalent linkages primarily form at the C6 position of the sugar^{235,265}, LCCs at C2 and C3 positions have also been shown to be thermodynamically facile. Therefore, this study also aims to investigate whether the site of LCC linkage influences cellulose activation. To address this, covalent linkages were established not only at the C6 position but also at the C2 and C3 positions (refer to Scheme 4.2).

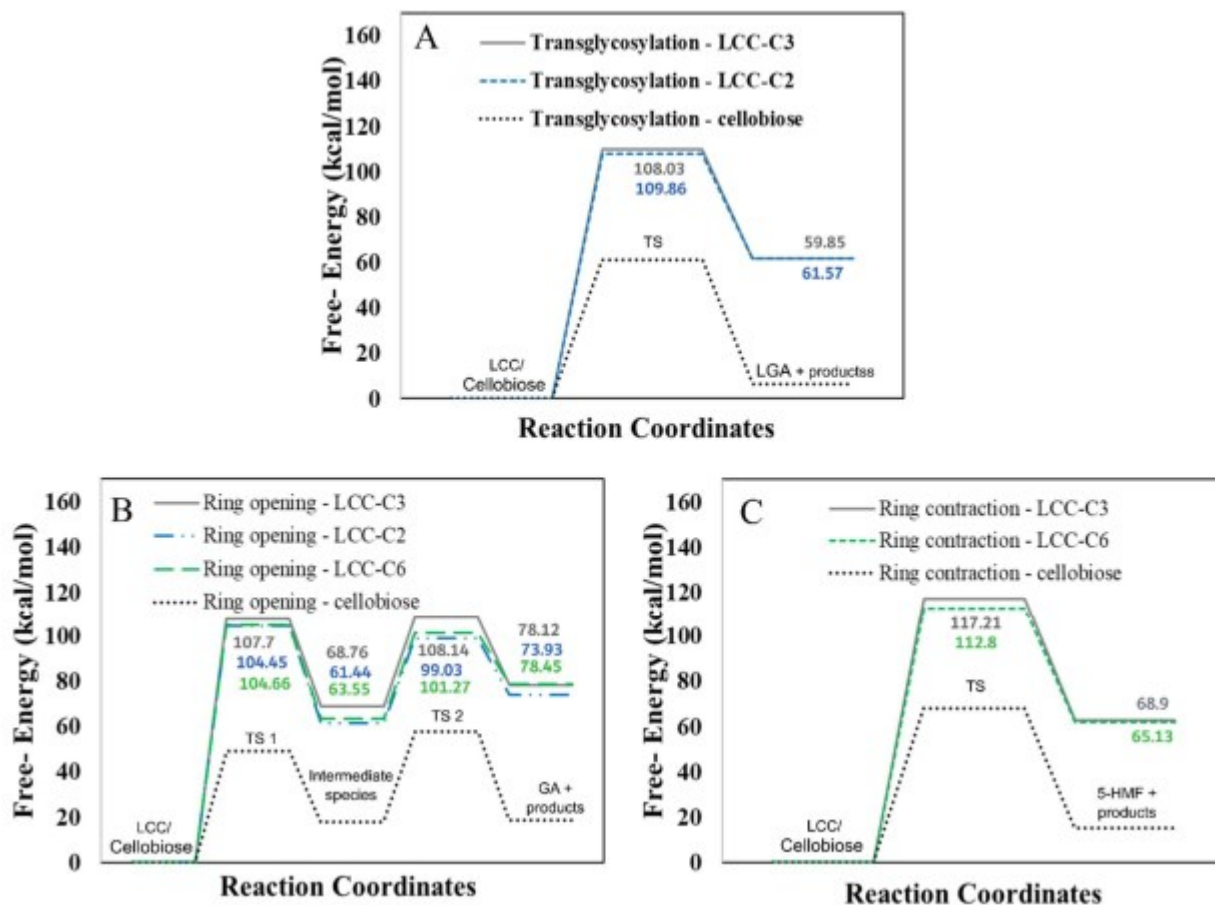


Figure 4.2 Free energy barriers for LCC decomposition via A) Transglycosylation B) Ring opening and C) Ring contraction mechanisms.

4.3.3 Activation barriers for competing cellulose decomposition reactions in the presence of LCC

DFT calculations were performed for the decomposition of cellobiose moiety via all three mechanisms for the 3 lowest energy conformers (LCC-C2, LCC-C3 and LCC-C6) each with a benzyl ether bond at the C2, C3 and C6 positions on cellobiose (*c.f.* Scheme 4.2). The transition states (TS) were calculated for transglycosylation, ring contraction and ring opening mechanism at 500K. All mechanisms are feasible for LCC-C3 and all LCCs can undergo ring opening. However, LCC-C2 can't undergo ring contraction because the mechanism requires a C2 hydroxyl group that protonates the glycosidic oxygen, which is replaced by the ether linkage in the LCC-C2 molecule. Similarly, LCC-C6 can't undergo transglycosylation as the mechanism requires the protonation of the glycosidic oxygen by

the C6 hydroxyl group; but the C6 oxygen is involved in the LCC ether linkage. These DFT calculations revealed that the activation barrier for transglycosylation in the LCC-C2 and LCC-C3 molecules are 108.04 kcalmol⁻¹ and 109.86 kcalmol⁻¹ (*cf.* Figure 4.2A). These barriers calculated in LCC molecules (cross-linked cellobiose) are almost twice of that in a pure cellobiose molecule (60.98 kcal/mol) for the same mechanism. The activation barrier for ring contraction in the LCC-C3 and LCC-C6 molecules are 117.21 kcalmol⁻¹ and 112.8 kcalmol⁻¹, respectively (*cf.* Figure 4.2C). For the 2-step ring opening mechanism in LCC-C2, LCC-C3 and LCC-C6 (*cf.* Figure 4.2B), the barriers for the first dehydration step are 104.44 kcalmol⁻¹, 107.7 kcalmol⁻¹ and 104.66 kcalmol⁻¹, respectively. Subsequently, the activation barriers for the second ring opening step in cellobiose cross-linked at the C2, C3 and C6 positions are 37.59 kcalmol⁻¹, 39.38 kcalmol⁻¹ and 37.72 kcalmol⁻¹, respectively. Unlike the large barriers calculated in the decomposition of cross-linked cellobiose in LCC via other mechanisms, the second ring opening step exhibits relatively low activation barriers. This indicates that once the 1,2-dehydration step is complete forming a C=C bond on the cellobiose ring, the formation of glycolaldehyde by ring opening is kinetically facile. Comparing the three mechanisms for an LCC conformer cross-linked at a particular site, ring contraction has the highest barrier, followed by transglycosylation, while the first dehydration (rate determining) step in ring opening has the lowest barriers. This lower barrier for dehydration and subsequent formation of lower oxygenates (like GA) is supported by the high yields of GA measured in cellulose pyrolysis experiments¹²⁶. For all three mechanisms and in turn all three products (LGA, furans, GA) formation, the barriers in cross-linked cellobiose in LCC are almost twice of those in the isolated cellobiose. Additionally, the decomposition reaction of LCC molecules is also significantly more endergonic (as compared to pure cellobiose). This indicates that the pyrolysis energetics and the kinetics of cellobiose with LCC are different from that of pure cellobiose. Such high activation barriers for the primary decomposition of cellobiose moiety in the presence of LCC has not been reported before. To develop a molecular level understanding and a mechanistic reason for the high barrier to cleave cellulose moiety in the presence of LCC, the reaction energies are compared, and the frontier molecular orbitals are also visualized.

Table 4.1 Reaction free energies (kcal/mol) for thermal cleavage of cellobiose via 3 key mechanisms when isolated and when cross-linked to lignin in LCC at C2, C3 and C6 positions.

Reaction mechanism	Cellobiose	LCC		
		C2	C3	C6
Transglycosylation	6.54	59.85	61.57	-
Ring contraction	15.10	-	68.90	65.13
Ring opening	18.00	61.45	68.76	63.56
	0.79	12.49	14.31	14.89

The reaction free energies of all three mechanisms in isolated and cross-linked cellobiose are reported in Table 4.1. For pure cellobiose the reaction energies for transglycosylation and ring contraction are 6.54 kcalmol⁻¹ and 15.1 kcalmol⁻¹, respectively while that for the 2-step ring opening mechanism are 18.0 kcalmol⁻¹ and 0.79 kcalmol⁻¹. These reaction energies are in excellent agreement with previously published DFT calculations²⁰⁴. However, the LCC cross-linked cellobiose exhibits significantly higher reaction energies, similar to the large deviation observed in activation energies. The reaction energy for transglycosylation in cellobiose cross-linked at the C2 and C3 positions are 59.85 kcalmol⁻¹ and 61.57 kcalmol⁻¹ while for ring contraction cross-linked at the C3 and C6 positions are 68.9 kcalmol⁻¹ and 65.13 kcalmol⁻¹, respectively. For the ring opening, the reaction energies of the first dehydration step for LCC conformers binding at C2, C3 and C6 positions are 61.45 kcalmol⁻¹, 68.76 kcalmol⁻¹ and 63.56 kcalmol⁻¹ while for the second step it is 12.49 kcalmol⁻¹, 14.3 kcalmol⁻¹ and 14.89 kcalmol⁻¹, respectively. The calculation of conformational changes in LCC molecules revealed a maximum change of ~15 kcal/mol. Despite considering a conformational penalty (which we have minimized using the sampling), the reaction energies observed in LCC were found to be more than 40 kcal/mol higher compared to those in pure cellobiose. These reaction energies follow the

same trend as the activation barriers with only the second ring opening step having lower values compared to the energetics in isolated cellobiose. This indicates that it is not the preferential destabilization of the TS that leads to these high barriers for cellulose decomposition in LCCs. The lignin moiety in LCC seems to shield the cross-linked cellobiose leading to a higher barrier for cellulose cleavage via conventional reaction mechanisms. These representative reaction mechanisms were proposed for the cleavage of cellulose and its oligomers. However, for the cleavage of cross-linked cellobiose in LCC, there could potentially be more energetically favorable mechanisms. The changes in relative stabilities of cross-linked cellobiose (evident from the higher barriers compared to pure cellobiose) can be evaluated using the quantum chemical indicators calculated using the frontier molecular orbitals ²⁷⁶. Electron transfer between/within the reactants is most likely to occur in the frontier orbital and they have been widely used in predicting activity ²⁷⁷, absorption selectivity ²⁷⁶, binding properties ²⁷⁸ and so on. In this work, the frontier orbital in the cellobiose and LCC molecules are visualized to investigate the electronic structure's contributions to the higher barriers for the cleavage of cellulose moiety in LCC.

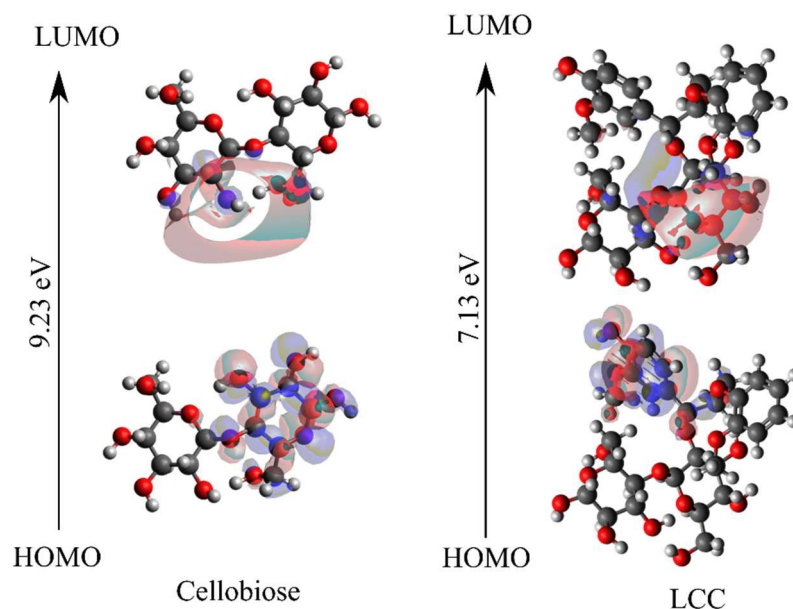


Figure 4.3 HOMO-LUMO orbitals are visualized using Frontier Orbital analysis performed on isolated cellobiose and cross-linked cellobiose in LCC.

Within the framework of frontier molecular orbital theory, the highest energy level occupied orbital is denoted as the highest occupied molecular orbital (HOMO), while the lowest energy level unoccupied orbital is referred to as the lowest unoccupied molecular orbital (LUMO). HOMO reflects the ability to give electrons, and LUMO reflects the ability to accept electrons. The exchange of frontier electrons significantly influences reactions since the interaction between the HOMO and LUMO also correlates with the energy barrier ^{279,280}. Figure 4.3 shows the frontier orbitals, HOMO and LUMO, for cellobiose and cross-linked cellobiose in LCC. In an isolated cellobiose, both the frontier orbitals are spatially close and are located on the cellobiose molecule. In the LCC molecule, while the LUMO is on the cellobiose moiety, the HOMO is located away on the nucleophilic lignin moiety. The chemical reaction is likely to occur in the position and direction where HOMO and LUMO overlap effectively ²⁸¹. By examining the spatial extent and localization of the HOMO and LUMO orbitals, specific regions or atoms within a molecule that are more reactive or prone to participate in chemical reactions can be identified. These regions are often associated with higher electron density in the HOMO or regions where the LUMO has significant overlap, indicating favorable sites for electron transfer or bond formation. The sites of HOMO and LUMO orbitals in the cellobiose molecule match with previous calculations investigating adsorption selectivity in anticorrosion coating with biopolymer extracts (specifically cellobiose) ²⁷⁶. These favorable sites are active centers that contribute to covalent bonding in cellulose. Unlike the spatial overlap of the HOMO-LUMO orbitals in the isolated cellobiose molecule, in the LCC molecule, they are spatially far. Moreover, the localization of the HOMO orbital on the electron rich lignin and LUMO orbital on the cellobiose moiety suggests that electron transfer between the lignin and cellobiose moiety might be favored over intra-moiety electron transfer. In addition to the position and direction of HOMO and LUMO overlap, the HOMO-LUMO gap has been used to study the molecular stability and activity for cellulose and related systems^{10,120,277}.

The magnitude of the HOMO-LUMO gap correlates with the level of HOMO-LUMO interaction and stability ²⁸² in the reaction and a larger HOMO-LUMO gap is indicative of greater kinetic stability and diminished chemical reactivity ^{276,283}. Therefore, the lower HOMO-LUMO gap in cross-linked cellobiose (c.f. Figure 4.3) as compared to pure cellobiose seems to suggest higher reactivity meaning lower activation barrier. Since the

activation barriers are higher for the intra-moiety cellobiose reaction mechanisms reported in Figure 4.2, these are possibly not the mechanism through which cross-linked cellulose cleaves. The HOMO-LUMO energy gap is indicative of the inter-moiety reaction but not that of the activity of intra-moiety reaction mechanisms studied here. The HOMO orbital shifting from the cellobiose moiety to lignin moiety in LCC supports this. New mechanisms for cross-linked cellobiose cleavage involving atoms in the lignin and cellobiose moiety could possibly be more favored. Cellobiose decomposition mechanisms involving just the cellobiose moiety investigated here have higher energy penalty as they require the HOMO to be on the cellobiose moiety. However, the highest energy occupied molecular orbital is on lignin moiety which can possibly explain the higher barrier for cross-linked cellulose decomposition calculated in LCCs.

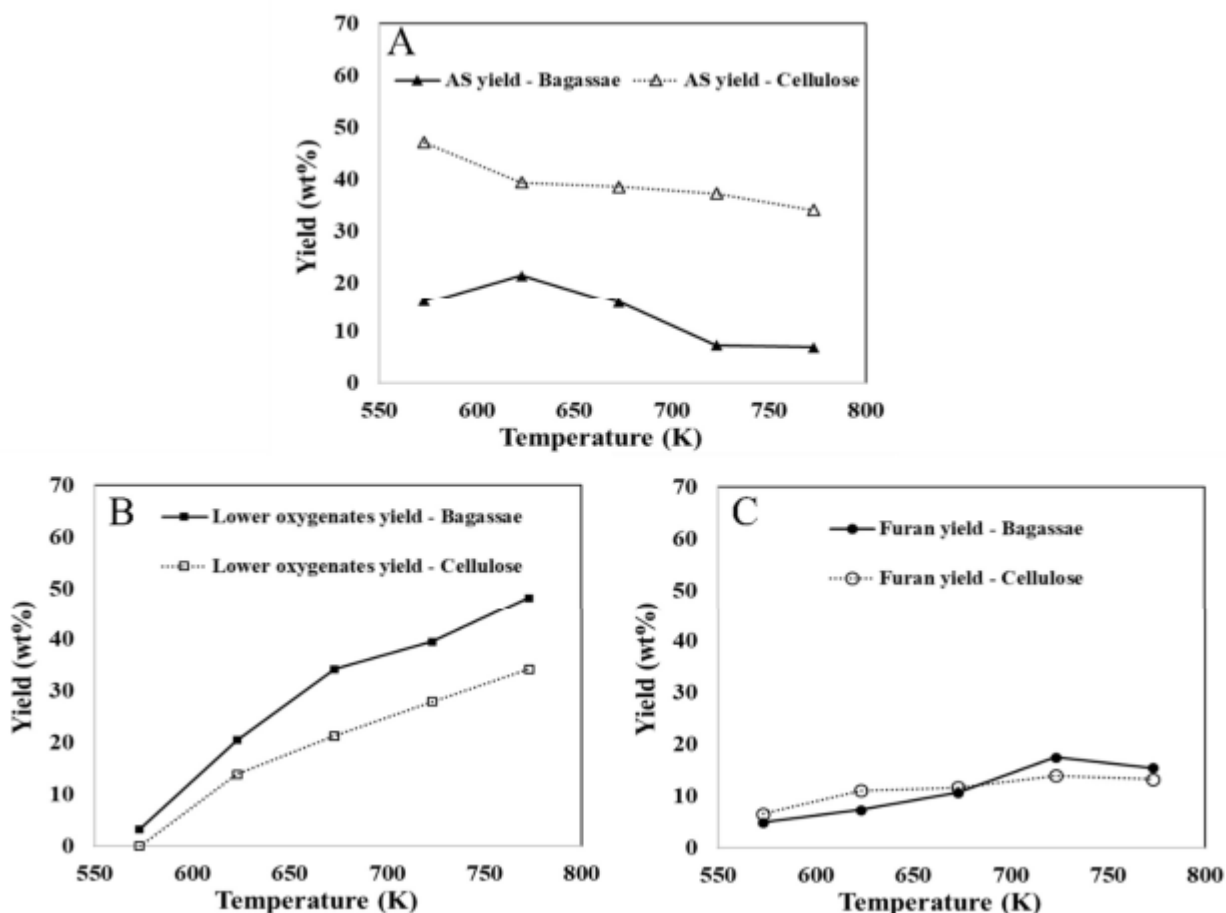


Figure 4.4 Yields (wt%) of bio-oil components (A. Anhydrosugars, B. Lower oxygenates, C. Furans) in the thin-film pyrolysis of native biomass, bagasse (solid line) and that of pure cellulose (dash line).

Table 4.2 Thin-film pyrolysis product distribution at 573K-773K for native biomass bagasse and cellulose ¹³⁷

Temperature (K)	Bagasse Product distribution			Cellulose Product distribution		
	Gases (wt%)	Bio-oil (wt%)	Char (wt%)	Gases (wt%)	Bio-oil (wt%)	Char (wt%)
573	1.34 ± 0.08	36.74 ± 0.14	44.04 ± 0.45	0.12 ± 0.01	61.16 ± 0.22	32.58 ± 0.48
623	1.48 ± 0.05	56.68 ± 0.24	32.86 ± 0.43	2.07 ± 0.013	69.47 ± 0.88	25.53 ± 0.29
673	2.38 ± 0.06	62.36 ± 0.33	27.59 ± 0.35	5.35 ± 0.07	76.23 ± 0.1	17.12 ± 0.2
723	2.8 ± 0.05	66.23 ± 0.11	22.96 ± 0.93	6.41 ± 0.04	82.81 ± 0.1	11.13 ± 0.9
773	3.85 ± 0.29	68.44 ± 0.12	17.77 ± 0.15	7.04 ± 0.07	84.99 ± 0.1	8.79 ± 0.12

The reported activation barriers for the three mechanisms produce three major bio-oil components – anhydrosugars (LGA), furans (5-HMF) and lower oxygenates (GA). To validate these first principles calculations and the corresponding activation barriers, thin-film pyrolysis experiments were conducted on bagasse as model biomass for cross-linked cellulose. The product distribution and bio-oil composition are then compared to previously reported thin-film pyrolysis of pure cellulose ¹³⁷. This enables comparison between the first principles barriers and the experimental yields of the three bio-oil components.

4.3.4 Thin-film pyrolysis experiment product yields for pure cellulose and cross-linked cellulose in native biomass (Bagasse)

In this section the overall product yield, including the percentages of non-condensable gases, bio-oil, and char, as well as the individual yields of bio-oil components such as anhydrosugars (including LGA), furans, and light oxygenates (including glycolaldehyde) are examined. The effect of cross-linked cellulose on the yields of these bio-oil components, non-condensable gases, and char is highlighted. Further, the experimental data from thin-film pyrolysis provides valuable insights into the thermal decomposition pathways of both cross-linked and pure cellulose. These findings are then compared to first principles calculations to establish parallels between the experimental and theoretical results.

The pyrolysis of bagasse thin films in the temperature range of 573-773 K resulted in the production of non-condensable gases (1.3-3.9 wt%), bio-oil (36-69 wt%), and char (17-45 wt%) as major products, as shown in Table 4.2. The total yield of pyrolysis products, including non-condensable gases, bio-oil, and char, ranged from 86 to 93 wt% (see Table 4.2), the carbon balance is consistent with previous experiments ²⁷⁰. These pyrolysis yields for bagasse are compared to those reported for cellulose thin-films under similar pyrolysis conditions ¹³⁷. Increasing temperature resulted in a marginal increase in non-condensable gas production in bagasse (1.3-3.9 wt%) and a prominent increase in pure cellulose (0.12-7.04 wt%). Both materials showed a decreasing trend in char yield with higher pyrolysis temperatures, with bagasse thin-films yielding more char (44.04 to 17.77) than pure cellulose (32.58 to 8.79). The condensable volatile products (bio-oil) during bagasse pyrolysis had higher yields at elevated temperatures, while the char yield decreased, competing with other pyrolysis products ^{270,284}. However, while the trends in char/bio-oil behavior are similar between cellulose and bagasse pyrolysis, bagasse containing cross-linked cellulose (in LCC) exhibits significantly higher char yields (> 7wt% across all temperatures) compared to pure cellulose. The reduced bio-oil yield in bagasse aligns with the higher activation barriers calculated for decomposition of cellobiose with LCC, compared to pure cellobiose, as discussed in Section 4.3.2. Further, the major components of bio-oil, including LGA, 5-HMF, and GA, which are products of

transglycosylation, ring contraction, and ring opening mechanisms, respectively, were considered for comparison between experimental data and first principles calculations. To facilitate this comparison, the chemical compounds present in bio-oil derived from bagasse were categorized into anhydrosugars, furans, light oxygenates, and phenolic compounds. The formation of anhydrosugars (e.g., levoglucosan), furans (e.g., 5-HMF), and lower oxygenates (e.g., glycolaldehyde) can be attributed to the three mechanisms investigated using first principles calculations. Furthermore, phenolic compounds derived from lignin are found in bagasse bio-oil, while pyrans are present in cellulose-derived bio-oil¹³⁷. However, the pyrolysis of lignin into phenolic compounds falls beyond the scope of this paper.

The yields of bio-oil components from bagasse and pure cellulose, are measured as a percentage of their carbohydrate content. Biomass pyrolysis research has focused on cellulose-based materials due to their abundance in biomass and their potential impact on bio-oil yield and composition^{252,270,285}. In this context, comparing the decomposition of bagasse with that of cellulose under similar reaction conditions is valuable. The findings reveal that within the temperature range of 573-773 K, the anhydrosugar yield in bagasse pyrolysis decreased from 16 wt% to 6.85 wt%, while the yields of furans and lower oxygenates increased from 6.57 wt% to 13.22 wt% and from 0 wt% to 34.16 wt%, respectively. The results also demonstrate that furans derived from bagasse thin-film pyrolysis exhibit a similar temperature-dependent trend as observed in cellulose thin-film pyrolysis. However, the anhydrosugar yields in bagasse were significantly lower compared to cellulose pyrolysis (ranging from 34 wt% to 48 wt%). This study further highlights the influence of cross-linked cellulose with lignin in lignocellulosic complexes (LCCs) on anhydrosugar yields, which are compensated by increased C1-C3 product yields (lower oxygenates). Moreover, the compensation by lower oxygenates is also supported by first-principles calculated reaction energies reported in Table 4.1. The reaction energy is more endergonic (~10kcal/mol) for the formation of glycolaldehyde compared to LGA or furan, making it more thermodynamically favorable at higher temperatures. A recent publication¹⁶⁵ investigating the impact of cross-linking in fast pyrolysis of lignocellulosic biomass presents the only notable comparability to the findings of this study. The selective removal of lignin or hemicellulose from treated biomass led to

significant changes in LCC composition, affecting the yields of levoglucosan (LGA) and C1-C3 products, in alignment with the results obtained from pure cellulose ¹³⁷. The observed trends in product yields from bagasse pyrolysis correspond with the literature for untreated herbaceous biomass, particularly in terms of bio-oil compounds, anhydrosugars, and light oxygenates.

4.3.5 Reaction kinetics and thermochemistry for cross-linked cellulose (in LCC) decomposition

We have reported a significant increase in the activation barrier (~2X) for the formation of three major pyrolysis products in cross-linked cellobiose (LCC) as compared to pure cellobiose (*c.f.* Figure 4.2). Additionally, cross-linking between lignin and cellulose also seems to alter the thermodynamics of the reaction. The reaction energies (*c.f.* Table 4.1) also increase significantly (~3X-4X). Probing primary decomposition reaction kinetics experimentally is limited by the timescale difference between product evolution and analysis. However, the apparent activation energies of product formations calculated from millisecond scale kinetics can be used as reactivity criteria for comparing different biomass feedstocks and relative rates of product formations. The only millisecond scale data available is for woody biomass (loblolly) ¹⁶⁶ which has been suggested to have significantly low number of LCC linkages as compared to herbaceous biomass. Consequently, the overall kinetics between pure cellulose and such woody biomass exhibits minimum difference as it's the LCC linkage that alters product yields and not the mere presence of lignin ¹⁶⁵. Such millisecond scale experimental kinetics is currently unavailable for herbaceous biomass hindering the investigation of the direct role of cross-linked cellulose on its decomposition kinetics and thermochemistry. However, as mentioned in the previous section, product yields from the pyrolysis of chemically treated and untreated native biomass reveals a drastic shift in LGA and C₁-C₃ product yields. The difference in product yields was suggested to be because of the LCC linkage being made at the glycosyl C6 position that hinders the formation of C6-O-C1 bridge resulting in less efficient release of LGA end-groups ²⁵⁹. However, other thermodynamically feasible LCCs ³⁴ made at 3 linkage sites (LCC-C2, LCC-C3, LCC-C6) exhibited comparable activation barriers (*c.f.* Figure 4.2) for cellobiose decomposition with LCC-C3 having marginally

higher barriers. Further details about these minimal deviations among different LCC sites can be found in the SI.

The increased experimental yield of light oxygenates compared to LGA could be a result of altered kinetics, thermochemistry and/or reaction pathway. The higher reaction energy (~10-15 kcal/mol) and the endergonic nature of GA (light oxygenate) compared to LGA indicate that the formation of GA will be relatively more favored at higher temperatures. Higher temperatures also facilitate the overcoming of kinetic barriers, making the more endergonic formation of light oxygenates favored. Moreover, in addition to the enhancement of kinetic or thermochemistry, the breakdown of cellulose in LCC molecules could involve alternate reaction pathways, such as ring opening and dehydration rearrangement, leading to the formation of C1-C3 small molecules²⁸⁶. The lower HOMO-LUMO energy gap and the position of the HOMO orbital on electron-rich phenyl groups suggest that inter-moiety mechanisms could be more favourable. These findings indicate that the difference in product distribution during the pyrolysis of cross-linked cellobiose, compared to pure cellobiose, not only reflects a change in kinetics but also potentially a difference in reaction pathway. To gain further insights into alternate chemistry and kinetics, one can draw parallels between the experimental yields measured in this study and first principles calculated activation barriers. The presence of LCC linkages can alter kinetic and thermodynamic parameters for cellulose cleavage, such as reaction energy and activation barriers for the same reaction mechanism. Alternatively, the LCC linkage can promote alternate reaction pathways (other than cleavage of glycosidic linkage in cellulose as the first step in cellulose decomposition), thereby changing the ultimate product yields. Comparing the relative differences in product yields between cellulose and lignocellulosic complexes (LCCs), such as bagasse, provides qualitative insights to distinguish between the effects of altered kinetics or altered reaction pathway and reaction pathways. Analysis of Figure 4.4 shows a consistent gap in the yields of anhydrosugars between bagasse and cellulose (with a constant relative yield), indicating kinetic inhibition in LCCs while maintaining the reaction mechanism for LGA formation. For C1-C3 products, both relative and absolute yields change, indicating changes in both kinetics and reaction pathways. On the other hand, the absolute and relative yields of furans are comparable, suggesting that the reaction pathway and kinetics of furan

formation during cellulose decomposition remain unchanged in both bagasse and cellulose. This also indicates that the LCC linkage only affects the primary decomposition of cellulose, as a significant portion of furans is formed through secondary reactions during cellulose pyrolysis¹²⁶, which remain unaffected. Furthermore, the modification of lignin functional groups has been observed to facilitate lignin depolymerization [78]. Similarly, the interaction between lignin and carbohydrates in LCCs could induce novel chemical reactions, such as inter-moiety mechanisms, leading to cellulose cleavage involving lignin depolymerization.

4.4 Conclusions

This study investigates the role of cross-linked cellulose with lignin in lignin-carbohydrate complexes (LCC) during cellulose decomposition, focusing on its effects on reaction kinetics, thermochemistry and reaction pathways. Ab initio molecular dynamics and metadynamics simulations are employed to model LCC molecules with β -O-4 benzyl ether linkages, connecting cellulose and lignin dimers (cellobiose and quinone methide intermediate) at thermodynamically feasible positions in different conformations. First principles density functional theory (DFT) calculations are then conducted to screen for the lowest energy conformers and to determine the transition states for three major reaction mechanisms (transglycosylation, ring contraction, ring opening) producing bio-oil components (levoglucosan, 5-hydroxymethylfurfural, glycolaldehyde) at 500K. Activation barriers, reaction energies, and frontier molecular orbital interactions are analyzed to gain insights into the role of LCC linkages in cellulose decomposition. Experimental measurements of anhydrosugars, furans, and lower oxygenates in native herbaceous biomass (bagasse) pyrolysis are compared with yields from pure cellulose pyrolysis. The calculated activation barriers and experimental product yields provide evidence of different kinetics, thermochemistry and potentially reaction pathways induced by cross-linked lignin in LCC. Notably, higher activation barriers and reaction energies are observed for cross-linked cellobiose cleavage in LCC compared to pure cellobiose, indicating altered kinetics/thermochemistry. The higher endergonic nature (reaction energy) of GA formation in comparison to LGA suggests that cellulose decomposition can be effectively promoted at higher temperatures, favoring the production of lighter

oxygenates, particularly GA. This is in strong agreement with the increased relative yields of lower oxygenates over anhydrosugars in bagasse. In addition, the preference for inter-moiety mechanisms over intra-moiety cellulose decomposition is indicated by the high activation barrier for the intra-moiety mechanism and the low HOMO-LUMO energy gap. Comparison of relative differences in product yields between bagasse and cellulose provides additional evidence supporting the presence of alternative reaction pathways. This combined computational and experimental study sheds light on the distinct role played by cross-linked lignin-carbohydrate bonding in influencing reaction kinetics, thermochemistry and mechanisms of cellulose decomposition.

Chapter 5 Conclusions and Future Perspectives

5.1 Conclusions

This thesis has established the role of thermal changes in the pyrolysis condensed phase and direct covalent bonding with lignin on cellulose pyrolysis chemistry. The formation of major cellulose pyrolysis products levoglucosan (LGA) and 5-hydroxymethyl furan (5-HMF) is studied using the glycosidic bond cleavage mechanisms transglycosylation and ring contraction. Condensed phase effects induced by high temperature pyrolysis environment on cellulose decomposition are quantified by calculating the free energy barriers in pure cellulose. To overcome the limitations of traditional ab-initio methods, a novel computational strategy known as the ReSolv method has been developed, effectively combining quantum mechanics (QM) and molecular mechanics (MM) approaches to circumvent computationally expensive AIMD calculations. Through the integration of first principles density functional theory (DFT) calculations in the gas phase with thermodynamic integration techniques based on molecular mechanics (MM), the ReSolv method enables the accurate estimation of free energy barriers for cellulose primary decomposition reaction mechanisms in the pyrolysis melt-phase.

This investigation of pure cellobiose pyrolysis chemistry at finite temperatures in the condensed phase challenges the conventional hypothesis of mechanistic differences in cellulose cleavage leading to the two kinetic regimes. The low temperature regime is enthalpy controlled exhibiting a high enthalpic barrier while the high temperature regime has a low enthalpic barrier. Entropic activation leads to a thermal drop in the free energy barrier (by 264 kJ/mol for transglycosylation and 179 kJ/mol for ring contraction) resulting in the regime change for either mechanism studied. Glycosidic bond cleavage requires conformational change from chair to boat and this is hindered by the directional hydrogen bond network. The additional energy required to break the hydrogen bonds and create enough torsional freedom for conformation change is reflected in the higher activation barrier for glycosidic bond cleavage. Beyond 900K, the hydrogen bond network is completely disrupted, and maximum torsional freedom is gained. This destabilization of the reactant cellulose in the condensed phase by the thermal cleavage of hydrogen bonds results in a lower activation barrier.

This high temperature melting (melt-phase) process in native biomass is studied using two distinct local reaction environments: 1. melt-phase with covalent lignin-carbohydrate complex (LCC) linkages and 2. lignin-rich melt-phase devoid of such linkages. Unlike the the large thermal change in free energy barrier in pure cellobiose melt-phase, the LCC melt-phase demonstrates a more moderate drop. In the lignin-rich melt-phase, the condensed phase environment exerts no significant influence, and the activation free energy barriers remain comparable to those in the gas phase. The pure cellobiose melt-phase exhibits drastic thermal disruption of directional hydrogen bonding at high temperatures. While in the LCC melt-phase, the presence of lignin partially disrupts the formation of long-range hydrogen bonds and provides torsional freedom in the condensed phase even at lower temperatures. Despite the different thermal responses, in all three local reaction environments, the thermal shift in the condensed phase with the disruption of the hydrogen bonding network and in turn the conformational flexibility in hydroxymethyl group orientation seem to directly map onto the thermal shift in the free-energy barriers for cellobiose activation. These findings underscore the critical importance of considering finite temperature condensed phase effects and highlight the distinct impact of physical interactions with lignin on cellulose activation.

Apart from condensed phase effects, the direct covalent bonding between cellobiose and lignin also influences cellulose decomposition chemistry. The role of cross-linked lignin on cellulose chemistry is studied using lignin-carbohydrate complexes (LCCs) with cellulose and lignin dimers (cellobiose and quinone methide intermediate) connected at thermodynamically feasible positions on the sugar - C2, C3, C4. The low energy LCC conformers with β -O-4 benzyl ether linkages are identified using ab initio molecular dynamics and metadynamics techniques followed by systematical screened using DFT calculations. Three widely reported reaction mechanisms (transglycosylation, ring contraction, and ring opening), which are responsible for the formation of major bio-oil components (LGA, 5-HMF and glycolaldehyde (GA)) at 500 K are investigated. The product yields of these bio-oil components are further measured using thin-film pyrolysis of native herbaceous biomass (bagasse). The high endergonic nature of GA formation over other products promoted a higher yield of GA at high temperatures. This agrees with the thermal increase in GA product yields compensated for by the reduction in LGA.

Moreover, in the LCC molecule, while the LUMO is on the cellobiose moiety, the HOMO is located away on the nucleophilic lignin moiety. This indicated that the electron rich phenyl groups in lignin are likely to participate in cellulose decomposition reactions leading to the cleavage of the LCC bond. Therefore, conventional intra-moiety cellobiose reaction mechanisms in LCC exhibit significantly high activation barriers (2X) and reaction energies (3-4X) when compared to cellobiose across all three reaction mechanisms. The relative yield between cellulose and bagasse pyrolysis for GA increases while it remains constant for the other two products. This reveals that the reaction mechanism for GA formation changes in LCC molecule while only the kinetics is altered for LGA and furan formation.

In summary, this comprehensive investigation has provided invaluable insights into the complex interplay between cellulose reaction energetics, thermal effects, and the presence of lignin in the pyrolysis reaction environment. The findings significantly contribute to our understanding of cellulose chemistry under pyrolysis conditions and offer critical insights into the role of condensed phase effects and lignin-carbohydrate interactions in reaction kinetics and chemistry. A future direction for this work involves the inclusion of finite temperature melt-phase effects in investigating the impact of covalent bonding in LCC. Further, such first principles modelling can be extended to secondary pyrolysis reactions to be integrated in particles models enabling comparison with kinetic experiments.

5.2 Future Perspectives

Looking forward, this research can delve deeper into understanding how condensed phase effects influence the breakdown of cellulose when it is bonded to lignin within lignin-carbohydrate complexes (LCCs). While our current focus centers on the benzyl ether linkage in woody plants, future investigations may extend to other linkages such as Phenyl Glycosidic LCC linkages. Moreover, while our primary emphasis lies in cellulose chemistry and intra-molecular mechanisms, we recognize the potential for exploring inter-molecular mechanisms within the covalently bonded lignin-carbohydrate matrix present in native biomass.

Further avenues for research include:

- Examining the impact of varying chain lengths, including the presence of other carbohydrates like hemicellulose.
- Investigating the role of inorganic compounds such as magnesium, calcium, and sodium, which are commonly found in native biomass.
- Facilitating direct comparisons between experimental results and our first principles calculations by utilizing chemically tailored native biomass samples with known LCC linkages.
- Designing experimental protocols that enable the kinetic analysis of primary decomposition reactions.

This forward-looking perspective underscores the potential for expanding our understanding of cellulose-lignin interactions, thereby contributing significantly to the field of biomass conversion.

Bibliography

- (1) Miret, C.; Chazara, P.; Montastruc, L.; Negny, S.; Domenech, S. Design of Bioethanol Green Supply Chain: Comparison between First and Second Generation Biomass Concerning Economic, Environmental and Social Criteria. *Comput. & Chem. Eng.* **2016**, *85*, 16–35. <https://doi.org/https://doi.org/10.1016/j.compchemeng.2015.10.008>.
- (2) Huber, G. W.; Iborra, S.; Corma, A. Synthesis of Transportation Fuels from Biomass: Chemistry, Catalysts, and Engineering. *Chem. Rev.* **2006**, *106* (9), 4044–4098. <https://doi.org/10.1021/cr068360d>.
- (3) Magdalena, G.; Joshi, S.; Maclean, H. A Review of US and Canadian Biomass Supply Studies. *BioResources* **2009**, *4*.
- (4) Bradley, D.; Solutions, C. C. Canada Biomass-Bioenergy Report. *Clim. Chang. Solut. Bioenergy Task* **2006**.
- (5) Alam, M. B.; Pulkki, R.; Shahi, C. Woody Biomass Availability for Bioenergy Production Using Forest Depletion Spatial Data in Northwestern Ontario. *Can. J. For. Res.* **2012**, *42* (3), 506–516. <https://doi.org/10.1139/x2012-011>.
- (6) Naik, S. N.; Goud, V. V.; Rout, P. K.; Dalai, A. K. Production of First and Second Generation Biofuels: A Comprehensive Review. *Renew. Sustain. Energy Rev.* **2010**, *14* (2), 578–597. <https://doi.org/https://doi.org/10.1016/j.rser.2009.10.003>.
- (7) Organization, A. *The State of Food and Agriculture 2008: Biofuels: Prospects, Risks and Opportunities*; Food & Agriculture Org., 2008.
- (8) Sanderson, K. A Field in Ferment. *Nature* **2006**, *444* (7120), 673–676.
- (9) Laursen, W. Students Take a Green Initiative. *Chem. Eng.* **2006**, *774*, 32–34.
- (10) Vispute, T.; Huber, G. Breaking the Chemical and Engineering Barriers to Lignocellulosic Biofuels. *Int. Sugar J.* **2008**, *110*, 138–149.
- (11) Zhou, C.-H.; Xia, X.; Lin, C.-X.; Tong, D.-S.; Beltramini, J. Catalytic Conversion of

- Lignocellulosic Biomass to Fine Chemicals and Fuels. *Chem. Soc. Rev.* **2011**, *40* (11), 5588–5617. <https://doi.org/10.1039/C1CS15124J>.
- (12) Yousuf, A.; Pirozzi, D.; Sannino, F. Chapter 1 - Fundamentals of Lignocellulosic Biomass. In *Lignocellulosic Biomass to Liquid Biofuels*; Yousuf, A., Pirozzi, D., Sannino, F., Eds.; Academic Press, 2020; pp 1–15.
<https://doi.org/https://doi.org/10.1016/B978-0-12-815936-1.00001-0>.
- (13) Vassilev, S. V.; Baxter, D.; Andersen, L. K.; Vassileva, C. G. An Overview of the Chemical Composition of Biomass. *Fuel* **2010**, *89* (5), 913–933.
<https://doi.org/https://doi.org/10.1016/j.fuel.2009.10.022>.
- (14) Batidzirai, B.; Mignot, A. P. R.; Schakel, W. B.; Junginger, H. M.; Faaij, A. P. C. Biomass Torrefaction Technology: Techno-Economic Status and Future Prospects. *Energy* **2013**, *62*, 196–214.
<https://doi.org/https://doi.org/10.1016/j.energy.2013.09.035>.
- (15) Arsène, M.-A.; Bilba, K.; Jr, H.; Ghavami, K. Treatments of Non-Wood Plant Fibres Used as Reinforcement in Composite Materials. *Mater. Res.* **2013**, *16*, 903–923. <https://doi.org/10.1590/S1516-14392013005000084>.
- (16) Smit, A.; Huijgen, W. Effective Fractionation of Lignocellulose in Herbaceous Biomass and Hardwood Using a Mild Acetone Organosolv Process. *Green Chem.* **2017**, *19*. <https://doi.org/10.1039/C7GC02379K>.
- (17) Nhuchhen, D.; Basu, P.; Acharya, B. A Comprehensive Review on Biomass Torrefaction. *Int. J. Renew. Energy Biofuels* **2014**, DOI: 10.51, 56.
<https://doi.org/10.5171/2014.506376>.
- (18) Yu, J.; Paterson, N.; Blamey, J.; Millan, M. Cellulose, Xylan and Lignin Interactions during Pyrolysis of Lignocellulosic Biomass. *Fuel* **2017**, *191*, 140–149. <https://doi.org/https://doi.org/10.1016/j.fuel.2016.11.057>.
- (19) Zhang, J.; Choi, Y. S.; Yoo, C. G.; Kim, T. H.; Brown, R. C.; Shanks, B. H. Cellulose–Hemicellulose and Cellulose–Lignin Interactions during Fast Pyrolysis.

- ACS Sustain. Chem. Eng.* **2015**, 3 (2), 293–301.
<https://doi.org/10.1021/sc500664h>.
- (20) Haykiri-Acma, H.; Yaman, S.; Kucukbayrak, S. Comparison of the Thermal Reactivities of Isolated Lignin and Holocellulose during Pyrolysis. *Fuel Process. Technol.* **2010**, 91 (7), 759–764.
<https://doi.org/https://doi.org/10.1016/j.fuproc.2010.02.009>.
- (21) Dionisi, D.; Anderson, J. A.; Aulenta, F.; McCue, A.; Paton, G. The Potential of Microbial Processes for Lignocellulosic Biomass Conversion to Ethanol: A Review. *J. Chem. Technol. Biotechnol.* **2015**, 90 (3), 366–383.
<https://doi.org/10.1002/jctb.4544>.
- (22) Adams, P.; Bridgwater, T.; Lea-Langton, A.; Ross, A.; Watson, I. Biomass Conversion Technologies. In *Greenhouse Gas Balances of Bioenergy Systems*; 2018; pp 107–139. <https://doi.org/10.1016/B978-0-08-101036-5.00008-2>.
- (23) Goyal, H.; Seal, D.; Saxena, R. Bio-Fuels from Thermochemical Conversion of Renewable Resources: A Review. *Renew. Sustain. Energy Rev.* **2008**, 12, 504–517. <https://doi.org/10.1016/j.rser.2006.07.014>.
- (24) FAO. Unified Bioenergy Terminology. Food and Agriculture Organization of the United Nations Rome 2004.
- (25) Lee, S. Y.; Sankaran, R.; Chew, K. W.; Tan, C. H.; Krishnamoorthy, R.; Chu, D.-T.; Show, P.-L. Waste to Bioenergy: A Review on the Recent Conversion Technologies. *BMC Energy* **2019**, 1 (1), 4. <https://doi.org/10.1186/s42500-019-0004-7>.
- (26) Balat, M. Biomass Energy and Biochemical Conversion Processing for Fuels and Chemicals. *Energy Sources, Part A Recover. Util. Environ. Eff.* **2006**, 28 (6), 517–525. <https://doi.org/10.1080/009083190927994>.
- (27) Cantrell, K. B.; Ducey, T.; Ro, K. S.; Hunt, P. G. Livestock Waste-to-Bioenergy Generation Opportunities. *Bioresour. Technol.* **2008**, 99 (17), 7941–7953.

<https://doi.org/10.1016/j.biortech.2008.02.061>.

- (28) Abo, B. O.; Gao, M.; Wang, Y.; Wu, C.; Ma, H.; Wang, Q. Lignocellulosic Biomass for Bioethanol: An Overview on Pretreatment, Hydrolysis and Fermentation Processes. *Rev. Environ. Health* **2019**, *34* (1), 57–68.
<https://doi.org/10.1515/reveh-2018-0054>.
- (29) Bibi, R.; Ahmad, Z.; Imran, M.; Hussain, S.; Ditta, A.; Mahmood, S.; Khalid, A. Algal Bioethanol Production Technology: A Trend towards Sustainable Development. *Renew. Sustain. Energy Rev.* **2017**, *71* (C), 976–985.
<https://doi.org/10.1016/j.rser.2016.12.12>.
- (30) Balat, M. Production of Bioethanol from Lignocellulosic Materials via the Biochemical Pathway: A Review. *Energy Convers. Manag.* **2011**, *52* (2), 858–875.
<https://doi.org/https://doi.org/10.1016/j.enconman.2010.08.013>.
- (31) Teter, S. A.; Sutton, K. B.; Emme, B. 7 - Enzymatic Processes and Enzyme Development in Biorefining. In *Advances in Biorefineries*; Waldron, K., Ed.; Woodhead Publishing, 2014; pp 199–233.
<https://doi.org/https://doi.org/10.1533/9780857097385.1.199>.
- (32) Sun, Y.; Cheng, J. Hydrolysis of Lignocellulosic Materials for Ethanol Production: A Review. *Bioresour. Technol.* **2002**, *83* (1), 1–11.
[https://doi.org/https://doi.org/10.1016/S0960-8524\(01\)00212-7](https://doi.org/https://doi.org/10.1016/S0960-8524(01)00212-7).
- (33) Mushrif, S. Multiscale Molecular Modeling Can Be an Effective Tool to Aid the Development of Biomass Conversion Technology: A Perspective. *Chem. Eng. Sci.* **2015**, *121*, 217–235. <https://doi.org/10.1016/j.ces.2014.08.019>.
- (34) Hu, J.; Jiang, B.; Liu, J.; Sun, Y.; Jiang, X. Influence of Interactions between Biomass Components on Physicochemical Characteristics of Char. *J. Anal. Appl. Pyrolysis* **2019**, *144*, 104704.
- (35) Werpy, T.; Petersen, G. *Top Value Added Chemicals from Biomass: Volume I-- Results of Screening for Potential Candidates from Sugars and Synthesis Gas*;

2004.

- (36) Alamillo, R.; Tucker, M.; Chia, M.; Pagan-Torres, Y.; Dumesic, J. The Selective Hydrogenation of Biomass-Derived 5-Hydroxymethylfurfural Using Heterogeneous Catalysts. *Green Chem.* **2012**, *14*, 1413–1419. <https://doi.org/10.1039/C2GC35039D>.
- (37) Wang, D.; Osmundsen, C.; Taarning, E.; Dumesic, J. Selective Production of Aromatics from Alkylfurans over Solid Acid Catalysts. *ChemCatChem* **2013**, *5*. <https://doi.org/10.1002/cctc.201200757>.
- (38) Lin, Y.-C.; Huber, G. W. The Critical Role of Heterogeneous Catalysis in Lignocellulosic Biomass Conversion. *Energy Environ. Sci.* **2009**, *2* (1), 68–80. <https://doi.org/10.1039/B814955K>.
- (39) Zhou, X.; Nolte, M. W.; Mayes, H. B.; Shanks, B. H.; Broadbelt, L. J. Experimental and Mechanistic Modeling of Fast Pyrolysis of Neat Glucose-Based Carbohydrates. 1. Experiments and Development of a Detailed Mechanistic Model. *Ind. Eng. Chem. Res.* **2014**, *53* (34), 13274–13289. <https://doi.org/10.1021/ie502259w>.
- (40) Demirbas, A.; Arin, G. An Overview of Biomass Pyrolysis. *Energy Sources* **2002**, *24* (5), 471–482. <https://doi.org/10.1080/00908310252889979>.
- (41) Bridgwater, T. Biomass for Energy. *J. Sci. Food Agric.* **2006**, *86* (12), 1755–1768.
- (42) Vinu, R.; Broadbelt, L. A Mechanistic Model of Fast Pyrolysis of Glucose-Based Carbohydrates to Predict Bio-Oil Composition. *Energy Environ. Sci.* **2012**, *5*, 9808–9826. <https://doi.org/10.1039/C2EE22784C>.
- (43) Czernik, S.; Bridgwater, A. V. Overview of Applications of Biomass Fast Pyrolysis Oil. *Energy Fuels* **2004**, *18* (2), 590–598. <https://doi.org/10.1021/ef034067u>.
- (44) Mettler, M. S.; Vlachos, D. G.; Dauenhauer, P. J. Top Ten Fundamental Challenges of Biomass Pyrolysis for Biofuels. *Energy Environ. Sci.* **2012**, *5* (7), 7797–7809. <https://doi.org/10.1039/C2EE21679E>.

- (45) Mansoori, G. A.; Enayati, N.; Agyarko, L. B. Energy: Sources, Utilization, Legislation, Sustainability, Illinois as Model State Is an 800-Page.
- (46) Anex, R. P.; Aden, A.; Kazi, F. K.; Fortman, J.; Swanson, R. M.; Wright, M. M.; Satrio, J. A.; Brown, R. C.; Daugaard, D. E.; Platon, A.; Kothandaraman, G.; Hsu, D. D.; Dutta, A. Techno-Economic Comparison of Biomass-to-Transportation Fuels via Pyrolysis, Gasification, and Biochemical Pathways. *Fuel* **2010**, *89*, S29– S35. <https://doi.org/https://doi.org/10.1016/j.fuel.2010.07.015>.
- (47) Mettler, M. S.; Paulsen, A. D.; Vlachos, D. G.; Dauenhauer, P. J. Pyrolytic Conversion of Cellulose to Fuels: Levoglucosan Deoxygenation via Elimination and Cyclization within Molten Biomass. *Energy Environ. Sci.* **2012**, *5* (7), 7864–7868.
- (48) Regulator, A. E. Alberta's Energy Reserves 2013 and Supply/Demand Outlook 2014--2023. *Alberta Energy Regul. Calgary, AB., Stat. Ser. ST98* **2014**, 1.
- (49) Hart, A. A Review of Technologies for Transporting Heavy Crude Oil and Bitumen via Pipelines. *J. Pet. Explor. Prod. Technol.* **2014**, *4* (3), 327–336.
- (50) Nolte, M. W.; Liberatore, M. W. Viscosity of Biomass Pyrolysis Oils from Various Feedstocks. *Energy Fuels* **2010**, *24* (12), 6601–6608. <https://doi.org/10.1021/ef101173r>.
- (51) Brown, T. R.; Thilakaratne, R.; Brown, R. C.; Hu, G. Techno-Economic Analysis of Biomass to Transportation Fuels and Electricity via Fast Pyrolysis and Hydroprocessing. *Fuel* **2013**, *106*, 463–469.
- (52) Agarwal, V.; Dauenhauer, P. J.; Huber, G. W.; Auerbach, S. M. Ab Initio Dynamics of Cellulose Pyrolysis: Nascent Decomposition Pathways at 327 and 600 °C. *J. Am. Chem. Soc.* **2012**, *134* (36), 14958–14972. <https://doi.org/10.1021/ja305135u>.
- (53) Carlson, T. R.; Vispute, T. P.; Huber, G. W. Green Gasoline by Catalytic Fast Pyrolysis of Solid Biomass Derived Compounds. *ChemSusChem* **2008**, *1* (5),

397–400.

- (54) Bridgwater, T. Renewable Fuels and Chemicals by Thermal Processing of Biomass. *Chem. Eng. J.* **2003**, *91*, 87–102.
[https://doi.org/10.1016/S1385-8947\(02\)00142-0](https://doi.org/10.1016/S1385-8947(02)00142-0).
- (55) Nachenius, R. W.; Ronsse, F.; Venderbosch, R. H.; Prins, W. Chapter Two - Biomass Pyrolysis. In *Chemical Engineering for Renewables Conversion*; Murzin, D. Y., Ed.; Advances in Chemical Engineering; Academic Press, 2013; Vol. 42, pp 75–139. [https://doi.org/https://doi.org/10.1016/B978-0-12-386505-2.00002-X](https://doi.org/10.1016/B978-0-12-386505-2.00002-X).
- (56) Pictet, A.; Sarasin, J. Sur La Distillation de La Cellulose et de l'amidon Sous Pression Réduite. *Helv. Chim. Acta* **1918**, *1* (1), 87–96.
<https://doi.org/10.1002/hlca.19180010109>.
- (57) Sharifzadeh, M.; Sadeqzadeh, M.; Guo, M.; Borhani, T. N.; Konda, N. V. S. N. M.; Garcia, M. C.; Wang, L.; Hallett, J.; Shah, N. The Multi-Scale Challenges of Biomass Fast Pyrolysis and Bio-Oil Upgrading: Review of the State of Art and Future Research Directions. *Prog. Energy Combust. Sci.* **2019**, *71*, 1–80.
[https://doi.org/https://doi.org/10.1016/j.pecs.2018.10.006](https://doi.org/10.1016/j.pecs.2018.10.006).
- (58) Wang, Q.; Li, X.; Wang, K.; Zhu, Y.; Wang, S. Commercialization and Challenges for the Next Generation of Biofuels: Biomass Fast Pyrolysis. In *2010 Asia-Pacific Power and Energy Engineering Conference*; 2010; pp 1–4.
<https://doi.org/10.1109/APPEEC.2010.5448437>.
- (59) Balonek, C. M.; Colby, J. L.; Persson, N. E.; Schmidt, L. D. Rapid Ablative Pyrolysis of Cellulose in an Autothermal Fixed-Bed Catalytic Reactor. *ChemSusChem* **2010**, *3* (12), 1355–1358.
- (60) Antal, M. J. J.; Varhegyi, G. Cellulose Pyrolysis Kinetics: The Current State of Knowledge. *Ind. Eng. Chem. Res.* **1995**, *34* (3), 703–717.
<https://doi.org/10.1021/ie00042a001>.
- (61) Collard, F.-X.; Blin, J. A Review on Pyrolysis of Biomass Constituents:

- Mechanisms and Composition of the Products Obtained from the Conversion of Cellulose, Hemicelluloses and Lignin. *Renew. Sustain. Energy Rev.* **2014**, *38*, 594–608. <https://doi.org/https://doi.org/10.1016/j.rser.2014.06.013>.
- (62) Aqsha, A.; Mahinpey, N.; Mani, T.; Salak, F.; Murugan, P. Study of Sawdust Pyrolysis and Its Devolatilisation Kinetics. *Can. J. Chem. Eng.* **2011**, *89* (6), 1451–1457. <https://doi.org/https://doi.org/10.1002/cjce.20584>.
- (63) Thurner, F.; Mann, U. Kinetic Investigation of Wood Pyrolysis. *Ind. Eng. Chem. Process Des. Dev.* **1981**, *20* (3), 482–488. <https://doi.org/10.1021/i200014a015>.
- (64) McKendry, P. Energy Production from Biomass (Part 1): Overview of Biomass. *Bioresour. Technol.* **2002**, *83* (1), 37–46. [https://doi.org/https://doi.org/10.1016/S0960-8524\(01\)00118-3](https://doi.org/https://doi.org/10.1016/S0960-8524(01)00118-3).
- (65) Shafizadeh, F. Introduction to Pyrolysis of Biomass. *J. Anal. Appl. Pyrolysis* **1982**, *3* (4), 283–305. [https://doi.org/https://doi.org/10.1016/0165-2370\(82\)80017-X](https://doi.org/https://doi.org/10.1016/0165-2370(82)80017-X).
- (66) Sanders, E. B.; Goldsmith, A. I.; Seeman, J. I. A Model That Distinguishes the Pyrolysis of D-Glucose, d-Fructose, and Sucrose from That of Cellulose. Application to the Understanding of Cigarette Smoke Formation. *J. Anal. Appl. Pyrolysis* **2003**, *66* (1), 29–50. [https://doi.org/https://doi.org/10.1016/S0165-2370\(02\)00104-3](https://doi.org/https://doi.org/10.1016/S0165-2370(02)00104-3).
- (67) Bauer, W. D.; Talmadge, K. W.; Keegstra, K.; Albersheim, P. The Structure of Plant Cell Walls: II. The Hemicellulose of the Walls of Suspension-Cultured Sycamore Cells. *Plant Physiol.* **1973**, *51* 1, 174–187.
- (68) Patwardhan, P. R.; Satrio, J. A.; Brown, R. C.; Shanks, B. H. Product Distribution from Fast Pyrolysis of Glucose-Based Carbohydrates. *J. Anal. Appl. Pyrolysis* **2009**, *86* (2), 323–330. <https://doi.org/https://doi.org/10.1016/j.jaap.2009.08.007>.
- (69) Patwardhan, P. R.; Dalluge, D. L.; Shanks, B. H.; Brown, R. C. Distinguishing Primary and Secondary Reactions of Cellulose Pyrolysis. *Bioresour. Technol.* **2011**, *102* (8), 5265–5269.

<https://doi.org/https://doi.org/10.1016/j.biortech.2011.02.018>.

- (70) Mayes, H. B.; Nolte, M. W.; Beckham, G. T.; Shanks, B. H.; Broadbelt, L. J. The Alpha-Bet(a) of Glucose Pyrolysis: Computational and Experimental Investigations of 5-Hydroxymethylfurfural and Levoglucosan Formation Reveal Implications for Cellulose Pyrolysis. *ACS Sustain. Chem. Eng.* **2014**, *2* (6), 1461–1473. <https://doi.org/10.1021/sc500113m>.
- (71) Piskorz, J.; Radlein, D.; Scott, D. S. On the Mechanism of the Rapid Pyrolysis of Cellulose. *J. Anal. Appl. Pyrolysis* **1986**, *9*, 121–137.
- (72) Demirbaş, A. Mechanisms of Liquefaction and Pyrolysis Reactions of Biomass. *Energy Convers. Manag.* **2000**, *41* (6), 633–646. [https://doi.org/https://doi.org/10.1016/S0196-8904\(99\)00130-2](https://doi.org/https://doi.org/10.1016/S0196-8904(99)00130-2).
- (73) Lin, Y.-C.; Cho, J.; Tompsett, G. A.; Westmoreland, P. R.; Huber, G. W. Kinetics and Mechanism of Cellulose Pyrolysis. *J. Phys. Chem. C* **2009**, *113* (46), 20097–20107. <https://doi.org/10.1021/jp906702p>.
- (74) Patwardhan, P. R.; Satrio, J. A.; Brown, R. C.; Shanks, B. H. Influence of Inorganic Salts on the Primary Pyrolysis Products of Cellulose. *Bioresour. Technol.* **2010**, *101* (12), 4646–4655. <https://doi.org/https://doi.org/10.1016/j.biortech.2010.01.112>.
- (75) Varhegyi, G.; Jakab, E.; Antal, M. J. Is the Broido-Shafizadeh Model for Cellulose Pyrolysis True? *Energy & Fuels* **1994**, *8* (6), 1345–1352. <https://doi.org/10.1021/ef00048a025>.
- (76) Diebold, J. P. A Unified, Global Model for the Pyrolysis of Cellulose. *Biomass and Bioenergy* **1994**, *7* (1), 75–85. [https://doi.org/https://doi.org/10.1016/0961-9534\(94\)00039-V](https://doi.org/https://doi.org/10.1016/0961-9534(94)00039-V).
- (77) Broido, A.; Nelson, M. A. Char Yield on Pyrolysis of Cellulose. *Combust. Flame* **1975**, *24*, 263–268.
- (78) Bradbury, A. G. W.; Sakai, Y.; Shafizadeh, F. A Kinetic Model for Pyrolysis of

- Cellulose. *J. Appl. Polym. Sci.* **1979**, *23* (11), 3271–3280.
- (79) Lédé, J. Cellulose Pyrolysis Kinetics: An Historical Review on the Existence and Role of Intermediate Active Cellulose. *J. Anal. Appl. Pyrolysis* **2012**, *94*, 17–32. <https://doi.org/10.1016/J.JAAP.2011.12.019>.
- (80) White, J. E.; Catallo, W. J.; Legendre, B. L. Biomass Pyrolysis Kinetics: A Comparative Critical Review with Relevant Agricultural Residue Case Studies. *J. Anal. Appl. Pyrolysis* **2011**, *91* (1), 1–33.
- (81) Şerbănescu, C. Kinetic Analysis of Cellulose Pyrolysis: A Short Review. *Chem. Pap.* **2014**, *68* (7), 847–860. <https://doi.org/10.2478/s11696-013-0529-z>.
- (82) Mettler, M. S.; Mushrif, S. H.; Paulsen, A. D.; Javadekar, A. D.; Vlachos, D. G.; Dauenhauer, P. J. Revealing Pyrolysis Chemistry for Biofuels Production: Conversion of Cellulose to Furans and Small Oxygenates. *Energy Environ. Sci* **2012**, *5* (1), 5414–5424. <https://doi.org/10.1039/C1EE02743C>.
- (83) Krumm, C.; Pfaendtner, J.; Dauenhauer, P. J. Millisecond Pulsed Films Unify the Mechanisms of Cellulose Fragmentation. *Chem. Mater.* **2016**, *28* (9), 3108–3114. <https://doi.org/10.1021/acs.chemmater.6b00580>.
- (84) Schmidt, L. D. Millisecond Chemical Reactions and Reactors. In *12th International Congress on Catalysis*; Corma, A., Melo, F. V, Mendioroz, S., Fierro, J. L. G. B. T.-S. in S. S. and C., Eds.; Elsevier, 2000; Vol. 130, pp 61–81. [https://doi.org/https://doi.org/10.1016/S0167-2991\(00\)80945-3](https://doi.org/https://doi.org/10.1016/S0167-2991(00)80945-3).
- (85) Zhu, C.; Krumm, C.; Facas, G. G.; Neurock, M.; Dauenhauer, P. J. Energetics of Cellulose and Cyclodextrin Glycosidic Bond Cleavage. *React. Chem. Eng.* **2017**, *2* (2), 201–214. <https://doi.org/10.1039/C6RE00176A>.
- (86) Zhou, X.; Nolte, M. W.; Shanks, B. H.; Broadbelt, L. J. Experimental and Mechanistic Modeling of Fast Pyrolysis of Neat Glucose-Based Carbohydrates. 2. Validation and Evaluation of the Mechanistic Model. *Ind. Eng. Chem. Res.* **2014**, *53* (34), 13290–13301. <https://doi.org/10.1021/ie502260q>.

- (87) Vinu, R.; Broadbelt, L. J. Unraveling Reaction Pathways and Specifying Reaction Kinetics for Complex Systems. *Annu. Rev. Chem. Biomol. Eng.* **2012**, *3* (1), 29–54. <https://doi.org/10.1146/annurev-chembioeng-062011-081108>.
- (88) Murillo, J. D.; Biernacki, J. J.; Northrup, S.; Mohammad, A. S. BIOMASS PYROLYSIS KINETICS: A REVIEW OF MOLECULAR-SCALE MODELING CONTRIBUTIONS. *Brazilian J. Chem. Eng.* **2017**, *34*, 1–18.
- (89) ATALLA, R. H.; VANDERHART, D. L. Native Cellulose: A Composite of Two Distinct Crystalline Forms. *Science (80-.)*. **1984**, *223* (4633), 283–285. <https://doi.org/10.1126/science.223.4633.283>.
- (90) Pe, S.; others. Conformations, Structures, and Morphologies of Celluloses. In *Polysaccharides*; CRC Press, 2004; pp 53–80.
- (91) Somerville, C. Cellulose Synthesis in Higher Plants. *Annu. Rev. Cell Dev. Biol.* **2006**, *22*, 53–78.
- (92) VanderHart, D. L.; Atalla, R. H. Studies of Microstructure in Native Celluloses Using Solid-State Carbon-13 NMR. *Macromolecules* **1984**, *17* (8), 1465–1472. <https://doi.org/10.1021/ma00138a009>.
- (93) Horii, F.; Yamamoto, H.; Kitamaru, R.; Tanahashi, M.; Higuchi, T. Transformation of Native Cellulose Crystals Induced by Saturated Steam at High Temperatures. *Macromolecules* **1987**, *20* (11), 2946–2949. <https://doi.org/10.1021/ma00177a052>.
- (94) Viëtor, R. J.; Mazeau, K.; Lakin, M.; Pérez, S. A Priori Crystal Structure Prediction of Native Celluloses. *Biopolym. Orig. Res. Biomol.* **2000**, *54* (5), 342–354.
- (95) Nishiyama, Y.; Sugiyama, J.; Chanzy, H.; Langan, P. Crystal Structure and Hydrogen Bonding System in Cellulose I α from Synchrotron X-Ray and Neutron Fiber Diffraction. *J. Am. Chem. Soc.* **2003**, *125* (47), 14300–14306. <https://doi.org/10.1021/ja037055w>.
- (96) Matthews, J. F.; Skopec, C. E.; Mason, P. E.; Zuccato, P.; Torget, R. W.;

- Sugiyama, J.; Himmel, M. E.; Brady, J. W. Computer Simulation Studies of Microcrystalline Cellulose I β . *Carbohydr. Res.* **2006**, *341* (1), 138–152.
- (97) Bergenstr hle, M.; Berglund, L. A.; Mazeau, K. Thermal Response in Crystalline I β Cellulose: A Molecular Dynamics Study. *J. Phys. Chem. B* **2007**, *111* (30), 9138–9145. <https://doi.org/10.1021/jp072258i>.
- (98) Matthews, J. F.; Bergenstr hle, M.; Beckham, G. T.; Himmel, M. E.; Nimlos, M. R.; Brady, J. W.; Crowley, M. F. High-Temperature Behavior of Cellulose I. *J. Phys. Chem. B* **2011**, *115* (10), 2155–2166. <https://doi.org/10.1021/jp1106839>.
- (99) Agarwal, V.; Huber, G. W.; Conner Jr, W. C.; Auerbach, S. M. Simulating Infrared Spectra and Hydrogen Bonding in Cellulose I β at Elevated Temperatures. *J. Chem. Phys.* **2011**, *135* (13), 10B605.
- (100) Chen, P.; Nishiyama, Y.; Mazeau, K. Torsional Entropy at the Origin of the Reversible Temperature-Induced Phase Transition of Cellulose. *Macromolecules* **2012**, *45* (1), 362–368. <https://doi.org/10.1021/ma201954s>.
- (101) Watanabe, A.; Morita, S.; Ozaki, Y. Temperature-Dependent Changes in Hydrogen Bonds in Cellulose I α Studied by Infrared Spectroscopy in Combination with Perturbation-Correlation Moving-Window Two-Dimensional Correlation Spectroscopy: Comparison with Cellulose I β . *Biomacromolecules* **2007**, *8* (9), 2969–2975. <https://doi.org/10.1021/bm700678u>.
- (102) Wada, M. Lateral Thermal Expansion of Cellulose I β and IIII Polymorphs. *J. Polym. Sci. Part B* **2002**, *40*, 1095–1102.
- (103) Wada, M.; Hori, R.; Kim, U.-J.; Sasaki, S. X-Ray Diffraction Study on the Thermal Expansion Behavior of Cellulose I β and Its High-Temperature Phase. *Polym. Degrad. Stab.* **2010**, *95* (8), 1330–1334. <https://doi.org/https://doi.org/10.1016/j.polymdegradstab.2010.01.034>.
- (104) Paavilainen, S.; R ng, T.; Vattulainen, I. Analysis of Twisting of Cellulose Nanofibrils in Atomistic Molecular Dynamics Simulations. *J. Phys. Chem. B* **2011**,

- 115 (14), 3747–3755. <https://doi.org/10.1021/jp111459b>.
- (105) Jarvis, M. Cellulose Stacks Up. *Nature* **2003**, 426 (6967), 611–612. <https://doi.org/10.1038/426611a>.
- (106) Coote, M. Quantum-Chemical Modeling of Free-Radical Polymerization. *Macromol. Theory Simulations* **2009**, 18, 388–400. <https://doi.org/10.1002/mats.200900050>.
- (107) Broadbelt, L. J.; Pfaendtner, J. Lexicography of Kinetic Modeling of Complex Reaction Networks. *AIChE J.* **2005**, 51 (8), 2112–2121.
- (108) Vasiliu, M.; Jones, A. J.; Guynn, K.; Dixon, D. A. Prediction of the Thermodynamic Properties of Key Products and Intermediates from Biomass. II. *J. Phys. Chem. C* **2012**, 116 (39), 20738–20754. <https://doi.org/10.1021/jp306596d>.
- (109) Assary, R. S.; Curtiss, L. A. Comparison of Sugar Molecule Decomposition through Glucose and Fructose: A High-Level Quantum Chemical Study. *Energy & Fuels* **2012**, 26 (2), 1344–1352. <https://doi.org/10.1021/ef201654s>.
- (110) Zhang, X.; Li, J.; Yang, W.; Blasiak, W. Formation Mechanism of Levoglucosan and Formaldehyde during Cellulose Pyrolysis. *Energy & Fuels* **2011**, 25 (8), 3739–3746. <https://doi.org/10.1021/ef2005139>.
- (111) Assary, R. S.; Curtiss, L. A. Thermochemistry and Reaction Barriers for the Formation of Levoglucosenone from Cellobiose. *ChemCatChem* **2012**, 4 (2), 200–205.
- (112) Zhang, M.; Geng, Z.; Yu, Y. Density Functional Theory (DFT) Study on the Dehydration of Cellulose. *Energy & Fuels* **2011**, 25 (6), 2664–2670. <https://doi.org/10.1021/ef101619e>.
- (113) Arora, J. S.; Chew, J. W.; Mushrif, S. H. Influence of Alkali and Alkaline-Earth Metals on the Cleavage of Glycosidic Bond in Biomass Pyrolysis: A DFT Study Using Cellobiose as a Model Compound. *J. Phys. Chem. A* **2018**, 122 (38), 7646–7658. <https://doi.org/10.1021/acs.jpca.8b06083>.

- (114) Irvine, J. C.; Oldham, J. W. H. CXCVIII. The Constitution of Polysaccharides. Part III. The Relationship of l-Glucosan to d-Glucose and to Cellulose. *J. Chem. Soc. Trans.* **1921**, 119, 1744–1759.
- (115) Ivanov, V. I.; Golova, O. P.; Pakhomov, A. M. Main Direction of Reaction in the Thermal Decomposition of Cellulose in a Vacuum. *Russ. Chem. Bull.* **1956**, 5 (10), 1295–1296.
- (116) Pakhomov, A. M. Free-Radical Mechanism of the Thermodegradation of Cellulose and Formation of Levoglucosan. *Bull. Acad. Sci. USSR, Div. Chem. Sci.* **1957**, 6 (12), 1525–1527. <https://doi.org/10.1007/BF01169764>.
- (117) Shen, D.; Gu, S. The Mechanism for Thermal Decomposition of Cellulose and Its Main Products. *Bioresour. Technol.* **2009**, 100 24, 6496–6504.
- (118) Mayes, H. B.; Broadbelt, L. J. Unraveling the Reactions That Unravel Cellulose. *J. Phys. Chem. A* **2012**, 116 (26), 7098–7106. <https://doi.org/10.1021/jp300405x>.
- (119) Ponder, G. R.; Richards, G. N. A Review of Some Recent Studies on Mechanisms of Pyrolysis of Polysaccharides. *Biomass and Bioenergy* **1994**, 7 (1), 1–24. [https://doi.org/https://doi.org/10.1016/0961-9534\(94\)00043-S](https://doi.org/https://doi.org/10.1016/0961-9534(94)00043-S).
- (120) Cho, J.; Davis, J. M.; Huber, G. W. The Intrinsic Kinetics and Heats of Reactions for Cellulose Pyrolysis and Char Formation. *ChemSusChem* **2010**, 3 (10), 1162–1165.
- (121) Yamamoto, E.; Bokelman, G. H.; Lewis, N. G. Phenylpropanoid Metabolism in Cell Walls; 1989; pp 68–88. <https://doi.org/10.1021/bk-1989-0399.ch005>.
- (122) Hosoya, T.; Nakao, Y.; Sato, H.; Kawamoto, H.; Sakaki, S. Thermal Degradation of Methyl β -d-Glucoside. A Theoretical Study of Plausible Reaction Mechanisms. *J. Org. Chem.* **2009**, 74 (17), 6891–6894. <https://doi.org/10.1021/jo900457k>.
- (123) Huang, J.; Wu, D.; Tong, H.; Ren, L. Density Functional Theory Studies on Pyrolysis Mechanism of β -O-4 Type Lignin Dimer Model Compound. *J. Anal. Appl. Pyrolysis* **2014**, 109. <https://doi.org/10.1016/j.jaap.2014.07.007>.

- (124) Climent, M. J.; Corma, A.; Iborra, S. Converting Carbohydrates to Bulk Chemicals and Fine Chemicals over Heterogeneous Catalysts. *Green Chem.* **2011**, *13* (3), 520–540. <https://doi.org/10.1039/C0GC00639D>.
- (125) Momany, F.; Appell, M.; Strati, G.; Willett, J. B3LYP/6-311++G** Study of Monohydrates of α - and β -D-Glucopyranose: Hydrogen Bonding, Stress Energies, and Effect of Hydration on Internal Coordinates. *Carbohydr. Res.* **2004**, *339*, 553–567. <https://doi.org/10.1016/j.carres.2003.10.013>.
- (126) Wang, Q.; Song, H.; Pan, S.; Dong, N.; Wang, X.; Sun, S. Initial Pyrolysis Mechanism and Product Formation of Cellulose: An Experimental and Density Functional Theory(DFT) Study. *Sci. Rep.* **2020**, *10* (1), 3626. <https://doi.org/10.1038/s41598-020-60095-2>.
- (127) Teixeira, A. R.; Gantt, R.; Joseph, K. E.; Maduskar, S.; Paulsen, A. D.; Krumm, C.; Zhu, C.; Dauenhauer, P. J. Spontaneous Aerosol Ejection: Origin of Inorganic Particles in Biomass Pyrolysis. *ChemSusChem* **2016**, *9* (11), 1322–1328.
- (128) Zhu, C.; Krumm, C.; Facas, G. G.; Neurock, M.; Dauenhauer, P. J. Energetics of Cellulose and Cyclodextrin Glycosidic Bond Cleavage. *React. Chem. Eng.* **2017**, *2* (2), 201–214. <https://doi.org/10.1039/C6RE00176A>.
- (129) Maliekkal, V.; Maduskar, S.; Saxon, D. J.; Nasiri, M.; Reineke, T. M.; Neurock, M.; Dauenhauer, P. Activation of Cellulose via Cooperative Hydroxyl-Catalyzed Transglycosylation of Glycosidic Bonds. *ACS Catal.* **2019**, *9* (3), 1943–1955. <https://doi.org/10.1021/acscatal.8b04289>.
- (130) Klein, M. T.; Virk, P. S. Modeling of Lignin Thermolysis. *Energy Fuels* **2008**, *22* (4), 2175–2182. <https://doi.org/10.1021/ef800285f>.
- (131) Wang, S.; Guo, X.; Wang, K.; Luo, Z. Influence of the Interaction of Components on the Pyrolysis Behavior of Biomass. *J. Anal. Appl. Pyrolysis* **2011**, *91* (1), 183–189. <https://doi.org/https://doi.org/10.1016/j.jaap.2011.02.006>.
- (132) Wu, S.; Shen, D.; Hu, J.; Zhang, H.; Xiao, R. Cellulose-Lignin Interactions during

- Fast Pyrolysis with Different Temperatures and Mixing Methods. *Biomass and Bioenergy* **2016**, *90*, 209–217.
<https://doi.org/https://doi.org/10.1016/j.biombioe.2016.04.012>.
- (133) Zhu, L.; Zhong, Z. Effects of Cellulose, Hemicellulose and Lignin on Biomass Pyrolysis Kinetics. *Korean J. Chem. Eng.* **2020**, *37* (10), 1660–1668.
- (134) Fahmi, R.; Bridgwater, A. V.; Thain, S. C.; Donnison, I.; Morris, P. M.; Yates, N. Prediction of Klason Lignin and Lignin Thermal Degradation Products by Py–GC/MS in a Collection of Lolium and Festuca Grasses. *J. Anal. Appl. Pyrolysis* **2007**, *80* (1), 16–23. <https://doi.org/10.1016/j.jaap.2006.12.018>.
- (135) Antal, M. J. Effects of Reactor Severity on the Gas-Phase Pyrolysis of Cellulose- and Kraft Lignin-Derived Volatile Matter. *Ind. Eng. Chem. Prod. Res. Dev.* **1983**, *22* (2), 366–375. <https://doi.org/10.1021/i300010a039>.
- (136) Evans, R. J.; Milne, T. A. Molecular Characterization of the Pyrolysis of Biomass. 2. Applications. *Energy & Fuels* **1987**, *1*, 311–319.
- (137) Ansari, K. B.; Arora, J. S.; Chew, J. W.; Dauenhauer, P. J.; Mushrif, S. H. Fast Pyrolysis of Cellulose, Hemicellulose, and Lignin: Effect of Operating Temperature on Bio-Oil Yield and Composition and Insights into the Intrinsic Pyrolysis Chemistry. *Ind. Eng. Chem. Res.* **2019**, *58* (35), 15838–15852.
<https://doi.org/10.1021/acs.iecr.9b00920>.
- (138) Antal, M. J. Biomass Pyrolysis: A Review of the Literature Part 1—Carbohydrate Pyrolysis; 1983.
- (139) Shen, D.; Xiao, R.; Gu, S.; Luo, K. The Pyrolytic Behavior of Cellulose in Lignocellulosic Biomass: A Review. *RSC Adv.* **2011**, *1* (9), 1641–1660.
<https://doi.org/10.1039/C1RA00534K>.
- (140) Hosoya, T.; Kawamoto, H.; Saka, S. Cellulose–Hemicellulose and Cellulose–Lignin Interactions in Wood Pyrolysis at Gasification Temperature. *J. Anal. Appl. Pyrolysis* **2007**, *80* (1), 118–125.

<https://doi.org/https://doi.org/10.1016/j.jaap.2007.01.006>.

- (141) Liu, Q.; Zhong, Z.; Wang, S.; Luo, Z. Interactions of Biomass Components during Pyrolysis: A TG-FTIR Study. *J. Anal. Appl. Pyrolysis* **2011**, *90* (2), 213–218.
<https://doi.org/https://doi.org/10.1016/j.jaap.2010.12.009>.
- (142) Couhert, C.; Commandre, J.-M.; Salvador, S. Is It Possible to Predict Gas Yields of Any Biomass after Rapid Pyrolysis at High Temperature from Its Composition in Cellulose, Hemicellulose and Lignin? *Fuel* **2009**, *88* (3), 408–417.
<https://doi.org/https://doi.org/10.1016/j.fuel.2008.09.019>.
- (143) Hosoya, T.; Kawamoto, H.; Saka, S. Influence of Inorganic Matter on Wood Pyrolysis at Gasification Temperature. *J. Wood Sci.* **2007**, *53* (4), 351–357.
<https://doi.org/10.1007/s10086-006-0854-8>.
- (144) de Wildt, P. Biomass Pyrolysis for Chemicals, Rijksuniversiteit Groningen, 2011.
- (145) Demirbas, A. The Influence of Temperature on the Yields of Compounds Existing in Bio-Oils Obtained from Biomass Samples via Pyrolysis. *Fuel Process. Technol.* **2007**, *88* (6), 591–597. <https://doi.org/https://doi.org/10.1016/j.fuproc.2007.01.010>.
- (146) Liu, Z.; Wang, L.; Zhang, Y.; Li, Y.; Li, Z.; Cai, H. Cellulose-Lignin and Xylan-Lignin Interactions on the Formation of Lignin-Derived Phenols in Pyrolysis Oil. *BioResources* **2017**, *12* (3), 4958–4971.
- (147) Wu, S.; Shen, D.; Hu, J.; Zhang, H.; Xiao, R. Intensive Interaction Region during Co-Pyrolysis of Lignin and Cellulose: Experimental Observation and Kinetic Assessment. *BioResources* **2014**, *9* (2), 2259–2273.
- (148) Lam, T. B.-T.; Iiyama, K.; Stone, B. A. Hot Alkali-Labile Linkages in the Walls of the Forage Grass *Phalaris Aquatica* and *Lolium Perenne* and Their Relation to in Vitro Wall Digestibility. *Phytochemistry* **2003**, *64* (2), 603–607.
[https://doi.org/10.1016/s0031-9422\(03\)00301-7](https://doi.org/10.1016/s0031-9422(03)00301-7).
- (149) Zhao, X.; Qi, F.; Liu, D. Hierarchy Nano- and Ultrastructure of Lignocellulose and

- Its Impact on the Bioconversion of Cellulose; 2017. https://doi.org/10.1007/978-3-319-45459-7_6.
- (150) Balakshin, M. Y.; Capanema, E. A.; Chang, H. MWL Fraction with a High Concentration of Lignin-Carbohydrate Linkages: Isolation and 2D NMR Spectroscopic Analysis. **2007**, *61* (1), 1–7. <https://doi.org/doi:10.1515/HF.2007.001>.
- (151) Kim, J. S.; Lee, Y. Y.; Kim, T. H. A Review on Alkaline Pretreatment Technology for Bioconversion of Lignocellulosic Biomass. *Bioresour. Technol.* **2016**, *199*, 42–48. <https://doi.org/10.1016/j.biortech.2015.08.085>.
- (152) Charlier, L.; Mazeau, K. Molecular Modeling of the Structural and Dynamical Properties of Secondary Plant Cell Walls: Influence of Lignin Chemistry. *J. Phys. Chem. B* **2012**, *116* (14), 4163–4174. <https://doi.org/10.1021/jp300395k>.
- (153) Freudenberg, K.; Neish, A. C. *Constitution and Biosynthesis of Lignin*; Springer Berlin Heidelberg: Berlin, Heidelberg, 1968. <https://doi.org/10.1007/978-3-642-85981-6>.
- (154) Jin, Z.; Katsumata, K. S.; Lam, T. B. T.; Iiyama, K. Covalent Linkages between Cellulose and Lignin in Cell Walls of Coniferous and Nonconiferous Woods. *Biopolym. Orig. Res. Biomol.* **2006**, *83* (2), 103–110.
- (155) McCammon, J. A.; Harvey, S. C. *Dynamics of Proteins and Nucleic Acids*; Cambridge University Press: Cambridge, 1987. <https://doi.org/DOI:10.1017/CBO9781139167864>.
- (156) Elder, T. Application of Computational Methods to the Chemistry of Lignin. In *Lignin*; ACS Symposium Series; American Chemical Society, 2019; Vol. 397, pp 262–271. <https://doi.org/10.1021/bk-1989-0397.ch019>.
- (157) Besombes, S.; Mazeau, K. The Cellulose/Lignin Assembly Assessed by Molecular Modeling. Part 1: Adsorption of a Threo Guaiacyl β -O-4 Dimer onto a β -D-Glucopyranose Cellulose Whisker. *Plant Physiol. Biochem.* **2005**, *43* (3), 299–308.

<https://doi.org/https://doi.org/10.1016/j.plaphy.2005.02.005>.

- (158) Zhang, X.; Yang, W.; Blasiak, W. Modeling Study of Woody Biomass: Interactions of Cellulose, Hemicellulose, and Lignin. *Energy Fuels* **2011**, *25* (10), 4786–4795. <https://doi.org/10.1021/ef201097d>.
- (159) Seshadri, V.; Westmoreland, P. R. Roles of Hydroxyls in the Noncatalytic and Catalyzed Formation of Levoglucosan from Glucose. *Catal. Today* **2016**, *269*, 110–121. <https://doi.org/https://doi.org/10.1016/j.cattod.2015.10.033>.
- (160) Dauenhauer, P.; Neurock, M.; Maduskar, S. On the Yield of Levoglucosan from Cellulose. *ACS Sustain. Chem. Eng.* **2018**, *6*. <https://doi.org/10.1021/acssuschemeng.8b00853>.
- (161) Hilbers, T. J.; Wang, Z.; Pecha, B.; Westerhof, R. J. M.; Kersten, S. R. A.; Pelaez-Samaniego, M. R.; Garcia-Perez, M. Cellulose-Lignin Interactions during Slow and Fast Pyrolysis. *J. Anal. Appl. Pyrolysis* **2015**, *114*, 197–207. <https://doi.org/https://doi.org/10.1016/j.jaap.2015.05.020>.
- (162) Li, W.; Zhou, S.; Xue, Y.; Lee, Y.-J.; Smith, R.; Bai, X. Understanding Low-Pressure Hydrolysis of Lignin Using Deuterated Sodium Formate. *ACS Sustain. Chem. Eng.* **2017**, *5* (10), 8939–8950. <https://doi.org/10.1021/acssuschemeng.7b01748>.
- (163) Lu, Q.; Wang, Z.; Guo, H.; Li, K.; Zhang, Z.; Cui, M.; Yang, Y. Selective Preparation of Monocyclic Aromatic Hydrocarbons from Ex-Situ Catalytic Fast Pyrolysis of Pine over Ti(SO₄)₂-Mo₂N/HZSM-5 Catalyst. *Fuel* **2019**, *243*, 88–96. <https://doi.org/https://doi.org/10.1016/j.fuel.2019.01.102>.
- (164) Leng, E.; Zhang, Y.; Peng, Y.; Gong, X.; Mao, M.; Li, X.; Yu, Y. In Situ Structural Changes of Crystalline and Amorphous Cellulose during Slow Pyrolysis at Low Temperatures. *Fuel* **2018**, *216*, 313–321. <https://doi.org/https://doi.org/10.1016/j.fuel.2017.11.083>.
- (165) Zhang, Y.; Xu, W.; Ma, N.; Shen, Y.; Xu, F.; Wang, Y.; Wu, N.; Guo, Z.; Jiang, L.

- Revealing the Key Role of Structural Cross-Link between Lignin and Polysaccharides during Fast Pyrolysis of Lignocellulose. *Bioresour. Technol.* **2022**, *361*, 127714. <https://doi.org/10.1016/j.biortech.2022.127714>.
- (166) Maduskar, S.; Facas, G. G.; Papageorgiou, C.; Williams, C. L.; Dauenhauer, P. J. Five Rules for Measuring Biomass Pyrolysis Rates: Pulse-Heated Analysis of Solid Reaction Kinetics of Lignocellulosic Biomass. *ACS Sustain. Chem. Eng.* **2018**, *6* (1), 1387–1399. <https://doi.org/10.1021/acssuschemeng.7b03785>.
- (167) Kim, T. H.; Lee, Y. Y. Fractionation of Corn Stover by Hot-Water and Aqueous Ammonia Treatment. *Bioresour. Technol.* **2006**, *97* (2), 224–232. <https://doi.org/10.1016/j.biortech.2005.02.040>.
- (168) Rowell, R. M. *Handbook of Wood Chemistry and Wood Composites*; CRC press, 2005.
- (169) Ragauskas, A. J.; Williams, C. K.; Davison, B. H.; Britovsek, G.; Cairney, J.; Eckert, C. A.; Frederick, W. J.; Hallett, J. P.; Leak, D. J.; Liotta, C. L. The Path Forward for Biofuels and Biomaterials. *Science (80-.)*. **2006**, *311* (5760), 484–489.
- (170) Pandey, A. *Handbook of Plant-Based Biofuels*; CRC press, 2008.
- (171) Ruddy, D. A.; Schaidle, J. A.; Ferrell III, J. R.; Wang, J.; Moens, L.; Hensley, J. E. Recent Advances in Heterogeneous Catalysts for Bio-Oil Upgrading via “Ex Situ Catalytic Fast Pyrolysis”: Catalyst Development through the Study of Model Compounds. *Green Chem.* **2014**, *16* (2), 454–490. <https://doi.org/10.1039/C3GC41354C>.
- (172) Sharma, R. K.; Bakhshi, N. N. Catalytic Upgrading of Pyrolysis Oil. *Energy & Fuels* **1993**, *7* (2), 306–314. <https://doi.org/10.1021/ef00038a022>.
- (173) Alonso, D. M.; Wettstein, S. G.; Dumesic, J. A. Bimetallic Catalysts for Upgrading of Biomass to Fuels and Chemicals. *Chem. Soc. Rev.* **2012**, *41* (24), 8075–8098. <https://doi.org/10.1039/C2CS35188A>.

- (174) Bond, J. Q.; Upadhye, A. A.; Olcay, H.; Tompsett, G. A.; Jae, J.; Xing, R.; Alonso, D. M.; Wang, D.; Zhang, T.; Kumar, R.; Foster, A.; Sen, S. M.; Maravelias, C. T.; Malina, R.; Barrett, S. R. H.; Lobo, R.; Wyman, C. E.; Dumesic, J. A.; Huber, G. W. Production of Renewable Jet Fuel Range Alkanes and Commodity Chemicals from Integrated Catalytic Processing of Biomass. *Energy Environ. Sci.* **2014**, *7* (4), 1500–1523. <https://doi.org/10.1039/C3EE43846E>.
- (175) Taarning, E.; Osmundsen, C. M.; Yang, X.; Voss, B.; Andersen, S. I.; Christensen, C. H. Zeolite-Catalyzed Biomass Conversion to Fuels and Chemicals. *Energy Environ. Sci.* **2011**, *4* (3), 793–804. <https://doi.org/10.1039/C004518G>.
- (176) Wang, D.; Ámundadóttir, M. L.; van Gunsteren, W. F.; Hünenberger, P. H. Intramolecular Hydrogen-Bonding in Aqueous Carbohydrates as a Cause or Consequence of Conformational Preferences: A Molecular Dynamics Study of Cellobiose Stereoisomers. *Eur. Biophys. J.* **2013**, *42* (7), 521–537. <https://doi.org/10.1007/s00249-013-0901-5>.
- (177) Bridgwater, A. V; Meier, D.; Radlein, D. An Overview of Fast Pyrolysis of Biomass. *Org. Geochem.* **1999**, *30* (12), 1479–1493. [https://doi.org/https://doi.org/10.1016/S0146-6380\(99\)00120-5](https://doi.org/https://doi.org/10.1016/S0146-6380(99)00120-5).
- (178) Mettler, M. S.; Vlachos, D. G.; Dauenhauer, P. J. Top Ten Fundamental Challenges of Biomass Pyrolysis for Biofuels. *Energy Environ. Sci.* **2012**, *5* (7), 7797–7809. <https://doi.org/10.1039/C2EE21679E>.
- (179) Cherubini, F. The Biorefinery Concept: Using Biomass Instead of Oil for Producing Energy and Chemicals. *Energy Convers. Manag.* **2010**, *51*, 1412–1421. <https://doi.org/10.1016/j.enconman.2010.01.015>.
- (180) Zinoviev, S.; Müller-Langer, F.; Das, P.; Bertero, N.; Fornasiero, P.; Kaltschmitt, M.; Centi, G.; Miertus, S. Next-Generation Biofuels: Survey of Emerging Technologies and Sustainability Issues. *ChemSusChem* **2010**, *3* (10), 1106–1133.

- (181) Wooten, J. B.; Seeman, J. I.; Hajaligol, M. R. Observation and Characterization of Cellulose Pyrolysis Intermediates by ^{13}C CPMAS NMR. A New Mechanistic Model. *Energy & Fuels* **2004**, *18* (1), 1–15. <https://doi.org/10.1021/ef0300601>.
- (182) Kim, D.-Y.; Nishiyama, Y.; Wada, M.; Kuga, S.; Okano, T. Thermal Decomposition of Cellulose Crystallites in Wood. *HOLZFORSCHUNG* **2001**, *55*, 521–524. <https://doi.org/10.1515/HF.2001.084>.
- (183) Hori, R.; Wada, M. The Thermal Expansion of Wood Cellulose Crystals. *Cellulose* **2005**, *12* (5), 479. <https://doi.org/10.1007/s10570-005-5967-5>.
- (184) Hori, R.; Wada, M. The Thermal Expansion of Cellulose II and III Crystals. *Cellulose* **2006**, *13* (3), 281–290. <https://doi.org/10.1007/s10570-005-9038-8>.
- (185) Watanabe, A.; Morita, S.; Ozaki, Y. Temperature-Dependent Structural Changes in Hydrogen Bonds in Microcrystalline Cellulose Studied by Infrared and Near-Infrared Spectroscopy with Perturbation-Correlation Moving-Window Two-Dimensional Correlation Analysis. *Appl. Spectrosc.* **2006**, *60* (6), 611–618.
- (186) Watanabe, A.; Morita, S.; Ozaki, Y. Temperature-Dependent Changes in Hydrogen Bonds in Cellulose I α Studied by Infrared Spectroscopy in Combination with Perturbation-Correlation Moving-Window Two-Dimensional Correlation Spectroscopy: Comparison with Cellulose I β . *Biomacromolecules* **2007**, *8* (9), 2969–2975. <https://doi.org/10.1021/bm700678u>.
- (187) Szcześniak, L.; Rachocki, A.; Tritt-Goc, J. Glass Transition Temperature and Thermal Decomposition of Cellulose Powder. *Cellulose* **2008**, *15*, 445–451. <https://doi.org/10.1007/s10570-007-9192-2>.
- (188) Picker, K. M. The Relevance of Glass Transition Temperature for the Process of Tablet Formation. *J. Therm. Anal. Calorim.* **2003**, *73* (2), 597–605. <https://doi.org/10.1023/A:1025486331234>.
- (189) Baranov, A. I.; Anisimova, V. N.; Khripunov, A. K.; Baklagina, Y. G. Dielectric Properties and Dipole Glass Transition in Cellulose Acetobacter Xylinium.

- Ferroelectrics* **2003**, 286 (1), 141–151.
<https://doi.org/10.1080/00150190390206329>.
- (190) Seshadri, V.; Westmoreland, P. R. Concerted Reactions and Mechanism of Glucose Pyrolysis and Implications for Cellulose Kinetics. *J. Phys. Chem. A* **2012**, 116 (49), 11997–12013. <https://doi.org/10.1021/jp3085099>.
- (191) Lédé, J.; Diebold, J. P.; Peacocke, G. V. C.; Piskorz, J. The Nature and Properties of Intermediate and Unvaporized Biomass Pyrolysis Materials. In *Developments in thermochemical biomass conversion*; Springer, 1997; pp 27–42.
- (192) Antal, M. J.; Várhegyi, G.; Jakab, E. Cellulose Pyrolysis Kinetics: Revisited. *Ind. Eng. Chem. Res.* **1998**, 37 (4), 1267–1275. <https://doi.org/10.1021/ie970144v>.
- (193) Burnham, A. K.; Zhou, X.; Broadbelt, L. J. Critical Review of the Global Chemical Kinetics of Cellulose Thermal Decomposition. *Energy & Fuels* **2015**, 29 (5), 2906–2918. <https://doi.org/10.1021/acs.energyfuels.5b00350>.
- (194) Krumm, C.; Pfaendtner, J.; Dauenhauer, P. J. Millisecond Pulsed Films Unify the Mechanisms of Cellulose Fragmentation. *Chem. Mater.* **2016**, 28 (9), 3108–3114. <https://doi.org/10.1021/acs.chemmater.6b00580>.
- (195) Nishiyama, Y.; Johnson, G. P.; French, A. D.; Forsyth, V. T.; Langan, P. Neutron Crystallography, Molecular Dynamics, and Quantum Mechanics Studies of the Nature of Hydrogen Bonding in Cellulose I β . *Biomacromolecules* **2008**, 9 (11), 3133–3140. <https://doi.org/10.1021/bm800726v>.
- (196) Nishiyama, Y.; Langan, P.; Chanzy, H. Crystal Structure and Hydrogen-Bonding System in Cellulose I β from Synchrotron X-Ray and Neutron Fiber Diffraction. *J. Am. Chem. Soc.* **2002**, 124 (31), 9074–9082. <https://doi.org/10.1021/ja0257319>.
- (197) Qian, X.; Ding, S.-Y.; Nimlos, M. R.; Johnson, D. K.; Himmel, M. E. Atomic and Electronic Structures of Molecular Crystalline Cellulose I β : A First-Principles Investigation. *Macromolecules* **2005**, 38 (25), 10580–10589. <https://doi.org/10.1021/ma051683b>.

- (198) Chen, P.; Nishiyama, Y.; Mazeau, K. Torsional Entropy at the Origin of the Reversible Temperature-Induced Phase Transition of Cellulose. *Macromolecules* **2012**, *45* (1), 362–368. <https://doi.org/10.1021/ma201954s>.
- (199) Gardner, K. H.; Blackwell, J. The Structure of Native Cellulose. *Biopolym. Orig. Res. Biomol.* **1974**, *13* (10), 1975–2001.
- (200) Horii, F.; Hirai, A.; Kitamaru, R. Solid-State ¹³C-NMR Study of Conformations of Oligosaccharides and Cellulose. *Polym. Bull.* **1983**, *10* (7), 357–361.
- (201) Bergenstråhle, M.; Berglund, L. A.; Mazeau, K. Thermal Response in Crystalline I β Cellulose: A Molecular Dynamics Study. *J. Phys. Chem. B* **2007**, *111* (30), 9138–9145. <https://doi.org/10.1021/jp072258i>.
- (202) Zhang, Q.; Bulone, V.; Ågren, H.; Tu, Y. A Molecular Dynamics Study of the Thermal Response of Crystalline Cellulose I β . *Cellulose* **2011**, *18* (2), 207–221.
- (203) Shen, D.; Gu, S. The Mechanism for Thermal Decomposition of Cellulose and Its Main Products. *Bioresour. Technol.* **2009**, *100* 24, 6496–6504.
- (204) Arora, J.; S.; Chew, J. W.; Mushrif, S. H. Influence of Alkali and Alkaline-Earth Metals on the Cleavage of Glycosidic Bond in Biomass Pyrolysis: A DFT Study Using Cellobiose as a Model Compound. *J. Phys. Chem. A* **2018**, *122* (38), 7646–7658. <https://doi.org/10.1021/acs.jpca.8b06083>.
- (205) Jorgensen, W. L.; Madura, J. D. Quantum and Statistical Mechanical Studies of Liquids. 25. Solvation and Conformation of Methanol in Water. *J. Am. Chem. Soc.* **1983**, *105* (6), 1407–1413.
- (206) Bordwell, F. G.; Cheng, J. P.; Harrelson, J. A. Homolytic Bond Dissociation Energies in Solution from Equilibrium Acidity and Electrochemical Data. *J. Am. Chem. Soc.* **1988**, *110* (4), 1229–1231. <https://doi.org/10.1021/ja00212a035>.
- (207) Kollman, P. Free Energy Calculations: Applications to Chemical and Biochemical Phenomena. *Chem. Rev.* **1993**, *93* (7), 2395–2417. <https://doi.org/10.1021/cr00023a004>.

- (208) Zhao, Y.; Truhlar, D. G. The M06 Suite of Density Functionals for Main Group Thermochemistry, Thermochemical Kinetics, Noncovalent Interactions, Excited States, and Transition Elements: Two New Functionals and Systematic Testing of Four M06-Class Functionals and 12 Other Function. *Theor. Chem. Acc.* **2008**, *120* (1), 215–241. <https://doi.org/10.1007/s00214-007-0310-x>.
- (209) Csonka, G. I.; French, A. D.; Johnson, G. P.; Stortz, C. A. Evaluation of Density Functionals and Basis Sets for Carbohydrates. *J. Chem. Theory Comput.* **2009**, *5* (4), 679–692. <https://doi.org/10.1021/ct8004479>.
- (210) Wodrich, M. D.; Corminboeuf, C.; Schreiner, P. R.; Fokin, A. A.; Schleyer, P. von R. How Accurate Are DFT Treatments of Organic Energies? *Org. Lett.* **2007**, *9* (10), 1851–1854. <https://doi.org/10.1021/ol070354w>.
- (211) Arora, J. S.; Ansari, K. B.; Chew, J. W.; Dauenhauer, P. J.; Mushrif, S. H. Unravelling the Catalytic Influence of Naturally Occurring Salts on Biomass Pyrolysis Chemistry Using Glucose as a Model Compound: A Combined Experimental and DFT Study. *Catal. Sci. Technol.* **2019**, *9* (13), 3504–3524. <https://doi.org/10.1039/C9CY00005D>.
- (212) Maliekkal, V.; Dauenhauer, P. J.; Neurock, M. Glycosidic C–O Bond Activation in Cellulose Pyrolysis: Alpha Versus Beta and Condensed Phase Hydroxyl-Catalytic Scission. *ACS Catal.* **2020**, *10* (15), 8454–8464. <https://doi.org/10.1021/acscatal.0c02133>.
- (213) Saenger, W.; Betzel, C.; Hingerty, B.; Brown, G. M. Flip-Flop Hydrogen Bonding in a Partially Disordered System. *Nature* **1982**, *296* (5857), 581–583. <https://doi.org/10.1038/296581a0>.
- (214) Mellmer, M. A.; Sener, C.; Gallo, J. M. R.; Luterbacher, J. S.; Alonso, D. M.; Dumesic, J. A. Solvent Effects in Acid-catalyzed Biomass Conversion Reactions. *Angew. chemie Int. Ed.* **2014**, *53* (44), 11872–11875.
- (215) Pootakham, T.; Kumar, A. Bio-Oil Transport by Pipeline: A Techno-Economic Assessment. *Bioresour. Technol.* **2010**, *101* (18), 7137–7143.

<https://doi.org/https://doi.org/10.1016/j.biortech.2010.03.136>.

- (216) Diebold, J. P. A Review of the Chemical and Physical Mechanisms of the Storage Stability of Fast Pyrolysis Bio-Oils. **1999**. <https://doi.org/10.2172/753818>.
- (217) Bridgwater, A.; Czernik, S.; Diebold, J.; Meier, D.; Oasmaa, A.; Peacocke, C.; Piskorz, J.; Radlein, D. Fast Pyrolysis of Biomass: A Handbook. **1999**.
- (218) Fahmi, R.; Bridgwater, A. V; Donnison, I.; Yates, N.; Jones, J. M. The Effect of Lignin and Inorganic Species in Biomass on Pyrolysis Oil Yields, Quality and Stability. *Fuel* **2008**, *87* (7), 1230–1240.
- (219) Evans, R. J.; Milne, T. A. Molecular Characterization of the Pyrolysis of Biomass. 2. Applications. *Energy Fuels* **1987**, *1* (4), 311–319.
<https://doi.org/10.1021/ef00004a001>.
- (220) Varhegyi, G.; Antal Jr, M. J.; Jakab, E.; Szabó, P. Kinetic Modeling of Biomass Pyrolysis. *J. Anal. Appl. Pyrolysis* **1997**, *42* (1), 73–87.
- (221) Rao, T. R.; Sharma, A. Pyrolysis Rates of Biomass Materials. *Energy* **1998**, *23* (11), 973–978.
- (222) Raveendran, K.; Ganesh, A.; Khilar, K. C. Pyrolysis Characteristics of Biomass and Biomass Components. *Fuel* **1996**, *75* (8), 987–998.
[https://doi.org/https://doi.org/10.1016/0016-2361\(96\)00030-0](https://doi.org/https://doi.org/10.1016/0016-2361(96)00030-0).
- (223) Yang, H.; Yan, R.; Chen, H.; Zheng, C.; Lee, D. H.; Liang, D. T. In-Depth Investigation of Biomass Pyrolysis Based on Three Major Components: Hemicellulose, Cellulose and Lignin. *Energy Fuels* **2006**, *20* (1), 388–393.
<https://doi.org/10.1021/ef0580117>.
- (224) Manyà, J. J.; Velo, E.; Puigjaner, L. Kinetics of Biomass Pyrolysis: A Reformulated Three-Parallel-Reactions Model. *Ind. Eng. Chem. Res.* **2003**, *42* (3), 434–441. <https://doi.org/10.1021/ie020218p>.
- (225) Gómez, C. J.; Manyà, J. J.; Velo, E.; Puigjaner, L. Further Applications of a

- Revisited Summative Model for Kinetics of Biomass Pyrolysis. *Ind. Eng. Chem. Res.* **2004**, *43* (4), 901–906. <https://doi.org/10.1021/ie030621b>.
- (226) Wang, G.; Li, W.; Li, B.; Chen, H. TG Study on Pyrolysis of Biomass and Its Three Components under Syngas. *Fuel* **2008**, *87* (4), 552–558. <https://doi.org/https://doi.org/10.1016/j.fuel.2007.02.032>.
- (227) Skreiberg, A.; Skreiberg, Ø.; Sandquist, J.; Sørum, L. TGA and Macro-TGA Characterisation of Biomass Fuels and Fuel Mixtures. *Fuel* **2011**, *90* (6), 2182–2197. <https://doi.org/https://doi.org/10.1016/j.fuel.2011.02.012>.
- (228) Qu, T.; Guo, W.; Shen, L.; Xiao, J.; Zhao, K. Experimental Study of Biomass Pyrolysis Based on Three Major Components: Hemicellulose, Cellulose, and Lignin. *Ind. Eng. Chem. Res.* **2011**, *50* (18), 10424–10433. <https://doi.org/10.1021/ie1025453>.
- (229) Yoon, H. C.; Pozivil, P.; Steinfeld, A. Thermogravimetric Pyrolysis and Gasification of Lignocellulosic Biomass and Kinetic Summative Law for Parallel Reactions with Cellulose, Xylan, and Lignin. *Energy & Fuels* **2012**, *26* (1), 357–364. <https://doi.org/10.1021/ef201281n>.
- (230) Pang, C. H.; Gaddipatti, S.; Tucker, G.; Lester, E.; Wu, T. Relationship between Thermal Behaviour of Lignocellulosic Components and Properties of Biomass. *Bioresour. Technol.* **2014**, *172*, 312–320. <https://doi.org/https://doi.org/10.1016/j.biortech.2014.09.042>.
- (231) Hosoya, T.; Kawamoto, H.; Saka, S. Solid/Liquid- and Vapor-Phase Interactions between Cellulose- and Lignin-Derived Pyrolysis Products. *J. Anal. Appl. Pyrolysis* **2009**, *85* (1), 237–246. <https://doi.org/https://doi.org/10.1016/j.jaap.2008.11.028>.
- (232) Agarwal, V.; Huber, G. W.; Conner Jr, W. C.; Auerbach, S. M. Simulating Infrared Spectra and Hydrogen Bonding in Cellulose I β at Elevated Temperatures. *J. Chem. Phys.* **2011**, *135* (13), 10B605.

- (233) Eriksson, Ö.; Goring, D. A. I.; Lindgren, B. O. Structural Studies on the Chemical Bonds between Lignins and Carbohydrates in Spruce Wood. *Wood Sci. Technol.* **1980**, *14* (4), 267–279. <https://doi.org/10.1007/BF00383454>.
- (234) Košíková, B.; Ebringerová, A. Lignin-Carbohydrate Bonds in a Residual Soda Spruce Pulp Lignin. *Wood Sci. Technol.* **1994**, *28* (4), 291–296. <https://doi.org/10.1007/BF00204215>.
- (235) Zhou, Y.; Stuart-Williams, H.; Farquhar, G. D.; Hocart, C. H. The Use of Natural Abundance Stable Isotopic Ratios to Indicate the Presence of Oxygen-Containing Chemical Linkages between Cellulose and Lignin in Plant Cell Walls. *Phytochemistry* **2010**, *71* (8), 982–993. <https://doi.org/https://doi.org/10.1016/j.phytochem.2010.03.001>.
- (236) Minor, J. L. Chemical Linkage of Polysaccharides to Residual Lignin in Loblolly Pine Kraft Pulps. *J. Wood Chem. Technol.* **1986**, *6* (2), 185–201. <https://doi.org/10.1080/02773818608085223>.
- (237) Zhou, Y.; Stuart-Williams, H.; Farquhar, G. D.; Hocart, C. H. The Use of Natural Abundance Stable Isotopic Ratios to Indicate the Presence of Oxygen-Containing Chemical Linkages between Cellulose and Lignin in Plant Cell Walls. *Phytochemistry* **2010**, *71* (8), 982–993. <https://doi.org/https://doi.org/10.1016/j.phytochem.2010.03.001>.
- (238) Vinu, R.; Broadbelt, L. J. A Mechanistic Model of Fast Pyrolysis of Glucose-Based Carbohydrates to Predict Bio-Oil Composition. *Energy Environ. Sci.* **2012**, *5* (12), 9808–9826. <https://doi.org/10.1039/C2EE22784C>.
- (239) Dauenhauer, P. J.; Colby, J. L.; Balonek, C. M.; Suszynski, W. J.; Schmidt, L. D. Reactive Boiling of Cellulose for Integrated Catalysis through an Intermediate Liquid. *Green Chem.* **2009**, *11* (10), 1555. <https://doi.org/10.1039/b915068b>.
- (240) Padmanathan, A. M. D.; Mushrif, S. H. Pyrolytic Activation of Cellulose: Energetics and Condensed Phase Effects. *React. Chem. Eng.* **2022**, *7* (5), 1136–1149. <https://doi.org/10.1039/D1RE00492A>.

- (241) Kollman, P. Free Energy Calculations: Applications to Chemical and Biochemical Phenomena. *Chem. Rev.* **1993**, *93* (7), 2395–2417.
<https://doi.org/10.1021/cr00023a004>.
- (242) Mayes, H. B.; Broadbelt, L. J. Unraveling the Reactions That Unravel Cellulose. *J. Phys. Chem. A* **2012**, *116* (26), 7098–7106. <https://doi.org/10.1021/jp300405x>.
- (243) Bordwell, F. G.; Cheng, J. P.; Harrelson, J. A. Homolytic Bond Dissociation Energies in Solution from Equilibrium Acidity and Electrochemical Data. *J. Am. Chem. Soc.* **1988**, *110* (4), 1229–1231. <https://doi.org/10.1021/ja00212a035>.
- (244) Csonka, G. I.; French, A. D.; Johnson, G. P.; Stortz, C. A. Evaluation of Density Functionals and Basis Sets for Carbohydrates. *J. Chem. Theory Comput.* **2009**, *5* (4), 679–692. <https://doi.org/10.1021/ct8004479>.
- (245) Wodrich, M. D.; Corminboeuf, C.; Schreiner, P. R.; Fokin, A. A.; Schleyer, P. von R. How Accurate Are DFT Treatments of Organic Energies? *Org. Lett.* **2007**, *9* (10), 1851–1854. <https://doi.org/10.1021/ol070354w>.
- (246) Arora, J. S.; Ansari, K. B.; Chew, J. W.; Dauenhauer, P. J.; Mushrif, S. H. Unravelling the Catalytic Influence of Naturally Occurring Salts on Biomass Pyrolysis Chemistry Using Glucose as a Model Compound: A Combined Experimental and DFT Study. *Catal. Sci. Technol.* **2019**, *9* (13), 3504–3524.
<https://doi.org/10.1039/C9CY00005D>.
- (247) McCammon, J. A.; Harvey, S. C. *Dynamics of Proteins and Nucleic Acids*; Cambridge University Press, 1988.
- (248) Neves, D.; Thunman, H.; Matos, A.; Tarelho, L.; Gómez-Barea, A. Characterization and Prediction of Biomass Pyrolysis Products. *Prog. Energy Combust. Sci.* **2011**, *37* (5), 611–630.
<https://doi.org/https://doi.org/10.1016/j.pecs.2011.01.001>.
- (249) Kudo, S.; Huang, X.; Asano, S.; Hayashi, J. Catalytic Strategies for Levoglucosenone Production by Pyrolysis of Cellulose and Lignocellulosic

- Biomass. *Energy & Fuels* **2021**, *35* (12), 9809–9824.
<https://doi.org/10.1021/acs.energyfuels.1c01062>.
- (250) Arseneau, D. F. Competitive Reactions in the Thermal Decomposition of Cellulose. *Can. J. Chem.* **1971**, *49* (4), 632–638. <https://doi.org/10.1139/v71-101>.
- (251) Milosavljevic, I.; Oja, V.; Suuberg, E. M. Thermal Effects in Cellulose Pyrolysis: Relationship to Char Formation Processes. *Ind. Eng. Chem. Res.* **1996**, *35* (3), 653–662. <https://doi.org/10.1021/ie950438l>.
- (252) Mettler, M.; Mushrif, S.; Paulsen, A.; Javadekar, A.; Vlachos, D.; Dauenhauer, P. Revealing Pyrolysis Chemistry for Biofuels Production: Conversion of Cellulose to Furans and Small Oxygenates. *Energy Environ. Sci.* **2012**, *5*, 5414–5424.
<https://doi.org/10.1039/C1EE02743C>.
- (253) Arora, J. S.; Chew, J. W.; Mushrif, S. H. Influence of Alkali and Alkaline-Earth Metals on the Cleavage of Glycosidic Bond in Biomass Pyrolysis: A DFT Study Using Cellobiose as a Model Compound. *J. Phys. Chem. A* **2018**, *122* (38), 7646–7658. <https://doi.org/10.1021/acs.jpca.8b06083>.
- (254) Hosoya, T.; Nakao, Y.; Sato, H.; Kawamoto, H.; Sakaki, S. Thermal Degradation of Methyl Beta-D-Glucoside. a Theoretical Study of Plausible Reaction Mechanisms. *J. Org. Chem.* **2009**, *74* (17), 6891–6894.
<https://doi.org/10.1021/jo900457k>.
- (255) Banyasz, J.; Li, S.; Lyons-Hart, J.; Shafer, K. Cellulose Pyrolysis: The Kinetics of Hydroxyacetaldehyde Evolution. *J. Anal. Appl. Pyrolysis* **2001**, *57*, 223–248.
[https://doi.org/10.1016/S0165-2370\(00\)00135-2](https://doi.org/10.1016/S0165-2370(00)00135-2).
- (256) Nimlos, M. R.; Blanksby, S. J.; Qian, X.; Himmel, M. E.; Johnson, D. K. Mechanisms of Glycerol Dehydration. *J. Phys. Chem. A* **2006**, *110* (18), 6145–6156. <https://doi.org/10.1021/jp060597q>.
- (257) Mishra, S.; Singh, P. K.; Dash, S.; Pattnaik, R. Microbial Pretreatment of Lignocellulosic Biomass for Enhanced Biomethanation and Waste Management.

- 3 *Biotech* **2018**, 8 (11), 458. <https://doi.org/10.1007/s13205-018-1480-z>.
- (258) Zhang, Y.; Liu, C.; Chen, X. Unveiling the Initial Pyrolytic Mechanisms of Cellulose by DFT Study. *J. Anal. Appl. Pyrolysis* **2015**, 113, 621–629. <https://doi.org/https://doi.org/10.1016/j.jaap.2015.04.010>.
- (259) Zhang, J.; Choi, Y. S.; Yoo, C. G.; Kim, T. H.; Brown, R. C.; Shanks, B. H. Cellulose–Hemicellulose and Cellulose–Lignin Interactions during Fast Pyrolysis. *ACS Sustain. Chem. Eng.* **2015**, 3 (2), 293–301. <https://doi.org/10.1021/sc500664h>.
- (260) Lawoko, M.; Henriksson, G.; Gellerstedt, G. Structural Differences between the Lignin-Carbohydrate Complexes Present in Wood and in Chemical Pulps. *Biomacromolecules* **2005**, 6 (6), 3467–3473. <https://doi.org/10.1021/bm058014q>.
- (261) Henriksson, G.; Lawoko, M.; Eugenio, M.; Gellerstedt, G. Lignin-Carbohydrate Network in Wood and Pulps: A Determinant for Reactivity. *Holzforschung* **2007**, 61, 668–674. <https://doi.org/10.1515/HF.2007.097>.
- (262) Silva, V.; Jameel, H.; Gomes, F.; Batalha, L.; Coura, M.; Colodette, J. Effect of Lignin Carbohydrate Complexes of Hardwood Hybrids on the Kraft Pulping Process. *J. Wood Chem. Technol.* **2016**, 37, 1–10. <https://doi.org/10.1080/02773813.2016.1235584>.
- (263) Lawoko, M. Lignin Polysaccharide Networks in Softwood and Chemical Pulps : Characterisation, Structure and Reactivity, KTH, Fibre and Polymer Technology, School of Chemical Science and Engineering (CHE), KTH, 2005. <http://kth.diva-portal.org/smash/get/diva2:12959/FULLTEXT01.pdf>.
- (264) Fry, S. C. Plant Cell Walls. From Chemistry to Biology. *Annals of Botany*. July 2011, pp viii–ix. <https://doi.org/10.1093/aob/mcr128>.
- (265) Choi, J. W.; Choi, D.-H.; Faix, O. Characterization of Lignin-Carbohydrate Linkages in the Residual Lignins Isolated from Chemical Pulps of Spruce (*Picea Abies*) and Beech Wood (*Fagus Sylvatica*). *J. Wood Sci.* **2007**, 53 (4), 309–313.

<https://doi.org/10.1007/s10086-006-0860-x>.

- (266) Giummarella, N.; Zhang, L.; Henriksson, G.; Lawoko, M. Structural Features of Mildly Fractionated Lignin Carbohydrate Complexes (LCC) from Spruce. *RSC Adv.* **2016**, *6* (48), 42120–42131. <https://doi.org/10.1039/C6RA02399A>.
- (267) Giummarella, N.; Lawoko, M. Structural Insights on Recalcitrance during Hydrothermal Hemicellulose Extraction from Wood. *ACS Sustain. Chem. Eng.* **2017**, *5* (6), 5156–5165. <https://doi.org/10.1021/acssuschemeng.7b00511>.
- (268) Beck, S.; Choi, P.; Mushrif, S. H. Origins of Covalent Linkages within the Lignin Carbohydrate Network of Biomass. *Phys. Chem. Chem. Phys.* **2022**. <https://doi.org/10.1039/D2CP01683D>.
- (269) Car, R.; Parrinello, M. Unified Approach for Molecular Dynamics and Density-Functional Theory. *Phys. Rev. Lett.* **1985**, *55* (22), 2471–2474. <https://doi.org/10.1103/PhysRevLett.55.2471>.
- (270) Paulsen, A.; Mettler, M.; Dauenhauer, P. The Role of Sample Dimension and Temperature in Cellulose Pyrolysis. *Energy & Fuels* **2013**, *27*, 2126–2134. <https://doi.org/10.1021/ef302117j>.
- (271) Ansari, K. B.; Arora, J. S.; Chew, J. W.; Dauenhauer, P. J.; Mushrif, S. H. Effect of Temperature and Transport on the Yield and Composition of Pyrolysis-Derived Bio-Oil from Glucose. *Energy & Fuels*. May 17, 2018, pp 6008–6021. <https://doi.org/10.1021/acs.energyfuels.8b00852>.
- (272) Giummarella, N.; Pu, Y.; Ragauskas, A. J.; Lawoko, M. A Critical Review on the Analysis of Lignin Carbohydrate Bonds. *Green Chem.* **2019**, *21* (7), 1573–1595. <https://doi.org/10.1039/C8GC03606C>.
- (273) Zhang, Y.-H. P.; Ding, S.-Y.; Mielenz, J. R.; Cui, J.-B.; Elander, R. T.; Laser, M.; Himmel, M. E.; McMillan, J. R.; Lynd, L. R. Fractionating Recalcitrant Lignocellulose at Modest Reaction Conditions. *Biotechnol. Bioeng.* **2007**, *97* (2), 214–223. <https://doi.org/10.1002/bit.21386>.

- (274) Ralph, J.; Grabber, J. H.; Hatfield, R. D. Lignin-Ferulate Cross-Links in Grasses: Active Incorporation of Ferulate Polysaccharide Esters into Ryegrass Lignins. *Carbohydr. Res.* **1995**, *275* (1), 167–178.
[https://doi.org/https://doi.org/10.1016/0008-6215\(95\)00237-N](https://doi.org/https://doi.org/10.1016/0008-6215(95)00237-N).
- (275) Zeng, Y.; Zhao, S.; Yang, S.; Ding, S.-Y. Lignin Plays a Negative Role in the Biochemical Process for Producing Lignocellulosic Biofuels. *Curr. Opin. Biotechnol.* **2014**, *27*, 38–45.
<https://doi.org/https://doi.org/10.1016/j.copbio.2013.09.008>.
- (276) Daoudi, W.; El Aatiaoui, A.; Dagdag, O.; Zaidi, K.; Haldhar, R.; Kim, S.-C.; Oussaid, A.; Aouinti, A.; Berisha, A.; Benhiba, F.; Ebenso, E. E.; Oussaid, A. Anti-Corrosion Coating Formation by a Biopolymeric Extract of Artemisia Herba-Alba Plant: Experimental and Theoretical Investigations. *Coatings*. 2023.
<https://doi.org/10.3390/coatings13030611>.
- (277) Fang, J.; Zheng, W.; Liu, K.; Li, H.; Li, C. Molecular Design and Experimental Study on the Synergistic Catalysis of Cellulose into 5-Hydroxymethylfurfural with Brønsted–Lewis Acidic Ionic Liquids. *Chem. Eng. J.* **2020**, *385*, 123796.
<https://doi.org/https://doi.org/10.1016/j.cej.2019.123796>.
- (278) Singh, K.; Kumar, A.; Pandey, S. K.; Awasthi, S.; Gupta, S. P.; Mishra, P. Interpretation of Adsorption Behavior of Carboxymethyl Cellulose onto Functionalized Accurel Polymeric Surface. *Ind. Eng. Chem. Res.* **2020**, *59* (43), 19102–19116. <https://doi.org/10.1021/acs.iecr.0c03894>.
- (279) Bradley, J. ~D.; Gerrans, G. ~C. Frontier Molecular Orbitals. A Link between Kinetics and Bonding Theory. *J. Chem. Educ.* **1973**, *50* (7), 463.
<https://doi.org/10.1021/ed050p463>.
- (280) Fukui, K. Role of Frontier Orbitals in Chemical Reactions. *Science* **1982**, *218* (4574), 747–754. <https://doi.org/10.1126/science.218.4574.747>.
- (281) Fukui, K. The Role of Frontier Orbitals in Chemical Reactions (Nobel Lecture). *Angew. Chemie Int. Ed. English* **1982**, *21* (11), 801–809.

<https://doi.org/https://doi.org/10.1002/anie.198208013>.

- (282) Azeem, U.; Khera, R. A.; Naveed, A.; Imran, M.; Assiri, M. A.; Khalid, M.; Iqbal, J. Tuning of a A–A–D–A–A-Type Small Molecule with Benzodithiophene as a Central Core with Efficient Photovoltaic Properties for Organic Solar Cells. *ACS Omega* **2021**, *6* (43), 28923–28935. <https://doi.org/10.1021/acsomega.1c03975>.
- (283) Pontoh, R.; Rarisavitri, V. E.; Yang, C.; Putra, M. F.; Anugrah, D. S. B. Density Functional Theory Study of Intermolecular Interactions between Amylum and Cellulose. *Indones. J. Chem.* **2022**.
- (284) Mortensen, P. M.; Grunwaldt, J.-D.; Jensen, P. A.; Knudsen, K. G.; Jensen, A. D. A Review of Catalytic Upgrading of Bio-Oil to Engine Fuels. *Appl. Catal. A Gen.* **2011**, *407* (1), 1–19. <https://doi.org/https://doi.org/10.1016/j.apcata.2011.08.046>.
- (285) Hutchinson, C.; Lee, Y. jin. Evaluation of Primary Reaction Pathways in Thin-Film Pyrolysis of Glucose Using ¹³C Labeling and Real-Time Monitoring. *ACS Sustain. Chem. Eng.* **2017**, *5*. <https://doi.org/10.1021/acssuschemeng.7b01601>.
- (286) Patwardhan, P. R. *Understanding the Product Distribution from Biomass Fast Pyrolysis*; Iowa State University, 2010.
- (287) Perdew, J. P.; Burke, K.; Ernzerhof, M. Generalized Gradient Approximation Made Simple. *Phys.Rev.Lett.* **1996**, *77* (18), 3865–3868. <https://doi.org/10.1103/PhysRevLett.77.3865>.
- (288) Zhang, Y.; Yang, W. Comment on “Generalized Gradient Approximation Made Simple”. *Phys. Rev. Lett.* **1998**, *80* (4), 890. <https://doi.org/10.1103/PhysRevLett.80.890>.
- (289) Guo, Z.; Wang, J.; Qin, F.; Ge, L.; Li, Z.; Shen, W. Facile Adjusting of a Right-Handed Helical Structure of Cellulose-Based Carbon Material for Chiral Separation. *ACS Sustain. Chem. Eng.* **2020**, *8* (8), 3401–3411. <https://doi.org/10.1021/acssuschemeng.9b07540>.
- (290) Nosé, S. A Unified Formulation of the Constant Temperature Molecular Dynamics

Methods. *Jcp* **1984**, *81* (1), 511–519. <https://doi.org/10.1063/1.447334>.

- (291) Hoover, W. G. Canonical Dynamics: Equilibrium Phase-Space Distributions. *Phys. Rev. A* **1985**, *31* (3), 1695–1697. <https://doi.org/10.1103/PhysRevA.31.1695>.
- (292) Jia, W.; Wang, H.; Chen, M.; Lu, D.; Lin, L.; Car, R.; E, W.; Zhang, L. Pushing the Limit of Molecular Dynamics with Ab Initio Accuracy to 100 Million Atoms with Machine Learning. In *Proceedings of the International Conference for High Performance Computing, Networking, Storage and Analysis; SC '20*; IEEE Press, 2020.
- (293) Iannuzzi, M.; Laio, A.; Parrinello, M. Efficient Exploration of Reactive Potential Energy Surfaces Using Car-Parrinello Molecular Dynamics. *Phys. Rev. Lett.* **2003**, *90*, 238302. <https://doi.org/10.1103/PhysRevLett.90.238302>.

Appendix

A.1 Computational methods

Matter is a collection of molecules which in turn is a collection of atoms or negatively charged electrons and positively charged nuclei. Molecular modelling involves solving governing equations of fundamental units of matter to calculate the structure, property and reactivity of molecules using computational tools. Depending on if the molecules are considered as a collection of atoms or a collection of sub-atomic particles, there are two molecular modelling methods – Force-field and first principle methods. In computational chemistry, molecular modelling is used to find the molecular structures and least-energy reaction pathways while in molecular dynamics they are used to capture the motion of atoms and molecules. Molecular dynamics was first introduced by Alder and Wainright in the 1950's. Details on the molecular modelling methods to perform computational chemistry or molecular dynamic simulations are provided below.

A.1.1 Force-field method

In force-field/atomistic calculations, atoms are the basic unit and it is described by a 'ball and spring' model where atoms and bonds are considered to be balls and springs respectively. This modelling method can't simulate reactions because the bonds can't be broken as they are considered to be springs. However, bonds can be stretched and contracted. Non-bonded interactions such as van der Waals interactions and electrostatic interactions are also taken into account. In this method, Newtonian physics is used to calculate the potential energy surfaces (PES) of inter-atomic interactions in the system. The potential energy of the system is calculated as the sum of the bond stretching $E_{stretch}$, angle bending (E_{bend}), bond twisting ($E_{torsion}$), van der Waals interaction (E_{vdW}) and electrostatic interaction ($E_{electrostatic}$) where the former three energy terms are bonded interactions and the latter two are non-bonded interactions.

$$E_{potential} = E_{stretch} + E_{bend} + E_{torsion} + E_{vdW} + E_{electrostatic} \quad (B.1)$$

Many models are available for calculating these energy terms. For instance, bond stretching energy can be modelled using a harmonic approximation. However, this might

be unreasonable for H-H bond therefore, in order to account for anharmonicity a quadratic equation is used. Moreover, Morse potential can also capture bond breaking.

$$V_{\text{harm}}(r) = -k_{\text{harm}}(r - r_{\text{eq}})^2 \quad (\text{B.2})$$

$$V_{\text{anharm}}(r) = p(r - r_{\text{eq}})^2 + q(r - r_{\text{eq}})^2 + s(r - r_{\text{eq}})^2 \quad (\text{B.3})$$

$$V_{\text{morse}}(r) = D_e(1 - e^{-a(r-r_{\text{eq}})})^2 \quad (\text{B.4})$$

Here, k_{harm} , D_e , a , p , q and s are all parameters while r is the distance between the bonds and r_{eq} is the equilibrium distance.

Many such models are available for the different energy terms but they will not be explored as this is not the major focus of this thesis. There are two types of force-fields based on the models used – Class I involves simple functional forms and Class II involves additional energy terms and is heavily parameterized using first principle calculations (Jensen 2007). The parameters involved in energy calculation are empirically fitted and can differ based on the application. Many commercial force-fields are available that differ in the model and parameters used. The forces on atoms are calculated as a gradient of the potential energy calculated. Newtonian equations of motion are then solved to find the velocity and forces at an appropriate time step by numerically integrating using techniques such as Verlet (44) and velocity-Verlet (45). Force-field calculations are relatively fast and have the ability to perform nanosecond and nanometer scale simulations but have certain limitations. The limitations are –

- Inability to simulate reactions.
- Difficulty in parameterizing for diverse molecules in one force-field.
- Difficulty in parameterizing for ‘exotic’ species because of limited data.
- Difficulty in simulating transition state metals because of the free electrons as electronic effects are not considered in force-field calculations.

To overcome these limitations first principle methods are used with different degrees of accuracy.

A.1.2 First Principles Methods

In first principles calculations electrons and nuclei are the basic units. In this method, the PES is calculated by solving the Schrödinger equation with different degrees of approximation. Similar to Newton's equations of motion that describe the evolution of the position of a particle, Schrödinger equation describes the evolution of the wavefunction of a particle.

$$i\hbar \frac{\partial}{\partial t} |\psi(t)\rangle = \hat{H} |\psi(t)\rangle \quad (\text{B.5})$$

In the Born-Oppenheimer approximation, the nuclei are propagated classically (Newtonian), as the nuclei are much heavier than the electrons, while the electrons are propagated quantum mechanically. Since the bonds are not defined a priori and the electrons are allowed to arrange themselves, reactions can be simulated using first principle methods. The wavefunctions is a linear combination of atomic orbitals and atomic orbitals are described using functions called basis sets. However, Schrödinger equation can't be solved for more than one electron systems. Therefore, various approximations and optimizations techniques were developed.

A.1.2.1 Density Functional theory (DFT)

DFT was formulated by Hohenberg and Kohn (38) and later developed by Kohn and Sham (39). Kohn-Sham DFT uses the electronic density instead of the wave-function to calculate PES. They formulated the ground state energy of the electronic system to be a functional of the ground state electron density with an exchange-correlation function to account for the error. At each time-step the electronic density is optimized to reach the ground state and this increases the computational cost.

A.1.2.2 Car-Parinello Molecular Dynamics (CPMD)

In this method both the electron density and the nuclei are propagated classically and therefore reducing the computational cost. However, the simulations are limited to a few hundred picoseconds because of the restriction on the time-step. The time-scale for molecular reactions are significantly higher and therefore better techniques are necessary to simulate reactions.

Metadynamics – Bias potential methods are used to drive the system out of a local minima by filling the PES with potentials and thereby accelerating the simulation. Metadynamics is the technique used to combine dynamics and bias potential methods. CPMD-metadynamics simulation can therefore be used to simulate reaction mechanisms and find free energy landscapes.

A.2 Appendix to Chapter 2

Two novel computational strategies are employed in this work to capture the finite temperature condensed phase and entropic effects in cellulose decomposition. System size is limited by the tools used in each strategy. Table S1 provides details on the two strategies, tools and corresponding system configurations.

Table A.2.1 Computational methods and System configurations

Computational Strategy	Tools	Purpose	System (no. of molecules)	
			Solvent	Solute
ConTS	Gromacs v 2018.7	Finite temperature conformation	7 cellobiose	1 cellobiose
	VASP 5.4.1	TS search (enthalpic barrier)	7 cellobiose	1 reacting cellobiose
Free-energy barrier correction	Gaussian 09 code	TS search (gas phase free-energy barrier)		1 reacting cellobiose
	Gromacs v 2018.7 (Thermodynamic Integration)	Finite temperature condensed phase interactions	59 cellobiose	1 Transition State

A.2.1 Condensed phase TS-Search method

Transition states for cellobiose breakdown via transglycosylation and ring contraction are calculated in finite temperature melt-phase environment. Images of the TS are provided in Figure S1. Unlike the finite temperature condensed phase calculations reported in this paper, the enthalpic barriers in the crystal structure (Figure S2) shows a minimum difference in the barriers of only 12.62 kJ/mol between the two mechanisms.

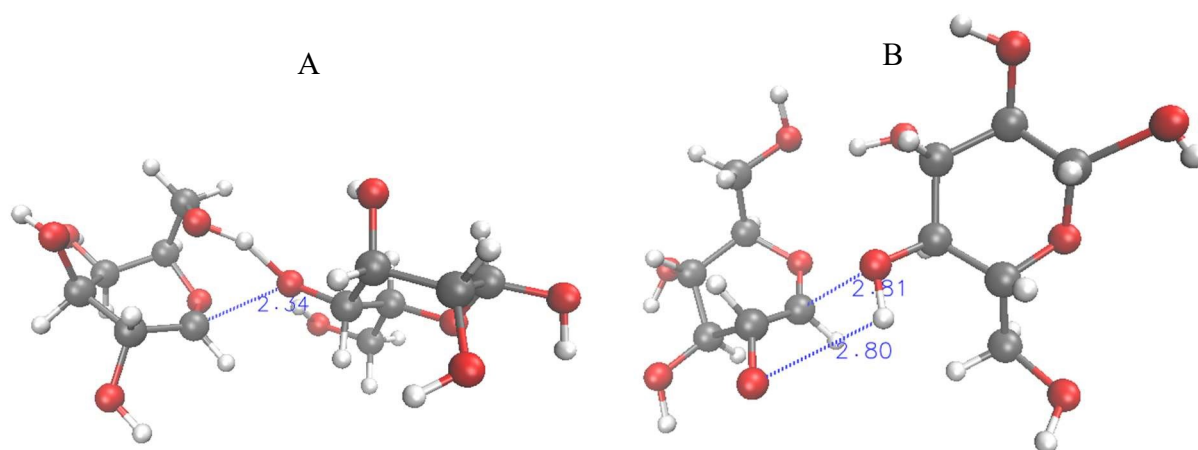


Figure A.2.1 DFT calculated transition states in condensed phase for (A) Transglycosylation (B) Ring contraction.

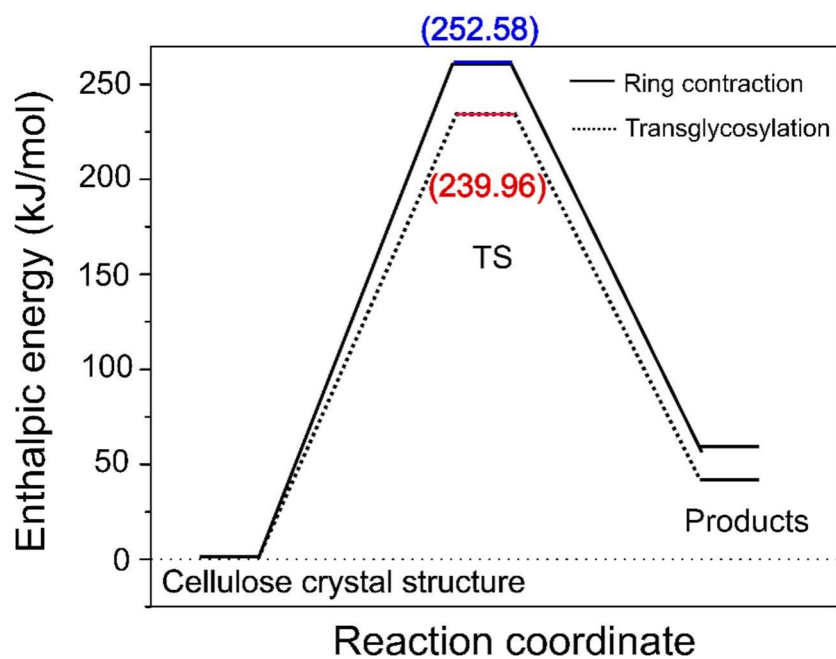


Figure A.2.2 DFT calculated activation barriers in crystal structure for Transglycosylation and Ring contraction

A.2.2 Dispersion Correction

DFT calculations in the study were performed using PBE exchange correlation functional. Dispersion corrections were accounted for by performing DFT-D3 calculations using the Grimme method. As shown in Table S2, the corrections to the functional lead to negligible

deviations from the original finite temperature barriers suggesting that the medium range non-covalent interactions have minimum effect of cellulose thermochemistry.

Table A.2.2 Comparison of finite temperature barriers calculated with and without dispersion corrections

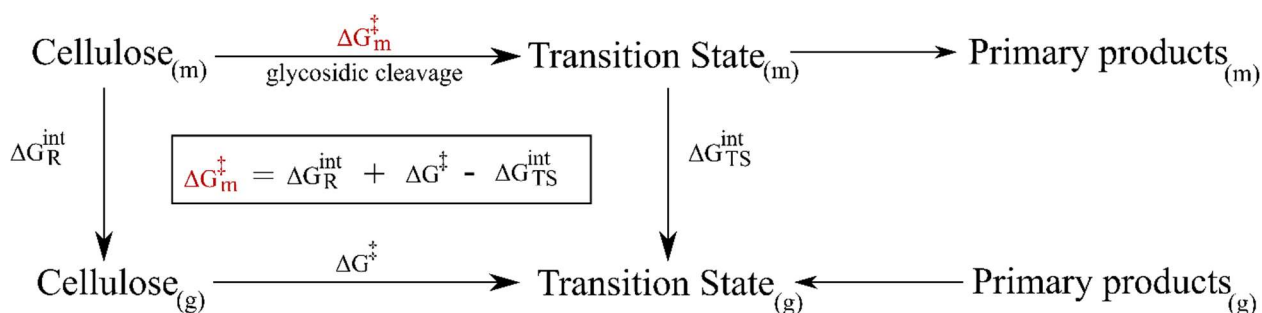
Mechanism	Temperature (K)	Enthalpic barrier (ΔH) (kJ/mol)	ΔH with VdW corrections (kJ/mol)
Transglycosylation	500	299.30	293.70
	1200	164.66	156.78
Ring contraction	500	399.73	394.56
	1200	294.22	288.50

A.2.3 Condensed phase free-energy barrier corrections

A.2.3.1 Interaction energy calculations (Thermodynamic Integration)

The interaction energy of the reactive solute molecule (reactant, TS, product) in the condensed phase is captured by calculating the relative solvation free energy using TI implementation in Gromacs 2018.7. The difference in the interaction between the reactant and TS ($\Delta G_{\text{R}}^{\text{int}} - \Delta G_{\text{TS}}^{\text{int}}$) gives the free energy correction to the gas phase barrier, as illustrated in Figure S3.

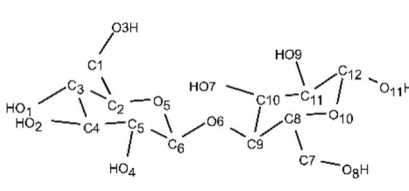
Scheme A.2.1 Schematic showing the calculation of condensed phase corrections to gas phase free energy barriers.



A.2.4 Simulation parameters

The non-bonded parameters of the reactant and transition state species used for the calculation of ΔG^\ddagger and ΔG in Gromacs is provided in Table S3.

Table A.2.3 Non-bonding force-field parameters for cellobiose and its transitions states

Molecule	Atom name	σ (nm)	ϵ (kJ mol)
	C1/C2/C3/C4/C5/C6/C7/C8/C9/C10/ C11	0.350	0.27 6
	H11/H12/H21/H31/H41/H51/H61/H71 /H72/H81/H91/H101/H111/H121	0.250	0.12 6
	HO2/HO3/HO4/HO6/HO7/HO8/HO9/ HO11	0.000	0.00 0
	O2/O3/O4/O6/O7/O8/O9/O11	0.312	0.71 1
	O1/O5/O10	0.290	0.58 6
Atom name	Charge		
	Cellobiose	TS - ring contraction	TS - transglycosylation
C1	0.1132	0.081	0.1132
C10	0.1545	0.1545	0.1545
C11	0.151	0.151	0.151
C12	0.1961	0.1961	0.1961
C2	0.0795	0.0619	0.0795
C3	0.1108	0.1557	0.1108
C4	0.1343	-0.1532	0.1343
C5	0.1675	0.2375	0.1675
C6	0.1978	0.191	0.0778
C7	0.1148	0.1148	0.1148
C8	0.0742	0.0742	0.0742
C9	0.0079	0.0079	0.0079
H101	0.1144	0.1144	0.1144
H11	0.0921	0.1027	0.0921
H111	0.1274	0.1274	0.1274
H12	0.0921	0.1027	0.0921
H121	0.0988	0.0988	0.0988
H21	0.1264	0.1805	0.1264
H31	0.1161	0.1362	0.1161

H41	0.1126	0.105	0.1126
H51	0.1324	0.136	0.1324
H61	0.1046	0.2126	0.1046
H71	0.0992	0.0992	0.0992
H72	0.0992	0.0992	0.0992
H81	0.124	0.124	0.124
H91	0.1205	0.1205	0.1205
HO1	0.4153	0.4399	0.4153
HO11	0.4296	0.4296	0.4296
HO2	0.4143	0.452	0.4143
HO3	0.4147	0.4232	0.4047
HO4	0.449	0.4047	0.449
HO7	0.4402	0.4402	0.4402
HO8	0.4246	0.4246	0.4246
HO9	0.4246	0.4246	0.4246
O1	-0.6633	-0.6936	-0.6633
O10	-0.4105	-0.4105	-0.4105
O11	-0.5634	-0.5634	-0.5634
O2	-0.6679	-0.5404	-0.6679
O3	-0.6669	-0.6693	-0.5169
O4	-0.6802	-0.6756	-0.6802
O5	-0.4359	-0.2858	-0.4359
O6	-0.3606	-0.6068	-0.3806
O7	-0.6741	-0.6741	-0.6741
O8	-0.6942	-0.6942	-0.6942
O9	-0.6567	-0.6567	-0.6567

A.3 Appendix to Chapter 4

A.3.1 Literature review

Table A.3.1 Studies that do not show any significant interactions between the biomass components during pyrolysis.

Title	Authors	Year	Equipment	Temperature	Feed	Interactions between biomass components
Pyrolysis characteristics of biomass and biomass components	Raveendran et al.	1995	TG/Packed bed	1000°C (50°C/min)	14 native biomass & synthetic	No interactions. Char, liquid and gas yields match additive model.
Kinetics of Biomass Pyrolysis: a Reformulated Three-Parallel-Reactions Model	Manya et al.	2003	TG	900°C (20°C/min)	Sugarcane bagasse/waste wood (washed & untreated)	No interactions. Weight loss predicts match additive model.
Further Applications of a Revisited Summative Model for Kinetics of Biomass Pyrolysis	Gomez et al.	2004	TG	900°C (20°C/min)	pine, beech, thistle (washed & untreated)	No interactions. Weight loss predicts match additive model.
In-Depth Investigation of Biomass Pyrolysis Based on Three Major Components: Hemicellulose, Cellulose and Lignin	Yang et al.	2005	TG	105°C-900°C (10°C/min)	Synthetic mixture & Palm oil waste	No interactions. Biomass compents were predicted from weight loss measurements by additive model.
TG study on pyrolysis of biomass and its three components under syngas	Wang et al.	2007	TG	300°C-600° C (max 20°C/min)	sawdust	No interactions. Weight loss predicted by additive model. Lumped activation energy for native biomass within the range of its components.
TGA and macro-TGA characterisation of biomass fuels and fuel mixtures	Skreiberg et al.	2010	TG and macro-TG	60°C-900°C (max 100°C/min)	Wood, coffe waste, demolition wood and mixtures	No interactions. Combustion characteristics and gas yields showed qualitative additive behaviour.
Experimental Study of Biomass Pyrolysis Based on Three Major Components: Hemicellulose, Cellulose, and Lignin	Qu et al.	2011	Tube furnace	350°C-600° C	rice straw, corn stalk, peanut vine	No interactions. Char, gas and bio-oil yield trends are predicted by additive model.
Thermogravimetric Pyrolysis and Gasification of Lignocellulosic Biomass and Kinetic Summative Law for Parallel Reactions with Cellulose, Xylan, and Lignin.	Yoon et al.	2012	TG-GC	140°C-900°C (10°C/min)	Conifers & synthetic	No interactions. Total gas yields and carbon conversion predicted by additive model.
Relationship between thermal behaviour of lignocellulosic components and properties of biomass	Pang et al.	2014	TG	900°C (10°C/min)	11 native biomass & Synthetic	No interactions. Peak decomposition temperature and weight loss predicted by additive model.

Table A.3.2 Studies that show interactions between the biomass components during pyrolysis.

Title	Authors	Year	Equipment	Temperature	Feed	Interactions between biomass components
Influence of inorganic matter on wood pyrolysis at gasification temperature	Hosoya et al.	2007	Glass tubular furnace	800°C	Cedar (washed & untreated)	Yes. Hydrolysable sugar (yield and MW) affected.
The influence of temperature on the yields of compounds existing in bio-oils obtained from biomass samples via pyrolysis	Demirbas et al.	2007	Electrically heated tubular furnace	352°C-552°C (10°C/s)	Olive husk, hazelnut shells, spruce and beech wood	Yes. Drastic change in LGA product yields.
Solid/liquid- and vapor-phase interactions between cellulose- and lignin-derived pyrolysis products	Hosoya et al.	2009	Ampoule reactor	600°C	Synthetic	Yes. Change in tar, water and char yields.
Influence of the interaction of components on the pyrolysis behavior of biomass,	Wang et al.	2011	TG-FTIR	300°C-800°C	Synthetic	Yes. Extended LGA formation temperature range, 2-furfural and acetic acid yields change.
Is it possible to predict gas yields of any biomass after rapid pyrolysis at high temperature from its composition in cellulose, hemicellulose and lignin?	Couhert et al.	2011	Electrically heated flow reactor	950°C	Synthetic & native (beech, spruce, ricehusk, wood bark, grass)	Yes. Gas (CO, CO ₂ , CH ₄ , H ₂ , C ₂ H ₂ , C ₂ H ₄) yields cannot be predicted by additive model.
Pyrolytic Reactions of Lignin within Naturally Occurring Plant Matrices: Challenges in Biomass Pyrolysis Modeling Due to Synergistic Effects	George et al.	2014	Wire mesh pyrolysis	400°C-900°C (1°C/s & 1000°C/s)	Synthetic & native (silver birchwood, sugarcane baggase)	Yes. Char yields are altered.
Cellulose-Lignin interactions during slow and fast pyrolysis	Hilbers et al.	2015	TGA/Py-GC-MS	350°C & 500°C	Synthetic	Yes. Enhanced LGA and reduced dehydration reactions.
Cellulose-Hemicellulose and Cellulose-Lignin Interactions during Fast Pyrolysis	Zhang et al.	2015	Py-GC-MS	500°C	Synthetic & native [Cornstover, pine, red oak, switchgrass (washed + n at d)]	Yes, interactions in herbaceous cellulose-lignin samples. No interactions between synthetic, native cellulose-hemicellulose and woody cellulose-lignin samples.
Cellulose-lignin interactions during fast pyrolysis with different temperatures and mixing methods	Wu et al.	2016	Py-GC-MS	500°C, 600°C & 700°C	Synthetic and native pretreated	Yes, LGA yield promoted while C1-C3 products are inhibited.
Cellulose, xylan and lignin interactions during pyrolysis of lignocellulosic biomass,	Yu et al.	2017	Wire mesh reactor	50° C to 900° C(30° C/min)	Spruce, oak, pine	Yes, at high temperatures additive model cannot predict tar, char and other product yields. However at 325°C, no interactions.
Effects of cellulose, hemicellulose and lignin on biomass pyrolysis kinetics	Zhu et al.	2020	TGA	800° C(10° C/min)	Synthetic	Yes, change in decomposition temperature and other kinetic parameters

A.3.2 Non-bonded parameters

Table A.3.3 Non-bonding force-field parameters for cellobiose.

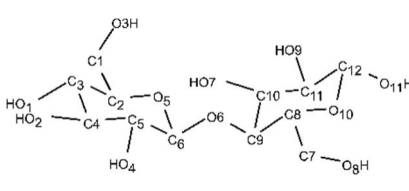
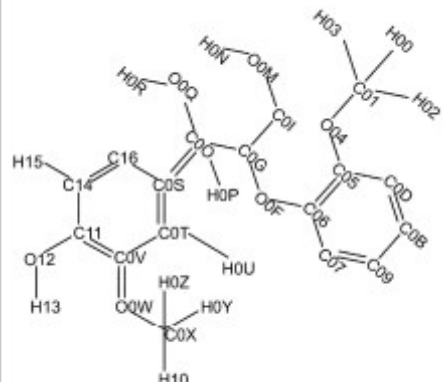
Molecule	Atom name	σ (nm)	ϵ (kJ mol)
 <p>Cellobiose (cellulose dimer)</p>	C1/C2/C3/C4/C5/C6/C7/C8/C9/C10/ C11	0.350	0.27 6
	H11/H12/H21/H31/H41/H51/H61/H71 /H72/H81/H91/H101/H111/H121	0.250	0.12 6
	HO2/HO3/HO4/HO6/HO7/HO8/HO9/ HO11	0.000	0.00 0
	O2/O3/O4/O6/O7/O8/O9/O11	0.312	0.71 1
	O1/O5/O10	0.290	0.58 6

Table A.3.4 Non-bonding force-field parameters for lignin dimer

Molecule	Atom name	σ (nm)	ϵ (kJ mol)
 <p>Quinone Methide Intermediate (lignin dimer)</p>	C05/C06/C07/C09/C0B/C0D/C0S/C0 T/C0V/C11/C14/C16	0.355	0.29 3
	C01/C0G/C0I/C0O/C0X	0.350	0.27 6
	O0M/O0Q/O12	0.312	0.71 1
	O04/O0F/O0W	0.290	0.58 6
	H08/H0A/H0C/H0E/H0U/H15/H17/H0 0/H02/H03/H0H/H0J/H0K/H0P/H0Y/ H0Z/H10	0.250	0.12 6
	H0N/H0R/H13	0.000	0.00 0

A.3.3 Molecule and system visualizations

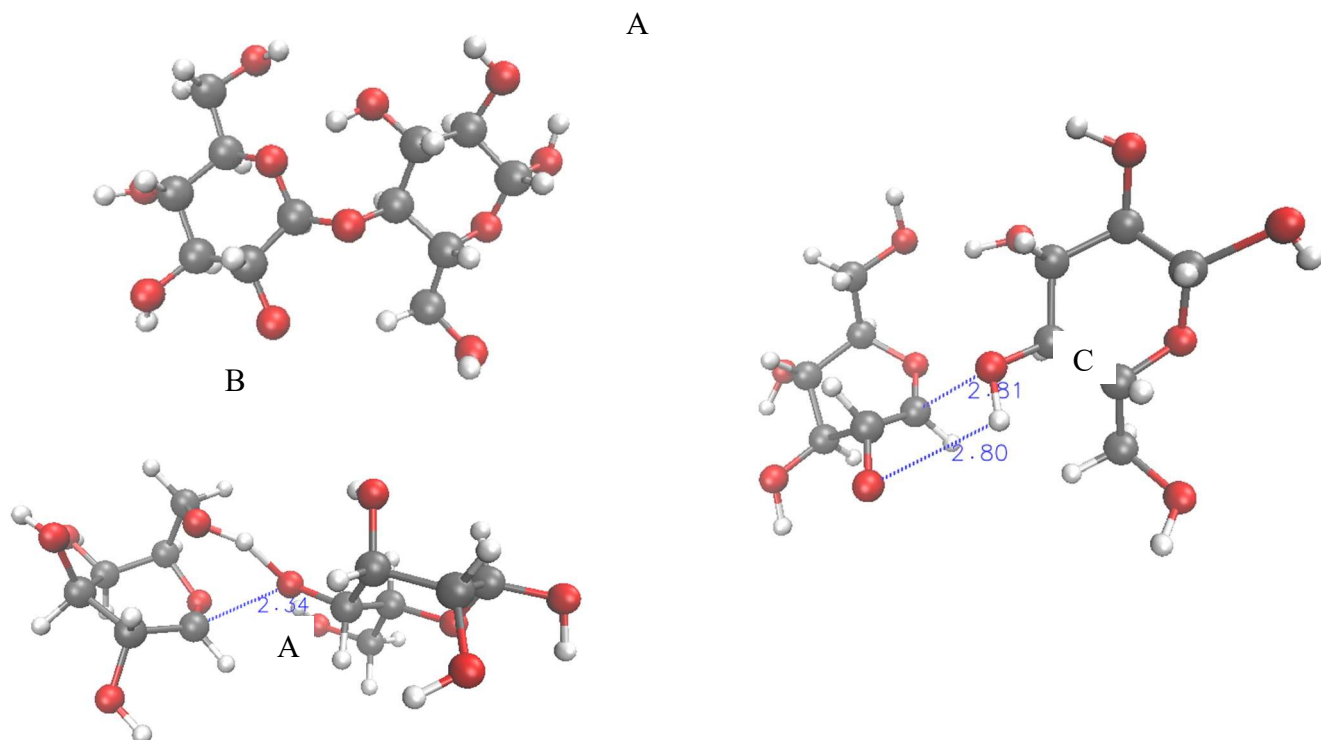


Figure A.3.1 DFT calculated structures of (A) Cellobiose molecule and transition states in gas phase for (B) Transglycosylation (C) Ring contraction mechanisms.

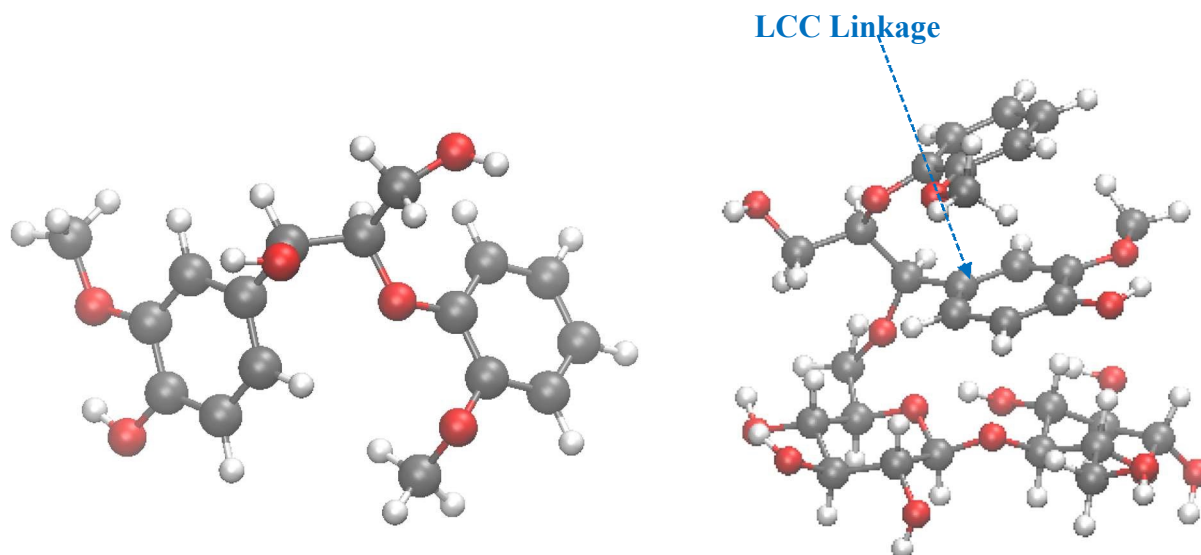


Figure A.3.2 DFT calculated structures of (A) Quinone methide intermediate (lignin dimer) (B) Lignin-Carbohydrate complex (LCC) molecule.

A.3.4 Molecule Coordinates

Cellulose

C	14.95	10.4	14.25
C	19.06	13.32	15.52
C	19.47	14.69	14.99
C	21	14.81	15.02
C	16.38	9.86	14.09
C	16.5	8.33	14.23
C	17.97	7.87	14.07
C	18.89	8.73	14.94
C	18.65	10.21	14.6
C	22.25	11.5	14.13
C	21.36	12.52	14.85
C	19.84	12.24	14.75
H	19.26	13.23	16.59
H	14.54	10.15	15.22
H	19.08	14.84	13.98
H	14.29	9.96	13.51
H	21.37	14.82	16.05
H	16.65	10.07	13.08
H	16.11	8.02	15.19
H	18.26	7.96	13.02
H	18.66	8.57	15.99
H	18.83	10.33	13.52
H	21.88	10.49	14.29
H	22.27	11.68	13.06
H	21.65	12.55	15.89
H	19.59	12.3	13.69
H	15.38	6.91	13.5
H	20.67	16.64	14.85
H	18.48	6.03	13.79
H	15.29	12.23	14.87
H	20.43	8.4	13.75
H	17.52	12.19	15.35
H	23.54	11.17	15.53
H	18.11	15.51	16.12
O	15.75	7.74	13.19
O	21.6	13.8	14.3
O	21.26	16	14.43
O	18.07	6.53	14.5
O	14.94	11.81	14.09
O	20.26	8.39	14.69
O	17.33	10.52	14.94

O	19.55	10.98	15.33
O	17.68	13.13	15.26
O	23.56	11.57	14.67
O	19.02	15.71	15.86

Transition state -Transglycosylation mechanism

C	19.91	13.16	15.78
C	21.01	14.04	15.18
C	20.44	15.44	14.92
C	17.03	9.89	16.19
C	16.7	9.73	14.68
C	16.56	8.28	14.15
C	17.94	7.6	13.91
C	18.92	8.52	13.17
C	18.84	9.92	13.7
C	17.2	14.81	13.48
C	18.29	14.67	14.55
C	18.63	13.22	14.94
H	20.26	12.13	15.83
H	21.89	14.06	15.83
H	16.29	10.54	16.66
H	20.11	15.9	15.86
H	16.98	8.93	16.69
H	15.72	10.19	14.56
H	16.04	8.31	13.19
H	17.84	6.7	13.31
H	19.93	8.18	13.34
H	19.65	10.25	14.35
H	16.87	15.84	13.41
H	17.62	14.56	12.5
H	18.04	15.18	15.47
H	18.78	12.65	14.02
H	21.09	17.14	14.52
H	14.85	7.64	15.04
H	17.56	6.99	15.66
H	17.86	11.26	15.89
H	17.81	9	11.64
H	18.85	13.22	17.4
H	16.02	13.83	14.67
H	20.73	13.98	13.31
O	19.41	15.32	14
O	21.39	16.24	14.39
O	15.81	7.46	15.05
O	18.4	7.21	15.19
O	18.3	10.46	16.45

O	18.64	8.54	11.78
O	17.59	10.47	13.85
O	17.58	12.65	15.71
O	19.62	13.68	17.07
O	16.1	13.96	13.72
O	21.36	13.57	13.9

Transition state – Ring contraction mechanism

C	18.35	13.48	17.76
C	17.14	13.09	16.87
C	17.47	13.28	15.37
C	18.79	12.44	12.46
C	19.16	10.98	12.9
C	18.11	10.09	13.65
C	17.95	8.73	13
C	21.23	9.62	15.28
C	21.13	10.21	13.97
C	20.51	15.27	15.74
C	19.71	13.97	15.66
C	19.64	13.18	16.99
H	18.38	12.91	18.69
H	16.88	12.04	17.03
H	19.48	12.8	11.71
H	17.92	12.35	15.04
H	19	13.14	13.24
H	19.5	10.43	12.02
H	18.41	9.94	14.7
H	17.33	8.64	12.12
H	21.95	8.8	15.31
H	21.97	10.12	13.3
H	20.46	15.79	14.79
H	20.05	15.94	16.47
H	20.23	13.36	14.93
H	20.49	13.45	17.61
H	15.64	13.73	15.18
H	16.82	11.39	13.13
H	17.53	7.15	13.95
H	17.07	13.23	12.82
H	20.45	11.34	16.38
H	17.69	15.22	17.4
H	21.91	14.52	16.87
H	16	13.98	18.14
O	18.39	14.32	15.21
O	16.36	13.49	14.59
O	16.81	10.61	13.66

O	18.34	7.6	13.66
O	17.44	12.71	12.1
O	20.6	9.97	16.28
O	20.28	11.25	13.74
O	19.61	11.76	16.79
O	18.28	14.86	18.06
O	21.87	15.03	16.07
O	16.04	13.91	17.18

Quinone Methide intermediate (Lignin dimer)

C	16.19	15.02	16.99
C	16.22	17.14	16.07
C	16.5	17.32	14.7
C	17.36	18.39	14.32
C	17.87	19.28	15.29
C	17.55	19.11	16.65
C	16.73	18.04	17.04
C	16.14	16.55	12.4
C	15.14	17.57	11.83
C	15.92	15.17	11.73
C	16.74	14	12.27
C	17.72	13.38	11.46
C	18.44	12.27	11.94
C	19.54	11.89	9.85
C	18.19	11.8	13.24
C	17.22	12.4	14.05
C	16.49	13.5	13.56
H	16.74	15.3	17.89
H	16.92	14.66	16.26
H	15.54	14.19	17.24
H	17.64	18.56	13.3
H	18.5	20.1	14.99
H	17.95	19.8	17.38
H	16.49	17.89	18.08
H	17.17	16.81	12.17
H	14.17	17.46	12.31
H	14.97	17.35	10.77
H	14.96	19.4	12.44
H	16.19	15.28	10.68
H	14.46	14.02	11.19
H	17.88	13.76	10.46
H	18.6	11.79	9.3
H	20.25	11.2	9.39
H	19.93	12.9	9.7
H	19.51	10.52	12.96

H	17.01	12.01	15.04
H	15.72	13.95	14.17
O	15.43	16.1	16.48
O	15.93	16.42	13.82
O	15.58	18.9	11.9
O	14.56	14.8	11.74
O	19.39	11.57	11.22
O	18.92	10.74	13.67

Lignin-carbohydrate complex (LCC) molecule

C	16.25	1.32	2.45
C	18.27	2.59	2.9
C	19.05	3.27	3.86
C	20.22	3.94	3.47
C	20.61	3.97	2.12
C	19.84	3.3	1.15
C	18.67	2.61	1.54
C	18.65	4.4	5.93
C	19.54	4.23	7.17
C	17.18	4.79	6.24
C	16.22	4.55	5.09
C	16	5.56	4.12
C	14.98	5.4	3.15
C	15.61	7.37	1.96
C	16.66	4.15	8.98
C	13.52	6.26	6.67
C	13.14	7.65	6.14
C	12.29	7.54	4.86
C	14.31	3.3	4.21
C	15.38	3.42	5.11
C	15.27	3.55	9.21
C	15.28	2.01	9.44
C	13.89	1.48	9.26
C	13.33	1.92	7.9
C	13.28	3.46	7.92
C	10.1	4.74	5.62
C	11.43	5.47	5.46
C	12.3	5.32	6.73
C	14.14	4.28	3.22
H	15.65	2.09	1.98
H	15.55	0.71	3.01
H	16.72	0.69	1.7
H	20.86	4.42	4.21
H	21.52	4.48	1.84

H	20.14	3.31	0.12
H	18.12	2.1	0.78
H	19.04	5.23	5.34
H	19.3	3.33	7.72
H	19.33	5.03	7.87
H	21.36	3.5	7.27
H	17.18	5.87	6.43
H	16.62	6.43	4.15
H	15.61	8.05	2.82
H	15.31	7.94	1.08
H	16.62	7.01	1.79
H	14.26	5.82	6.02
H	17.26	4.13	9.89
H	12.59	8.17	6.91
H	17.17	3.59	8.2
H	12.83	7.02	4.06
H	13.29	4.91	1.7
H	13.64	2.46	4.28
H	15.54	2.67	5.87
H	14.79	4.04	10.05
H	16.04	1.64	8.75
H	13.23	1.74	10.09
H	13.97	1.6	7.09
H	12.71	3.8	8.79
H	9.55	5.14	6.47
H	10.31	3.69	5.82
H	11.94	5.03	4.61
H	11.68	5.57	7.6
H	15.6	0.85	10.99
H	11.38	8.74	3.7
H	15.36	0.14	9.33
H	11.53	1.46	8.51
H	14.54	5.58	8.09
H	8.6	4.19	4.56
H	13.88	9.01	5.1
O	17.17	1.9	3.36
O	18.67	3.19	5.19
O	20.9	4.2	6.79
O	16.68	4.24	7.47
O	14.7	6.3	2.15
O	15.69	1.78	10.79
O	11.14	6.85	5.2
O	11.98	8.81	4.43
O	13.15	4.17	2.29
O	14.38	0.12	9.27

O	12.05	1.36	7.71
O	14.6	3.87	8
O	12.68	3.94	6.76
O	14.05	6.41	7.97
O	9.3	4.83	4.45
O	14.27	8.39	5.71

A.4 Appendix to Chapter 5

A.4.1 CPMD-Metadynamics calculations

All CPMD [48] and metadynamics calculations in this study employed CPMD code version 4.3.0¹⁷⁷ with the plane-wave-pseudopotential implementation of Kohn-Sham density functional theory (DFT)²⁷³. The Martins-Trouiller (MT) pseudopotential²⁸⁷ with the revised Perdew-Burke-Ernzerhof (revPBE) functional^{288,289} of the generalized gradient approximation (GGA) was used in all CPMD calculations. The plane-wave energy cut-off was set at 70 Ryd. A single k-point (Γ -point) was employed for the integration over the Brillouin zone in reciprocal space. CPMD calculations were performed at a temperature of 298K, and temperature control was achieved using the Nosé-Hoover thermostat^{290,291}. The frequency for the ionic thermostat was set to 3000 cm⁻¹ for all systems, corresponding to approximate frequencies of C-H and O-H bond vibrations. To prevent coupling between the ionic and electronic thermostats, the electronic frequency was set to 10000 cm⁻¹ for all systems. The fictitious electron mass was chosen as 300 a.u., the fictitious electronic kinetic energy was within the range of 0.004 a.u. to 0.005 a.u., and a timestep of 4 a.u. (~0.0968 fs) was selected for all calculations. The energies, including the fictitious electronic kinetic energy, were monitored to ensure that the systems did not deviate from the Born-Oppenheimer surface during the molecular dynamics simulations. Two torsion angles were employed as collective variables to enhance the sampling of the CPMD calculations and explore conformations with significant energy barriers using the metadynamics technique^{292,293}. Torsion angle 1 was used to rotate the position of the phenyl ring, while torsion angle 2 rotated the cellobiose moiety. This approach ensured that the system sampled all major conformational changes, specifically the variation in the relative position of the quinone methide intermediate to the cellobiose moiety. The height of the potential was maintained at approximately 0.63 kcal/mol. The convergence of the metadynamics simulations was considered complete if at least one of the torsion angles fully sampled the range of 0-360°, and the other angle explored over 90% of the torsional space. The free energy surfaces constructed for LCC-C2, LCC-C3 and LCC-C6 from which the low energy conformers are extracted are shown below in Figure S1. Subsequently, all structures corresponding to the minima were optimized using all-electron DFT calculations.

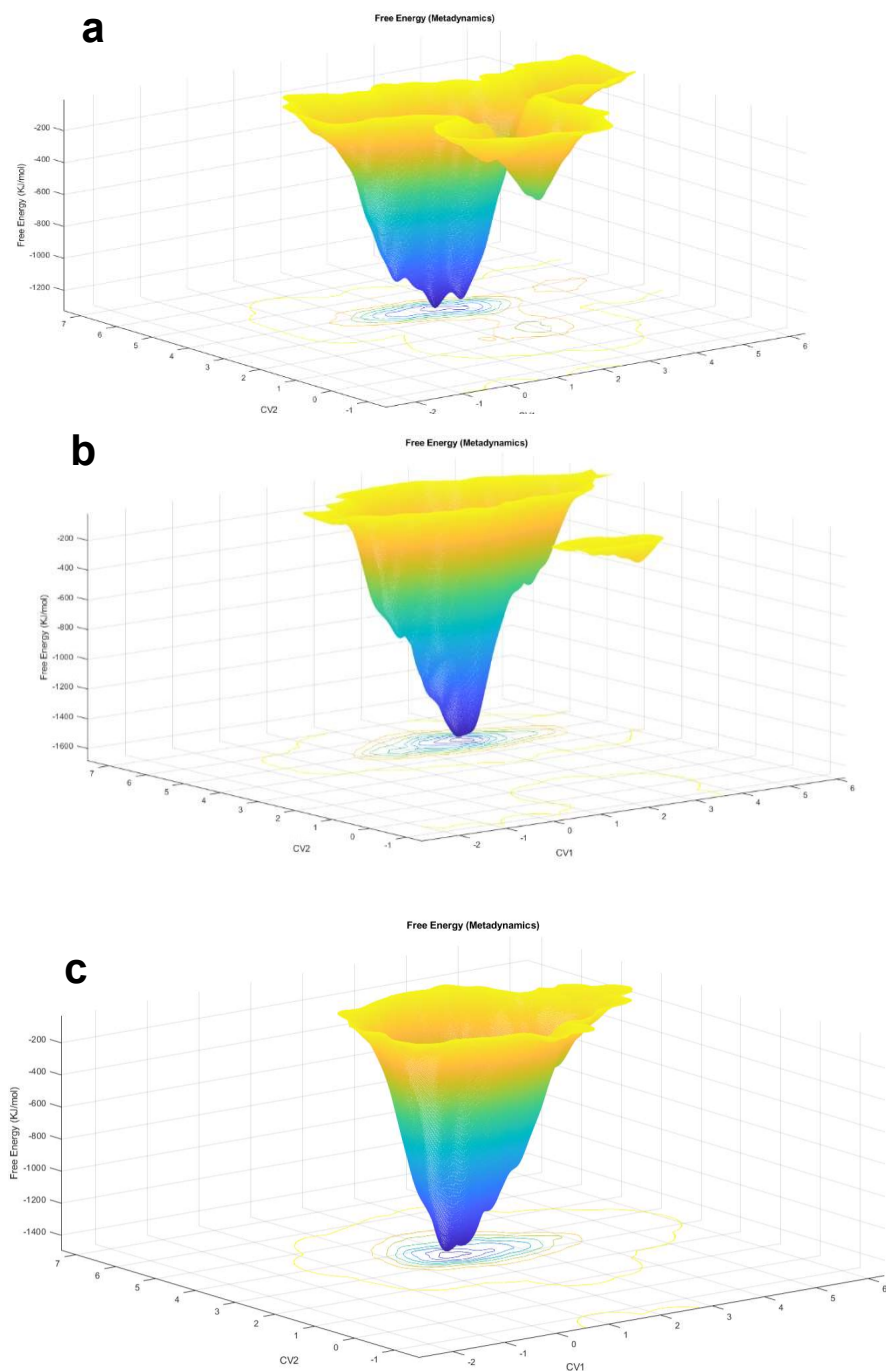


Figure A.4.1 Free energy surfaces constructed by rotating the LCC molecule along CV1 (Torsional angle along the phenyl ring in lignin) and CV2 (Torsional angle along the LCC bond). a) LCC-C2, b) LCC-C3, c) LCC-C6

A.4.2 Thin-film Preparation

Thin-film techniques are used to maintain the sample at isothermal and kinetically limited regime.

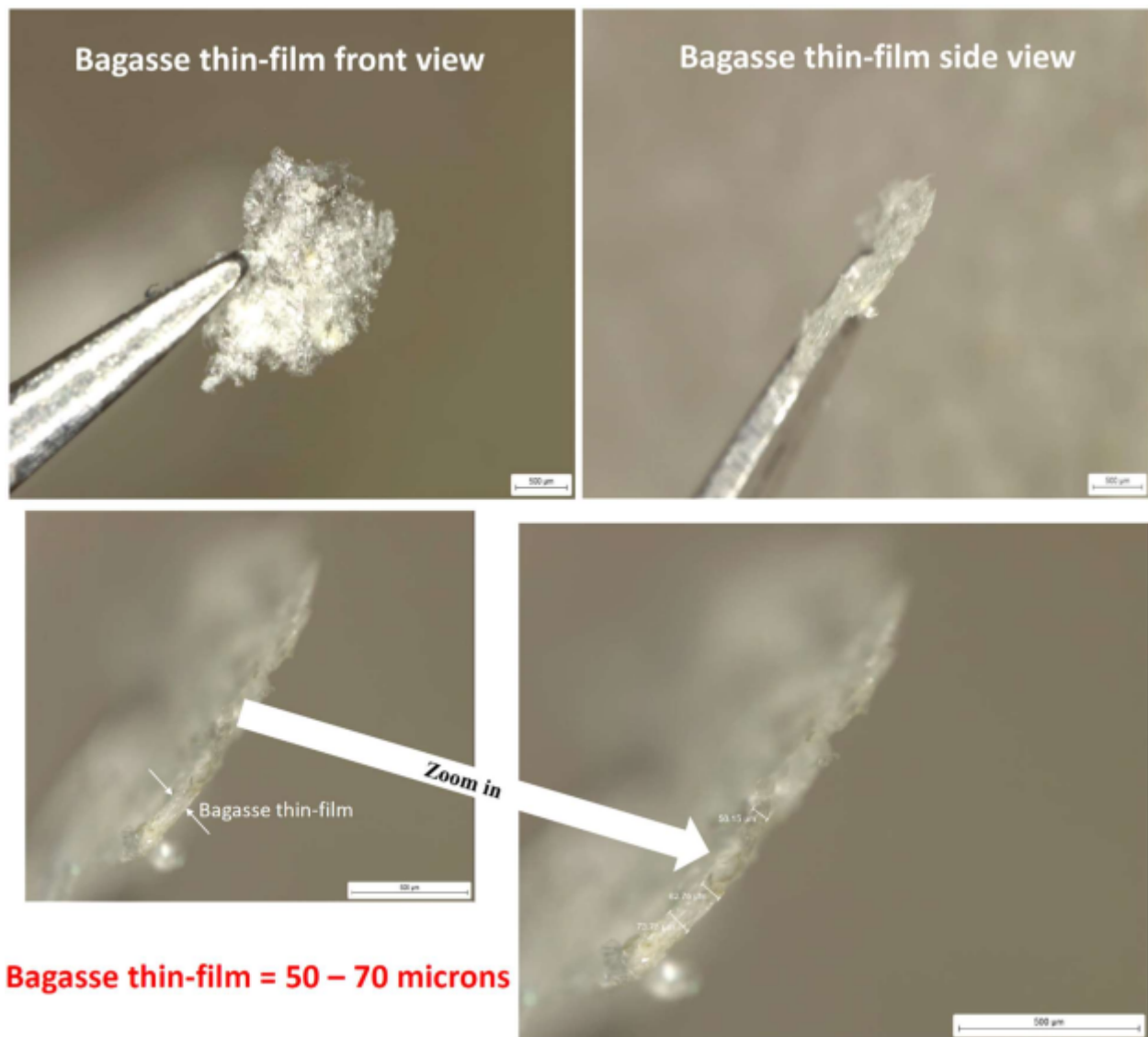


Figure A.4.2 Digital microscopy images of Bagasse thin-films – front, side and zoomed in views.

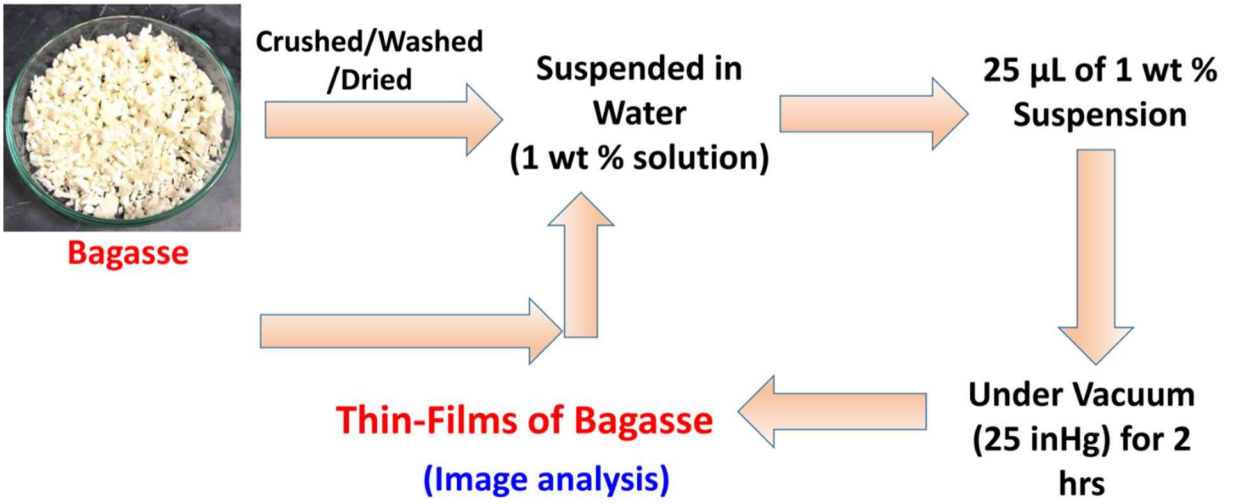


Figure A.4.3 Schematic of the steps involved in thin-film preparation from crushed bagasse.

A.4.3 Minimal change in kinetics between LCCs with different linkage sites (C2, C3, C6)

Table A.4.1 Inter- and Intra-moiety hydrogen bond lengths (Å) made by the cellobiose moiety when binding at C2, C3 and C6 positions with the lignin dimer.

Hydrogen bonds in cellulose dimer	Bond length		
	Reactant		
	LCC site -C2	LCC site- C3	LCC site - C6
C4-C3	2.42		2.42
C5'-C4'	2.29		2.29
C3-C2	2.36	2.53	2.36
O5-C3'	1.93	2.03	1.93
C3'-C4'	2.37	2.38	2.37
O5'-C6'	2.35	2.39	2.36
C2-C1		2.4	

In addition to the difference in activation barriers between pure cellobiose and cross-linked cellobiose in LCC, there are minimum differences in kinetics among various LCC molecules (LCC-C2, LCC-C3 and LCC-C6). C2 and C3 carbons in cellobiose are attached to a hydroxyl (-OH) group while C6 is attached to a hydroxymethyl (-CH₂OH) group. It is interesting to note that the LCC linkage made at different carbon atoms (C2 and C6) exhibit similar activation barriers for ring opening mechanism (c.f. Figure 2). Moreover, for all three mechanisms, LCC-C3 has a marginally higher activation barrier. Activation barriers in cellobiose have been shown to be influenced by the hydrogen bonds made in the reaction environment^{129,240}. Hydroxyl groups from neighboring cellulose sheets can catalyze and promote glycosidic C-O bond cleavage. Therefore, any conformational advantages in making such hydrogen bonds for LCCs linked at the C3 position to the sugar is investigated by identifying all intra- and inter-moiety hydrogen bonds made by cross-linked cellobiose in LCC. Their bond distances have been calculated and reported in Table 2. It can be noticed that for LCC bonding at the C2 and C6, 6 identical hydrogen bonds are identified with almost the same bond distances. However, when the lignin dimer and cellobiose are bound at the C3 position, there are

fewer number of hydrogen bonds with longer (weaker) bond distances. This small difference in the hydrogen bonding made by cross-linked cellobiose between the three bonding sites can potentially explain the difference in their activation energies (c.f. Figure 2). The availability of only weaker hydrogen bonds in the reaction site for cellobiose cross-linked at C3, could lead to less favored TS for the three mechanisms without access to hydrogen bonds to stabilize it. However, the difference in barriers between LCCs binding at different positions is < 5 kcal/mol, indicating that the site of linking between cellobiose and lignin does not have a highly significant role in cellulose decomposition. On the other hand, the deviation in activation energy between the same mechanism in cellobiose and in LCC are huge, indicating that LCC linkage plays a prominent role in cellulose decomposition kinetics.

A.4.4 Molecule and system visualizations

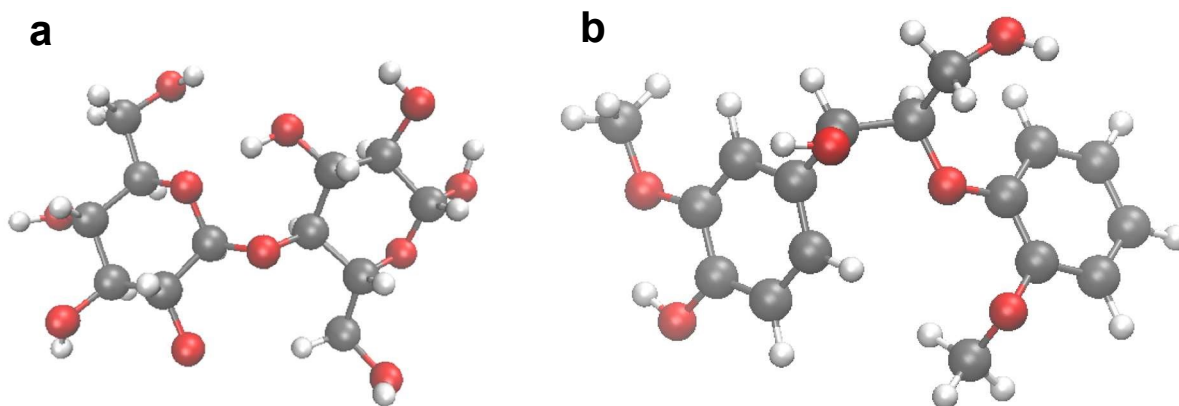


Figure A.4.4 DFT calculated structures of model molecules (a) Cellobiose (cellulose dimer) (b) Quinone methide intermediate (lignin dimer).

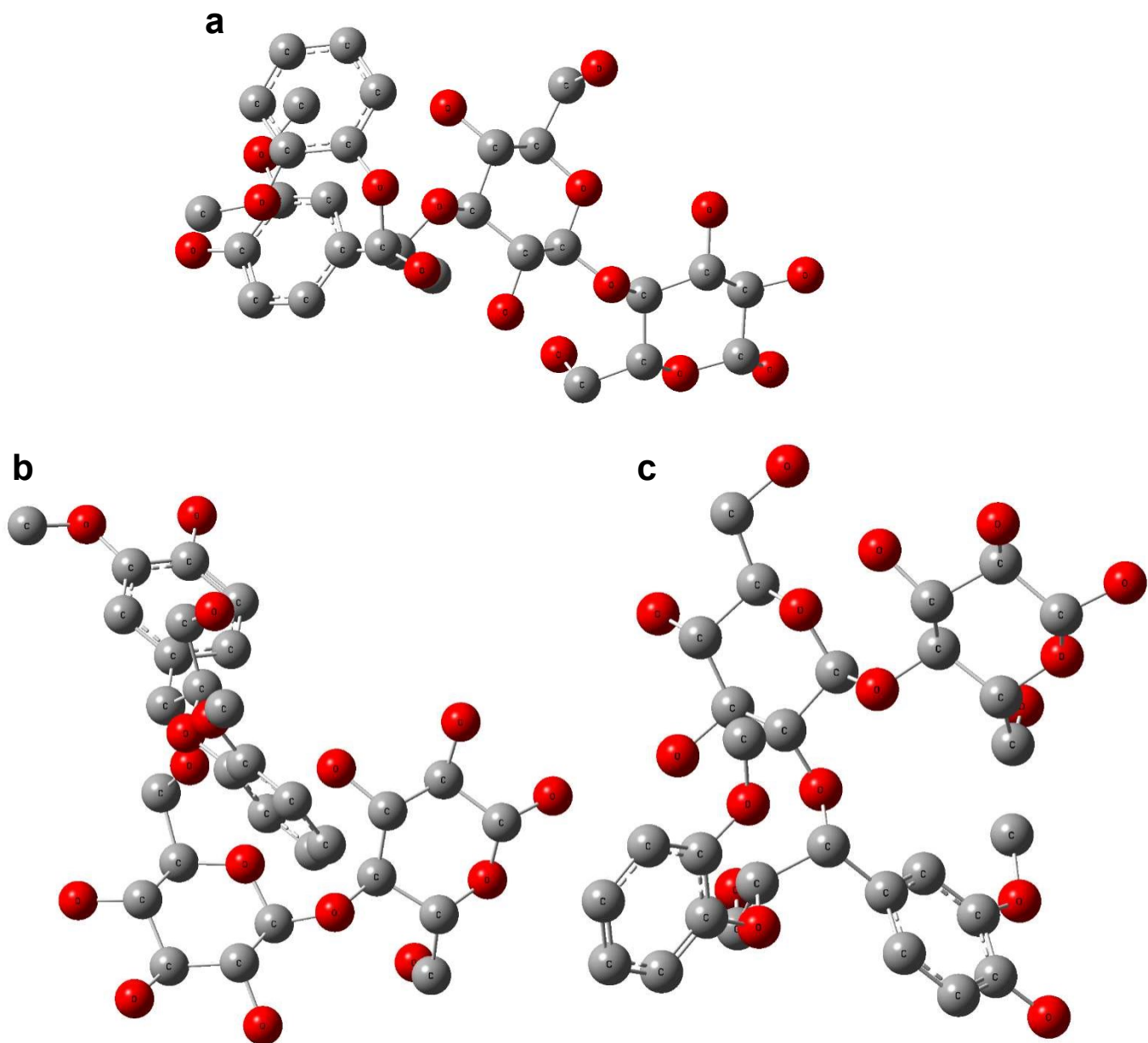


Figure A.4.5 DFT calculated structures of Lignin-carbohydrate complex molecules (a) LCC-C3 (b) LCC-C6 (c) LCC-C2